Interpretation of Transient Temperature Data from Permanent Down-hole Gauges (PDGs)

Yiqun Zhang

Submitted for the degree of Doctor of Philosophy

Heriot-Watt University

School of Energy, Geoscience, Infrastructure and Society

October 2015

Abstract

With the installation of Permanent Down−hole Gauges (PDGs) during oil field development, a large volume of high resolution pressure, temperature and sometimes flow-rate data are available for real-time and continuous reservoir monitoring. In practice, interpretations of these data can optimize well performance, provide information about the reservoir and continuously calibrate the reservoir model.

Although the wellbore is in a non-isothermal environment, heat transfer between the fluid in the wellbore and the formation is often ignored and temperature is usually assumed to be constant in the process of data interpretation, leading to misunderstanding of the pressure profile. Furthermore, the pressure transient analysis (PTA) often fails to determine accurate flow regimes, and may be erroneously applied in nonlinear reservoir-well systems. These problems motivated my detailed analysis of temperature data.

In this thesis, firstly, a non-isothermal wellbore model that is capable of predicting the temperature, pressure, and flow-rate profiles under multi-rate and multiphase production scenarios is established. Then this numerical wellbore model is coupled with a reservoir model to reproduce the transient temperature behaviour at gauge locations. Secondly, a new workflow for integrating transient down-hole data processing is introduced. The relationship between temperature change and flow-rate change is interpreted and a new nonlinearity diagnostic function (A_{Turc}) is presented. Thirdly, new procedures of model-independent transient temperature analysis are performed, followed by diagnosing the wellbore storage regime, verifying the PTA interpretation results, and reconstructing the flow-rate history using transient temperature data. Several case studies are conducted to demonstrate how transient temperature analysis, along with the transient pressure analysis can greatly reduce the uncertainties in well testing interpretation.

The applications of both synthetic datasets which are simulated by the fully coupled wellbore-reservoir model and real field datasets demonstrated that the temperature data can provide additional constraints for pressure analysis. Additionally, the reliability of the developed methods which reveal complementary reservoir information from transient temperature data has also been verified.

Dedication

This thesis is dedicated to my wife Lu Ji

&

my parents

Acknowledgement

I would like to thank my supervisor Professor. Shiyi Zheng with deepest gratitude, for providing me the opportunity to pursue Ph.D. degree in the IPE of Heriot-Watt University. My research work would not have been completed without his continuous guidance, fantastic advice, hard pushing and effective encouragement.

I would also like to express my appreciation to Conoco-Philips, BG Group, Wintershall AG, Weatherford and PetroChina for their financial support.

I am very grateful to the research staff, secretaries, and all other supporting staff of the IPE. I thank all my friends for technical discussions and social interactions – especially those I met with at regular lunch at Energy Academy. Although the PRIME project finished two years ago, I still would like to express particular appreciation to my colleagues Fuyong Wang and Lili Xue for their unconditional help and kind encouragement.

Last but not least, my special thanks would like to be given to my wife and parents who are willing to share this happiness with me, and support me with their selfless love.

ACADEMIC REGISTRY
Research Thesis Submission

Name*:*	Yiqun Zhang		
School/PGI:	School of Energy, Geoscience, Infrastructure and Society		
Version: *(i.e. First, Resubmission, Final)*	Final	Degree Sought (Award **and** Subject area)	PhD in Petroleum Engineering

Declaration

In accordance with the appropriate regulations I hereby submit my thesis and I declare that:

1) the thesis embodies the results of my own work and has been composed by myself
2) where appropriate, I have made acknowledgement of the work of others and have made reference to work carried out in collaboration with other persons
3) the thesis is the correct version of the thesis for submission and is the same version as any electronic versions submitted*.
4) my thesis for the award referred to, deposited in the Heriot-Watt University Library, should be made available for loan or photocopying and be available via the Institutional Repository, subject to such conditions as the Librarian may require
5) I understand that as a student of the University I am required to abide by the Regulations of the University and to conform to its discipline.

* *Please note that it is the responsibility of the candidate to ensure that the correct version of the thesis is submitted.*

Signature of Candidate*:*		Date:	

Submission

Submitted By *(name in capitals):*	YIQUN ZHANG
Signature of Individual Submitting:	
Date Submitted:	

For Completion in the Student Service Centre (SSC)

Received in the SSC by *(name in capitals):*			
Method of Submission *(Handed in to SSC; posted through internal/external mail):*			
*E-thesis Submitted (**mandatory for final theses)***			
Signature:		Date:	

Table of Contents

List of Figures

List of Tables

Nomenclature

A = *drainage area, ft*^{2}

A_P = *amplitude of wavelet detail coefficient/ processed pressure*

A_T = *amplitude of wavelet detail coefficient/ processed temperature*

A_{Tf} = *earlier wavelet transform detail coefficient*

A_{Tl} = *later wavelet transform detail coefficient*

A_{Purc} = *pressure amplitude caused by unit-rate-change*

A_{Turc} = *temperature amplitude caused by unit-rate-change*

B = *formation volume factor*

C_A = *Dietz shape factor for drainage area, dimensionless*

C_j = *J-T coefficient,* $\frac{\beta T-1}{C_f}$, *K/pa*

C_P = *heat capacity, Btu/(lbm ˚F)*

C_f = *specific heat capacity of the fluid, Btu/(lbm ˚F)*

C_s/C_r = *specific heat capacity of the rock, Btu/(lbm ˚F)*

C_m = *volumetric heat capacity of fluid saturated rock,* $(1-\emptyset)\rho_s C_s + \emptyset(\rho_w C_{fw} S_w + \rho_o C_{fo} S_o)$, *Btu/(lbm ˚F)*

C_T = *thermal storage parameter represents the capacity of the wellbore to store or release heat as a multiple of the fluid mass and fluid heat capacity, dimensionless*

C_{rc} = *compressibility of reservoir rock, 1/psi*

C_t = *total compressibility of fluid and rock, 1/psi*

c = *ratio of the fluid heat capacity to the heat capacity of fluid statured rock,* $\frac{C_f \rho_f}{C_m}$, *dimensionless*

D = *pipe diameter, ft*

$f(t)$ = *a dimensionless function with respect to time and thermal conduction conditions*

f_F = *fanning friction factor*

g = *gravity acceleration, ft/sec*^{2}

g_c = *conversion factor*

h = *vertical depth / Reservoir thickness, ft*

H_L = *liquid hold-up, dimensionless*

J = *Productivity Index, MMscf/(day psi) or bbl/(day psi)*

k = *permeability*

k_g = *geothermal gradient, ˚F/ft*

k_{pc} = *thermal conductivity coefficient of production casing, Btu/(hr ft ˚F)*

k_{mud} = *thermal conductivity coefficient of mud, Btu/(hr ft ˚F)*

k_{cem} = *thermal conductivity coefficient of cement, Btu/(hr ft ˚F)*

k_{cas} = *thermal conductivity coefficient of casing, Btu/(hr ft ˚F)*

k_e = *thermal conductivity coefficient of formation, Btu/(hr ft ˚F)*

k_m = *thermal conductivity of fluid saturated rock,* $\emptyset k + (1 - \emptyset)k_e$ *, Btu/(hr ft ˚F)*

m = *fluid mass in control volume, lbm*

q = *flow rate*

Q = *accumulative flow rate*

Q_c = *heat flow rate from or to the wellbore, Btu/hr*

r = *radius, ft*

r_e = *reservoir outer radius, ft*

r_w = *wellbore radius, ft*

S = *skin factor*

T_e = *geothermal temperature of formation, ˚F*

T_{ebh} = *geothermal temperature of formation at bottom-hole, ˚F*

T_f = *fluid temperature,* ˚*F*

T_{ei} = *formation temperature,* ˚*F*

T_{fbh} = *fluid temperature entering the sand-face from formation,* ˚*F*

T_{fp} = *fluid temperature prior to shut-in,* ˚*F*

$\bar{t}$ = *average time*

Δt = *impulse time, it is a certain constant value when performing WT (decided by the WT scale parameter and the time step of transient data)*

U = *overall heat transfer coefficient, Btu/(hr ft °F)*

v_m = *mixture superficial velocity, ft/s*

v_{sl} = *superficial liquid velocity, ft/s*

v_{sg} = *superficial gas velocity, ft/s*

W_t = *mass rate, lbm/hr*

z = *length of calculation segments (from bottom), ft*

Greek

η = *adiabatic expansion coefficient,* $\frac{\beta T}{C_f}$, *K/pa*

β = *thermal expansion coefficient,* $\frac{1}{\rho}\frac{\partial \rho}{\partial T_p}$, *1/K*

$\overline{\rho_m}$ = *average density of the mixture, lbm/ft*^{3}

ρ_{NS} = *no-slip density (both phases move at the same velocity), lbm/ft*^{3}

ρ = *fluid density*

$\emptyset$ = *porosity*

$\emptyset(t)$ = *scale function*

$\psi(t)$ = *wavelet function*

τ = *time-dependent integration variable,* $\frac{\mathrm{A_P}}{\Delta \mathrm{q}}$

μ = *viscosity, cp*

$\gamma = e^{0.5772}$, *Euler constant*

$\pi = 3.14159$, *mathematical constant*

Subscripts

f = fluid

m = mixture

s = rock

g = gas/gauge

l = liquid

n = flow event index

r = reservoir

Name

BHT: Bottom-hole Temperature

BHP: Bottom-hole Pressure

BU: Build-up Test

CWT: Continuous Wavelet Transform

DD: Drawdown Test

DTS: Distributed Temperature Sensor

DWT: Discrete Wavelet Transform

ETR： Early Time Region

FVF: Formation Volume Factor

GOR: Gas Oil Ratio

JT: Joule-Thomson Effect

MPP: Middle Production Point

PDG: Permanent Down-hole Gauges

PI: Production Index

PTA: Pressure Transient Analysis

TTA: Temperature Transient Analysis

URSR: Unit Reservoir System Response

WOR: Water-Oil Ratio

WT: Wavelet Transform

Publications

Zheng, S., and Y. Zhang, 2014, A Non-Isothermal Wellbore Model with Complex Structure and Its Application in Well Testing: International Petroleum Technology Conference. IPTC-18152

Zheng, S., and Y. Zhang, 2015, Improved Analysis of Transient Temperature Data from Permanent Downhole Gauges (PDG): SPE Reservoir Characterisation and Simulation Conference and Exhibition. SPE-175579

Chapter 1 Introduction

1.1. Background

The term 'well testing' has been researched over the decades with the aim of monitoring production, estimating reservoir parameters, calibrating accurate reservoir models, and forecasting well performance. The interpretation of data can be made from analysing data from several kinds of measurement tools which have been widely applied in oil fields. Among the advanced types of equipment, Permanent Down-hole Gauges (PDGs) provide the possibility of investigating the reservoir at a larger radius than that from conventional well testing. These are usually installed at several hundred feet above the production zone during well completion and can provide continuous, real-time and high-resolution measurements of down-hole pressure, temperature and sometimes flow-rate data. The onset of PDGs inspired engineers to further interpret measured down-hole data and calculate the pressure and temperature profiles. The analytical solutions (reliable pressure equations and correlations) and interpretation methods (convolution and deconvolution techniques) for transient pressure data have been published in many articles in the past (Lee et al., 2003). However, the temperature changes during fluid flow in the porous media and the wellbore have been regarded as unimportant for flow behaviour analysis, and the transient temperature data have been under-investigated.

1.1.1 Temperature measurement tools

Effective down-hole data acquisition is crucial for reservoir management and field development. In 1906, Golubyatnikov utilized a maximal thermometer and first measured the temperature profile along an oil well (Ramazanov, 2006). Then, with the development of electronic thermometers, more investigations concerning the temperature in gas wells were conducted by Dakhnov (1952). Since the 1960s, pressure data have been used for production monitoring, and with the installation of PDGs (more sensitive thermometers with a resolution in the order of 0.01 K), the temperature changes caused by the Joule-Thomson effect and the adiabatic effect have been recognised. The measurements of down-hole transient data in subsea wells can be traced back to 1977, when PDG was first installed in a subsea well in the Campos Basin (Bezerra et al., 1992). However, PDGs were not widely used in the petroleum industry until in the 1980s. According to Baker et al. (1995), the original applications of PDGs suffered many failures, which were caused

by damage occurring during installation or caused by cable problems. These issues were resolved with the new tool structure and improved down-hole cables. Gisbergen and Vandeweijer (2001) evaluated the performance of 952 PDGs installed since 1987 and found that the 5-year survival probability improved from 40% for those pressure and temperature monitoring systems installed in the period of 1987-1988 to 75% for the period of 1991-1992. Figure 1-1 shows the comparison between current technology and the technology in the 1960s. The current electronic PDGs system consists of seven main components, which are temperature/pressure gauges, gauge mandrel, connectors, cables, acquisition systems, interpretation software and power supply.

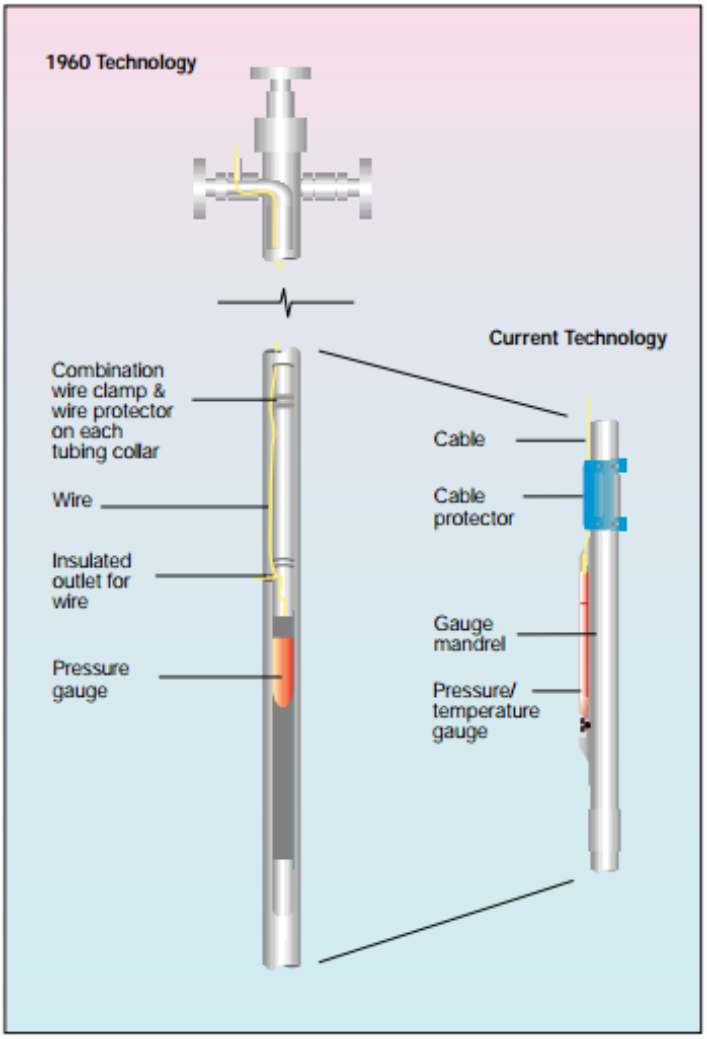

Figure 1-1：The technical evolution of electronic PDG (Baker et al., 1995)

In recent years, as the fibre optic technology has advanced, the temperature can now be measured by the permanent down-hole sensors with a resolution better than 0.0045 °F

(Sensornet Limited, 2007). Other advantages of optical fibre include the absence of down-hole electronics and the fact that it is available to install after completion. The typical fibre optic PDG system provides highly reliable temperature data and consists of four main components: the instrumentation unit, the wellhead outlet and surface cable, the in-well cable and connectors, and the sensor assembly (Kragas et al., 2002).

Another advanced commercial temperature monitoring system is the fibre optic DTS (Distributed Temperature Sensor), which can profile injection or production of wells. Nearly all the temperature measurement methods used in conjunction with DTS apply the vibration of molecules in the fibre optic, which is directly associated with the fibre's temperature and causes weak backscattering of the laser light. The working mechanism is briefly illustrated in Figure 1-2.

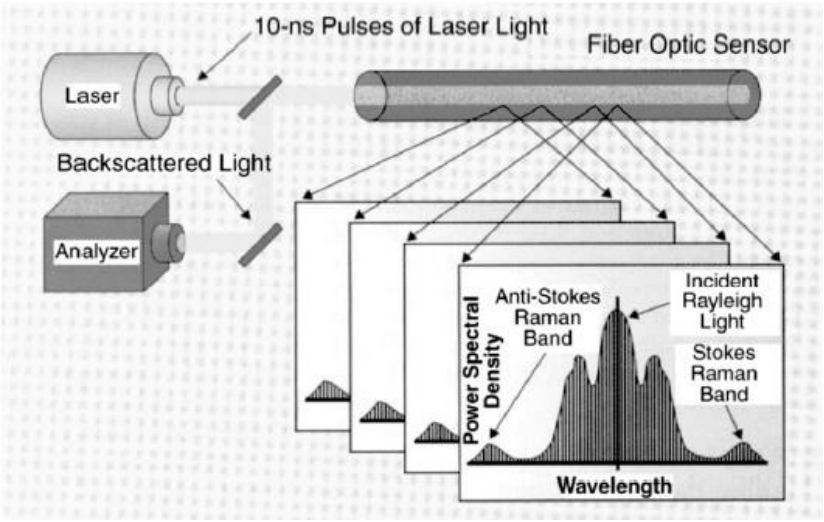

Figure 1-2：Mechanism of fibre-optic temperature monitoring (Ouyang and Belanger, 2006)

1.1.2 The applications of down-hole temperature data

Initially, temperature data acquired from an electronic thermometer were simply introduced and temperature logging data were mainly used for locating gas or water entry, detecting casing leaks, identifying injection or production zones, and determining cement top location. However, the thermodynamic effects such as the Joule-Thomson effect and adiabatic effect were usually ignored (Atkinson and Ramey, 1977; Meyer, 1989), and fluid flow in porous media was treated as isothermal, due to the small value of temperature changes during production (Lapuk, 1940).

With the development of temperature measurement tools, high resolution down-hole data can now be recorded. Therefore, the application of temperature data has entered a new stage. In summary, these current applications can be classified into three categories.

Reservoir description related applications

1. Explain anomalous pressure trends and assess the quality of the test data and test procedures
2. Monitor the changes of reservoir-wellbore properties and drive mechanism with time through analytical solutions
3. Detect the wellbore storage regime and verify the conventional well test (pressure analysis) interpretation parameters
4. Determine individual layer properties for multiple layers commingled reservoir

Reservoir and wellbore modelling related applications

1. Estimate reservoir and fluid thermodynamic parameters such as permeability, porosity and the Joule-Thomson coefficient through matching the simulated results with field data
2. Estimate flow-rate profile along the wellbore and allocate zonal flow-rate
3. Reconstruct unknown flow-rate history

Production monitoring related applications

1. Identify well problems quickly
2. Detect water and gas entry into the wellbore, identify breakthrough zones and development of steam zones
3. Diagnose the stimulation workovers such as acidizing or the formation fracturing, and evaluate the well performance
4. Diagnose near wellbore formation damage and wax deposition

More details about the temperature data applications will be described in the literature review in Chapter 2.

1.2. Statement of problem and motivation

Although down-hole transient pressure data modelling, processing and interpretation have been studied for decades and are significantly improved, there still remain some problems which will be discussed in this section in sequence. These challenging problems and the potential usefulness of temperature measurements are the motivations for making this study, which include interpreting temperature variation, identifying reservoir-well characteristics, calculating production and overcoming data limitation problems, when other sources of down-hole information are less sufficient.

1.2.1 Non-isothermal or isothermal conditions

Although there are articles that describe heat flow modeling for thermal recovery processes (Lasseter, 1976; Prats, 1985), temperature is often assumed as constant in the data interpretation. In other words, the temperature changes during fluid flow in porous media have been regarded unimportant for flow behaviour analysis. Reservoir temperature profiles, practically, are the results of the combination of flow-rate, pressure and reservoir-fluid properties and the flow is definitely not isothermal. The measured temperature can vary up to 8 °F with the gauge resolution of 0.001 °F in some circumstances (Sui and Zhu, 2009).

Furthermore, the wellbore has usually been assumed as an isothermal environment, which means that there is no heat transfer between the fluid in the wellbore and the formation; however, in the oilfield operations, the wellbore is in a non-isothermal environment, and the heat transfer along the tubing will affect the pressure profile. Therefore, placing the pressure gauge above the MPP (Middle Production Point) can result in misdiagnosis of reservoir problems, based on the pressure data alone (Wang and Horne, 2011). As demonstrated in Figure 1-3, putting the gauge at different points along the wellbore can result in totally different pressure data, which will yield different results in well test interpretation. Placing the gauge at the MPP, the pressure derivative shows a plateau, while putting the gauge at the wellhead, the pressure derivative shows a dip, which is misleading in this case. This example shows that gauge placement can affect the data interpretation result, especially in high transmissibility reservoirs or gas wells. Moreover, the thermodynamic behaviour of the flowing fluid is one of the dominant factors that affect multiphase flow in the wellbore. As PDGs (Permanent Down-hole Gauges) are

usually installed several hundred feet above the pay zones, the heat transfer along the well length, which will lead to misunderstanding of the pressure profile, should not be ignored.

In summary, there is a lack of a coupled wellbore-reservoir model that is capable of simulating comprehensive compositional and thermal phenomena for well test interpretation.

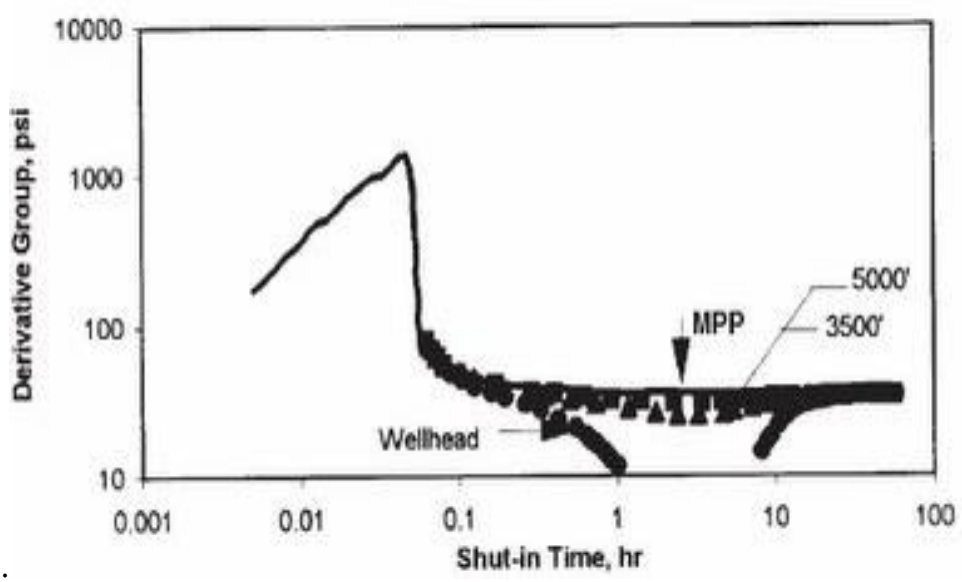

Figure 1-3：Effect of gauge positions on well testing (Kabir and Hasan, 1998)

1.2.2 Transient data processing

Together with the good news that large volumes of down-hole pressure, temperature and sometimes flow-rate data can be acquired by PDGs, there comes a new challenge for petroleum engineers - how to analyse those noisy transient data and convert them into useful information for reservoir model identification and parameter estimation. Typically, PDG data contain noise, outliers and other types of error signals (aberrations) which do not comport with known physics due to the uncontrolled collection conditions. With the intention of correctly interpreting transient pressure and temperature data, data processing is an essential preliminary step. Several effective methods and algorithms associated with pressure data processing have been applied in practice, but temperature data processing is rarely discussed. As mentioned in the previous background section, the temperature and pressure are measured by PDGs at the same time but independent of each other; hence, temperature data can be used to provide additional constraints for pressure data

processing. These issues motivated the current studies into data processing for transient identification, detection of outliers, and noise reduction.

1.2.3 Transient data interpretation - uncertainties of transient pressure analysis

Transient pressure data has been analyzed to estimate formation parameters and identify the reservoir model since 80 years ago. Currently, the common well-testing practice is pressure transient analysis; this method is based on the assumption of a linear system, which underlies the principle of superposition in time and space (Houzé et al., 2011). The nonlinearities which are caused by gas/multi-phase flow, non-Darcy flow or a change in well-reservoir parameters, may drive the diffusivity equation to become invalid and result in erroneous application of PTA methods (such as Horner analysis, pressure derivative, and deconvolution). Although several approaches for diagnosis of nonlinearities have been published, there are always limitations to them:

1. A full scale numerical model can obtain the most accurate results and is probably what we need, but it is too complex to use widely. Especially, in order to match the long-term field data, the numerical model should be calibrated continuously with the variable reservoir-well parameters.
2. Plotting all build-ups on the same log-log plot, known as '4D' pressure/pressure derivative analysis, is an extension of PTA, and it also depends on the appropriate superposition function and linear equations (Sammy et al., 2004; Gringarten et al., 2003). In addition, this method cannot diagnose nonlinearity in real-time due to the relatively poor quality of draw-down pressure data and limited number of effective pressure build-ups.
3. PI (Productivity Index, $\mathrm{PI} = \frac{q_m(t)}{[\bar{p}(t) - p_m(t)]}$) is a common and simple method for monitoring the oil and gas well's performance; it expresses the ratio of measured flow-rate and the difference between average reservoir pressure and measured down-hole pressure. Unneland (1998a) and Kuchuk et al. (2005) demonstrated the application of PI in monitoring well performance and diagnosing nonlinearity over time. The disadvantage of this method is that PI has to be estimated during the steady-state or pseudo-steady-state period; what is more, the average reservoir pressure needs to be updated with time. This method cannot diagnose nonlinearity in real-time in the strict sense, either.

4. Unit Reservoir System Response (URSR) is a more effective diagnostic method which analyzes the relationship between flow-rate change and pressure change (Wang, 2012). But it cannot distinguish the nonlinearities of pressure-dependent fluid parameters from the reservoir parameters' change.

As a result, a further method for nonlinearity diagnosis needs to be developed.

Furthermore, detecting the end of wellbore storage and flow regimes by transient pressure data is uncertain in some circumstances (even for the linear or pseudo-linear reservoir systems), which will cause problematic interpretation of the reservoir parameters. That is to say, if the near-wellbore area is small and the features' performance is close to that of the well, the reservoir characteristics contained in the pressure data may be masked by wellbore storage due to the high propagation speed of the pressure wave.

Compared with the pressure transient analysis, the temperature transient analysis is underutilized. It is taken for granted that the pressure diffusivity equation governing slightly compressible fluid flow in porous media is linear for the linear reservoir system. This principle also satisfies the temperature performance, because temperature (much slower propagation speed of thermal front) and pressure meet the same diffusion equation. If the reservoir with a single production well is treated as a system, the input signal of this system is flow-rate and the output signal can be regarded as either down-hole transient temperature or pressure data. For that reason, transient temperature data may be interpreted successfully and can provide complementary information for pressure analysis.

Moreover, although the measured dynamic temperature data have been interpreted in practice to predict flow profiling and provide characteristic information about the reservoir, almost all of the approaches rely on established non-isothermal models, which depend on thermodynamic parameters.

1.2.4 Unknown flow-rate history

Detailed flow-rate information is not only necessary for conventional pressure transient analysis, but also crucial for reservoir surveillance and management. Nevertheless the straight-forward flow-rate measurement techniques have their own disadvantages. For

instance, measuring flow-rate at the pay zone by using down-hole flow meters, which are cost-prohibitive, can obtain the most accurate production rate; surface flow meters cannot get reliable results, especially in multiphase reservoirs (high GOR); the utilization of production-logging tools not only interrupts daily production, but also fails to provide transient flow-rate data.

During field production, a more common practice is using surface separation equipment to measure several wells' entire cumulative production (Dake, 1983). It means the flow-rate is measured daily or weekly rather than continuously. Further operations such as separator tests and production allocation need to be carried out to assign the individual well's flow-rate history, but the obtained results are not particularly good, due to the limit of test frequency (gathering and separation equipment are shared by numerous producers).

In order to acquire the continuous flow-rate history without long intervals, other authors have attempted to reconstruct the flow-rate from transient pressure data. Athichanagorn et al. (1999) made an uncertain assumption about the reservoir model and proposed a wavelet-based approach for reconstructing the flowrate. Zheng and Wang (2011) presented the study of recovering flow-rate using the Wavelet Transform method in an oil and water two-phase flowing reservoir. Exact locations of the beginning of every pressure transient need to be identified in advance, so as to achieve this. But the pressure-based flow-rate reconstruction method is restricted by the signal (pressure data) quality and flow conditions; for example, it has rather poor performance with aberrant pressure data points and in nonlinear systems (such as the phase segregation effect after gas comes out of solution). By integrating the additional transient temperature data analysis, the pressure information can be constrained and the unreliability of the reconstructed flow-rate may be reduced.

1.3. Research objectives and study approach

The four problems mentioned in Section 1.2 discussed the issue that the transient pressure data alone is insufficient to provide accurate information for reservoir management, and the temperature is an additional and valuable item of data, which has a large potential in the understanding and management of the reservoir. Using temperature data along with pressure analysis will improve well testing accuracy and decrease uncertainty.

In brief, the current study focuses on utilizing temperature data as complementary interpretation sources to conventionally acquired pressure and sometimes flow-rate measurements. The objectives of this research can be summarized as:

1. Establishing a non-isothermal wellbore model which can calculate temperature profile, integrate pressure data, and determine the flow-rate profile more accurately and coupling it with a reservoir model.
2. Simulating the transient temperature behaviour at the location of gauges, and then matching the model with field data to estimate the representative thermodynamic parameters.
3. Developing a wavelet-based reliable approach for transient pressure and temperature data processing, then identifying the flow events and removing the outliers by using processed temperature and pressure data together.
4. Diagnosing the nonlinearity of the reservoir-well system from processed temperature data, and evaluating the degree of nonlinearity.
5. Based on the nonlinearity diagnostic method, developing new procedures for transient temperature analysis.
6. Analysing early time region (ETR) transient temperature data for detecting the wellbore storage regime and verifying the well-test interpretation parameters in nonlinear scenarios (not only in the gas production case, but also in multi-phase production case).
7. Reconstructing flow-rate history from temperature measurements in both linear and nonlinear systems.
8. Estimation of permeability, skin factor and thermal investigation radius by utilizing a simplified analytical relationship between the later-time region transient temperature data and flow-rate.

1.4. Thesis outline

The remaining chapters of this thesis are organized in the following way:

Chapter 2 reviews the related literature and theories, which concern wellbore and reservoir temperature modelling, data processing by wavelet transform method, and the transient temperature and pressure data interpretation.

Chapter 3 establishes a non-isothermal wellbore model for multiphase fluid flow, coupled with a reservoir model to account for transient temperature behaviour at the location of PDGs, and estimates some typical thermodynamic parameters by matching the simulated results with field data.

Chapter 4 firstly studies the relationships among down-hole temperature, pressure and flow-rate data. Next, the flow transients are identified and the outliers are removed by using the processed temperature and pressure data together. The nonlinearity of the reservoir is then diagnosed from processed temperature data, and finally the variable reservoir-well parameters are evaluated.

Chapter 5 presents new procedures for long-term transient temperature data analysis and uses sets of synthetic/field data to verify the effectiveness of the developed algorithms, which include wellbore storage detection, flow-rate history reconstruction and formation parameters estimation.

Chapter 6 summarizes this study, presents the major results, and gives recommendations for future work.

Chapter 2 Literature Review

2.1. Introduction

This chapter provides a brief overview of the literature related to the current research and the theories utilized. This study focuses on wellbore and reservoir temperature modelling, followed by integrated processing and interpretation of the simulated/real down-hole data by the wavelet transform method, and finally the transient temperature data are analysed for field application. The reviewed area of the literature specifically addresses the following areas:

Section 2.2 introduces and assesses the existing non-isothermal wellbore-reservoir models for simulating the distributed and transient temperature behaviour.

Section 2.3 briefly describes the theory of wavelet transform. The selection of the initial wavelet and the problems related to PDG pressure and temperature data processing are also discussed in this section.

Section 2.4 analyses the reasons for temperature change, and reviews the history of transient/distributed temperature and pressure data interpretation.

2.2. Coupled non-isothermal wellbore-reservoir models for simulating the distributed and transient temperature behaviour

Several authors have studied the thermodynamic flow through porous media, as well as the modelling of the wellbore temperature distribution and heat transfer between wellbore and formation, which requires a numerical fully coupled wellbore-reservoir model. In this section, the wellbore and reservoir temperature simulation will be reviewed separately.

2.2.1 Literature review of wellbore temperature simulation

Analytical approaches

The first analytical model for temperature prediction was developed by Ramey (1962) for an injection well. His model predicts wellbore fluid temperature as a function of depth

for injection wells. He also expanded this model to give the rate of heat loss from well to formation, by assuming steady-state heat flow in the wellbore and unsteady radial conduction to the formation. Despite his assumption of ignoring the early temperature changes (T tubing = T injection), for the first time, Ramey (1962) established an equation for wellbore temperature prediction, and his approach seems to work remarkably well. Heat transferred from the injected fluid to the formation can be represented by the following equations:

For liquid, $T_l(z,t) = az + b - aA + (T_0 + aA - b)e^{-z/A}$

For gas, $T_g(z,t) = az + b - A\left(a + \frac{1}{778c}\right) + [T_0 - b + A(a + \frac{1}{778c})]e^{-z/A}$

For long time, the time function, $f_{(t)} = \ln\frac{r_2'}{2\sqrt{at}} - 0.290$,

where A=$\frac{Wc[k+r_1Uf(t)]}{2\pi r_1 Uk}$, a - geothermal gradient, b - surface temperature, c - specific heat at constant pressure of fluid, k - thermal conductivity of formation, U - overall heat transfer coefficient, W - fluid injection rate, z - well depth, r_1- inside radius of tubing r_2- outside radius of casing and T_0- injected fluid temperature.

Based on Ramey's work, Horne and Shinohara (1979) determined the heat loss rate, q, as a function of flow-rate and reservoir properties. Moreover, their model succeeded in predicting temperature profiles (temperature of fluid in tubing, T_1) by giving entry temperature (T_0) and flow-rate (W). However, they only presented single-phase heat transfer equations for both production and injection wells.

Injection: $q = -Wc\left[az - (T_0 + aA - b)\left(1 - e^{\frac{-z}{A}}\right)\right] = Wc(T_0 - T_1)$

Production: $q = aWc[z + A(e^{\frac{-z}{A}} - 1)]$

In 1990, Wu and Pruess (1990) presented an analytical solution for wellbore heat transmission in a layered formation with different reservoir thermal properties, without introducing the assumptions by Ramey. Although they demonstrated that Ramey's method can result in large errors at an early time, they did not present any exact conditions in their paper. Hagoort (2004) then revisited Ramey's method, with the purpose of

assessing the approximations Ramey made. In Hagoort's work, the overestimation of temperature in the early transient period was demonstrated, and a graphical correlation was presented for the purpose of estimating the length of the early transient period.

Recently, a relatively new analytical model for calculating wellbore temperature distribution was published by Spindler (2011). In that paper, he not only developed an analytical transient model for either initial or boundary conditions, but also extended this model to include the heat conduction effect. In addition, he compared the solution without heat conduction with the one which included heat conduction.

Numerical models – coupled wellbore temperature and pressure models

Despite the advantages of fast calculation speed and explicit expression, an analytical approach usually requires items to be ignored in order to simplify complex scenarios. For that reason, an analytical model is too simple to accurately account for transient flow, multiphase flow and spatial variability of properties. Alternatively, the numerical method can be used through discretizing the segments along the wellbore and optimizing fluid PVT properties. Numerical models are categorized into black-oil models and compositional models according to the different treatments of fluid PVT properties. For black-oil models, fluid properties are regarded as a function of pressure and temperature; while for compositional models, more accurate fluid properties can be generated based on the utilization of the equation of state (EOS), as a mixture of in-situ components.

Compositional numerical wellbore thermal flow models have been developed by Stone and Bennett (2002) and Pourafshary et al. (2008). However, the first of these does not include slippage effects between phases, which is an important phenomenon in multiphase flow, and the model developed by Pourafshary does not consider transient effects in either mass or energy conservation equations.

For correctly simulating multi-phase flow, drift-flux models were first developed by Zuber and Findlay (1965) and Wallis (1969). These consider the gas-liquid mixture as a whole, rather than different phases separately. Hasan et al. (2007) presented a wellbore two-phase flow model through the application of the drift-flux approach to various kinds of well orientation, fluids and geometry. Another numerical model, built by Livescu et al. (2009) also used a drift-flux model which is relatively simple, continuous and

differentiable, to capture the slippage effects between phases. They included an accumulation term to model transient effects, but the effect of fluid viscosity which is vital in high flow-rate scenarios was neglected.

Yoshioka et al. (2005) developed a horizontal wellbore model for steady-state multiphase flow which counted in the Joule-Thomson and frictional heating effects. Although it is difficult to calculate production parameters in multiphase flow horizontal wells, Shirdel and Sepehrnoori (2009) developed a non-isothermal simulator to simulate fluid flow without using unrealistic assumptions or neglecting pressure drop in the horizontal sections. But its accuracy is uncertain.

Izgec (2008) coupled wellbore and reservoir systems to calculate transient temperature profiles for both pressure drawdown and build-up periods, and demonstrated that the distribution of wellbore fluid temperature can be obtained on the basis of depth. Although Trina (2012) established a non-isothermal multiphase wellbore model which calculates temperature and pressure profiles separately by integrating two traditional models (flow model and thermal model), it is relatively simple and only suitable for vertical wells. Later, Wang and Horne (2012) summarized previous work and analysed wellbore temperature distribution using non-isothermal multiphase flow simulation, but the configuration they considered was also a vertical well, for which DTS has less advantage over traditional measurement methods.

2.2.2 Literature review of reservoir temperature simulation

Although the study of heat transfer in porous media is crucial in the field of thermal recovery, most of the initial models ignored the minor effects, such as the Joule-Thomson effect and fluid expansion. With the development of computer technology, those simple models have been replaced by commercial simulators such as CMG Star^{TM} and Eclipse 300^{TM}, however the simulation software are complex and time-consuming.

In 1977, Atkinson and Ramey (1977) presented mathematical models for studying heat transfer behaviour in both fractured and non-fractured porous media; they emphasized the importance of the correct heat transfer coefficient but neglected the effects of viscous dissipation and compressibility. Similarly, Meyer (1989) developed another analytical heat transfer model for the combined convection along vertical fractures with conduction

and convection in the reservoir. However, the frictional heating and compressibility effects which may cause the temperature changes were not included in their model.

Maubeuge et al. (1994) proposed an energy equation for simulating the fluid heating or cooling in the reservoir. In this equation, they considered the Joule-Thomson effect as well as the fluid decompression and the frictional heating effects in formation. They also showed how this energy equation can be coupled with the pressure equation in a numerical wellbore model.

Ramazanov and Parshin (2006) presented an analytical model which is able to describe the formation temperature distribution with multi-phase flow. A steady-state convective thermal transport model was solved by using constant flow-rate. After that, Ramazanov and Nagimov (2007) went on to develop another analytical model for calculating the temperature changes in the saturated porous formation (single-phase flow in a homogenous reservoir) with variable bottom-hole pressure. They found that the Joule-Thomson effect can significantly affect the reservoir temperature if the pressure is changing with time. Later, this work was extended by Ramazanov and Valiullin (2010), they described the near wellbore parameters, such as permeability and flow-rate distributions, by analysing the influence of the reservoir geothermal gradient, the fluid Joule-Thomson effect and the adiabatic effect on non-steady state wellbore temperature profiles.

In order to predict the wellbore temperature profiles, Yoshioka et al. (2005, 2006, 2007) developed models which include the often-subtle thermal effects (Joule-Thomson, frictional heating effects, conductive and convective heat transfer) in both reservoir and wellbore. These models coupled the energy balance with mass and momentum balances to simulate temperature and pressure distribution in the reservoir. However, constant flow-rate and steady-state conditions were assumed.

Duru and Horne (2008) established a reservoir temperature transient model for single/multiphase fluids by performing energy, mass and momentum balances, and then estimated several reservoir thermodynamic parameters. This reservoir temperature model will be discussed in detail in Chapter 3.

2.3. Wavelet theory and down-hole data processing

2.3.1 Background of wavelet transform

Mathematically, wavelet transform is a multi-resolution frequency analysis method; it has been widely used for analysing signals which have the characteristic of time-variation, especially in the fields of petroleum engineering and geophysics. In order to overcome the deficiencies in Fourier transform, Morlet et al. (1982) processed the seismic signal by utilizing a wavelet algorithm, which initiated the wide development and application of wavelet transform in the petroleum industry. Gonzalez (1999) applied wavelet transform for de-noising the transient pressure data and concluded that the frequency spectrum of noise in a pressure signal is in the same frequency band as the reservoir signals. In 1998, Kikani and He (1998) first applied the wavelet analysis in PDG pressure data processing. Subsequently, many papers were published on this topic. More details about transient PDG data processing will be reviewed in Section 2.3.4. Soliman and Ansah (2003) provided guidelines on the application of Daubechies wavelet in well testing. The transient pressure data from four fields were analysed to determine wellbore anomalies, faults and other boundary effects, both qualitatively and quantitatively. Guan et al. (2004) reviewed the wavelet analysis methods in the petroleum industry, and discussed various applications, such as reservoir characterization, geological model upscaling, data noise removal and well test data analysis. Based on multiresolution wavelet analysis, Sahni and Horne (2005) came up with an algorithm for integrating transient pressure data with reservoir parameters.

2.3.2 Introduction to the theory of wavelet transform

Wavelet analysis is similar to the very popular Fourier analysis. Both of them are mathematical methods for revealing the information hidden in the signals by transforming the time-domain to the frequency-domain.

However, compared with Fourier transform, which ignores the time-variation frequency contents and averages the information contained in the signal, wavelet transform can analyse the signals by using different windows. For example, a long time window can be used to analyse low-frequency signals and a short time window is suitable for high-frequency signals.

Therefore, compared with Fourier analysis (either Fourier transform or short-time Fourier transform), wavelet transform can provide more accurate results for non-stationary signals with sudden transitions, such as transient down-hole pressure and temperature data. Figure 2-1 shows the comparison among Fourier transform, short-time Fourier transform and wavelet transform.

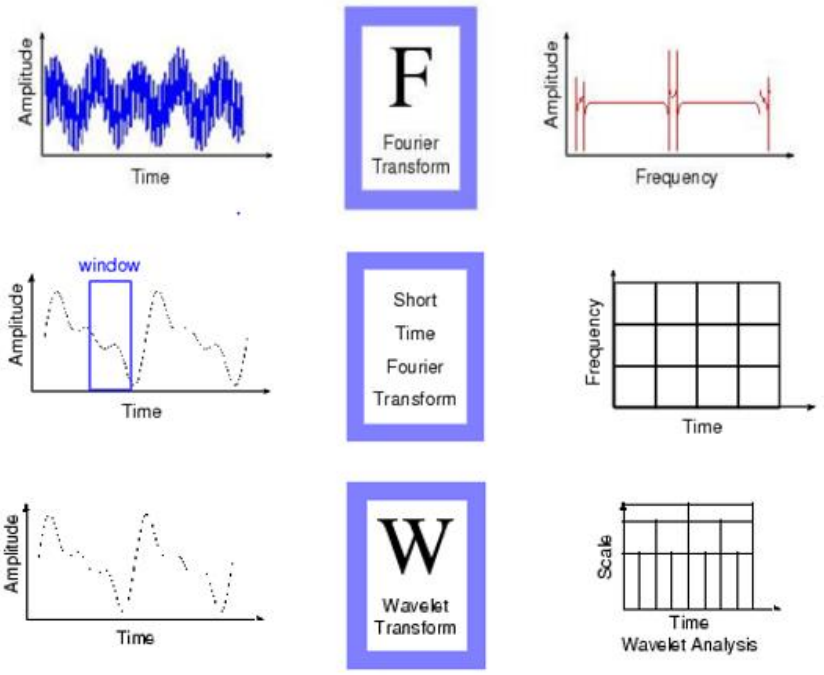

Figure 2-1：Different frequency analysis methods - compared with Fourier transform and short time Fourier transform, wavelet transform can analyse the signal with multi-resolution (source: Matlab/wavelet toolbox user's guide)

The integral wavelet transform of signal $f(t)$ at scale b and position a is defined as:

$$Wf(a,b) = \frac{1}{\sqrt{b}} \int_{-\infty}^{\infty} \psi\left(\frac{t-a}{b}\right) f(t)dt \ ,$$

where ψ is the original wavelet function.

In addition, wavelet transform can be divided into two categories: stationary Continuous Wavelet Transform (CWT) and down-sampled Discrete Wavelet Transform (DWT). CWT has a continuously changing scale parameter, s, and translation parameter, u, in order to perform WT at every scale and every location of the signal. Lots of information is obtained but too much space is occupied. To overcome this drawback, CWT can be performed on some suitable scale parameter, s, instead of on all the scale parameters. By

selecting different scale factors, *s*, the detailed information on different levels can be obtained. DWT performs wavelet transform on a partial scale and position with down sampling. Dyadic wavelet transform, which chooses the scale and position based on powers of two, can reduce the amount of work. The most efficient way to process DWT is the Mallat algorithm, which is a two-channel sub-band coder in signal processing.

In the current study, CWT performing on a particular scale level is utilized. After choosing a scale level, the decomposition process will be iterated and the original signal will be divided with decreasing resolutions, as illustrated in Figure 2-2. The original signal S is decomposed into a detailed signal cD1 and an approximation cA1 at level 1, a detailed signal cD2 and an approximation cA2 at level 2, and a detailed signal cD3 and an approximation cA3 at level 3. Each level of decomposition separates the signal (original and approximation signals) into two components. The WT detailed signals represent the changes between the inputs and local scale signals; the overall characteristics of the original signal are contained in the approximation signals. Figure 2-3 shows the wavelet decomposition on a transient signal at level 3. During this procedure, the original data number reduces to one eighth, due to down-sampling. The influence of scale on transient data interpretation will be discussed in detail in Chapter 4.

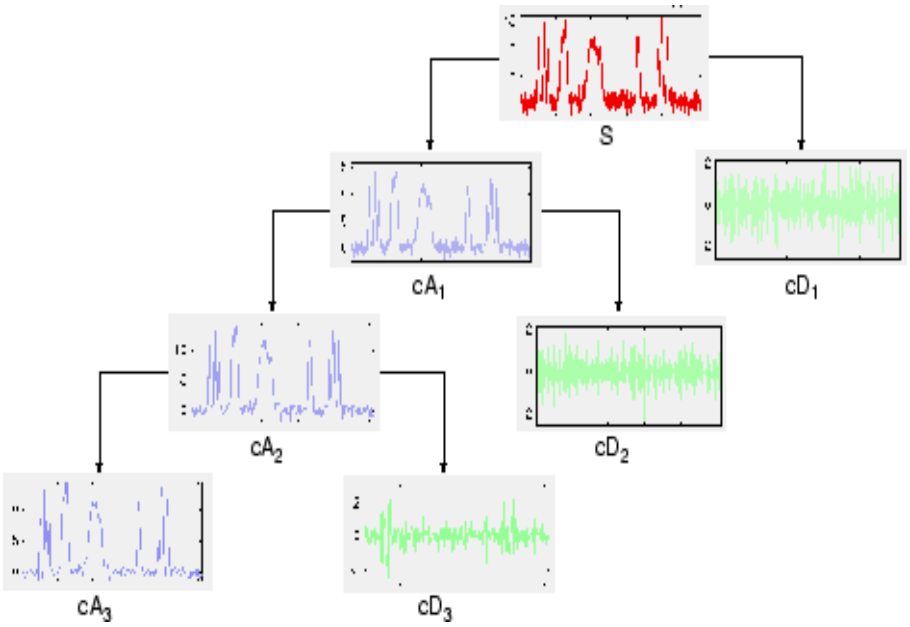

Figure 2-2： Wavelet decomposition tree - The original signal is decomposed into three detailed signals and approximations (source: MathWorks)

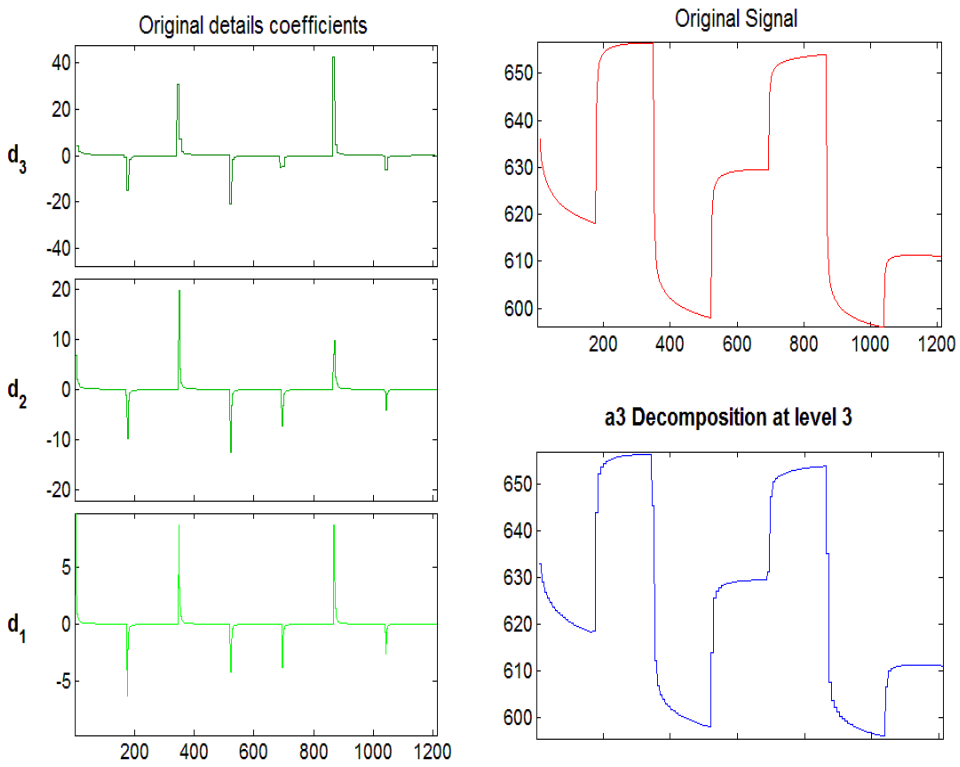

Figure 2-3： The original signal decomposed into several detailed signals, D, and approximations, A

2.3.3 Original wavelet selection

Some commonly-used wavelets and their types are listed below (Matlab wavelet toolbox):

- Haar family wavelets: orthogonal
- Daubechies family wavelets: orthogonal
- Symlets family wavelets: orthogonal
- Coiflets family wavelets : orthogonal
- Meyer family wavelets: with scale function
- DMeyer family wavelets: orthogonal
- Gaussian family wavelets: without scale function
- Mexican_hat family wavelets: without scale function
- Morlet family wavelets: without scale function
- Shannon family wavelets: complex wavelet
- Frequency B-Spline family wavelets: complex wavelet

Figure 2-4 shows the functions of five different original wavelets, and Figure 2-5 demonstrates their performance during the processing of a set of transient data. Although the flow events can be diagnosed from transient data (pressure or temperature) by using each of the wavelets and the locations of the breakpoints look as if they almost coincide in each plot, only the Haar wavelet presents single amplitude of the detail coefficient for every flow event. Furthermore, the wavelet with the smallest support length (Haar wavelet) has the fastest achieved speed which is good for processing PDG transient signals (hundreds of thousands of data points).

Therefore, in this study, the simplest and the most widely used method – the Haar wavelet was selected to process the down-hole transient pressure and temperature data for identification and further interpretation of transient periods.

The Haar sequence was proposed in 1909 by Alfred Haar. It is the most compactly supported wavelet (values of the wavelet function equal to zero, except for a small interval) of all the orthogonal wavelet families. Moreover, its discontinuous characteristic can be regarded as an advantage in analysing the transient pressure and temperature data, because of the existence of sudden transitions.

The original Haar wavelet function $\psi(t)$ is:

$$\psi(t) = \begin{cases} 1 & 0 \le t < 1/2 \\ -1 & 1/2 \le t < 1 \\ 0 & otherwise \end{cases}$$

Its scaling function $\emptyset(t)$ is:

$$\emptyset(t) = \begin{cases} 1 & 0 \le t < 1 \\ 0 & otherwise \end{cases}$$

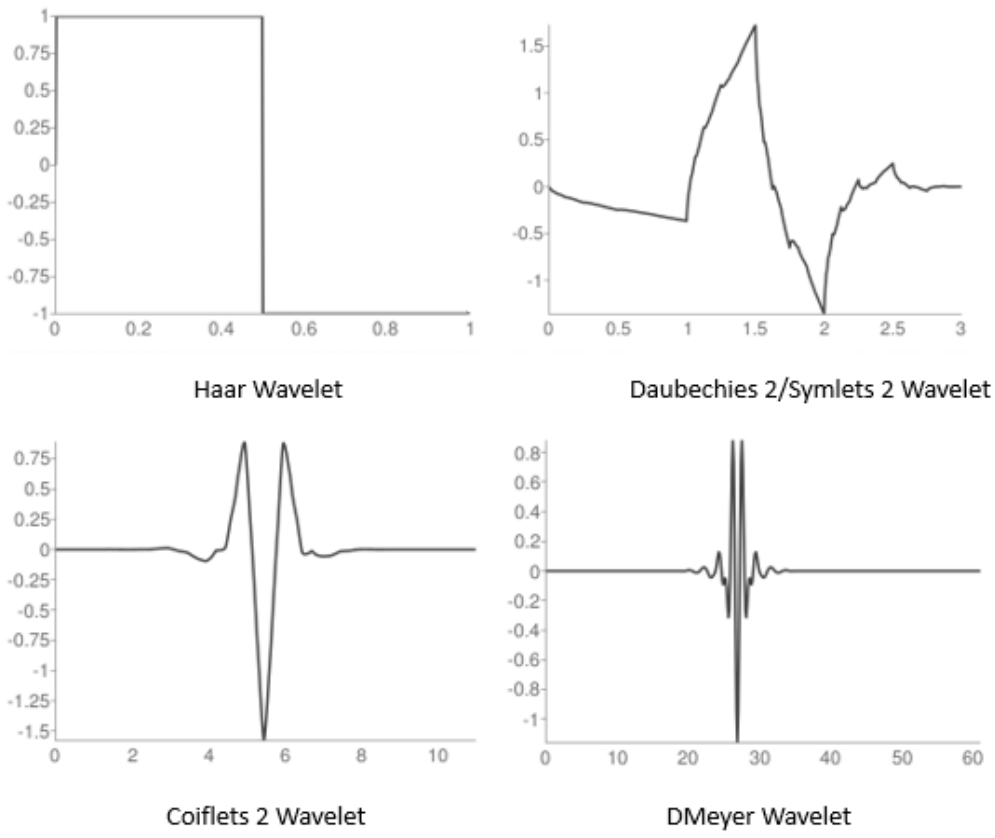

Figure 2-4: Different kinds of original wavelet function ψ

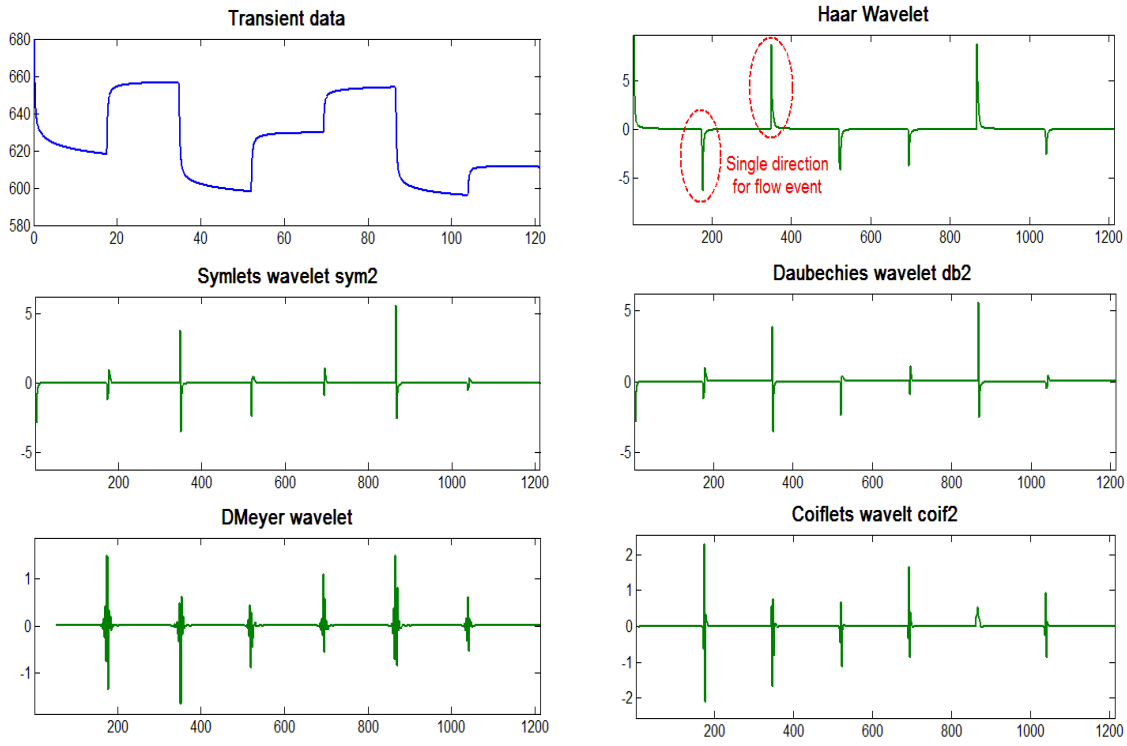

Figure 2-5：Transient data processed with five different original wavelets

2.3.4 Transient PDG data processing

The quality issues such as low resolution, insufficient signal contents and noise for the long term PDG data were first discussed by Veneruso (1992). Subsequently, Gisbergen and Vandeweijer (2001) evaluated the performance of PDGs and analyzed the reliability of the acquired pressure and temperature data. However, they only used a statistical method without considering any physical models.

Other authors emphasize the importance of processing the acquired down-hole data before interpretation. Athichanagorn et al. (1999) presented both wavelet-based data processing and nonlinear regression/moving window-based interpretation procedures. Their seven-step methodology includes outlier removal, de-noising, transient identification, data reduction, flow-rate reconstruction, behavioral filtering, and moving window analysis for time-dependent reservoir parameters.

Olsen and Nordtvedt (2005b) investigated the filtering and compression of real-time production data by means of wavelets, and demonstrated the excellent performance of the spline wavelet for pressure and flow-rate data. This work was then extended to develop two automated module procedures for filter and well testing, separately (Olsen and Nordtvedt, 2005a; Olsen and Nordtvedt, 2006). Li (2009) improved Olsen's work and proposed a new workflow for PDG data processing, but focused mainly on the transient pressure data and ignored the transient temperature data. His procedure includes data preprocessing, outlier removal, flow event detection, identification of BU and DD, data de-noising, data reduction and identifying abnormal events.

Outlier removal, transient identification and noise removal will be reviewed in this section and discussed further in Chapter 4.

Outlier removal

Considering the fact that PDGs and other down-hole gauges collect data in uncontrollable environments, it is common to acquire inaccurate data with outliers due to sensor failure. According to Khong (2001), the outliers can be divided into two types as spike outliers and step outliers. The spike outlier is described as a small amount of data away from the true data, which may be caused by a gauge error; the step outlier is defined as a group of

singularities away from the accurate data, which may be created due to the absence of transient data for period of time and can become serious if interpolation is applied to the original data gap. Athichanagorn et al. (1999) and later Ribeiro (2008) presented a very efficient wavelet-based method that can be used to identify the spike outliers. However, Khong (2001) recommended the use of manual removal to remove the step outliers.

Transient identification

Identifying the exact time of numerous flow events which are contained in the entire PDG pressure and temperature history is critical for further data interpretation. The wavelet modulus maxima method was first presented by Kikani and He (1998) and then improved by Athichanagorn et al. (1999). However, they only processed the transient pressure data and used it for transient identification; in addition, satisfactory results may not be obtained in the circumstances of high noise, where a threshold needs to be set. Considering the limitations of the Spline wavelet algorithm in transient identification, Rai and Horne (2005) proposed another two non-wavelet methods, known as the Savitzky-Golay polynomial smoothing filter algorithm and the Segmentation Method; however, the WT identified false breakpoints for big transients, the fact that they identified the wrong breakpoints was mainly caused by the data problem (but that is not the common cause in practice).

Subsequently, Duru (2011) developed an approach for the combined interpretation of synthetic pressure and temperature data which were generated for the single-phase oil flow. He tested the performance of the Canny algorithm (based on the first derivative of the Gaussian kernel), a second derivative-based algorithm (based on the second derivative of the Gaussian kernel), and a wavelet-based algorithm (based on the Spline wavelet) in transient identification, and concluded that the temperature and pressure data can be constrained by each other.

Noise removal

Noise estimation is crucial for selecting a suitable scale level. Khong (2001) estimated the noise level of transient pressure data by removing the trend from the original data (least square error straight line fit to the interval). This assumption was made as the data varies linearly with time, which is not common in practice. Other researchers (Ribeiro,

2008; Ortiz et al., 2009) used an alternative well-known method (Median Absolute Deviation) to estimate the noise level, where the median is taken over the details at the first decomposition level.

2.4. Transient temperature and pressure data interpretation

2.4.1 Pressure data interpretation

Pressure performance in reservoirs and wellbores has been studied extensively for estimation of reservoir parameters, reservoir description and fluid/wellbore performance evaluation. As mentioned before, PDG pressure data consists of many pressure build-up and draw-down periods. The common interpretation procedure requires transient identification in advance. Theoretically, both build-up and draw-down transient pressure data can be analysed in well testing. However, only build-up pressure data is usable in practice, as the draw-down data can be quite noisy (unknown or unstable flow-rate information). The approaches of transient pressure data interpretation can be summarized as: conventional well test methods (Bourdet et al., 1983), nonlinear regression methods (Earlougher and Kersch, 1972), deconvolution (Schroeter et al., 2001) and decline curve analysis (Unneland, 1998b). More specifically, the conventional well test methods (PTA) which can identify different flow regimes, from the early time wellbore storage effect to the late time boundary effect, may be deduced for temperature transient analysis; the nonlinear regression methods which can estimate the reservoir parameters by minimizing the differences between the measured pressure data and the calculated value (based on the reservoir model) can be used for the history/optimal matching of temperature data. Additionally, Wang and Zheng (2012) defined a nonlinearity diagnostic function, known as Unit Reservoir System Response (URSR), and used it for flow-rate reconstruction. The unit-rate-change coefficient is a relative value without any meaningful information, but the change of it is very useful instead. This nonlinearity diagnostic method may also be extended for transient temperature data interpretation.

2.4.2 Reasons for temperature change

In general, a temperature difference between objects results in heat transfer by conduction, convection and radiation. The temperature in reservoirs and wellbores changes mainly because of the geothermal gradient, frictional heating, injected fluid and Joule-Thomson

effects (Khanlarov, 2012). The combination of these effects creates a characteristic time-dependent thermal profile that can be recorded by DTS and PDG and analysed to give the flow in the wellbore, as well as an estimate of the formation properties.

The geothermal gradient varies from basin to basin. Typical gradients of hydrocarbon-production areas range from 0.6 to 1.6°F per 100 ft of depth increase.

Frictional heating is a warming effect of fluids as a result of friction when fluids are passing through porous media and the wellbore.

The Joule-Thomson effect is a warming or cooling effect of fluids as a result of expansion or compression preceded by pressure change in an adiabatic process (constant enthalpy). The Joule-Thomson coefficient is defined as temperature change per unit pressure at constant enthalpy, as illustrated below:

$$C_j = (\frac{\Delta T}{\Delta P})_H$$

Especially for an ideal gas, the Joule-Thomson coefficient is equal to zero, which means that the temperature of an ideal gas remains constant upon being expanded at constant enthalpy.

Figure 2-6 shows the thermal response of the Joule-Thomson effect on gas and oil flowing radially from a reservoir into a wellbore. Note that the largest cooling (or heating) takes place immediately around the wellbore, where the largest pressure drop also occurs. At the sand-face and near wellbore formation, the Joule-Thomson effect dominates the temperature change, because of the existence of perforation and damage to skin in this area, while away from the wellbore regime, into the reservoir, frictional heating becomes the determining factor.

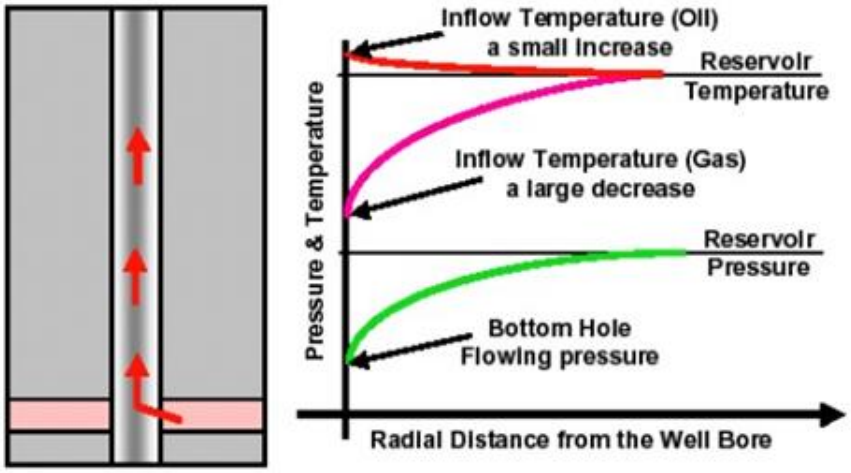

Figure 2-6：Reservoir Joule-Thomson effects (Sanchez et al., 2005)

2.4.3 Temperature data interpretation

In order to monitor the down-hole production and injection conditions as well as to make decisions for well performance optimization, the dynamic temperature data acquired from DTS and PDG have been interpreted both qualitatively and quantitatively in several projects.

Distributed temperature sensors

Nath et al. (2005) used DTS in a steam injection project to identify breakthrough zones and development of steam zones, while Johnson et al. (2006) examined several case histories and demonstrated that DTS transient analysis can be used for understanding oil/gas production/injection rates. Achinivu et al. (2008) developed both a forward model to predict well flowing pressure/temperature and an inversion model to detect water and gas entry (temperature can provide valuable information, especially in gas wells) into a wellbore. They also presented practical guidelines on how to initialize the inversion process and achieve a quick conversion. Later, Wang and Bussear (2011) applied the DTS technology in horizontal wells and illustrated that several benefits can be provided for operators, such as effectiveness of zonal isolation, pumping fluid movement within the target fracture stage during fracturing and the integrity of isolation packers.

Others tried to interpret DTS data quantitatively. Ouyang and Belanger (2006) estimated the flow-rate profile from the temperature profile. They concluded that DTS data can be

used to determine the production profile under certain circumstances, such as single-phase flow; however, under more complicated circumstances, such as multiphase flow or highly deviated wells, additional data may be required to obtain correct flow profiles. Even more can be learned about a well (the location of transverse fractures created from horizontal wells, permeability, skin factor, depths of damage of each layer etc.) when multiple measurements of the temperature profile at different times are available with DTS systems (Tabatabaei et al., 2011). In another study, Brown et al. (2005) used DTS to monitor injection and production in two developing fields. Instead of installing the optical fibre inside the tubing, they installed them on the periphery of the sand-screening shroud. They succeeded in estimating flow-rate even after gas breakthrough, which involved a multiphase flow and changing gas-oil ratio. Then, Brown (2006) further expanded the use of DTS measurement to monitor multilayered reservoir pressures and gas-oil ratio changes. He demonstrated that temperature data can be interpreted not only in terms of flow contribution from stacked multilayered reservoirs, by solving for various reservoir layer properties using a robust flow and thermal model, but also in terms of changes in reservoir layer properties, specifically changes in layer pressures and GORs, during the well's production, if baseline data is first obtained and reservoir parameters are known. A similar mathematical model which can predict and interpret DTS data and other down-hole measurements was built by Tardy et al. (2011), and a field case of matrix acidizing treatment was also presented as an example, in this paper.

Transient temperature - Permanent down-hole gauge

Most of the published articles analyzed the transient temperature data through established reservoir-well models. The research directions of temperature interpretation can be summarized as: using the transient temperature measurements to reconstruct the unknown flow-rate history, identify the features of the producing system (such as water or gas entrance) and determine formation properties.

Fairuzov and Gonzalez (1997) developed a numerical model for analysing two-phase flow and heat transfer in the wellbore during the build-up test. The results demonstrated that the variation of the wellbore fluid temperature with time has only a small effect on the bottom-hole pressure during the build-up test. Elshahawi et al. (1999) developed an approach for explaining anomalous pressure trends and assessing the quality of the test data and test procedures. Additionally, they estimated the down-hole flow-rate from

flowing temperature measurements, continuously measured pressure data and the known fluid composition. Based on their developed numerical model, Yoshioka et al. (2006) and App and Yoshioka (2011) identified the water entry locations from the temperature profile and examined the influence of effective permeability and flow-rate on the temperature profile. As pointed out by Duru (2008) and Duru and Horne (2011), the temperature change is closely related to some typical reservoir parameters and the flow-rate, which provides opportunities to estimate near wellbore characteristics and reconstruct flow-rate history. Two methods for estimating the flow-rate from wellhead pressure and temperature were developed by Izgec et al. (2010). For the entire-wellbore approach, the thermal properties of fluid, tubular and formation are needed, and this approach also relies on modelling. In contrast, the single-point method requires few input parameters and was recommended by the authors. Muradov (2010) presented a method of zone rate allocation based on measured down-hole pressure and temperature data in intelligent wells. This approach appears to be based on steady-state modelling. However, Lorentzen et al. (2010) combined a transient well flow model and the ensemble Kalman filter for individual well flow-rate allocation. They used both high frequency pressure and temperature measurements and focused on the early time period after changing influx conditions. Sui and Zhu (2008) proposed a new testing approach which can determine individual layer properties for multiple layers commingled in a well without the need of highly time-consuming and accurate transient flow rate measurements. After studying the sensitivity of the transient temperature on layer properties (using investigated mechanisms for transient temperature variation), they found that the temperature response is sensitive not just to skin, but to the damage radius and permeability, which cannot be discovered from pressure and rate measurements. The formation fluid temperature variation mechanisms are listed below. The transient temperature change (Term 1) is a consequence of six effects. Term 2 stands for the transient formation fluid expansion or compression, Term 3 represents the expansion or compression of rock (safe to ignore), Term 4 is heat convection, the combination of Term 5 and Term 6 comprises the Joule-Thomson effect, and Term 7 is heat conduction.

$$\underbrace{\overline{\rho C_p}\frac{\partial T}{\partial t}}_{\text{Term 1}} - \underbrace{\emptyset\beta T\frac{\partial p}{\partial t}}_{\text{Term 2}} - \underbrace{\emptyset C_{rc}(p+\rho_r C_r T)\frac{\partial p}{\partial t}}_{\text{Term 3}} = \underbrace{-\rho\vec{v}C_p\vec{\nabla}T}_{\text{Term 4}} + \underbrace{\beta T\vec{v}\vec{\nabla}p}_{\text{Term 5}} \underbrace{-\vec{v}\vec{\nabla}p}_{\text{Term 6}} + \underbrace{k_e\Delta T}_{\text{Term 7}}$$

where v - fluid velocity, β - fluid thermal expansion coefficient, $\emptyset$ - porosity, C_p - heat capacity, $\overline{\rho C_p}$ - average formation property of fluid and rock, C_{rc} - compressibility of rock, C_r - specific heat capacity of the rock, k_e - thermal conductivity of the formation.

Fewer papers have talked about developing approaches for interpreting transient temperature measurements directly. Kragas et al. (2004) analysed the real time down-hole temperature and pressure data acquired from fibre-optic gauges and demonstrated the possibility of detecting perforation and other well activities by the temperature and pressure changes. Bahrami and Siavoshi (2007) presented field cases with the observed temperature increase at the beginning of a pressure build-up. In their opinions, when the gas well is shut-in, the Joule-Thomson cooling effect vanishes causing a sharp increase in sandface temperature, and then the wellbore temperature gradually cools down due to heat conduction with the near wellbore regime. So transient temperature data can be used as a fast and reliable diagnostic tool in gas well test analysis. App (2009) emphasized the importance of paying special attention to early time temperature behaviour, because well bottom-hole temperature profiles often indicate a temperature change immediately after a rate change. This thermal behaviour depends on the rate of compression or expansion of the reservoir/wellbore fluid. An increase in rate represents an expansion process that results in a temperature reduction and a decrease in rate, such as a pressure build-up, represents a compression process that results in a temperature increase. Although Slider's method was initially used for analysing transient pressure data, Kutasov and Eppelbaum (2007) and Eppelbaum and Kutasov (2006) extended it for transient temperature well tests. They also described an approach for determining the formation thermal conductivity, skin factor and contact thermal resistance for boreholes where the temperature recovery process after drilling operations is not completed. Wu et al. (2013) examined the Joule-Thomson effect, which caused down-hole transient temperature change, and inferred the true reservoir temperature from the gauge measured data. An analytical solution of the temperature data and the PI (productivity index) was then presented. Based on this relationship, several useful surveillance studies, such as monitoring the skin change of the well and the impact of reservoir compaction during the depletion were conducted.

2.5. Chapter summary

In this chapter, the literature and theories related to the study of wellbore/reservoir temperature modelling, down-hole data processing and the transient temperature/pressure data interpreting have been reviewed. The main conclusions are:

1. Although there are articles that describe heat flow modelling, there is still a lack of a coupled wellbore-reservoir model which is capable of simulating comprehensive compositional and thermal phenomena.
2. As a multi-resolution frequency analysis method, the (continuous) wavelet transform is suitable for processing the transient pressure and temperature data which can be regarded as non-stationary signals. Particularly, the Haar wavelet is selected as the initial wavelet, and it can effectively identify transient periods among PDG data.
3. Several effective methods and algorithms associated with pressure data processing have been applied in practice, but temperature data processing is rarely discussed and more research work needs to be done.
4. Compared with the pressure transient analysis, the temperature transient analysis is not well utilized. Even though some measured dynamic temperature data have been interpreted for flow profile prediction and reservoir characterization, almost all of these approaches still rely on established non-isothermal models, which depend on thermodynamic parameters.

Chapter 3 A Non-isothermal Wellbore Model with Complex Structure and Its Application in Well Testing

3.1. Introduction

Although the wellbore is in a non-isothermal environment, heat transfer between the fluid in wellbore and the formation is often ignored and temperature is usually assumed constant in the data interpretation which will lead to misunderstanding of the pressure profile. In this chapter, a non-isothermal wellbore model that is capable of predicting the temperature, pressure, flow-rate and liquid fraction profiles under multi-rate and multiphase production scenarios is established. This numerical wellbore model was used to calculate temperature and pressure separately and iterate until the estimated and calculated values converge. After that, this model was compared with two other published heat transfer models to verify its reliability and coupled with a reservoir model to simulate the temperature at gauge location. Finally, based on the coupled wellbore-reservoir model, the transient temperature behaviour during flowing and shut-down periods was extracted for well testing analysis, and some typical thermodynamic parameters were also estimated by utilizing sets of field data.

This chapter provides a way to not only integrate pressure data, and determine the flow-rate profile more accurately, but also estimate typical reservoir and fluid parameters such as porosity, permeability, viscosity, and Joule-Thomson coefficient by matching the simulated results with the real transient temperature data measured by PDGs. In addition, the transient temperature data may also be used as a fast and reliable diagnostic tool in well testing analysis to detect the end of wellbore storage.

3.2. Solution procedure of the non-isothermal wellbore model

The non-isothermal wellbore model represented in this chapter is capable of predicting the temperature, pressure and flow-rate profiles under multi-rate and multiphase production scenarios. This numerical wellbore model calculates temperature and pressure from bottom-hole (reservoir inflow point) to well head (or gauge location) separately and iterates until the estimated and calculated values converge (Trina, 2012). It should be noted that the wellbore section is assumed to be sealed from the reservoir, and there is no

fluid entry along the wellbore section, with the aim of accounting for phase changes and flow conditions.

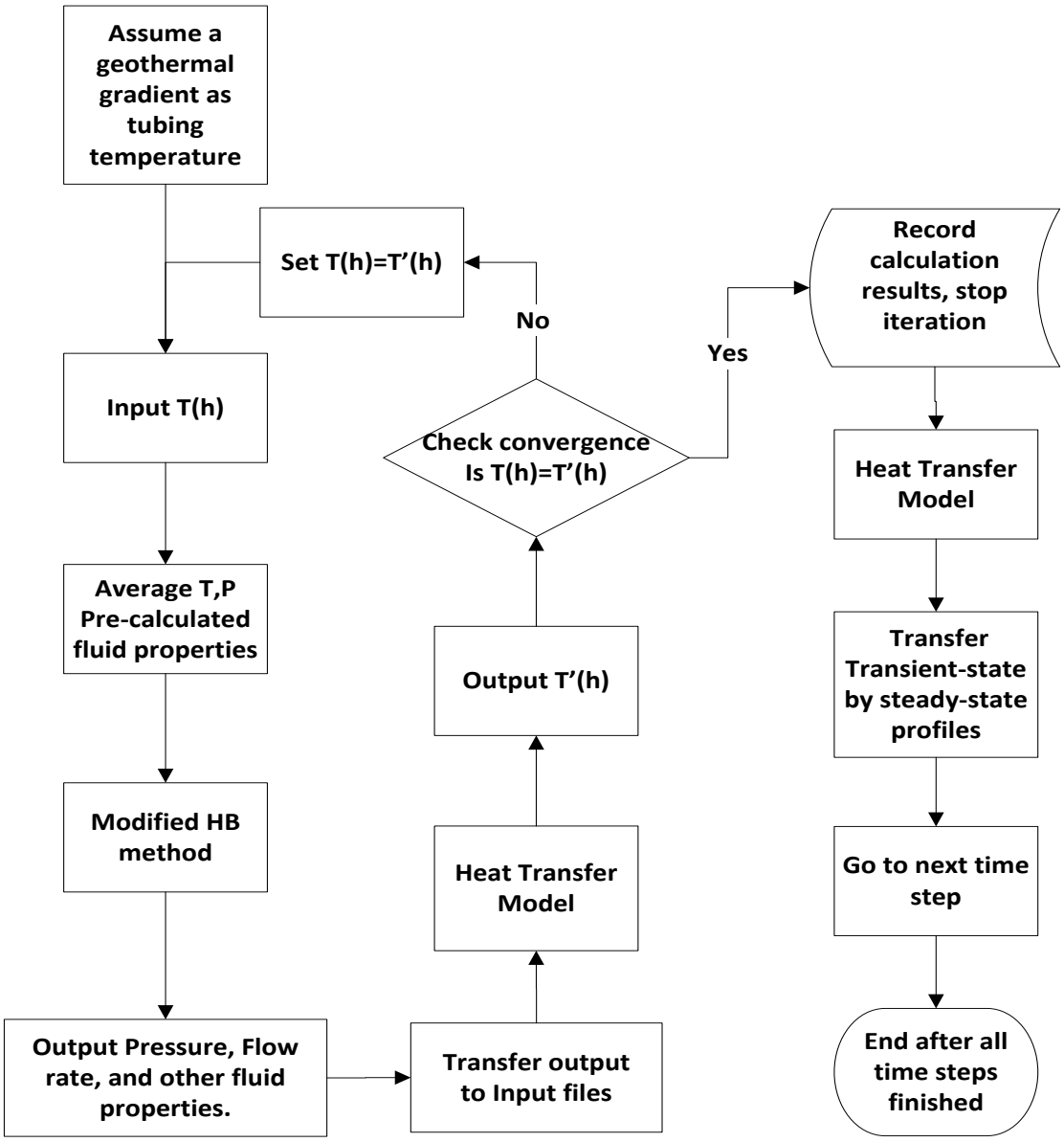

Figure 3-1：Numerical solution method for a non-isothermal wellbore model

As illustrated in the processing flowchart of Figure 3-1, first of all, we need to assume a geothermal gradient, set the time step, as well as inputting other wellbore/formation properties; the Hagedorn and Brown (1965) model, which will be introduced in detail in Section 3.4, is then modified and recoded to calculate pressure, flow-rate and liquid fraction profiles, after which this pressure calculation model is coupled with a heat transfer model to calculate the temperature profile; finally, the program will check the convergence of temperature profiles and continue to calculate for other time steps by

using the steady-state temperature and pressure profiles to replace the items in transient-state temperature calculation equations. Since the pressure model and temperature model calculate different parameters and are not run simultaneously, the fluid parameters can be amended by iteration, and the problem of having to input either the exact pressure or temperature profiles in advance is thus solved. Particularly, the differential equations for fluid temperature calculation are solved numerically in Matlab^{TM}, rather than through any analytical solution.

3.3. Heat transfer model

It is imperative to calculate the wellbore temperature profile so that the accurate pressure profile and then the operation conditions of the well can be determined. Additionally, fluid flowing in the wellbore heats up/cools down surrounding rock over time. In this section, two published temperature profile calculation methods and the temperature governing equations used in current thesis are described.

Ramey's method

Nearly all practical wellbore temperature profile calculation methods are based on the work of Ramey (1962). In the original article, Ramey presented an analytical equation for wellbore temperature, based on a simplified heat balance. As he pointed out in that work, the fluid temperature can be expressed as a function of depth. In the following equations, g is gravity acceleration, $g_c$is a conversion factor, C_j is the J-T coefficient, C_p is the heat capacity of the fluid, w is the mass rate, α is an angle of well inclination and Q_c represents the heat transfer rate. In particular, z and L represent variable well depth from surface and tubing length respectively, in these two published temperature profile calculation methods.

$$\frac{\partial T_f}{\partial z} = C_j \frac{\partial p}{\partial z} + \frac{1}{C_p}\left[\frac{Q_c}{w} - \frac{g sin\alpha}{g_c} - \frac{v}{g_c}\frac{\partial v}{\partial z}\right] \tag{3.1}$$

After assuming steady-state flow of an incompressible single phase fluid and dropping the kinetic energy term. The final form for a producing well is:

$$\frac{\partial T_f}{\partial z} = \frac{1}{A}\left[T_f - [T_{ei} - (L-z)g sin\alpha]\right] \tag{3.2}$$

After applying the boundary conditions

$$T_f = T_{ei} - gsin\alpha[(L-z) - (1 - exp(\tfrac{(z-L)}{A}))A] \quad , \tag{3.3}$$

where $T_{ei}$is the undisturbed earth or formation temperature, *A* is the inverse of parameter L_R, which will be described in detail in Eq. 3.12.

Izgec's method

Izgec's model is a modification of Ramey's model to account for heat transfer at both draw-down period and build-up period. He integrated the difference between loss in enthalpy and static head; and showed that the energy balance equation for fluid temperature in time as a linear differential equation can be written as:

$$\frac{\partial T_f}{\partial t} = \frac{wC_pL_R}{mC_p(1+C_T)}\left(T_{ei} - T_f\right) + \frac{wC_p}{mC_p(1+C_T)}[\frac{\partial T_f}{\partial z} + \frac{1}{C_p\rho} - \frac{gsin\alpha}{C_p}] \, , \tag{3.4}$$

where C_T is a dimensionless parameter with respect to thermal storage, m is the mass of fluid.

For the draw-down period, the analytic fluid-temperature model during production for every well segment, as a function of time, is given by

$$T_f = T_{ei} + \frac{1-e^{aL_Rt}}{L_R}[1 - e^{(z-L)L_R}](gsin\alpha + \frac{gsin\alpha}{C_pJg_c} + \frac{1}{C_p\rho}) \, , \tag{3.5}$$

where a is a defined lumped variable ($a = \frac{wC_p}{mC_p(1+C_T)}$) and J is the productivity index.

For the build-up period, the flow-rate is zero and heat transfer in the wellbore is only by conduction into the formation. So the distribution of temperature in a wellbore can be obtained, as a function of depth, by

$$T_f(r,t) = T_{ei} + \frac{1-e^{aL_Rt}}{L_R}\left[1 - e^{(z-L)L_R}\right]\left(gsin\alpha + \frac{1}{C_p\rho} - \frac{gsin\alpha}{C_pJg_c}\right) + e^{(z-L)L_R}(T_{fbh} - T_{ebh}) \tag{3.6}$$

Current model

The thermodynamic behaviour of the flowing fluid is one of the dominant factors that affect multiphase flow in the wellbore. In addition, permanent down-hole monitoring tools are usually installed several hundred feet above the perforation/pay zones, so the heat transfer along the distance, which will lead to misunderstanding of the pressure profile, should not be ignored. In order to study the principle of temperature well testing, we firstly need to figure out the temperature changes along the wellbore: heat transfer occurs by convection in the fluid and by conduction between wellbore and formation.

Based on the above wellbore structures shown in Figure 3-2, the following conditions are assumed for the wellbore:

- Oil and gas are well mixed flowing in the tubing and production casing;
- Heat transfer through the wellbore is in steady state;
- Heat transfer from the wellbore to the formation is only in the radial direction;
- Kinetic energy is neglected in the fluid flow process.

For the purpose of modelling the temperature distribution along a wellbore, energy conservation was considered with inflow heat equal to outflow heat (convective energy transport) plus conductive heat loss to/from formation. The well is assumed to be inclined at an angle θ with respect to the horizontal, as illustrated below in Figure 3-3.

The heat transfer coefficient depends on the cross-section profile of the wellbore, as shown in Figure 3-2. Its value can be calculated according to the different structures. If the production casing and surface casing are around the tubing (upper part), the overall heat transfer coefficient from inside of production casing is (Cui, 2012):

$$U_{pci} = [\frac{R_{pci}}{k_{pc}} ln\left(\frac{R_{pco}}{R_{pci}}\right) + \frac{R_{pci}}{k_{mud}} ln\left(\frac{R_{sci}}{R_{pco}}\right) + \frac{R_{pci}}{k_{cem}} ln\left(\frac{R_h}{R_{sco}}\right) + \frac{R_{pci}}{k_{cas}} ln\left(\frac{R_{sco}}{R_{sci}}\right) + \frac{R_{pci}}{k_e} ln\left(\frac{R_e}{R_h}\right)]^{-1} \quad 3.7$$

where $k_{subscripts}$ represent the thermal conductivity coefficients and $R_{subscripts}$ represent different radius.

Otherwise, when there is only the production casing surrounding the tubing for the lower part of the drill-hole, the overall heat transfer coefficient from inside of the production casing is:

$$U_{pci} = [\frac{R_{pci}}{k_{pc}} ln\left(\frac{R_{pco}}{R_{pci}}\right) + \frac{R_{pci}}{k_{mud}} ln\left(\frac{R_h}{R_{pco}}\right) + \frac{R_{pci}}{k_e} ln\left(\frac{R_e}{R_h}\right)]^{-1}$$

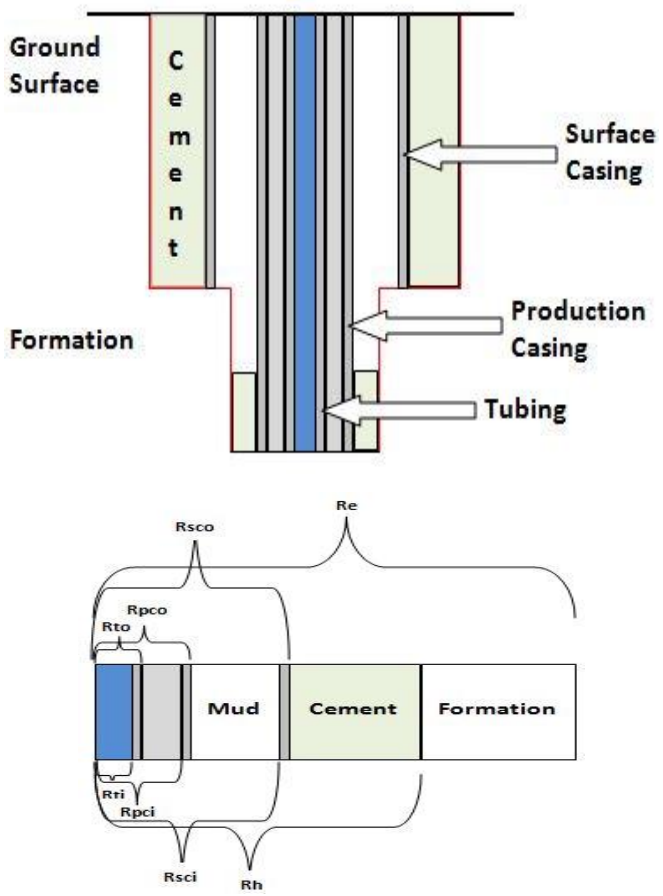

Figure 3-2：Complex wellbore structure - different overall heat transfer coefficients need to be assigned respectively

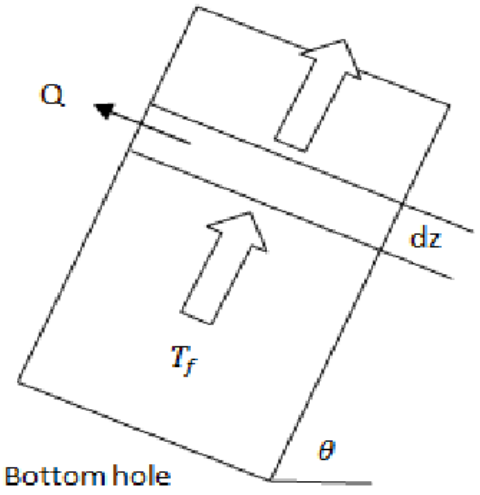

Figure 3-3：Energy conservation for a control volume of unit length in the wellbore

The energy equation in terms of enthalpy, H, is:

$$\rho v \frac{d}{dz}\left(H + gz + \frac{1}{2}v^2\right) = \frac{d}{dz}\left(k\frac{dT}{dz}\right) + \frac{Q}{\pi {R_{pci}}^2} \tag{3.8}$$

For fluids with no phase change, the enthalpy is a function of pressure and temperature, and can be expressed as:

$$dH = C_p dT - C_p C_j dp \tag{3.9}$$

Ignoring the heat conduction along the well, kinetic energy ($\frac{vdv}{C_p dz}$), and also the inertial term ($-\rho v\frac{dv}{dz}$), the energy balance equation and momentum equation are (Michel and Civan, 2008):

$$\frac{dT_f}{dz} = \frac{Q}{C_p W_t} + C_j\frac{dp}{dz} - \frac{g}{C_p}sin\theta \tag{3.10}$$

$\frac{dp}{dz} = -\frac{f_F {W_t}^2}{\pi^2 {R_{pci}}^5}\frac{1}{\rho} - \rho g sin\theta$, or it can be calculated by another pressure model.

where W_t is the mass rate, f_F is the fanning friction factor (Chen, 1979) with respect to all kinds of relative tubing roughness ($\frac{k}{D}$) and Reynolds number ($\mathrm{R_e} = \frac{\rho \mathrm{v} \mathrm{D}}{\mu}$). $\frac{1}{\sqrt{f_F}} = -4\log\{0.2698\left(\frac{k}{D}\right) - \frac{5.0452}{R_e} log\left[0.3539\left(\frac{k}{D}\right)^{1.1098} + \frac{5.8506}{{R_e}^{0.8981}}\right]\}$

The heat is transferred by conduction between fluid and formation. From the point where the fluid contacts the wellbore, the segments of material through which heat exchange occurs are shown in Figure 3-2. The heat flow of unit length from/to formation can be expressed as:

$$Q = [-\frac{2\pi R_{pci} U_{pci} k_e}{W_t C_p\left(k_e + f(t) R_{pci} U_{pci}\right)} T_f + \frac{2\pi R_{pci} U_{pci} k_e}{W_t C_p\left(k_e + f(t) R_{pci} U_{pci}\right)} T_e] W_t C_p \qquad 3.11$$

As shown in Eq. 3.11, the steady-state formation temperature (at large times) is required for calculating the steady-state fluid temperature profile. Substituting Eq. 3.11 into 3.10, the wellbore temperature profile during steady-state flow can be defined as:

$$\frac{dT_f}{dz} = \frac{2\pi R_{pci} U_{pci} k_e}{W_t C_p\left(k_e + f(t) R_{pci} U_{pci}\right)}\left(T_{ebh} - k_g z sin\theta - T_f\right) - C_j(\frac{f_F {W_t}^2}{\pi^2 {R_{pci}}^5}\frac{1}{\rho} + \rho g sin\theta) - \frac{g}{C_p} sin\theta \qquad 3.12$$

where k_g is the geothermal gradient, T_{ebh} is the formation temperature at bottom-hole, z is the length of wellbore segments from bottom, $f(t)$ is a dimensionless function with respect to time and thermal conduction conditions, $f(t) = ln[e^{0.2 t_D} + (1.5 - 0.3719 e^{-t_D})]\sqrt{t_D}$, $t_D = \frac{k_e t}{R^2}$.

The relaxation parameter L_R is set as:

$L_R = \frac{2\pi}{W_t C_p}\left[\frac{r_{pci} U_{pci} k_e}{k_e + r_{pci} U_{pci} f(t)}\right]$, w_t stands for the mass flux effect and can be neglected for a shut-in well.

$$\frac{dT_f}{dz} = L_R\left(T_{ebh} - k_g z sin\theta - T_f\right) - C_j(\frac{f_F {W_t}^2}{\pi^2 {R_{pci}}^5}\frac{1}{\rho} + \rho g sin\theta) - \frac{g}{C_p} sin\theta \qquad 3.13$$

with boundary conditions: $z = z_1 = 0, P = P_{bh}, T_e = T_{ebh}$, $T_f = T_{fbh}$ (solution of the reservoir model). Node: $z_1 < z_2 < \cdots < z_{bh}$, Step: $\Delta z = z_i - z_{i-1}$. This Ordinary

Differential Equation (ODE) can be solved by a modified Euler method. Consequently, the overall heat transfer coefficient U varies with depth change and the relaxation parameter L_R is depth-varying. Other parameters in Eq. 3.13 are either treated as inputs of the fluid properties or can be determined from the pressure/flow-rate profile calculation model which will be described later. Then, the accurate wellbore temperature profile at specific time can be calculated without the assumption of the constant L_R.

The temperature rise of the cement and tubular material may be taken to be a fraction of the rise in the fluid temperature at any time (Hasan and Kabir, 2005). Ignoring the kinetic energy term $\frac{v}{C_P}\frac{dv}{dz}$, the final form of the energy balance equation for fluid temperature in time as a linear differential equation can be written as (Izgec, 2008):

$$\frac{dT_f}{dt} = \frac{W_t C_P L_R}{mC_P(1+C_T)}\left(T_e - T_f\right) + \frac{W_t C_P}{mC_P(1+C_T)}\left(\frac{dT_f}{dz} + C_j\frac{dp}{dz} - \frac{g}{C_p}sin\theta\right) \tag{3.14}$$

Using the steady-state profiles to replace the items for transient-state profiles, the energy balance equation for fluid temperature in time as a linear differential equation can be rewritten as:

$$\frac{dT_f}{dt} = \frac{2W_t C_P L_R}{mC_p(1+C_T)}\left(T_e - T_f\right) - \frac{\mathrm{W}C_P}{mC_P(1+C_T)}\left[2C_j\left(\frac{f_F {W_t}^2}{\pi^2 {R_{pci}}^5}\frac{1}{\rho} + \rho g sin\theta\right) + \frac{2g}{C_p}sin\theta\right] \tag{3.15}$$

$$\frac{dT_f}{dt} = \frac{2W_t C_P}{mC_P(1+C_T)}\left[L_R\left(T_e - T_f\right) + C_j\frac{dp}{dz} - \frac{g}{C_p}sin\theta\right], \tag{3.16}$$

For a production well, the initial condition is set as: $t = 0, T_f = T_e$.

For a shut-in well with after-flow effect, the initial condition is set as: $t = 0, T_f = T_{fp}$, where T_{fp} is the last fluid temperature calculated for the production well.

Apart from giving the analytical solution (using the method of integrating factors), the differential Equation. 3.16 can also be solved numerically in Matlab™ (solver function: ode45).

3.4 Pressure and flow-rate profile calculation model

The Hagedorn-Brown Correlation is one of the most successful wellbore pressure drop calculation methods for multiphase steady-state flow. This correlation includes the effects of gas slippage and was generated by analysing a wide range of experimental/test data, such as liquid rates, gas-liquid ratios, tubing sizes, and different fluid properties, obtained from a vertical well.

Although the Hagedorn-Brown method was developed for vertical wells, in this paper a modification is made so that it suits inclined flow and even applies to horizontal wells. The fluid properties are also treated as a function of pressure and temperature rather than constants. In addition, the Hagedorn-Brown Correlation was found to be effective for slug flow prediction in oil wells, but based on other existing correlations and assumptions, different flow regimes such as bubble flow are taken into account.

Traditional Hagedorn and Brown Correlation

Generally speaking, hydrostatics and friction (ignoring the kinetic component) are the main factors that will cause pressure drop of fluid flow in wellbore. So the overall pressure drop equation is the sum of two terms:

$$\Delta P_{total} = \Delta P_{hydro} + \Delta P_{frictional} \tag{3.17}$$

As described by Hagedorn and Brown, the simplified pressure drop equation can be written as：

$$144\frac{\Delta p}{\Delta h} = \frac{g}{g_c}\left[\rho_L H_L + \rho_g(1-H_L)\right]\{1 + \frac{f{v_m}^2}{2g_c D} + \Delta\frac{[\frac{{v_m}^2}{2g}]}{\Delta h}\} \tag{3.18}$$

where H_L = liquid hold-up, Δh = depth increment, D = pipe diameter, f = Moody friction factor, $g_c$is a conversion factor, $v_m = \text{superficial velocities} = v_{sg} + v_{sl}$

A set of pre-calculations (fluid parameters such as $R_s, B_o, \mu_o, \sigma_o$) need to be performed and these can be evaluated by interpolating from data generated in PVTi^{TM}. Then the mixture liquid phase (oil and water) viscosity and the surface tension are expressed as:

$$\mu_L = \mu_o\left(\frac{1}{1+WOR}\right) + \mu_w\left(\frac{WOR}{1+WOR}\right);\quad \sigma_L = \sigma_o\left(\frac{1}{1+WOR}\right) + \sigma_w\left(\frac{WOR}{1+WOR}\right),$$

where *WOR* is the water-oil ratio.

The hold-up factor can be correlated with fluid and wellbore properties, which were defined as four dimensionless parameters (liquid velocity number, gas velocity number, pipe diameter number and liquid viscosity number):

$$N_{LV} = v_{sl}\sqrt[4]{\rho_L/g\sigma_L};\quad N_{GV} = v_{sg}\sqrt[4]{\rho_L/g\sigma_L};\quad N_D = D\sqrt{\rho_L g/\sigma_L};\quad N_L = \mu_L\sqrt[4]{g/\rho_L{\sigma_L}^3}$$

Several graphs were then utilized to calculate the hold-up correlation function. The graph of CN_L vs N_L gives CN_L and the graph of $H_L$vs $X_{HL}(X_{HL} = \frac{N_{LV}}{{N_{GV}}^{0.575}}(\frac{\bar{P}}{P})^{0.1}\frac{CN_L}{N_D})$ gives the hold-up factor. For programming, these graphs were converted into equations through Matlab™ curve fitting tool. Finally, the in-situ H_L can be calculated.

The incremental depth can be solved by rearranging momentum balance equation as:

$$\Delta h = \frac{144\Delta p - \overline{\rho_m}\Delta(\frac{v_m}{2g_c})^2}{\overline{\rho_m} + \frac{f{W_t}^2}{2.9652*10^{11}\overline{\rho_m}D^5}} \qquad 3.19$$

As can be seen from the calculations, this method calculates the pressure, flow-rate and liquid hold-up profiles of the well.

Modifications

Several modifications have been made based on the original HB method. Figure 3-4 shows the processing flowchart of the pressure model used in this study. This calculation schematic is suitable for either multi-phase or single phase flow.

Firstly, the hydrostatic pressure losses are related to the fluid mixture density and the height of the fluid column; the frictional losses are connected with flow regimes and compositional fluid properties along the wellbore. Thus, in this model, the hydrostatic pressure drop is calculated by using only the vertical depth of the tubing segment and the friction pressure loss is calculated based on the entire wellbore length.

Hydrostatic Pressure Difference: $\Delta P_H = \frac{\rho_m g \Delta h}{144 g_c}$, where $\rho_m = \rho_L H_L + \rho_g (1 - H_L)$, ρ_g with respect to $\frac{\bar{p}}{\bar{T}Z}$ and ρ_L based on R_s, B_o and WOR.

Friction Pressure Difference: $\Delta P_F = \frac{2 f_F \frac{\rho_{NS}{}^2}{\rho_m} v_m{}^2 z}{144 g_c D}$, as described before, friction factor f_F depends on Reynolds number, $\mu_m = \mu_L{}^{H_L} \mu_g{}^{(1-H_L)}$, $\rho_{NS} = \rho_L \frac{v_{sl}}{v_m} + \rho_g \left(1 - \frac{v_{sl}}{v_m}\right)$, and $z = \frac{\Delta h}{sin\theta}$.

The incremental depth can be rewritten as: $\Delta h = \frac{\Delta P_{total}}{\frac{\rho_m g}{144 g_c} + \frac{2 f_F \frac{\rho_{NS}{}^2}{\rho_m} v_m{}^2}{144 g_c D * sin\theta}}$

Secondly, as illustrated in the calculation schematic of Figure 3-4, by discretizing the segments along the wellbore and averaging pressure between each step change, we treat the fluid properties and compressibility factor as a function of pressure rather than a constant value. In addition, temperature difference is also considered to correct the fluid properties, so the frictional factor is not constant along the wellbore. In summary, the fluid properties are constant in each subdivided segment.

Average pressure calculated by Hagedorn and Brown: $\bar{P} = \frac{P_{bh} + P_{wh}}{2}$

The average pressure used in the current model for variable Z factor and other fluid properties: $\bar{P} = \frac{p_n + P_{n+1}}{2}$

The third modification takes into account the bubble flow regime; if $\frac{V_{sg}}{V_m} < 1.071 - 0.2218(\frac{v_m{}^2}{D})$, then the Griffith correlation (Griffith and Wallis, 1961) is applied by calculating the holdup as: $H_L = 1 - \frac{1}{2}[1 + \frac{v_m}{0.8} - \sqrt{(1 + \frac{v_m}{0.8})^2 - 4(\frac{v_g}{0.8})}]$. The minimum value of $[1.071 - 0.2218\left(\frac{v_m{}^2}{D}\right)]$ is set to 0.13: if a calculated value is less than 0.13, then this parameter will be set to 0.13 for the next step.

Fourthly, the known boundary condition used for the original HB method is tubing head pressure, so it starts at the tubing head and the calculation is downward. However, the

current modified pressure model calculates the pressure profile upwards through the discretisation of the depth. This is because the differences of boundary conditions - bottom-hole pressure and temperature - are treated as outputs of the reservoir model and inputs of the current wellbore model.

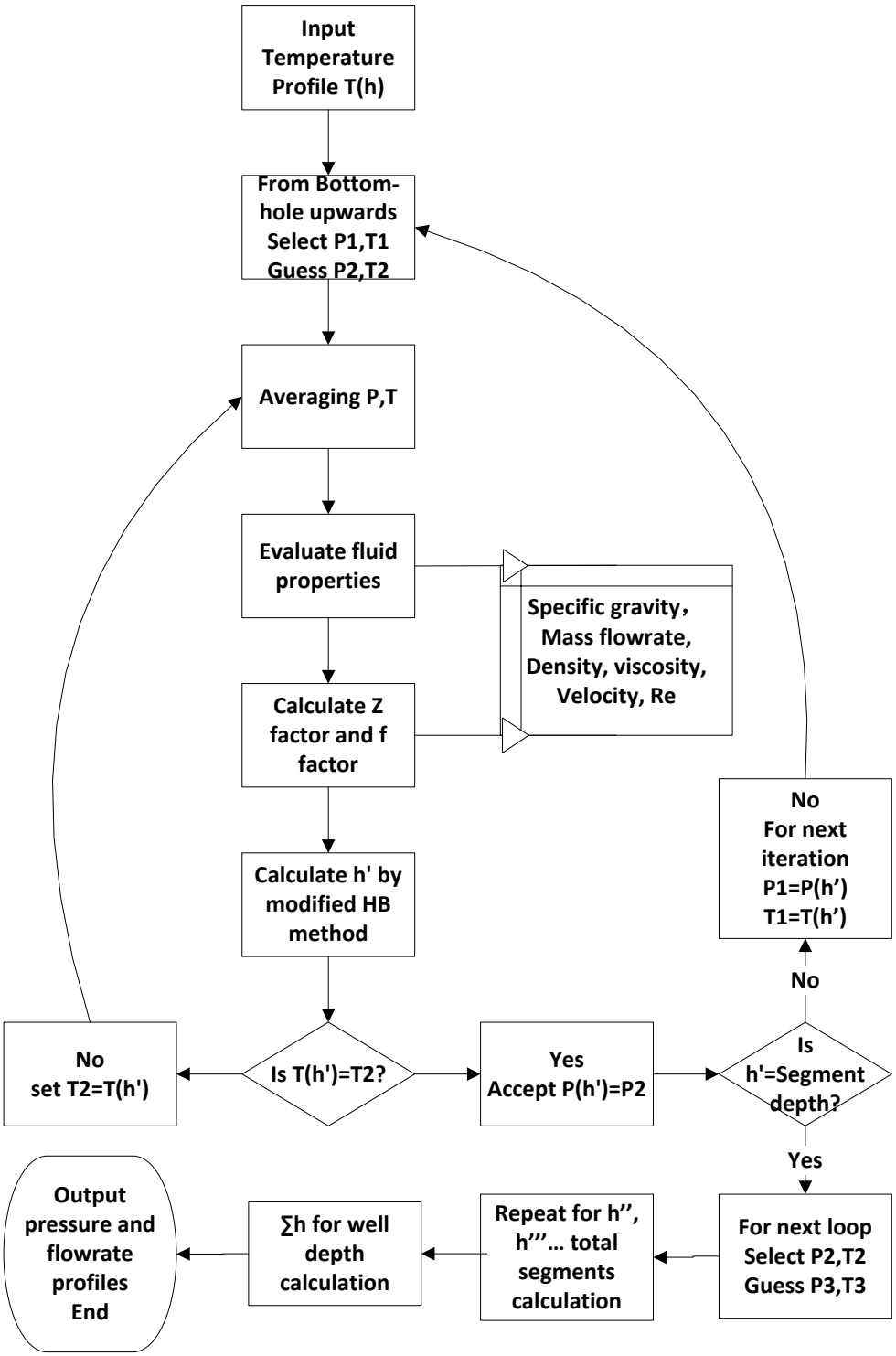

Figure 3-4：Modified Hagedorn and Brown calculation schematic and a set of pre-calculations

3.5 Application of the non-isothermal wellbore model in well testing

The PDG and DTS gauges are always located some distance away from the sand-face, approximately 400 feet, and in fact, heat transformation occurring between the wellbore fluids and surrounding formation will seriously affect the transient temperature recorded by gauges. In order to use those down-hole transient data for well testing interpretation, it is necessary to couple the wellbore model with another reservoir model to simulate actual transient temperature behaviour during production and shut-in periods. Then, some typical thermodynamic parameters can be estimated by matching the simulated results with the real data. In addition, the effect of wellbore storage on temperature can also be simulated by the model, and this provides a new method to assist in transient pressure analysis for well testing interpretation.

3.5.1 Coupling the wellbore model with the reservoir model

The bottom-hole temperature is used to couple the non-isothermal wellbore model and a reservoir model. In another words, the outputs (BHT) of the reservoir temperature model are transferred as inputs to the wellbore model, which will calculate the entire temperature profile along the wellbore section, especially at the gauge location. Moreover, the outputs of the reservoir flow (pressure) model are also used for the wellbore pressure profile calculation.

There are several typical parameters that affect the solution of this fully coupled non-isothermal well testing model, for instance: the distance between the gauge and the perforation, porosity of the formation, Joule-Thomson coefficient of the fluids, fluid viscosity and permeability, which will be tested in a sensitivity analysis. Generally speaking, the closer the gauge is located to the perforations, the more the behaviour will depend on the reservoir model, and the less dominant the wellbore model, and vice versa.

3.5.2 Reservoir model (from an existing reservoir model or commercial software)

The change of temperature in the formation is complex, particularly for a heterogeneous reservoir, because the reservoir consists of several porous media layers which will have different thermodynamic and physical properties.

The reservoir model used here was first developed by Duru (2008), and the standard codes for calculation were written using Matlab™. Duru's reservoir temperature model can be divided into two parts – a nonlinear convective transport part (analytical solution) and a nonlinear diffusion part (numerical solution), which are solved separately in each time step. The following assumptions were made:

- The fluid (oil/water) flow obeys Darcy's law.
- Joule-Thomson coefficient, adiabatic expansion coefficient and heat transfer coefficient are constant.
- The capillary force and gravity effect can be ignored.

Solution of convective transport part (initial condition of the diffusion part)

Transient well bottom-hole temperature:

$$T(r_w,t) = T_0(r_1) - C_j[p(r,0) - p(r,t)] - \frac{\eta^* - C_j}{ln\frac{r_e}{r_w}}\big(\Phi(t) - \Phi(0)\big) * ln(\frac{\sqrt{{r_1}^2 - 2\psi(p_e\bar{t} - s(\bar{t}))}}{r_e}) \ , \tag{3.20}$$

with $r_1 = \sqrt{{r_w}^2 - 2\psi(p_e t - s(t))},\ \psi = \frac{kC_p}{\mu ln\frac{r_e}{r_w}},\ \eta^* = \eta * \emptyset * c$

$s(\bar{t}) = \int_0^{\bar{t}} \Phi(\tau)d\tau_0 \,.\, \Phi(t)$ is the well bottom-hole pressure, which is obtainable from solutions of different reservoir flow models. Alternatively, in the current research, $\Phi(t) = P_e + \Delta P = P_e + \frac{q\mu}{4\pi kh} Ei(\frac{{r_w}^2 \pi\mu C_t}{4kt} + S)$.

$c = \frac{\rho_w C_{fw} S_w + \rho_o C_{fo} S_o}{C_m}$ represents the volumetric heat capacity ratio, C_t is the total compressibility of fluid and rock, S is the skin factor, k is the permeability, q is the flow-rate, P_e is the initial reservoir pressure and $r_e$is the reservoir radius.

Solution of diffusion part (final system temperature)

$$T(r,t) = \frac{1}{2\alpha t}\int_{r'}^{b} r'[exp(-\frac{r^2 + r'^2}{4\alpha t})F(r')I_0(\frac{rr'}{2\alpha t})]dr' \ , \tag{3.21}$$

where α = thermal diffusivity, $\frac{k_m}{C_m}$.

k_m = thermal conductivity of fluid saturated rock, $\emptyset k + (1-\emptyset)k_e$; C_m = volumetric heat capacity of fluid saturated rock, $(1-\emptyset)\rho_s C_s + \emptyset(\rho_w C_{fw} S_w + \rho_o C_{fo} S_o)$

$b =$ diffusivity length, $\sqrt{\alpha t}$. F (solution of Eq. 3.20) and I_0 are initial and boundary conditions.

The reservoir model developed by Duru (2008) is quite suitable for single-phase oil and two-phase oil-water systems. However, some pressure-dependent parameters such as fluid densities and fluid viscosities are not constant and should not be relaxed in gas systems. Moreover, high flow-rate gas flow in a reservoir may not obey Darcy's law. Accordingly, the commercial software – ECLIPSE 300 is used for simulating single-phase gas or three-phase gas-oil-water heat flow in the reservoir so that the developed non-isothermal wellbore model can be coupled with.

3.6 Results and case studies

The previous sections describe the solution procedures and calculation basis of the wellbore and reservoir models used in this study. In this section, the results obtained from the non-isothermal models for multi-phase fluid flow are presented; a few findings are discussed as well. In general, the simulated temperature, pressure and flow-rate results are specific for various reservoirs and fluids. In order to conduct synthetic case studies, different kinds of input files which contain reservoir and fluid properties need to be generated in advance. Fluid properties could be generated by PVTi™. Table 3-1 shows an example of the pre-existing fluid compositions which were used in the synthetic and sensitivity case studies. The bubble point pressure of the fluid is 3800 psi. The produced fluid specific results (PVT table), such as density, viscosity, FVF and Z factor with respect to different pressure and temperature, were written in the input file of Fluid.m.

Table 3-1：An example of the pre-existing fluid composition

Components	Weight fraction (%)	Mol weight (g/mol)
N2	1.257	28.013
CO2	1.5652	44.01
C1	40.014	16.043
C2	8.9152	30.7
C3	5.6722	44.097
IC4	1.1785	58.124
NC4	2.435	58.124
IC5	0.95925	72.151
NC5	1.1031	72.151
C6	1.7869	84
C7	3.0632	96
C8	3.2364	107
C9	2.3728	121
C10	2.1379	134
C11	1.8078	147
C12+	22.477	221

3.6.1 Progression of the non-isothermal wellbore model

For analysing the calculation results of the wellbore model quantitatively, a set of synthetic cases were simulated and various profiles of the fluid flow from the well bottom-hole to the surface were obtained by running the pressure model and the heat transfer model successively. In the synthetic cases, the well depth is set at 10000ft, the overall heat transfer coefficient is 18 Btu/hr ft °F, water cut is 0, the time step is 0.1 hour, and the entire simulation time is 50 hours, so that steady state already achieved.

Figure 3-5a demonstrates the initial input temperature profile which is equal to the first assumed temperature data for pressure profile calculation; Figure 3-5b shows a new temperature profile generated by inputting the pressure model results; after that, the program will check whether the differences between two temperature profiles (Figure 3-5a and Figure 3-5b) are within the allowable error, otherwise a second iteration will occur to simulate a new temperature profile, and the program will not stop running until the temperature profile (Figure 3-5c) in the most recent step matches the one before.

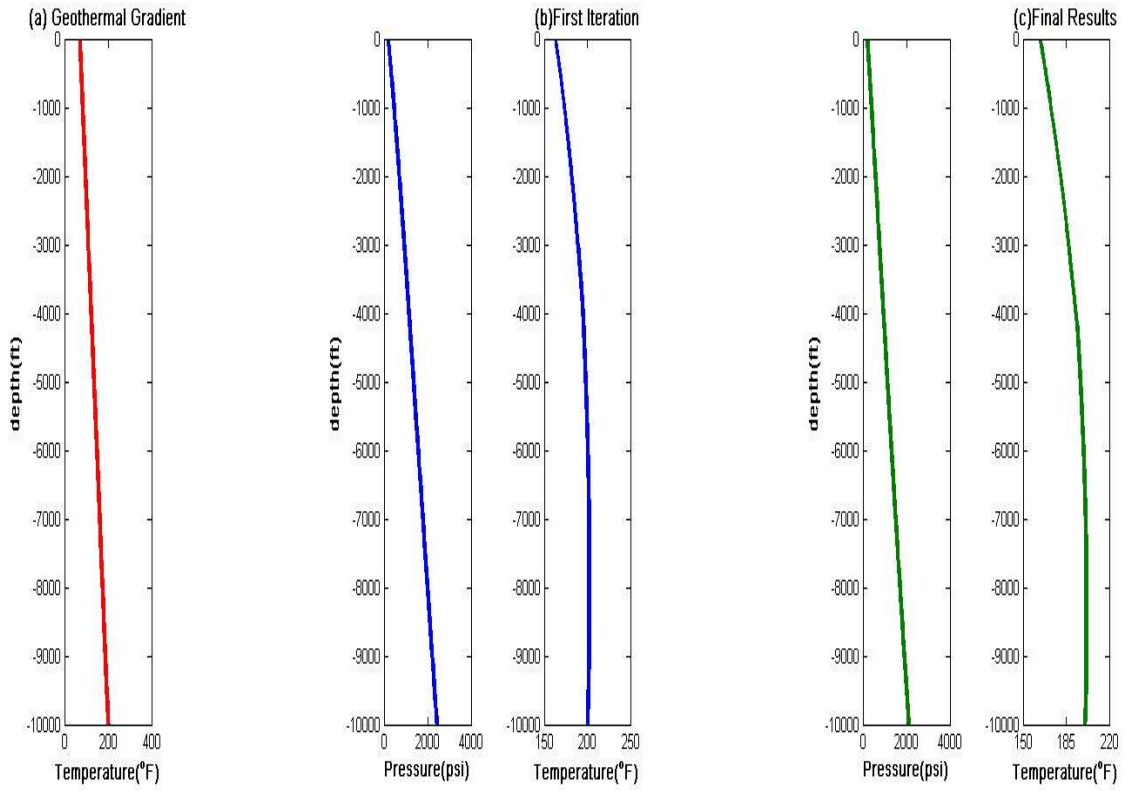

Figure 3-5：Results progression of the coupled temperature-pressure wellbore model

Figure 3-6 shows the results obtained at a relatively high bottom-hole oil flow-rate of 1400 bbl/d and Figure 3-7 shows the profiles with another lower bottom-hole oil flow-rate of 500 bbl/d.

The wellbore temperature was simulated starting from the bottom-hole temperature, which equals to the geothermal temperature at that depth, and then using this BHT as the boundary condition and moving upwards. It should be noted that the fluid temperature entering the sand-face from formation is not the reservoir temperature, so the BHT will be corrected by coupling with a reservoir model. The heat transfer effects are caused by convection in the fluid, conduction between wellbore and formation, geothermal temperature and frictional heating. The wellbore temperature decreases as it flows upwards and the fluid temperature with higher flow-rate (Figure 3-6) is higher than that with lower flow-rate (Figure 3-7), due to the more serious frictional heating effect happening in the higher fluid flow-rate tubing.

We also find that the pressure profiles decrease from bottom-hole to wellhead, which leads gas to discharge from the liquid. As illustrated in the liquid hold-up and flow-rate profiles, the distinct expansion of the lower density gaseous phase apparently causes the flow-rate to increase. However, compared with the gas flow-rate, the oil flow-rate does not change very much from bottom-hole to wellhead. Once more, the fluid pressure with higher flow-rate (Figure 3-6) is just above that with lower flow-rate (Figure 3-7) despite the serious frictional resistance and gravity occurring in the higher fluid flow-rate tubing.

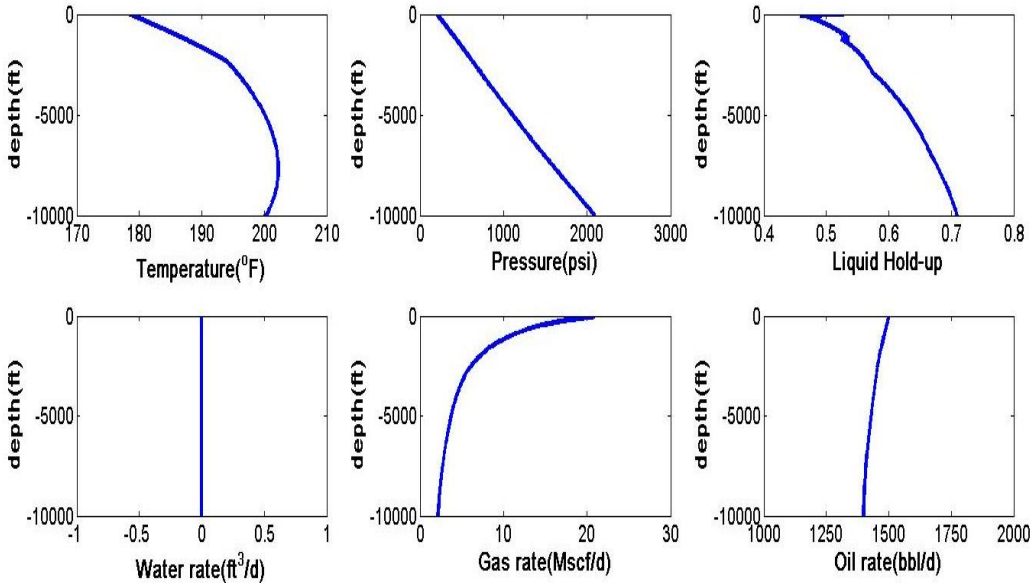

Figure 3-6：Calculated temperature, pressure and liquid hold-up profiles with higher bottom-hole flow-rate

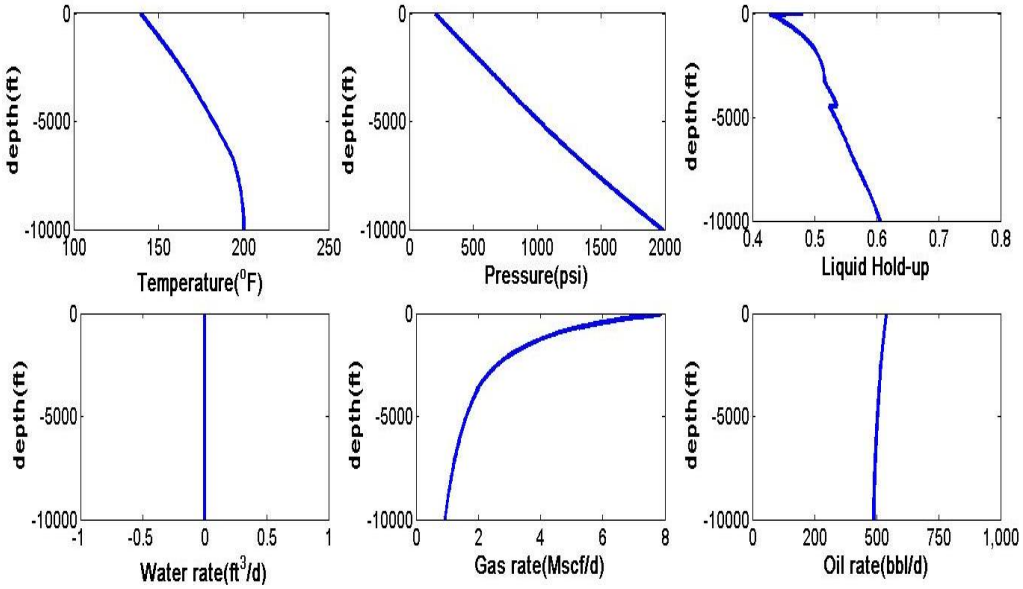

Figure 3-7：Calculated temperature, pressure and liquid hold-up profiles with lower bottom-hole flow-rate

In addition, it is apparent that the temperature of wellbore fluid changes with time, known as transient temperature. Figure 3-8 illustrates how the temperature profile is changing with time for a 50 hour production period. In this case, at the location of permanent gauges (400 feet away from the bottom), temperature increased about 0.6°F after 50 hours production. Generally speaking, for oil production wells, both frictional heating and Joule-Thomson heating effects lead the wellbore temperature to be higher than the reservoir temperature and increase with time, while for gas production wells, considering the Joule-Thomson cooling effect, there is no simple magnitude relationship between the transient wellbore temperature and the reservoir temperature. If we shut down the wells, either for gas wells or oil wells, the wellbore temperature will gradually drop with time, due to heat conduction which leads to the decrease of temperature difference between the wellbore fluid and the near wellbore regime. With the development of fibre optic technology, a temperature can be measured with a resolution in the order of 0.0045°F. If the estimated temperature change is larger than this resolution, it may benefit us to install the equipment and measure the temperature profile. Therefore, it is necessary to infer the possible temperature changes under synthetic scenarios by using the non-isothermal wellbore model in advance.

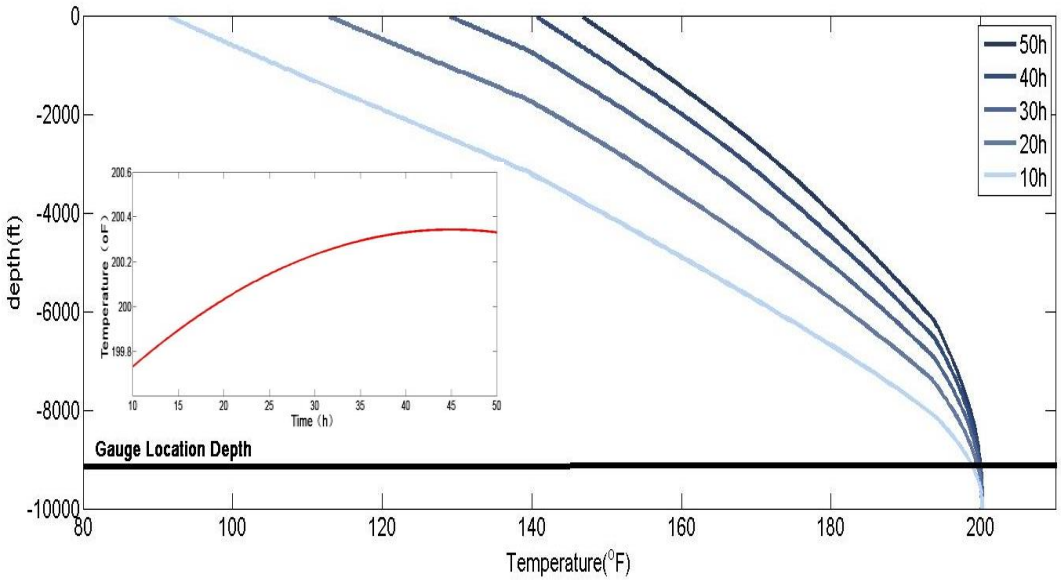

Figure 3-8：Temperature of wellbore fluid increase with production time elapsing

3.6.2 Verification of the non-isothermal wellbore model - Comparison of temperature profiles

This section is dedicated to comparing the simulation results among the non-isothermal wellbore model, Ramey's model which is an approximate analytical temperature profile calculation method commonly used in industry, and another, more accurate method, Izgec's model. The fluid properties and operation conditions were initially used to simulate high flow-rate gas condensate flow occurring in a vertical well, as presented by Alves et al. (1992). All of the following profiles were plotted with the same overall heat transfer coefficient of 10 Btu/(hr ft °F) and the same values of other wellbore and fluid conditions, as shown in Table 3-2 and Table 3-3.

Table 3-2：Operation conditions (data were taken from Alves et al., 1992)

Parameter	**value**
Vertical well depth, ft	7000
Bottom-hole Pressure, psi	3000
Bottom-hole temperature, °F	180
Geothermal gradient, °F /ft	0.02
Seabed Temperature, °F	40
Overall heat transfer	10
Mass flow-rate, lbm/d	86400

Table 3-3：Fluid composition (data were taken from Alves et al., 1992)

Components	**Weight fraction %**
Nitrogen	0.2
CO2	4.5
Methane	70.5
Ethane	8.0
Propane	4.2
I-butane	2.0
N-butane	2.0
I-pentane	1.0
N-pentane	1.0
Hexane	2.0
Hypothetical-1	2.5 (55 API)
Hypothetical-2	1.2 (50 API)
Hypothetical-3	1.3 (35 API)

Figure 3-9 shows how these three wellbore models compare with each other. After 80 hours production with 0.5 hour time step, the profiles simulated by the present numerical model and Izgec's model look as if they almost coincide, but Ramey's analytical model produced a quite different temperature profile, which is incorrect in this case. This is because of the different treatments of fluid properties, compressibility factor and friction effect between Ramey's model and the developed model in this study. This comparison demonstrates the necessity of developing a numerical model which can accurately simulate complex production scenarios such as inclined wellbore, high flow-rate, gas production and phase change.

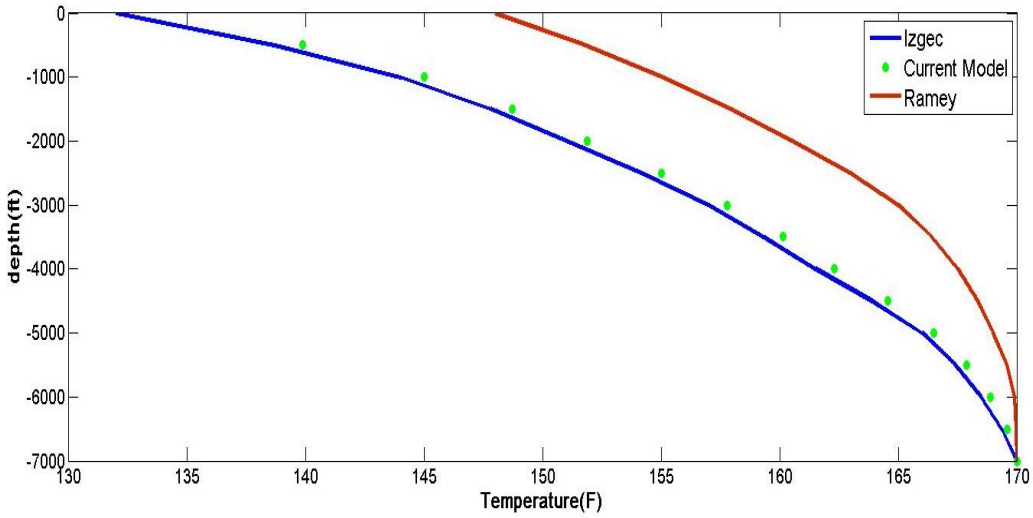

Figure 3-9：Temperature profiles along the wellbore calculated by different methods

Figure 3-10 shows the comparison of Ramey's model and Izgec's model with the current model for a drawdown test with a mass flow-rate of 86400lbm/d at 300ft above the production layer (which is always the case where the PDG is located). Significant differences can be seen at the beginning of the production period, and the difference will continue to reduce until 80 hours later (steady-state flow occurs). This is because both Ramey and the current model have dropped the kinetic term in the energy balance equation; in addition, the potential energy loss would become approximately equal to the enthalpy rise, due to Ramey's assumptions of single phase incompressible fluid flow, which mislead the simulation results in this case.

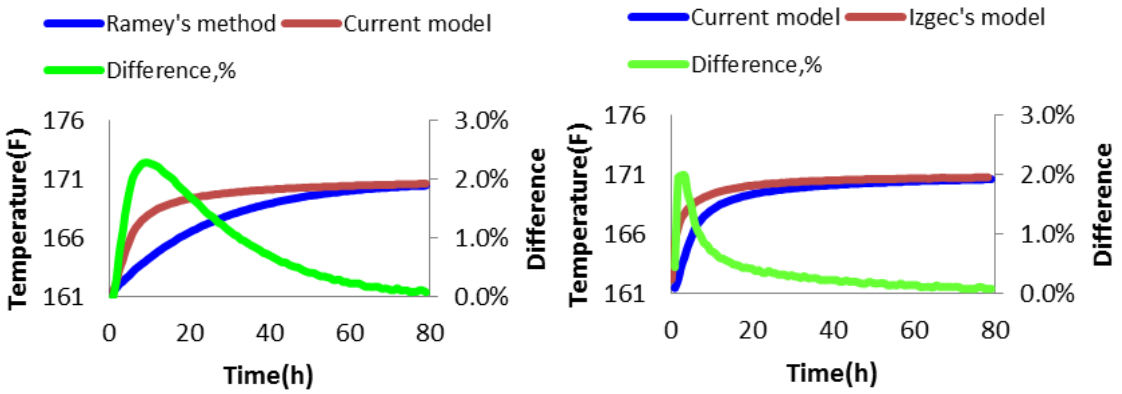

Figure 3-10：Comparison among three temperature models during a draw-down test

3.6.3 Sensitivity analysis of the non-isothermal well testing model

According to the established non-isothermal well testing model (coupling the wellbore model with the reservoir model), the temperature versus time curve at the location of PDGs can be calculated. For maximizing the influence of the established wellbore model, temperature was simulated at 500 ft (large distance increases the early time temperature jump) above the pay zone in these synthetic cases.

Several variables can increase the simulation uncertainty and reduce the model's accuracy, so it is necessary to conduct sensitivity tests and summarise the performance of different model parameters in generating the transient temperature data sets. After eliminating some minor parameters, such as geothermal gradient, reservoir thickness and thermal conductivity, the following parameters were tested for quantitative sensitivity analysis of the solution: porosity of the formation, Joule-Thomson coefficient of the fluids, fluid viscosity and permeability.

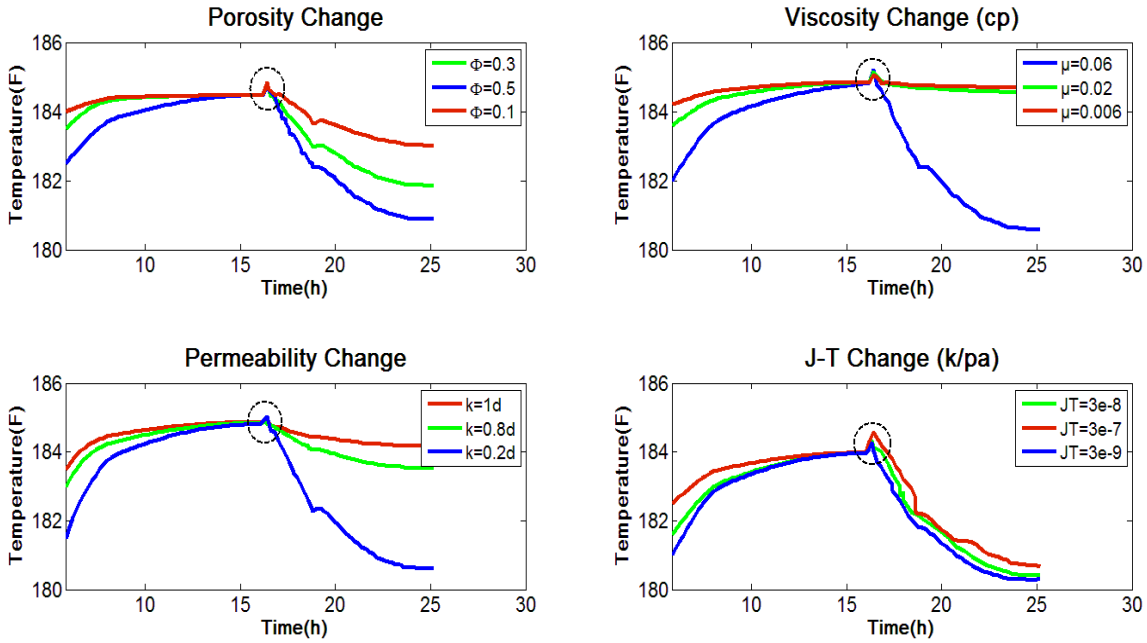

Figure 3-11：Effect of model parameters (porosity, permeability, viscosity and Joule-Thomson coefficient) on simulated transient temperature data at gauge location

Figure 3-11 shows that the global increase/decrease of the temperature profile is proportional to the rise in porosity and fluid viscosity, but is inversely proportional to the rise in permeability; changing the Joule-Thomson coefficient has relatively little effect on temperature. Although these parameters are available from well-logs, it is more convenient and cheaper to estimate them through simulation. In addition, considering that viscosity can be measured through experiments and used as accurate inputs for the model, the number of parameters for the inverse problem which aims to evaluate the reservoir and fluid parameters by matching the simulated results with the real temperature data is reduced to three.

Furthermore, from the sensitivity analysis, we can also find that the size of the jump in temperature which happens after flow-rate change can provide qualitative information about the formation and fluid properties. The jump in temperature can be very small in the case of high permeability and small Joule-Thomson coefficient, but can be relatively big when low porosity and large viscosity exist. Figure 3-12 demonstrates the performance more clearly, in these two plots of pressure build-up tests, the x axis stands for the logarithm of shut-in time and the y axis represents the simulated temperature. The early time temperature increase is affected by wellbore storage, in which there is a down-

hole flow-rate from the reservoir towards the wellbore and a gradual decline in pressure. So during this period, the frictional heating dominates the temperature behaviour (maximal increases are 0.2 °F and 0.4 °F respectively), and the effect of wellbore storage becomes more obvious with the decrease of permeability/increase of viscosity. However, as the effect of wellbore storage ends, the main factor affecting the wellbore temperature changes to heat conduction between wellbore and formation, so that wellbore temperature gradually declines towards the reservoir temperature at that depth.

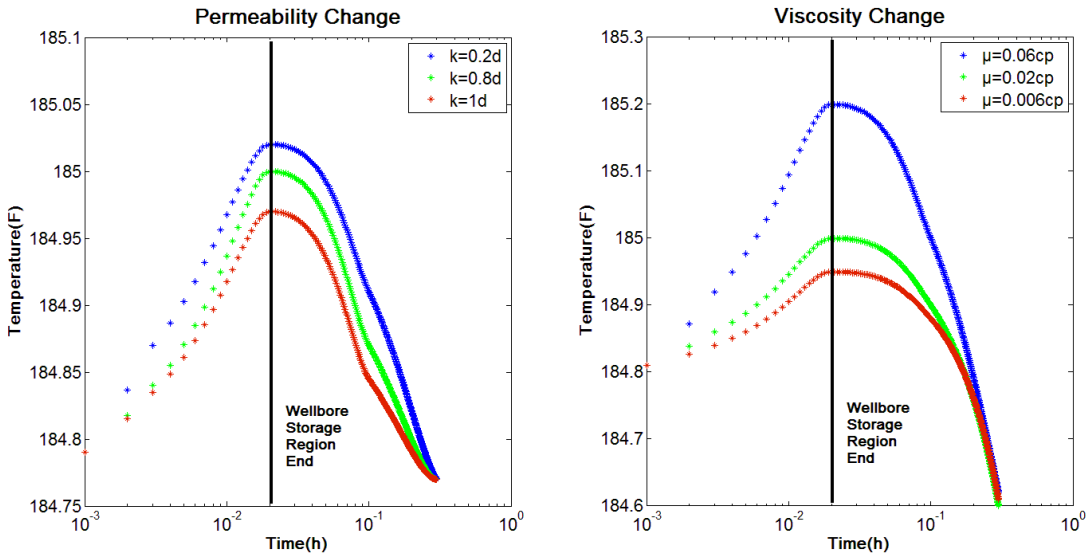

Figure 3-12：Semi-log plots of transient temperature with different parameters during build-up (time starts from well shut-in)

Therefore, considering the fact that some factors, such as reservoir heterogeneity, wellbore storage, and skin, can affect the pressure response, we may use the transient temperature behaviour for well testing interpretation to detect the end of wellbore storage and flow regimes.

3.6.4 Field data analysis

In order to obtain reservoir information and fluid thermodynamic parameters through optimal matching between the model results (input flow-rate data) and the temperature data, one set of field data which comprises a 9945 hours measurement period with each measurement taken at 10 seconds intervals and another set of field data with a 6 second time step and 5000 hours of measurement were utilized. Both of the field datasets were acquired from oil production wells, the temperature gauges were located at 300 feet and

200 feet above the production zones separately. The long-term PDG data may represents a change in the reservoir parameters, so in order to keep the constant reservoir parameters, simplify the model calibration process and ensure the utilization of constant diffusivity lengths, two representative transient regions of 70 hours period and 26 hours period were selected. The parameters used in the inverse problem were porosity, fluid mobility (permeability/viscosity) and Joule-Thomson coefficient; other thermodynamic and reservoir parameters such as fluid heat capacity, thermal conductivity, fluid density, flow-rate history and reservoir thickness were acquired from the literature and treated as known inputs.

Figure 3-13 and Figure 3-14 demonstrate the good history matching results of both field case one and field case two. The calculated RMS error ($\sqrt{\frac{\sum_1^n (T_{model}-T_{data})^2}{n}}$) of these two cases equals to 0.15 and 0.1 respectively. For the first case, the values of the model parameters at optimal matching are ∅=0.35, JT coefficient=3.4e-4 K/psi, and k/μ=5.5 md/cp; for the second case, the estimated parameters for history matching are ∅=0.2, JT coefficient=5e-3 K/psi, and k/μ=40 md/cp. These porosities and fluid mobilities coincide with the PTA interpreted values, and the estimated Joule-Thomson coefficients are within the ranges of crude oil which are mentioned in the literature. However, the method of optimal matching used in this section is manual which require numerous attempts and therefore is time consuming and inconvenient. Numerical optimization of temperature history matching will be discussed in the proposals for future work in Chapter 6.

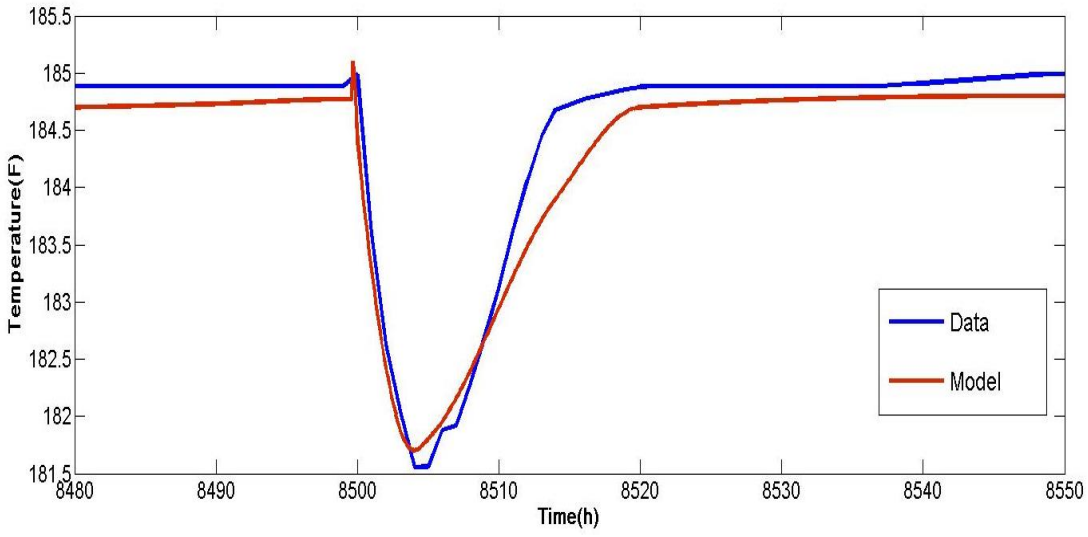

Figure 3-13：Matching the simulation results with temperature data (field case one)

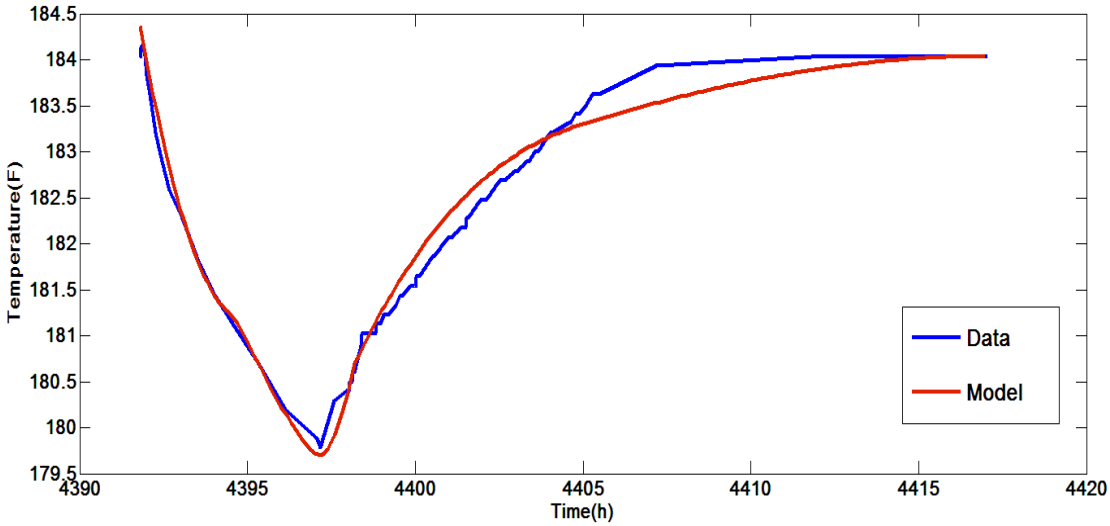

Figure 3-14：Matching the simulation results with temperature data (field case two)

3.7 Chapter Summary

The model presented in this chapter provides a way not only to integrate pressure data and determine the flow-rate profile more accurately, but also to estimate typical reservoir information and fluid thermodynamic parameters such as porosity, permeability, viscosity, and Joule-Thomson coefficient by matching the simulated results with the real transient temperature data measured by PDGs. In addition, the transient temperature data may also be used as a fast and reliable diagnostic tool in well testing analysis to detect the end of wellbore storage. The following conclusions can be summarized:

1. A non-isothermal wellbore model was developed and its reliability has been verified by comparing it with other published models.
2. The established wellbore model can calculate the temperature profile, integrate with pressure data, and determine the flow-rate profile more accurately.
3. The transient temperature behaviour at the location of gauges can be simulated by coupling the wellbore model with a reservoir model.
4. Temperature changes are very sensitive to the Joule-Thomson coefficient, viscosity, permeability and porosity among other parameters, and in accordance with established non-isothermal well testing models, these representative fluid thermodynamic parameters and reservoir parameters can be obtained accurately.
5. For pressure build-up tests, the wellbore storage effect starts from the wellbore temperature increase and ends when the temperature decreases. In addition, the

jump in temperature can be very small in case of high permeability and small Joule-Thomson effect (it depends on either the Joule-Thomson coefficient or the extra pressure drop caused by the skin factor), but can be relatively big when low porosity and large viscosity exist. So the transient temperature data may be used as a fast and reliable diagnostic tool in well testing analysis to detect the end of wellbore storage.

Chapter 4 Transient Temperature, Pressure and Flow-rate Data Processing and Integrated Interpretation for Nonlinearity Diagnostic

4.1. Introduction

With the installation of Permanent Down-hole Gauges (PDGs), continuous and real-time pressure, temperature and sometimes flow rate data are available. Considering the fact that the transient data acquisition process is relatively independent, integrating the analysis of the transient temperature, pressure and flow-rate data can include lots of useful information and significantly reduce the interpretation uncertainties. For instance, errors that are caused by measurement technical problems or interpretation constraints in pressure data are not expected to appear in the transient temperature data again. In addition, the flow-rate history can be reconstructed from the pressure data which has been published in several articles and proven in practice. However, any existing aberrant points in pressure data may affect the reconstruction of results and cause the inaccurate interpretation of production events/reservoir reactions. What is more, in order to reconstruct the flow-rate history, the times of flow events need to be identified. But the outliers in pressure data may increase the difficulty of transient identification. Therefore, it is necessary to verify the results of one dataset analysis by using other measurements. Especially with the development of techniques for temperature measurement, it is effortless to acquire high resolution and high accuracy temperature data that can improve the conventional pressure interpretation methods. However, gauge location affects the transient temperature preference. If the gauge is located far away from the middle of the perforated interval, the difference between the geothermal temperature and the sand-face temperature is very large, which will increase the ETR temperature jump. Consequently, it is necessary to take into account the temperature change along the wellbore. According to the established fully coupled reservoir-wellbore model, the accurate transient temperature and pressure data at gauge locations can be simulated.

This chapter describes how transient temperature, pressure and flow-rate data were processed and then interpreted. The relationships amongst down-hole temperature, pressure and flow-rate were firstly studied by using a wavelet transform together with a

nonlinear regression analysis method. Secondly, a workflow for transient down-hole data processing was developed. Thirdly, the simplest wavelet transform method, the Haar wavelet, was selected as the transient identification algorithm. It was found that not only in the pressure case but also in the temperature case, large amplitudes in the wavelet detail coefficients were caused by flow events. Fourthly, the relationship between wavelet transform amplitude and rate change (unit-rate-change coefficient) was analysed, and an improved diagnostic method of nonlinearity from both transient pressure and temperature data was also developed. According to the derived analytical solutions, the nonlinearities caused by a change in well-reservoir properties can be identified by both transient temperature and pressure data. Finally, how unit-rate-change coefficients behave with the changes of different thermodynamic parameters was also researched by conducting sensitivity studies.

4.2. BHT, BHP and flow-rate relationships

Figure 4-1 shows a set of field transient down-hole data which contains many different flow periods within 10000 hours. This dataset was acquired from an oil production well with no injectors around. The measured temperature increased progressively while pressure decreased gradually. So it is worth noting that formation pressure and temperature performed similarly and this similarity emerged in many characteristics. Firstly, temperature and pressure follow the same diffusion equation. Secondly, at the junction between formation and well, near-wellbore damage should be considered for pressure, at the same time, on the temperature side, we should also consider the heat loss which occurs in the formation, casing, tubing and cement. Thirdly, wellbore storage can be used to estimate heat capacity coefficient in wells. Fourthly, constant pressure and impermeable boundaries have been set for pressure boundaries, but we always regard the temperature boundary as infinite-acting. Consequently, the relationship between temperature and flow-rate may also be deduced similarly to the relationship between pressure and flow-rate. This section uses the measured PDG data to qualitatively reveal the existing relationships and inform the following detailed analyses for temperature data.

On the basis of energy conservation, if the initial conditions and boundary conditions have been established, we can derive the relationship between temperature, pressure and

flow-rate according to Fourier's law. Finally, the combination of temperature data can be used to provide complementary reservoir information and calculate yield quantitatively.

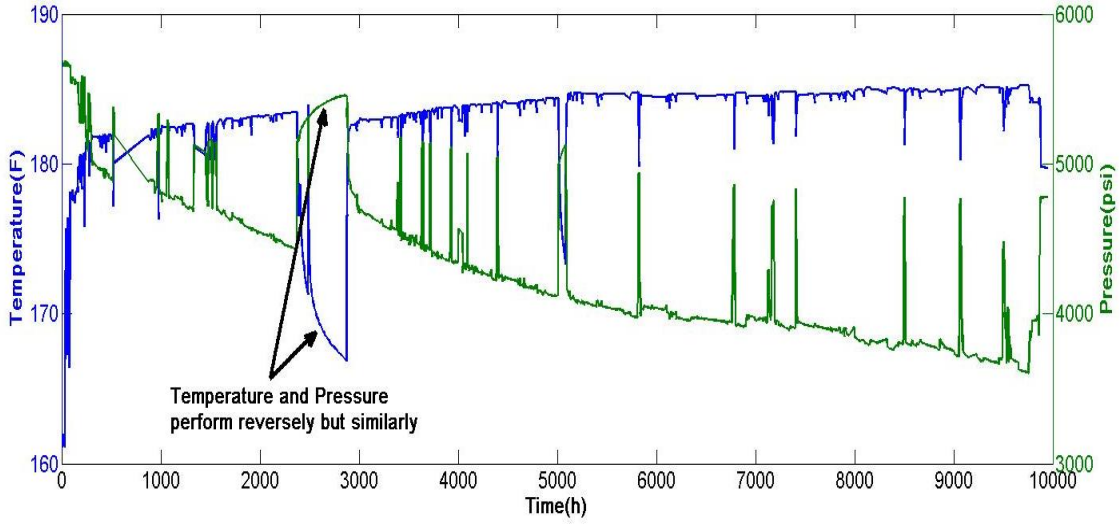

Figure 4-1：Long term temperature and pressure data measured by PDGs

4.2.1 Nonlinear regression analysis - optimal transformation for estimation of functional relationship

A Nonlinear Regression Analysis method which performs a calculation of optimal transformations from datasets is applied for the purpose of demonstrating an existing relationship between flow-rate, pressure (predictor variables), and temperature (response variable). The algorithm was invented by Breiman and Friedman (1985), known as the Alternating Conditional Expectations (ACE) method, which contains two basic mathematical operations of conditional expectations and iterative minimisation. ACE method is able to perform the regression without requiring a priori assumption of any functional form for the variables. The optimal transformations are derived solely from the input datasets. Consequently, the physical parameters, such as permeability and porosity, which are involved in the functions (existing relationships among down-hole data) may be identified through ACE method.

A programme which performs the calculation of optimal transformations from datasets was developed using Matlab^{TM} (Voss, 2013). It follows the algorithm closely and produces two kinds of variables, the first output contains the maximal correlation and the

second output represents the transformed values of inputs. The input data include six main components:

- The original signals for analysing, they should have the same time counts
- The number of dimension terms (signal types), which can be 1, 2, or 3
- The number of data points of each dimension term
- The total dataset size which is equal to the dimension terms plus one
- The maximum number of iterations of outer loop/inner loop
- The small (1e-12) outer iteration stop criterion and larger (1e-4) inner iteration stop criterion

The ACE method was utilized for a set of transient down-hole data which were recorded by Permanent Down-hole Gauges (PDGs). Then the maximal correlation and the set of optimal transformations which contained the transformed values in the same order as the inputs were produced. Figure 4-2 illustrates the diagrams of temperature, pressure and flow-rate data, as well as the plot of the ACE regression result (the maximum linear effect between the transformed response variable and the transformed predictor variables). A correlation coefficient of 0.9679 means that the temperature response to changes of flow-rate and pressure, and this optimal transformation function can be determined from either the entire dataset or a selected representative transient region.

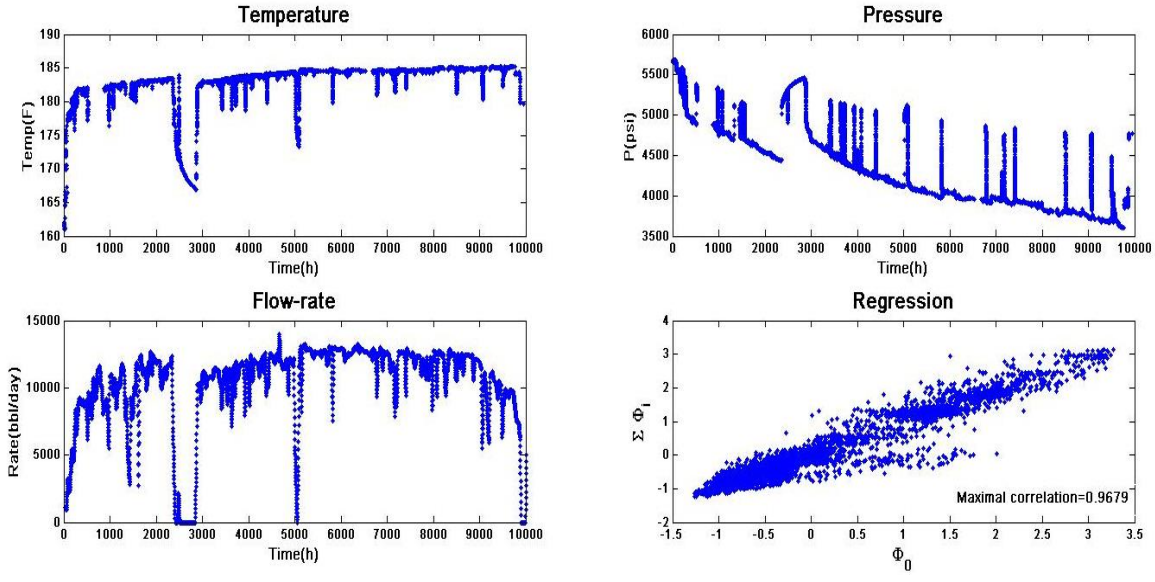

Figure 4-2：PDG data and ACE regression results ($\sum\Phi_i$: sum of transformed pressure and flow-rate, Φ_0 : transferred temperature)

4.2.2 Wavelet transform analysis

A wavelet transform is a mathematical method to analyse signals which have a characteristic time-variation. In another word, it is a multi-resolution frequency analysis method. Compared with other signal analysis techniques such as the nonlinear signal processing method, the wavelet transfer can provide more accurate analysis results for certain classes of signals and images. The integral wavelet transform of signal f(t) at scale b and position a is defined as:

$$Wf(a,b) = \frac{1}{\sqrt{\mathrm{b}}}\int_{-\infty}^{\infty} \psi\left(\frac{t-a}{\mathrm{b}}\right) f(t)dt \qquad 4.1$$

There are several kinds of original wavelet (ψ). In this study, the simplest and the most widely used method - the Haar wavelet - was selected to process the down-hole transient pressure and temperature data acquired by PDG.

If we treat the transient pressure data as signal f(t), as supposed by Wang and Zheng (2012), for drawdown period the amplitude of the WT coefficients is positive, and for pressure build-up the amplitude is negative, so the timing of the flow events can be identified with the wavelet transform.

However, their study only analysed the relationship between flow-rate and pressure. The transient temperature data can also be regarded as signal f(t). As Figure 4-3 and Figure 4-4 illustrate (processed transient data of Figure 4-1), not only in the pressure case but also in the temperature case, large amplitudes of wavelet detail coefficients are caused by flow events, while the small wavelet detail coefficients around zero reflect the data noise, which can be removed by setting a noise threshold. The non-effect flow events which are marked in Figure 4-3 may be caused by the outliers of the original pressure data, these uncertainties can be reduced through integrated processing of temperature and pressure data.

Moreover, for a reservoir with constant reservoir-well parameters, the amplitude of temperature transforms is proportional to the change of flow-rate, and the calculation of rate history from down-hole transient temperature data using wavelet transform will be discussed in Chapter 5. Alternatively, the flow-rate can be estimated from the pressure

and temperature profiles by using the established non-isothermal wellbore-reservoir model and the results then depend on thermodynamic parameters.

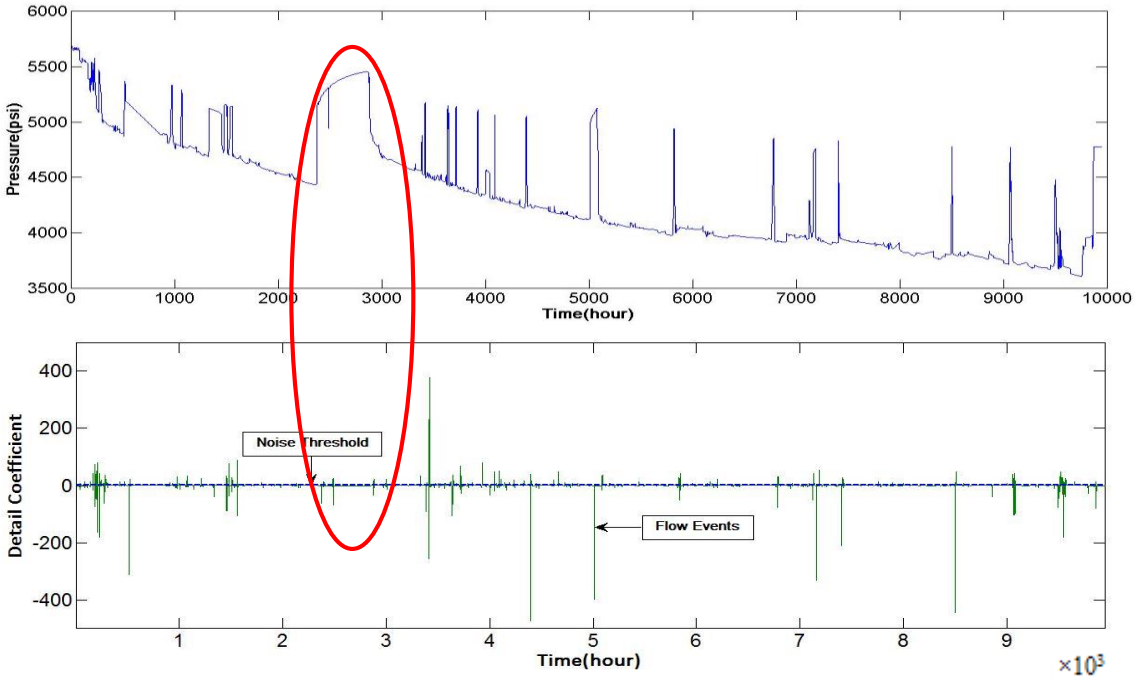

Figure 4-3：Pressure data and its detail coefficient after wavelet transform

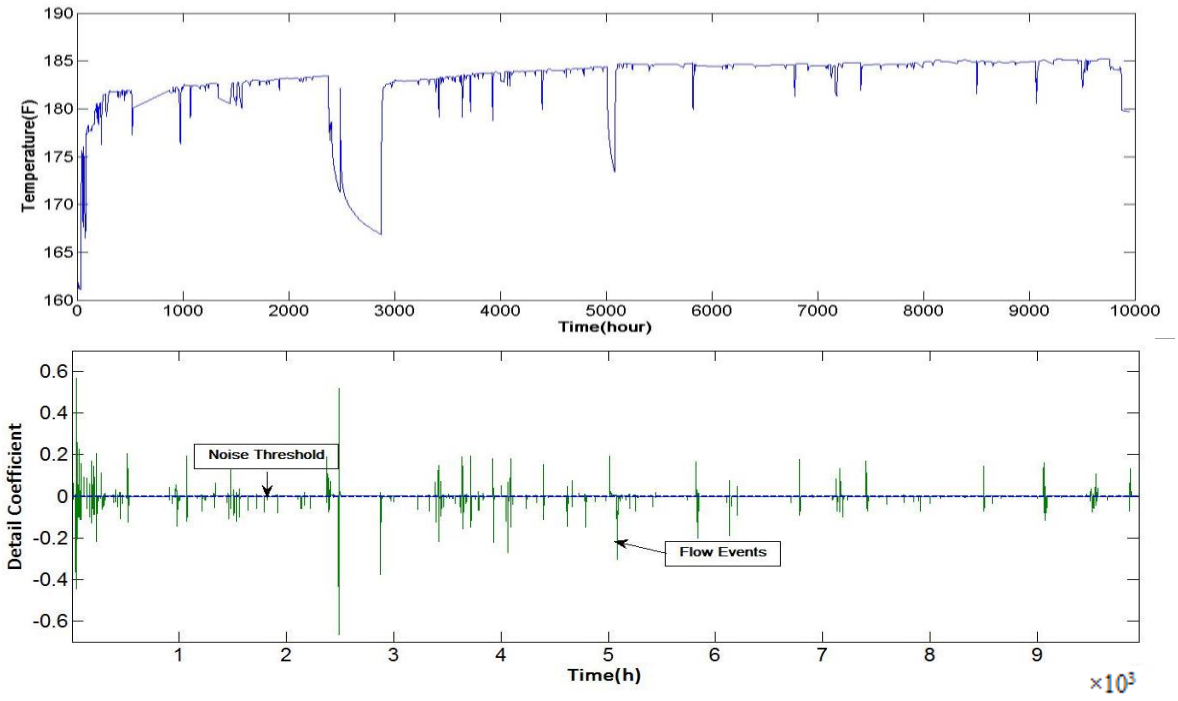

Figure 4-4：Temperature data and its detail coefficient after wavelet transform

4.3. Procedures of transient data processing

Compared with conventional wireline well-testing pressure and temperature data, the transient data collected from PDGs contain some differences. The long term fluctuations measured by PDGs are always too complex to analyze directly due to the existence of noise, outliers and a lot of flow events. Therefore, a considerable and reliable processing procedure needs to be discussed in advance (Li, 2009). This section describes the wavelet based approach for pressure and temperature data processing as well as some typical notes.

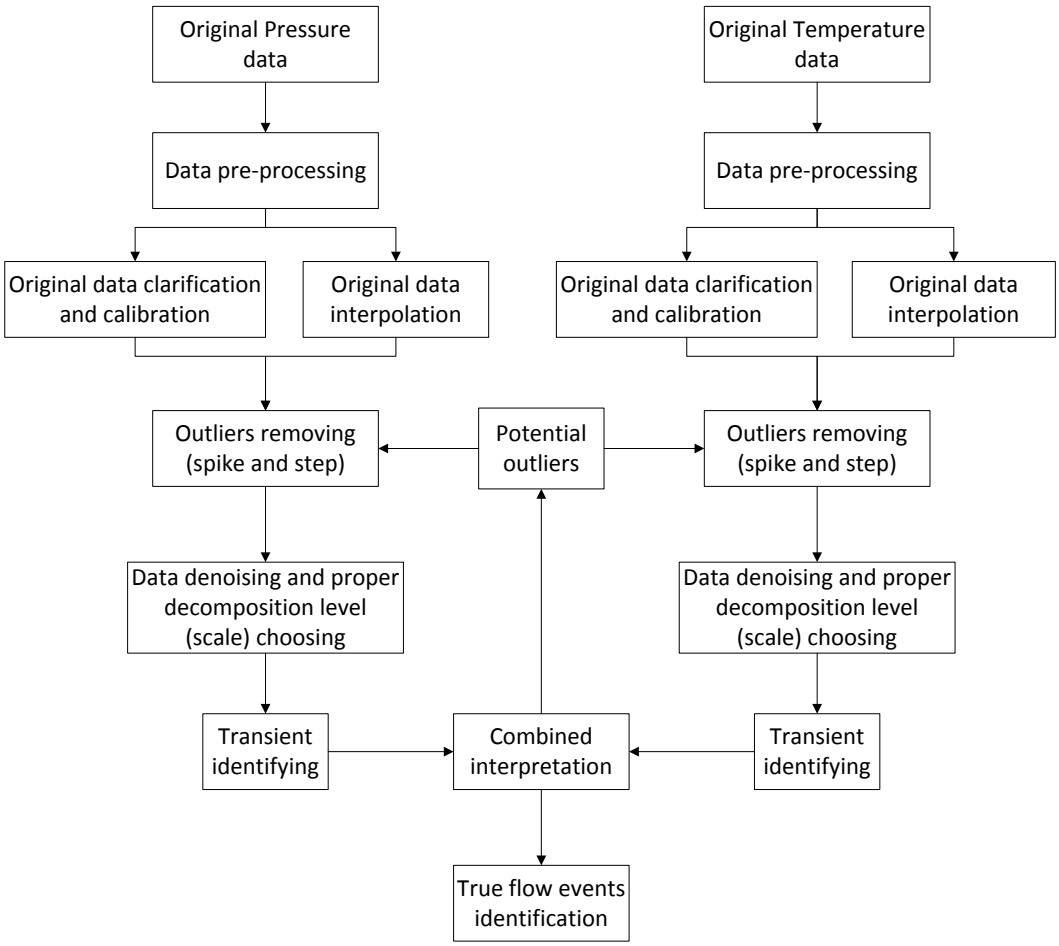

Figure 4-5：Workflow of transient data processing

Figure 4-5 shows the detailed workflow of transient data processing: firstly, data pre-processing for optimizing the original data to usable data; secondly, removal of single spike outliers; after that, data de-noising and selection of appropriate decomposition level (scale); transient periods are then identified by temperature and pressure data separately, which will be discussed in detail in the next section; finally, true flow events will be

identified and potential step outliers diagnosed by combining the processed temperature and pressure data.

4.3.1 Pre-processing PDG data

Before processing the transient temperature and pressure data, they should be prepared in advance in respect to the following aspects.

Original data clarification and calibration

The transient temperature and pressure data measured by PDGs commonly contain different degrees of singularities. For example, negative values of temperature and pressure data are invalid either in the reservoir or in the wellbore, but they can be observed in the real data (gauge error or unpredictable factor). In addition, unit conversions, such as time conversion and pressure and temperature unit calibrations, also need to be conducted in advance. The following four main steps for further analysis are summarized:

1) Singularities removal: negative temperature and pressure data.

2) Time format conversion: transfer the "day/month/year 00:00:00" format to hours.

3) Pressure data unit conversion: calibrate to field unit - psi.

4) Temperature data unit conversion: calibrate to field unit - °F.

Figure 4-6 and Figure 4-7 show a set of real PDG pressure and temperature data as well as the clean calibrated data after carrying out the four steps. These down-hole gauges were installed on 08/08/2001 for recording both pressure and temperature. The original datasets contain several singularities which should be removed before processing, for better understanding of the transient pressure and temperature data. A number of build-up and draw-down tests included in the 1500 hours of production can be observed from either the clean calibrated pressure data or the clean calibrated temperature data.

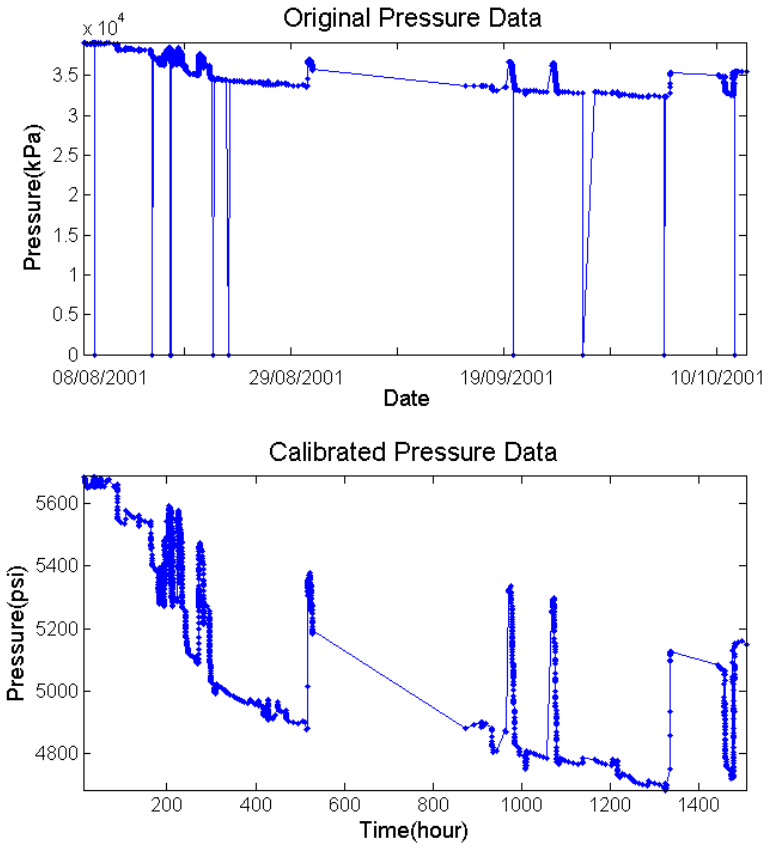

Figure 4-6：Real PDG pressure data and calibrated clean data

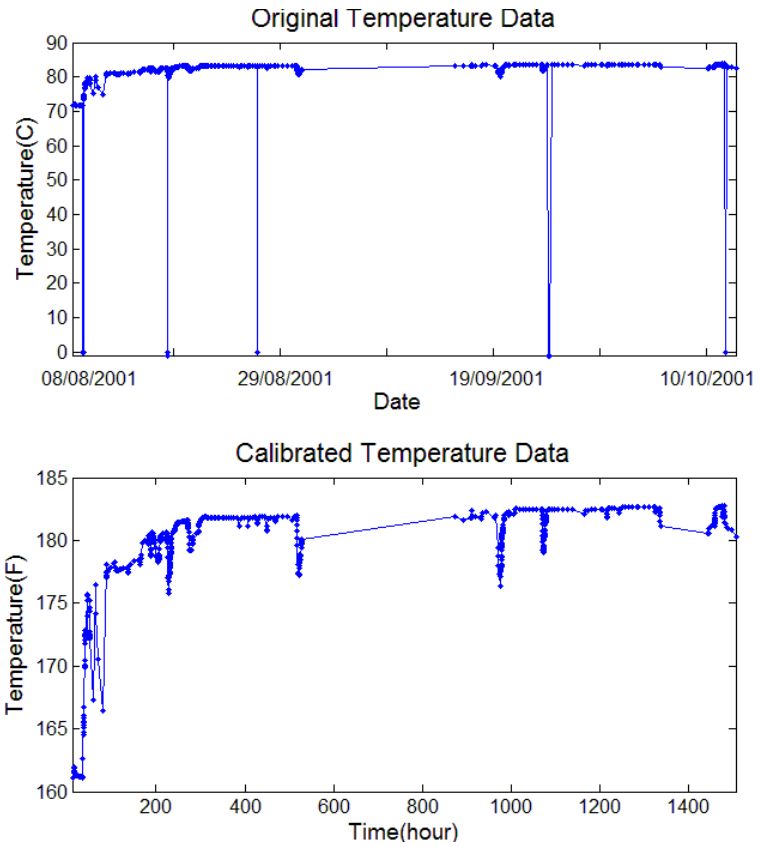

Figure 4-7：Real PDG temperature data and calibrated clean data

Synchronization issues

In order to process the down-hole transient data and check the consistency among breakpoints (flow-rate change points) of temperature, pressure and flow-rate, time synchronization should be considered. In other words, we need to keep the time interval coincident not only in synthetic case simulation but also in real data collection. Therefore, data evaluation should be conducted before data processing. In oil field operations, the time interval of transient data depends mainly on the recording frequency. The minimal time interval is about one second, but data gaps and missing data problems always exist. It is safe to adjust the data length if the frequencies of all the transient data are the same. However, if the frequencies of temperature, pressure and flow-rate measurements are different, interpolations using either high degree polynomials or functions are required. Additionally, it is worth pointing out that some errors may be caused by interpolation, especially in the areas close to the breakpoints.

Interpolation

As mentioned in the synchronization issues, interpolation is a necessary step for implementing wavelet decomposition. In the circumstances of unequal time intervals, the anomalously placed temperature and pressure data should be interpolated to evenly sampled datasets. Generally speaking, interpolation is a method of constructing new data among original data by defining a function that takes on specified values at specified points. In this section, it will be classified into four main types for discussion: linear interpolation, nearest neighbour interpolation, spline interpolation and pchip interpolation (Piecewise Cubic Hermite Interpolating Polynomial).

Nearest neighbour interpolation (also known as proximal interpolation or point sampling) is a simple method of multivariate interpolation in one or more dimensions. The nearest neighbour algorithm simply selects the value of the nearest point, and does not consider the values of other neighbouring points at all, yielding a piecewise-constant interpolation. The algorithm is very simple from the implementation point of view.

Linear interpolation (or lerp) is one of the simplest interpolation methods. If two data points are given as (x_a, y_a), (x_b, y_b) in the Cartesian coordinate system, the linear

interpolation is the straight line between them. For a value x between x_a and x_b, the corresponding value y can be given by:

$$y = y_a + (y_b - y_a)\frac{(x-x_a)}{(x_b-x_a)}.$$

Spline interpolation is a form of interpolation where the interpolant is a special type of piecewise polynomial called a spline. It provides an interpolation of the data points into smooth curves. Compared with polynomial interpolation, spline interpolation can make smaller errors, even when using low degree of polynomials for the spline. The corresponding mathematical spline must have a continuous second derivative and satisfy the same interpolation constraints.

The Pchip interpolation is any piecewise cubic polynomial that interpolates the given data. It has specified derivatives at the interpolation points. Just as two points determine a linear function, two points and two given slopes determine a cubic. The data points are known as 'knots'. If the y-values at the knots are known, in order to get a particular 'Pchip', we have to somehow specify the values of the derivative, y', at the knots. The Pchip interpolation can correctly reflect both the shape and trends of the data points. Compared with spline interpolation, it is more applicable for interpolating transient pressure and temperature data.

Figure 4-8 shows the interpolation results of transient temperature and pressure data by using four different approaches. Two representative time regions were selected from a set of transient PDG field data. In the first and third plots of temperature data, both the nearest approach and the spline approach produce inconsistent results. However, the linear and pchip methods give more reasonable interpolations, while in the second and fourth plots of pressure data, only the spline approach represents relatively weak interpolations. It is notable that in the second transient region, as shown in plots three and four, an outlier and a nearby gap (lack of original data) are illustrated from 87.75 to 87.9 hours. In this circumstance, the interpolation produces more outlier data points which are incorrect. Therefore, some researchers suggest removing outliers without interpolating the data, as described by Athichanagorn et al. (1999).

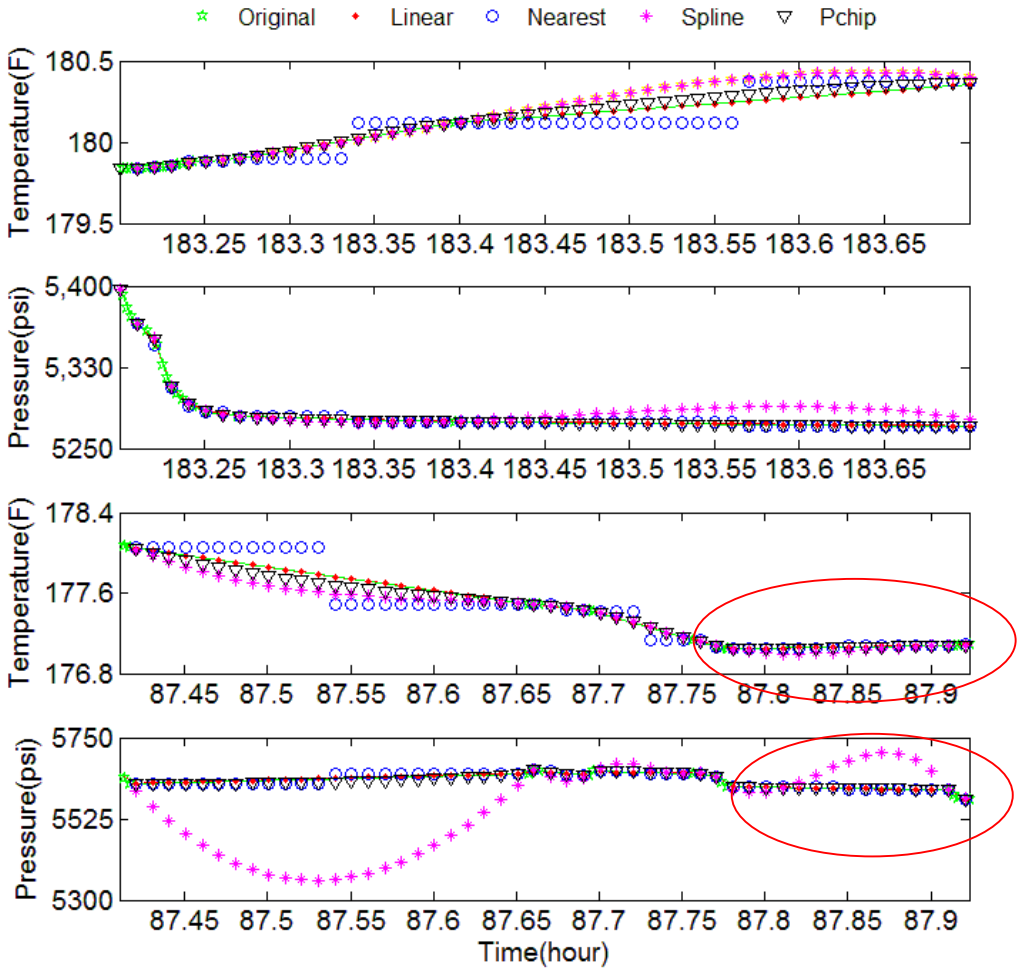

Figure 4-8：Interpolation of two sets of transient temperature and pressure data

4.3.2 De-noising

Noise is a small but high frequency fluctuation which is commonly seen in PDG pressure and temperature data. It can not only affect the transient identification, but also cause inaccurate well testing interpretation. De-noising is a good way to avoid noise effect by reducing the fluctuation and scattering to extract the main feature of the data (Wang and Zheng, 2012). The first step of de-noising is selecting original wavelet and scale level for decomposing. After wavelet decomposition, the high frequency sub-bands (detail coefficients) contain most of the noise information and little signal information, so we can remove the small fluctuations in detail signal and reconstruct the de-noised data. There are two kinds of thresholding methods:

Hard thresholding can be described as the usual process of setting to zero the elements whose absolute values are lower than the threshold. The hard threshold signal is x, if x is greater than the threshold, and is 0 if x is less than or equal to the threshold.

Soft thresholding is an extension of hard thresholding, first setting to zero the elements whose absolute values are lower than the threshold, and then shrinking the nonzero coefficients towards 0. The soft threshold signal changes the magnitude if x is greater than the threshold (Matlab^{TM} function: $Soft(Y) = sign(x)(|_x| - thr)$), and is 0 if x is less than or equal to the threshold.

As recommended by Kikani and He (1998), in order to avoid discontinuities which arise in the hard thresholding method, the figures below present the de-noised transient pressure and temperature data that are smoother and better for analysis by applying soft thresholding. The de-noising procedure is as follows:

- Firstly, the original signal of Figure 4-1 is decomposed into three level signals with the Haar wavelet
- Then, the fixed soft threshold is selected, as shown in Figure 4-9 and Figure 4-10
- Thirdly, the threshold is applied for the detail coefficients for each level from one to three
- Finally, the temperature and pressure signals are reconstructed by using the original approximation coefficients of level three and the modified detail coefficients of levels from one to three

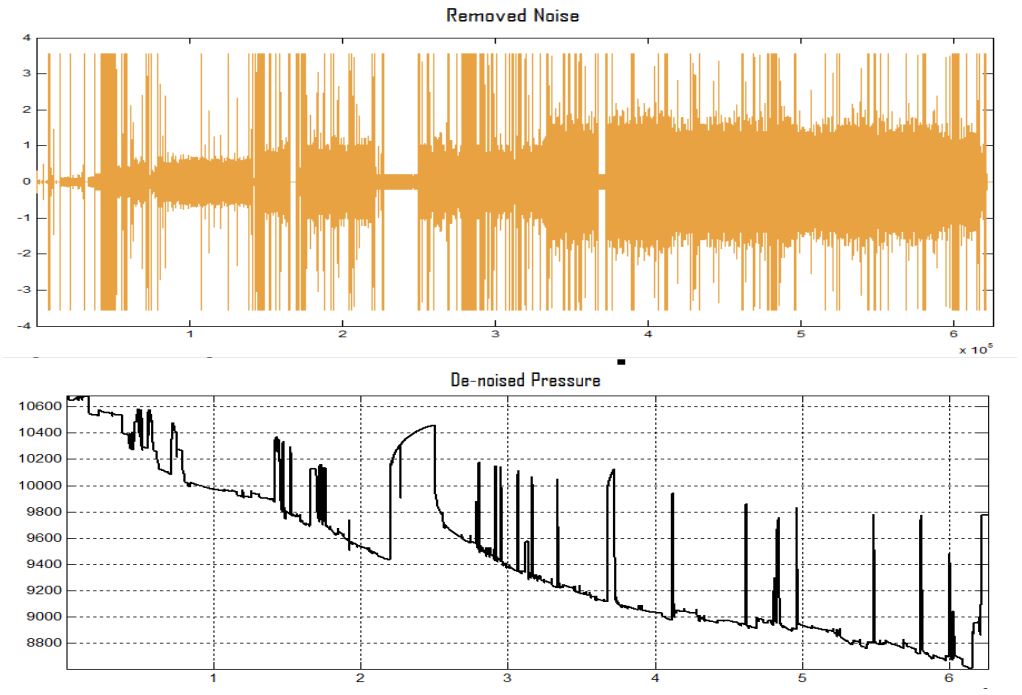

Figure 4-9：Removed noise signal and de-noised pressure data through soft thresholding method

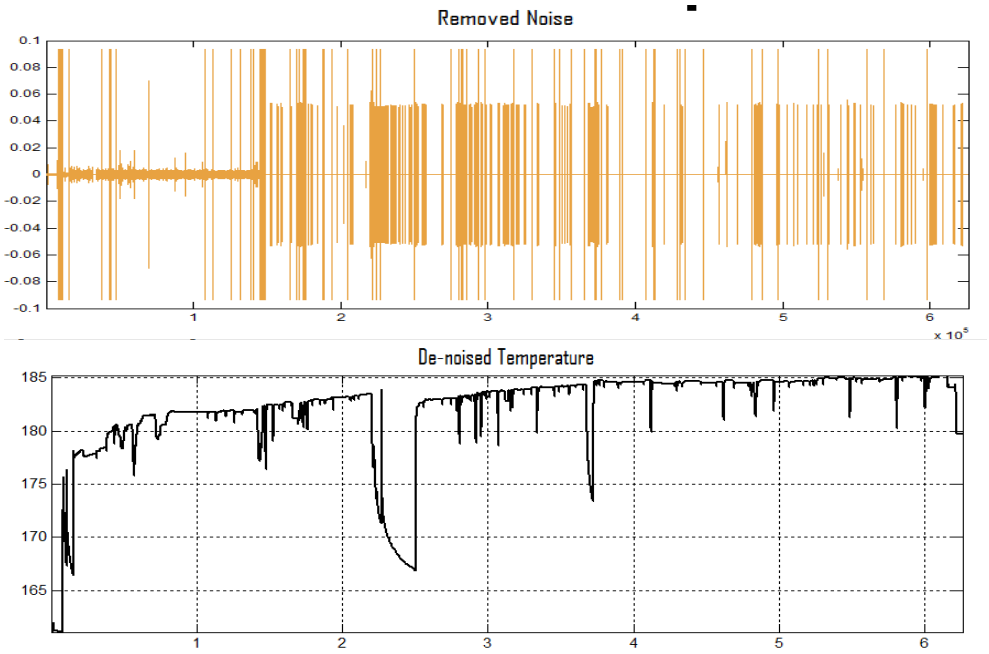

Figure 4-10：Removed noise signal and de-noised temperature data through soft thresholding method

4.4. Transient identification by using temperature and pressure data together

As explained in previous sections, the wavelet based data processing algorithm analyzes the temperature and pressure changes within unit time interval. In this section, the simplest Haar wavelet transform is utilized to identify the transient periods that are divided by flow-rate changes. In order to test the performance of the wavelet transform and determine the biggest differences between transient temperature and pressure data, two sets of synthetic data were generated by using the fully coupled reservoir-wellbore model, as discussed in Chapter 3. In addition, a field application of transient-identification-based outliers and aberrations (non-signal data) removal method is also demonstrated in this section.

4.4.1 Application of synthetic data, base case one - single phase gas production

In this case, a single phase, high flow-rate gas production well is simulated. Table 4-2 shows the fluid, thermal and reservoir parameters of the homogeneous and single phase reservoir model. The gas formation volume factor (FVF) and viscosity (ignoring temperature influence as the variation of temperature is relatively small) vary a lot with the pressure change, especially when the pressure is low, as illustrated in Table 4-1. Consequently, in this synthetic model of a shallow gas reservoir which located at the depth of 1500 ft, the influence of the pressure-dependent fluid properties can be expanded due to the relatively low reservoir pressure of 725 psi.

Table 4-1： Pressure-dependent gas formation volume factor (FVF) and viscosity (100 °F); these initial input fluid properties are linearly interpolated for simulation

Pressure/psi	FVF (rb/Mscf)	Viscosity/cp
362.5	5.509	0.0143
725	2.028	0.0149
1087.5	1.014	0.0161
1450	0.809	0.0172
1812.5	0.727	0.0184
2175	0.686	0.0196
2900	0.665	0.0207
3625	0.652	0.0241

Table 4-2：Fluid, wellbore, reservoir parameters and thermal parameters used in the synthetic model

Parameter	**Value**
Initial reservoir pressure, p_i	725 psi
Reservoir thickness, h	98.4ft
Permeability, k	Kx=ky=20md, kz=1md
Porosity, $\emptyset$	0.3
Rock compressibility, C_t	3.45e-5 1/psi
Well radius, r_w	0.328ft
Skin factor, s	3
Fluid thermal conductivity, λ_f	0.003 W/m.K
Fluid heat capacity, C_f	2 kJ/kg.K
Rock thermal conductivity, λ_r	5.0 W/m.K
Rock heat capacity, C_r	750 J/m^3.K
Joule-Thomson coefficient, C_{JT}	6.9e-3 K/psi
Adiabatic expansion coefficient, η	5.5 K/psi

Figure 4-11 shows the simulation results of transient temperature, pressure and flow-rate data. The production history was the input dataset, the temperature and pressure were generated at 200 feet above pay zone and treated as bottom-hole data. Other wellbore parameters, such as the overall heat transfer coefficient and the thermal conductivity coefficient, are the same as the synthetic data used in Chapter 3. It is well known that compared with liquid flow, gas flow in porous media has more complex characteristics due to the lower viscosity, lower density, higher compressibility and other pressure-dependent gas properties. In another words, the particularities of a gas production case are caused mainly by the effects of gas compressibility, non-Darcy flow, non-isothermal flow and slippage. Figure 4-12 demonstrates the processed production history, temperature and pressure data. The red marks stand for the flow-rate increase events and the green marks represent the flow-rate decrease events. The identified larger amplitude of detail coefficients are consistent with the locations of the singularities on the time axis, which means that both pressure and temperature changes can diagnose flow events by

using wavelet transform. Figure 4-13 shows the breakpoint locations (when the flow-rate changes) on the original data set. The relationship between WT amplitudes and flow-rate changes will be discussed in the next section.

It should be pointed out that the true breakpoint locations are illustrated precisely and exactly in this synthetic case, because all of the temperature, pressure and flow-rate data are generated without noise. It is not difficult to choose a proper level (small scale e.g. one, two or three) of decomposition, which is driven mainly by the interpreters' prior knowledge of the noise level estimation for the original signal de-noising. In addition, unlike the processed pressure and flow-rate data, the transformed temperature signal demonstrates two opposite amplitudes for every flow event. This is because of the specific behaviour of temperature during the early time of flow-rate change, which will be discussed in detail in the next sections.

Simply put: The earlier WT detail amplitudes correspond to the breakpoints which are caused by flow events, and the later WT detail coefficients respond to flow-rate change.

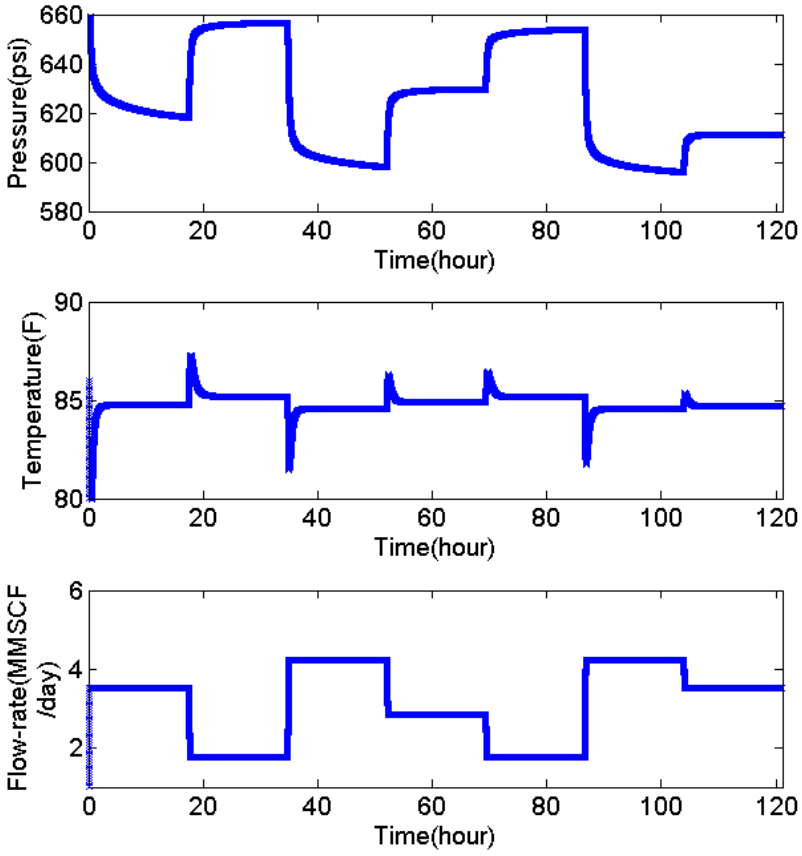

Figure 4-11：Simulated synthetic pressure, temperature and flow-rate data for gas production case

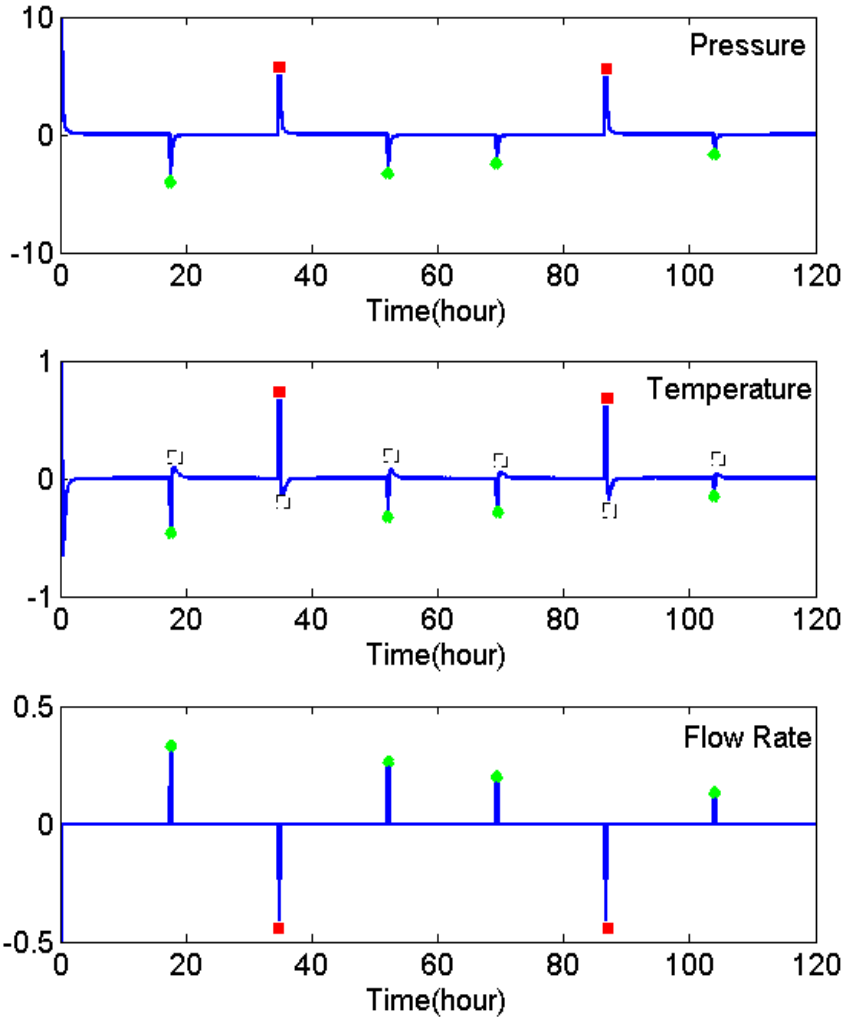

Figure 4-12：Transient data processed by wavelet transform and detected breakpoint locations for gas production case

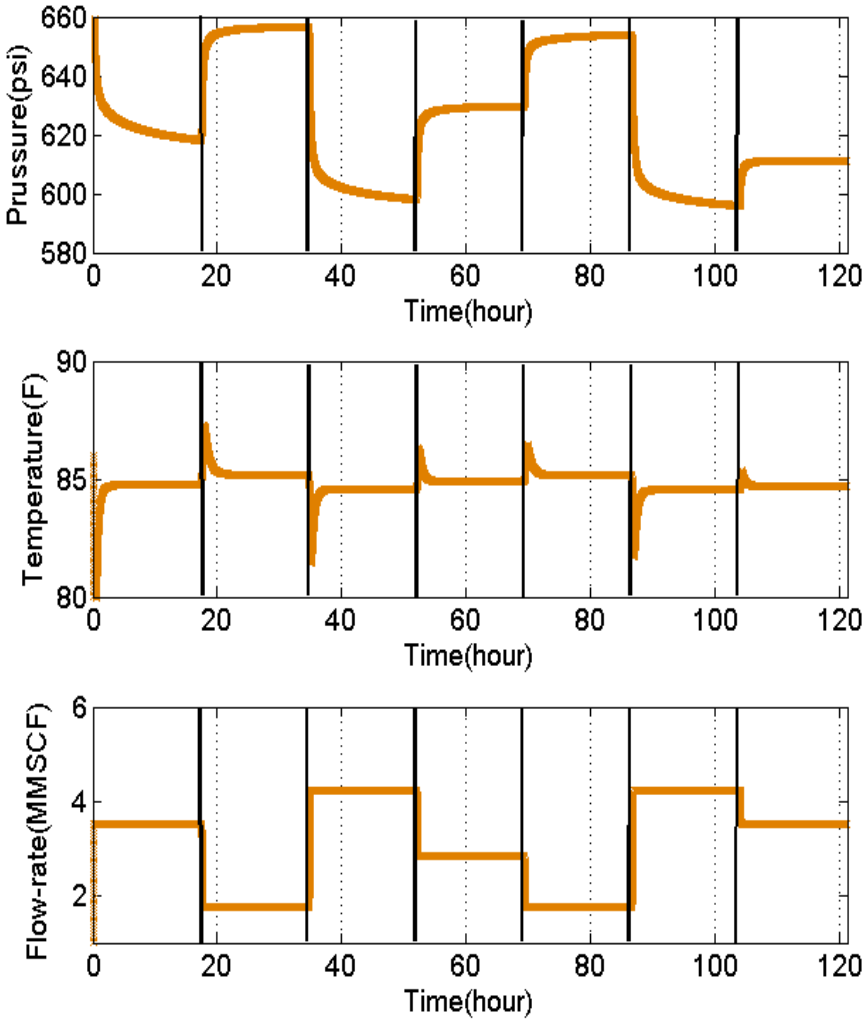

Figure 4-13：Detected breakpoint locations in the synthetic data for gas production case

The performance of the wavelet transform in transient identification is presented quantitatively in Table 4-3 which shows the detailed locations of the breakpoints in temperature, pressure and flow-rate plots respectively. In summary, the results are acceptable and this algorithm is able to locate the points of flow-rate change from both temperature and pressure signals.

Table 4-3：Detected breakpoint locations vs. true breakpoint locations and summary of performance of wavelet transform for the gas production case (level 3)

True Time/h		Flow-rate	Pressure	Temperature (earlier)	Temperature (later)
True Time= Rate Change Location (Data point counter)*Time Step	0	0	0	0	0.41
	17.47	17.47	17.47	17.47	17.95
	34.75	34.75	34.75	34.75	35.23
	52.03	52.03	52.03	52.03	52.51
	69.31	69.31	69.31	69.31	69.79
	86.59	86.59	86.59	86.59	87.07
	103.9	103.9	103.9	103.9	104.4
Summary		Very Good	Very Good	Very Good	

4.4.2 Application of synthetic data, base case two - single phase oil production

Single phase oil production is simulated in the second base case. Table 4-4 shows the fluid, wellbore, reservoir and thermal parameters used for generating the synthetic down-hole transient data. Particularly, there are no pressure-dependent fluid parameters and the oil thermal expansion coefficient is very small.

Table 4-4：Fluid, wellbore and reservoir parameters used in the synthetic model

Parameter	**Value**
Initial reservoir pressure, p_i	2900 psi
Permeability, k	100 md
Porosity, $\emptyset$	0.2
Total compressibility, C_t	6.89e-6 1/psi
Well radius, r_w	0.328 ft
Viscosity, μ_t	3 cp
Joule-Thomson coefficient, C_{JT}	2.76e-3 K/psi
Adiabatic coefficient of expansion/compression, η	9.65e-4 K/psi
Fluid thermal conductivity, λ_f	0.3 W/m.K
Fluid heat capacity, C_f	1500 J/kg.K
Fluid thermal expansion coefficient, β	N/A, can be ignored in slightly compressible fluid flow
Rock thermal conductivity, λ_r	7 W/m.K
Rock heat capacity, C_r	750 J/kg.K

Figure 4-14 illustrates the plots of simulated pressure, temperature and flow-rate data at 100 ft above the pay zone; the data are pure without any noise. The gauge location is closer to the production layer than that in the synthetic gas production case.

Figure 4-15 is a set of plots for the wavelet transformed down-hole transient data, and Figure 4-16 shows the plots of the breakpoint locations on the original synthetic data. Similarly to the marking method in synthetic case one, the red marks stand for the two flow-rate increase events and the green mark represents another flow-rate decrease event. According to these figures, the identified peaks (WT amplitude) are consistent with the locations of the breakpoints which are caused by flow events. In addition, as illustrated in Table 4-5, the exact locations of the flow-rate change can be diagnosed by either processed temperature or pressure data.

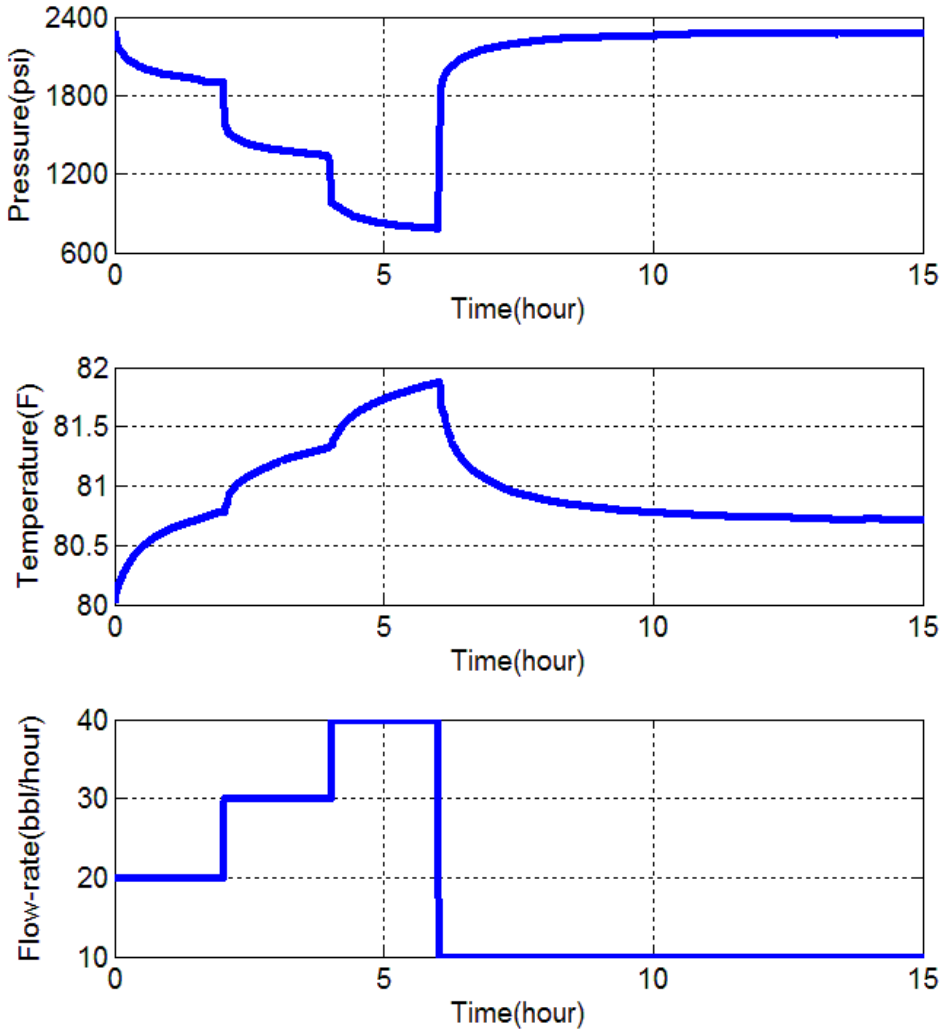

Figure 4-14：Simulated synthetic pressure, temperature and flow-rate data for oil production case

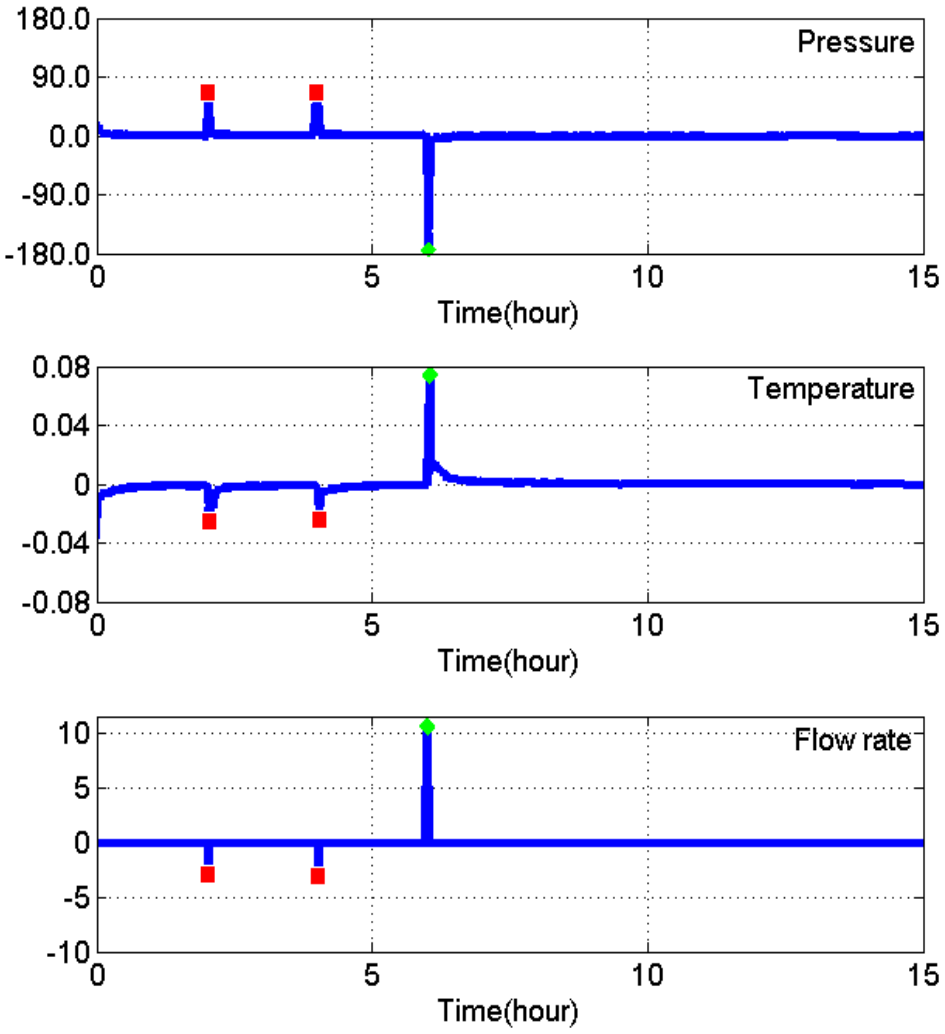

Figure 4-15：Transient data processed by wavelet transform and detected breakpoint locations for oil production case

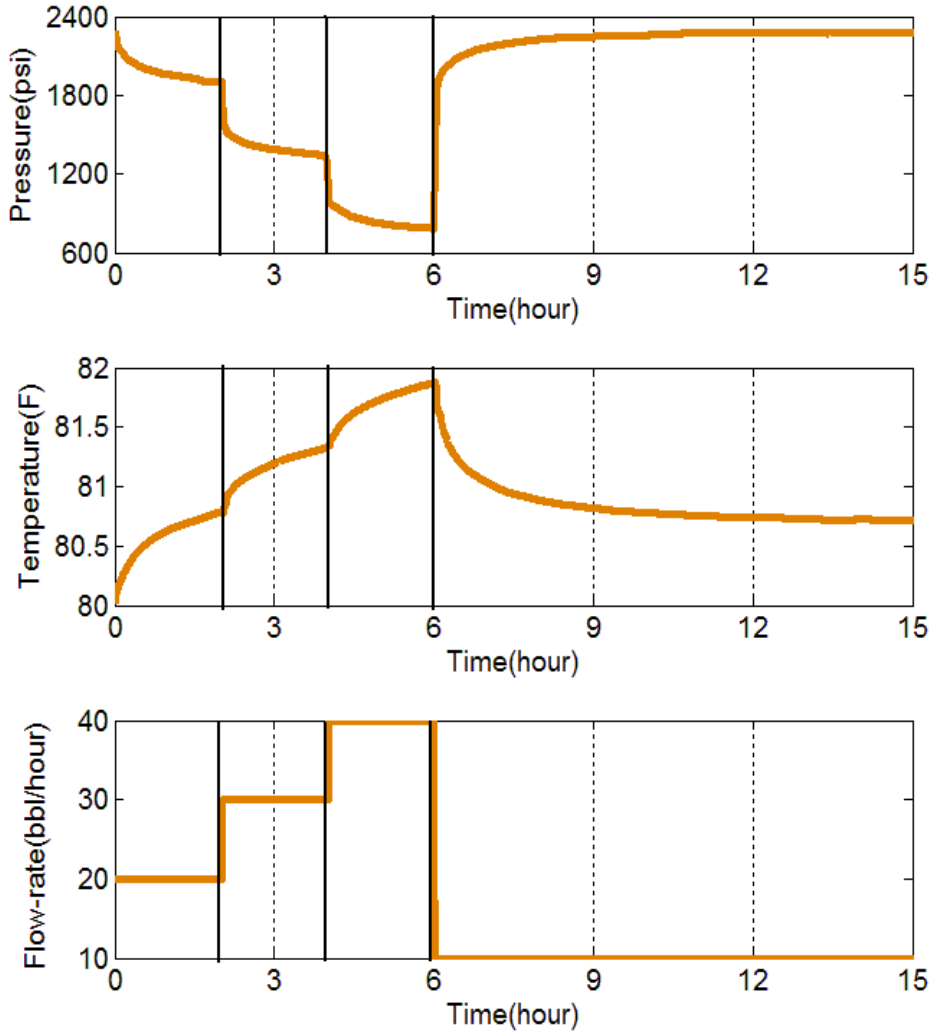

Figure 4-16：Detected breakpoint locations in the synthetic data of oil production case

Table 4-5：Detected breakpoint locations vs. true breakpoint locations and summary of performance of wavelet transform for the synthetic oil production case (level 3)

True Time/h		Flow-rate	Pressure	Temperature
True Time = Rate Change Location (Data point counter)*Time Step	0	0	0	0
	2.00	2.00	2.02	2.04
	4.00	4.00	4.00	4.00
	6.00	6.00	6.02	6.04
Summary of performance		Very Good	Good	Good

4.4.3 Field application and transient-identification-based outliers removal method

A set of long-term field PDG data was collected from an oil reservoir, with lots of flow events (dozens of shut-in and draw-down periods) over a period of 10,000 hours. Figure 4-17 presents a subset of the entire field transient pressure and temperature data. The data used for interpreting have been interpolated and resampled to keep the time intervals coincident, and the original non-uniform frequency, which ranges from several hours to sixty seconds, was increased/decreased to six minutes.

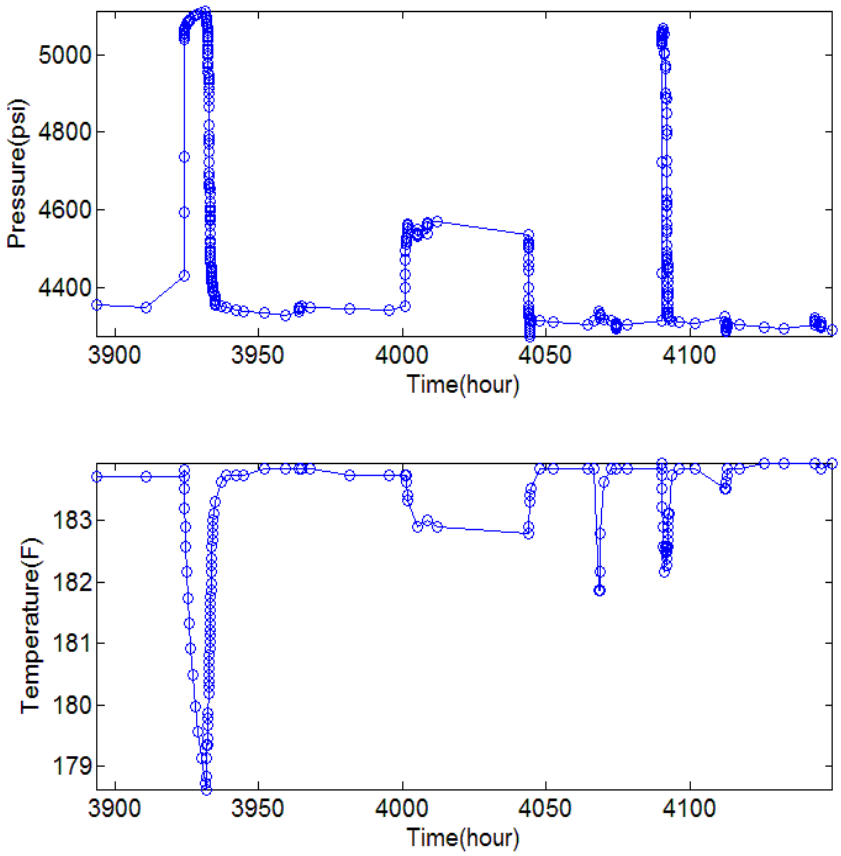

Figure 4-17：Original field data: pressure and temperature measurements

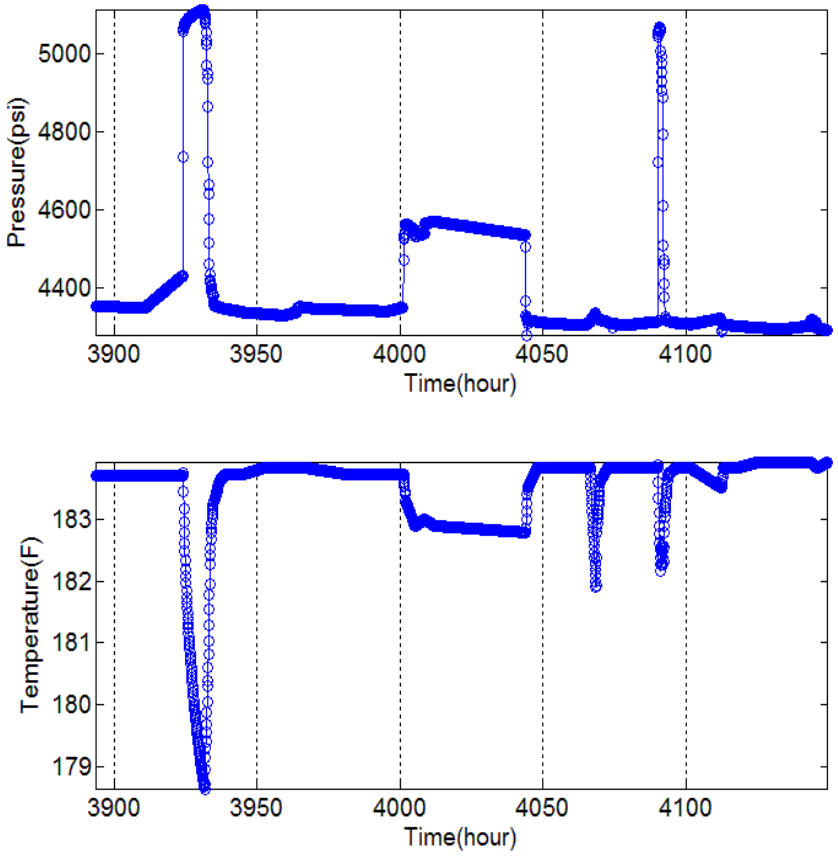

Figure 4-18：Interpolated field data: pressure and temperature

Transient Identification

As described in preceding sections, the first step is using the wavelet transform algorithm to locate the points of flow-rate change. The possible outliers and aberrant sections can be detected by integrally interpreting the transient down-hole data. In this case, the detailed flow-rate data is not available; the identification would therefore be constrained by temperature and pressure data only.

Figure 4-19 shows the breakpoints by calculated using the wavelet transform. Figure 4-20 demonstrates the combined interpretation of temperature and pressure data: the identified true transients have been extracted and marked. Because the errors in one dataset are not statistically expected to appear in another measurement, the agreement between temperature detected breakpoints and pressure detected breakpoints verified six flow events. The interpretation results which disagree with each other are treated as possible outliers which could be corrected.

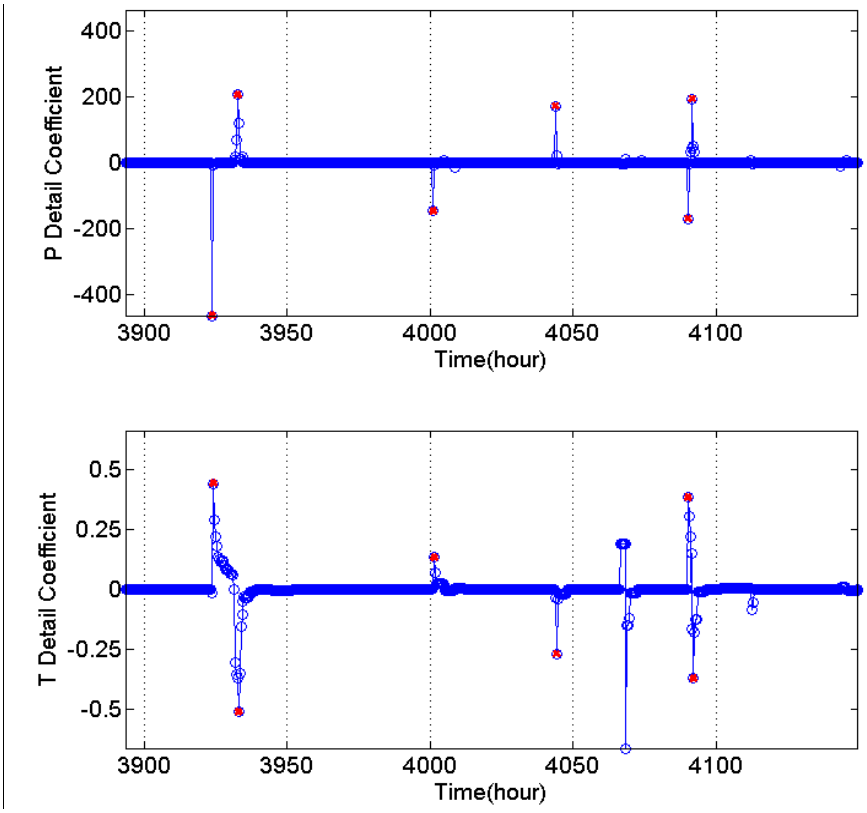

Figure 4-19：Processed transient data and detected breakpoint locations

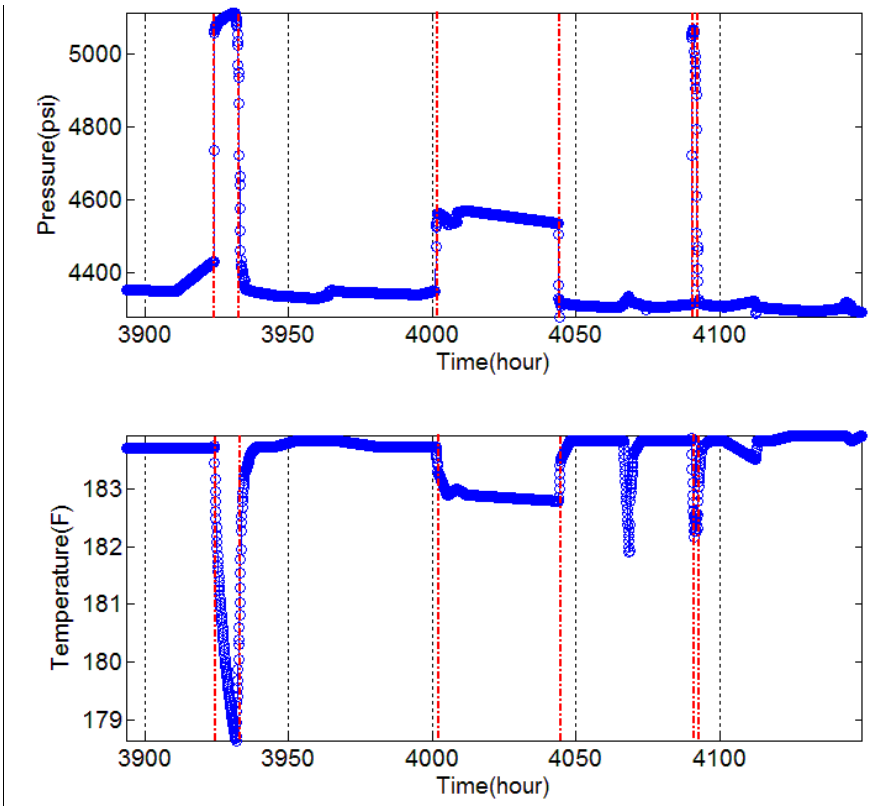

Figure 4-20：Combined interpretation of temperature and pressure data - identified true flow events

Detection and Removal of Outliers

Figure 4-21 shows the plots of outliers detected in the pressure and temperature data, as marked by the red ellipses; there is one set of continuous outliers in the transient pressure data and another set of outliers can be observed in the temperature data.

Strictly speaking, these potential outliers should not be removed directly, because transient identification is mainly a diagnostic but not correction approach. However, in this field case, simply removing those bad points is feasible because only a relatively small portion of the real data needs to be cut off.

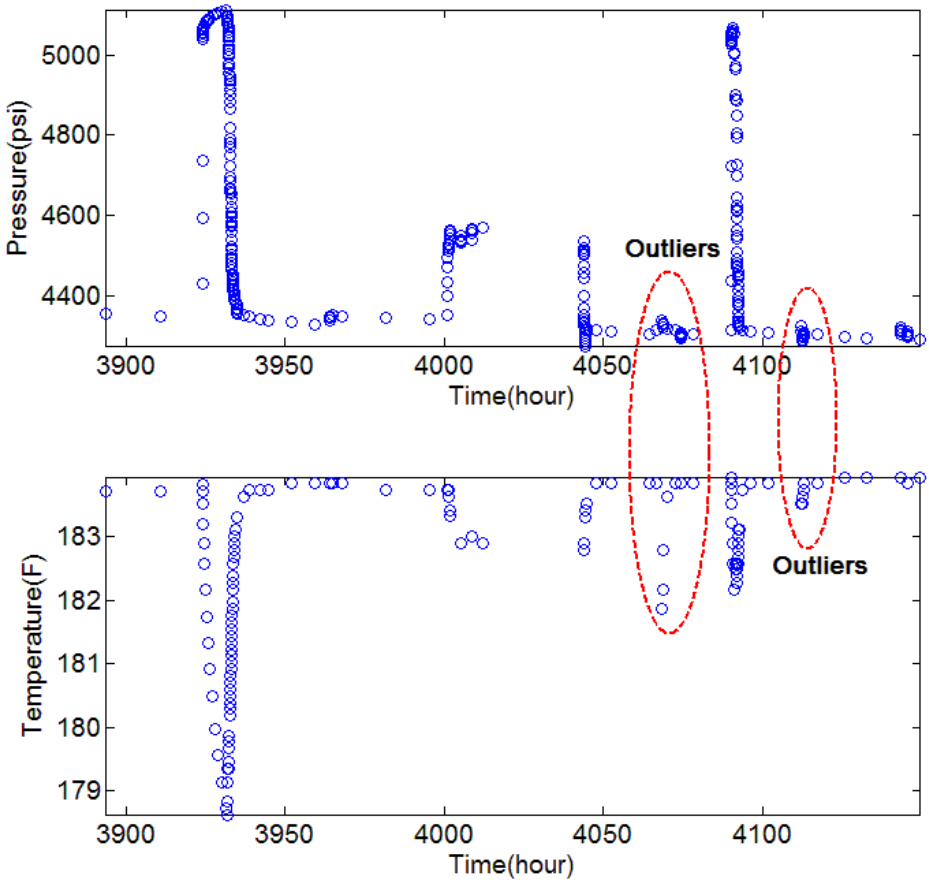

Figure 4-21：Detected outliers in the field pressure and temperature data

4.5. Relationship between WT amplitude and rate change – improved diagnostic method for reservoir-well nonlinearity from transient temperature and pressure data

Through the utilization of the wavelet transform, an improved nonlinearity diagnostic method is described in this section. It is well known that nonlinearities are caused by variations of reservoir properties, fluid characteristics and wellbore conditions. In this study, those nonlinear related effects such as non-Darcy gas flow, time-dependent skin, reservoir permeability change can be diagnosed from either transient pressure or transient temperature data.

This improved diagnostic method can ensure the correct application of conventional pressure-transient-analysis (PTA) methods, which are mostly based on the linearity assumption. By integrally interpreting the transient pressure and temperature data, the uncertainties of pressure analysis can also be reduced. If the detected nonlinearity is low, displayed as a little-changed value of the unit-rate-change coefficient ($A_{urc} = \text{WT detail coefficient}/\Delta q$), during a certain time region, the production case can be approximately treated as a linear system. However, for the pressure and temperature data with high nonlinearities, numerical methods are recommended to be used, as described in Chapter 3. In addition, this improved nonlinearity diagnostic method is an important step in the novel transient temperature analysis procedure which will be discussed in Chapter 5.

4.5.1 Theory description

PDG transient temperature and pressure history consist of many flow events, which can be divided into different flow regimes. The flow-rate variations cause the changes in temperature and pressure data, and these transient data can be processed by wavelet transform and displayed as different amplitudes on the time axis. Therefore, the properties of a reservoir-well system may be detected if a constant of proportionality exists between the WT detail coefficients and the corresponding flow-rate changes.

Pressure behaviour

Taking a simple linear system for example, the pressure change during the impulse time Δt (between two different flow-rate) is:

$$\mathrm{P}_n - \mathrm{P}_{n+1} = (\mathrm{q}_{n+1} - \mathrm{q}_n) \int_0^{\Delta \mathrm{t}} g(\tau) d\tau + \sum_{i=1}^{n} (\mathrm{q}_i - \mathrm{q}_{i-1}) \int_{\mathrm{t}_n - \mathrm{t}_{i-1}}^{\mathrm{t}_n - \mathrm{t}_{i-1} + \Delta \mathrm{t}} g(\tau) d\tau$$

The first term on the right side stands for the flow-rate change effect and the second term on the right side represents the production history effect.

If the impulse time Δt is much smaller than the steady production history time, it is safe to ignore the production history effect. Thus the relationship between processed pressure (amplitude A_P is proportional to the pressure change) and flow-rate change is expressed as (Zheng and Wang, 2011):

$$\mathrm{A}_P \propto \Delta \mathrm{q} \int_0^{\Delta \mathrm{t}} g(\tau) d\tau \,, \qquad 4.2$$

where $g(\tau)$ is a time-dependent integration variable, it only depends on the reservoir and well parameters. The quotient of the WT detail coefficient and flow-rate change was named as the Unit Reservoir System Response (URSR) function, and it can be used to diagnose if the system is linear (constant$\frac{\mathrm{A}_P}{\Delta \mathrm{q}}$) or nonlinear (time-varying$\frac{\mathrm{A}_P}{\Delta \mathrm{q}}$).

Temperature behaviour

In this section, the relationship between temperature change and flow-rate change will be discussed in detail.

For a slightly compressible/incompressible linear system, such as the single oil production case, the adiabatic fluid compression and expansion effects which dominate the early time temperature behaviour can be safely neglected. Otherwise, the heat transfer in the nonlinear gas production case will be described separately.

The Joule-Thomson coefficient is defined as temperature change per unit pressure at constant enthalpy, as illustrated below:

$$C_j = (\frac{\Delta T}{\Delta P})_H \quad 4.3$$

For a production well, the temperature and pressure change can be expressed as the differences between reservoir transient data (Tr,Pr) and the gauge measurements (Tg, Pg):

$$C_j = (\frac{T_r - T_g}{\overline{P_r} - P_g})_H \ , \quad 4.4$$

where $\overline{P_r}$ stands for the average reservoir pressure in pseudo-steady state and P_g represents the measured down-hole pressure.

If the pay zone (perforations) is close to the gauge location, the heat transfer between the wellbore and the formation can be neglected. Therefore, the assumption of Joule-Thomson isentropic is valid (Wu et al., 2013). In other words, the perforations act as a throttle which causes the fluid temperature changes due to the Joule-Thomson effect.

For transient flow and semi-steady state conditions, the rate can be defined as (Dake 1983) :

$$\mathrm{q} = \frac{4\pi kh}{\mu\left(ln\frac{4A}{\gamma C_A {r_w}^2} + 2S\right)}(\overline{P_r} - P_g) \quad 4.5$$

$$\left(\overline{P_r} - P_g\right) = \frac{q*\mu\left(ln\frac{4A}{\gamma C_A {r_w}^2} + 2S\right)}{4\pi kh} \quad 4.6$$

where S is the van Everdingen mechanical skin factor, C_A is the Dietz shape factor (Dietz 1965) which depends on the shape of area and position of well, A represents the reservoir area, $\gamma = e^{0.5772} = 1.781$ and 0.5772 is Euler's constant.

Eq. 4.4 can be rewritten as:

$$T_r - T_g = \frac{q*\mu*C_j\left(ln\frac{4A}{\gamma C_A {r_w}^2} + 2S\right)}{4\pi kh} \quad 4.7$$

For linear systems, the reservoir and fluid properties, such as permeability, porosity, viscosity and the Joule-Thomson coefficient are regarded as constant. In addition, the skin

factor is much more stable than the flow-rate, and it can last as long as several weeks, which is longer than the time for the flow-rate and temperature changes. If the well produces at constant flow-rate $q1$ for $t1$ time; and then, after a very small time, Δt, the flow-rate changes to $q2$; the reservoir temperature is assumed constant during the small time Δt. The first measured temperature is:

$$T_{g1} = T_r - \frac{q_1 * \mu * C_j \left(ln \frac{4A}{\gamma C_A {r_w}^2} + 2S \right)}{4\pi kh} \tag{4.8}$$

The second measured temperature is:

$$T_{g2} = T_r - \frac{q_2 * \mu * C_j \left(ln \frac{4A}{\gamma C_A {r_w}^2} + 2S \right)}{4\pi kh} \tag{4.9}$$

Therefore, the unknown reservoir temperature can be eliminated, and Eq. 4.7 is rewritten as:

$$T_{g2} - T_{g1} = (q_1 - q_2) * \frac{\mu * C_j \left(ln \frac{4A}{\gamma C_A {r_w}^2} + 2S \right)}{4\pi kh} \tag{4.10}$$

For n flow periods, the same procedure may be easily adapted to obtain the temperature change during the final impulse time Δt:

$$T_{gn} - T_{g(n-1)} = (q_{n-1} - q_n) * \frac{\mu * C_j \left(ln \frac{4A}{\gamma C_A {r_w}^2} + 2S \right)}{4\pi kh} \tag{4.11}$$

Simplified as:

$$\Delta T_g = \Delta \mathrm{q} * \mathrm{X} \ , \tag{4.12}$$

$$\text{where } \mathrm{X} = -\frac{\mu * C_j \left(ln \frac{4A}{\gamma C_A {r_w}^2} + 2S \right)}{4\pi kh} \tag{4.13}$$

As presented in the previous sections, both pressure changes and temperature changes between two continuous flow periods can be diagnosed and identified by the wavelet transform detail coefficients. For the wavelet processed transient temperature data in a

linear system, the amplitudes are positive for pressure build-up periods and negative for pressure drawdown periods. In addition, the values of those detail coefficients vary with the temperature changes.

The wavelet transform is a linear operation, thus the amplitude A_T is proportional to the measured temperature change ΔT_g :

$$A_T \propto \Delta T_g \tag{4.14}$$

Based on the above descriptions of a linear system, the following conditions are assumed:

- The impulse time Δt between every flow-rate change is extremely small and the entire production time is large;
- The reservoir properties such as permeability, porosity, drainage area and reservoir thickness are constant during production;
- The flow condition is steady with time and unchangeable;
- Fluid viscosity and the Joule-Thomson coefficient are treated as constant and can be measured in the laboratory;

Combining Eq. 4.12 and Eq. 4.14:

$$A_T \propto \Delta \mathrm{q} * \mathrm{X} \tag{4.15}$$

Eq. 4.15 establishes a relationship between the amplitude A_T and flow-rate change, and X is an unchangeable term for linear systems.

Therefore, the amplitudes of the wavelet transformed detail coefficients A_T caused by unit-rate-change can be written as:

$$\mathrm{A}_{Turc} = \frac{A_T}{\Delta \mathrm{q}} \qquad (\mathrm{A}_{Turc} \propto \mathrm{X}) \tag{4.16}$$

Because X depends on reservoir and fluid parameters, any changes which break the previous assumptions can be diagnosed with the A_{Turc} function. In summary, A_{Turc} is

constant with time in linear systems of slightly compressible fluid flow; when there are nonlinearities near the wellbore, A_{Turc} is time-varying.

On the other hand, for fluid flow with large compressibility, the adiabatic fluid compression and expansion effects which dominate the early time, the temperature behaviour should not be ignored. During the early-time region of each flow period, the temperature change follows the pressure change and the earlier amplitudes of the wavelet transformed detail coefficients A_{Tf} caused by unit-rate-change can be written as:

$$A_{Tfurc} = \frac{A_{Tf}}{\Delta q} \propto \frac{\emptyset \beta T}{\overline{\rho C_p}} * \frac{\Delta p}{\Delta q}, \qquad 4.17$$

where A_{Tf} is the earlier wavelet transform detail coefficient, $\emptyset$ is the porosity and β is the fluid thermal expansion coefficient.

Similarly, A_{Tfurc} can also be used as a nonlinearity diagnostic function for fluid flow with large compressibility. The derivation of Eq. 4.17 and more details will be described in the following base case and sensitivity studies.

4.5.2 Oil production base case – linear system

It is apparent that single phase flow of a slightly compressible fluid in a porous medium with constant reservoir-well parameters is a linear system. According to this principle, a previously described single oil production well which is located in a homogeneous reservoir is studied. Figure 4-22 and Figure 4-23 show the simulated production history, pressure and temperature data.

Figure 4-24 and Figure 4-25 show the processed pressure and temperature data by using Haar wavelet transform. According to these two figures, not only the pressure change caused by flow events (flow-rate change), but also the temperature change between successive flow periods can be identified and quantified by the WT detail coefficients.

In order to reconstruct the flow-rate history from pressure data, a new function has been defined to calculate the pressure amplitude caused by unit-rate-change:

$$A_{Purc} = \frac{A_p}{\Delta q}$$

Similarly, the temperature amplitude caused by unit-rate-change can be expressed in the same manner:

$$A_{Turc} = \frac{A_T}{\Delta q}$$

As shown in Table 4-6, the calculated unit-rate-change coefficients from processed pressure data and processed temperature data are 5.74 and -0.0024 respectively. Both of the time-constant A_{Purc} and A_{Turc} functions verify the linear system with unchangeable reservoir-well properties.

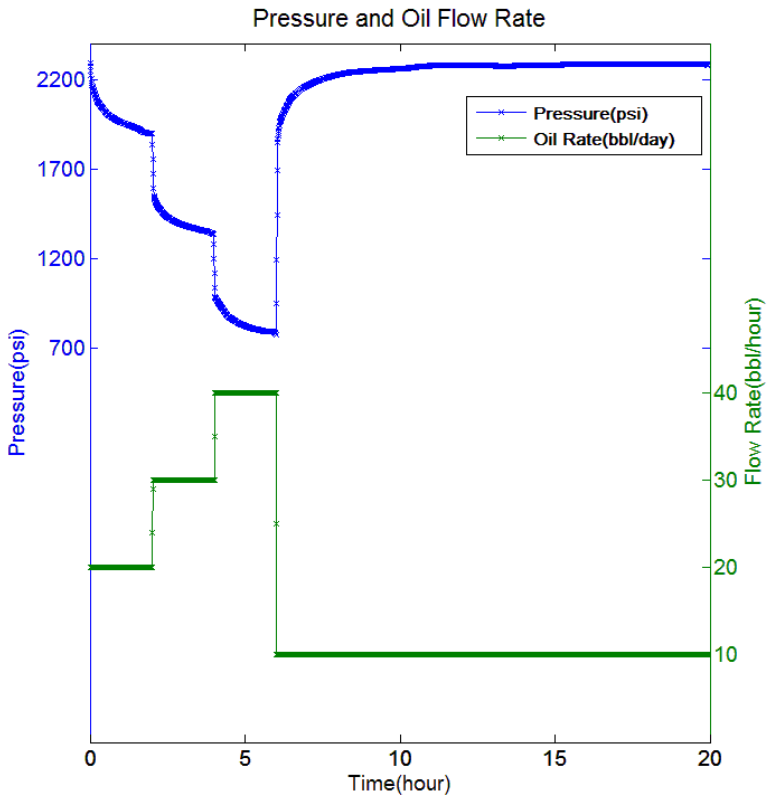

Figure 4-22：Production history and transient pressure data of the single oil phase scenario

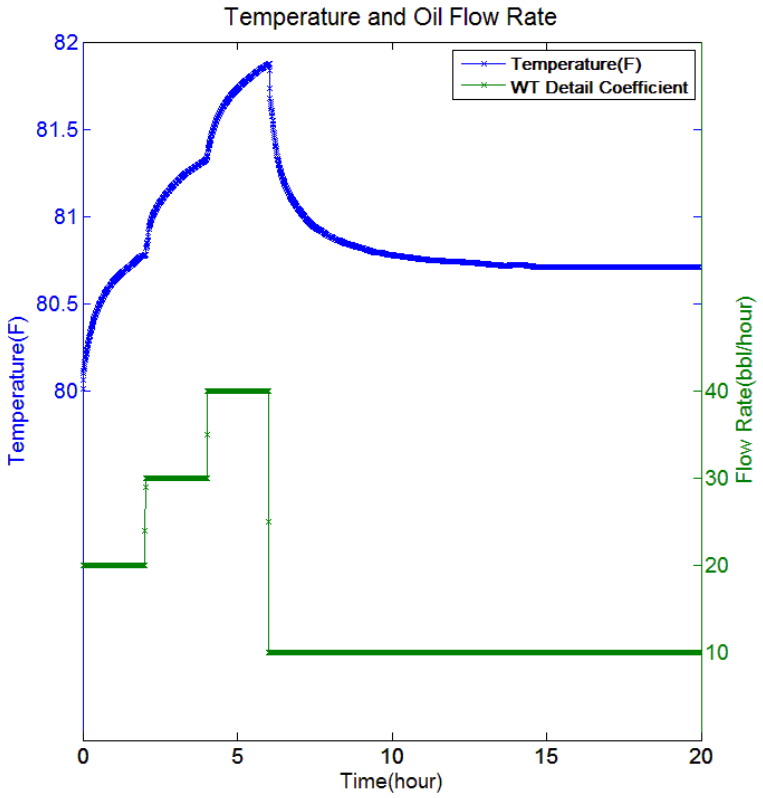

Figure 4-23：Production history and transient temperature data of the single oil phase scenario

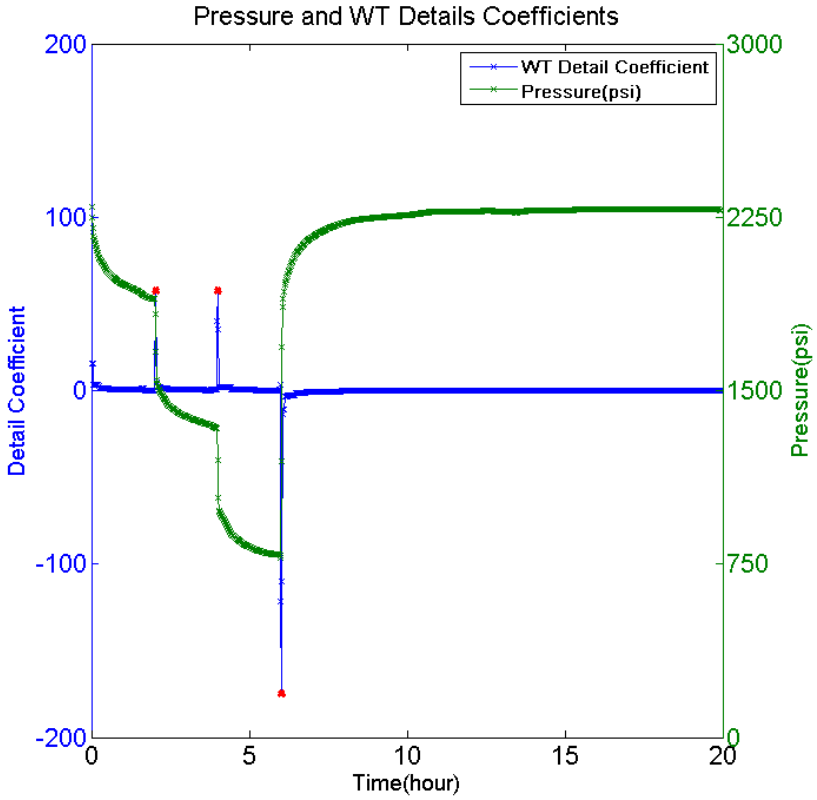

Figure 4-24：Transient pressure data processed by using Haar wavelet transform

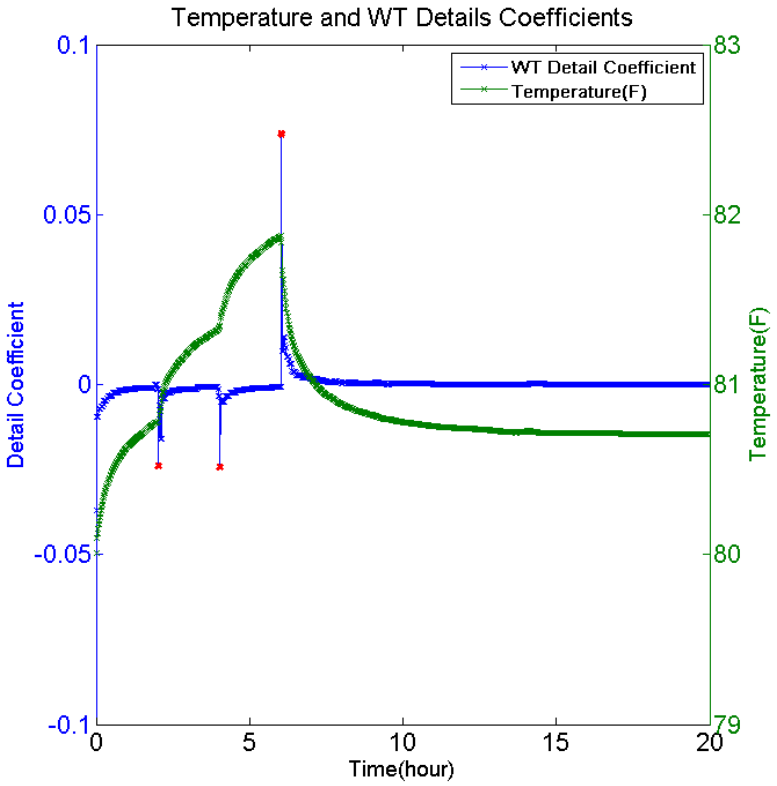

Figure 4-25：Transient temperature data processed by using Haar wavelet transform

Table 4-6：The A_{urc} function (WT Detail Coefficients/△q) calculated from both pressure and temperature data in this single oil synthetic case are almost the same

Pressure				
Time/t (hour)	Rate/q (bbl/hour)	Rate Change/△q (bbl/hour)	WT Detail Coefficients/A_P	$A_{Purc} = = A_P/\triangle$ q
0	20	N/A	N/A	
2.00	30	10	57.43	5.743
4.00	40	10	57.43	5.743
6.00	10	-30	-172.35	5.745
Temperature				
Time/t (hour)	Rate/q (bbl/hour)	Rate Change/△q	WT Detail Coefficients/A_T	$A_{Turc} = A_T/\triangle$ q
0	20	N/A	N/A	
2.00	30	10	-0.0243	-0.00243
4.00	40	10	-0.0243	-0.00243
6.00	10	-30	0.0737	-0.00245

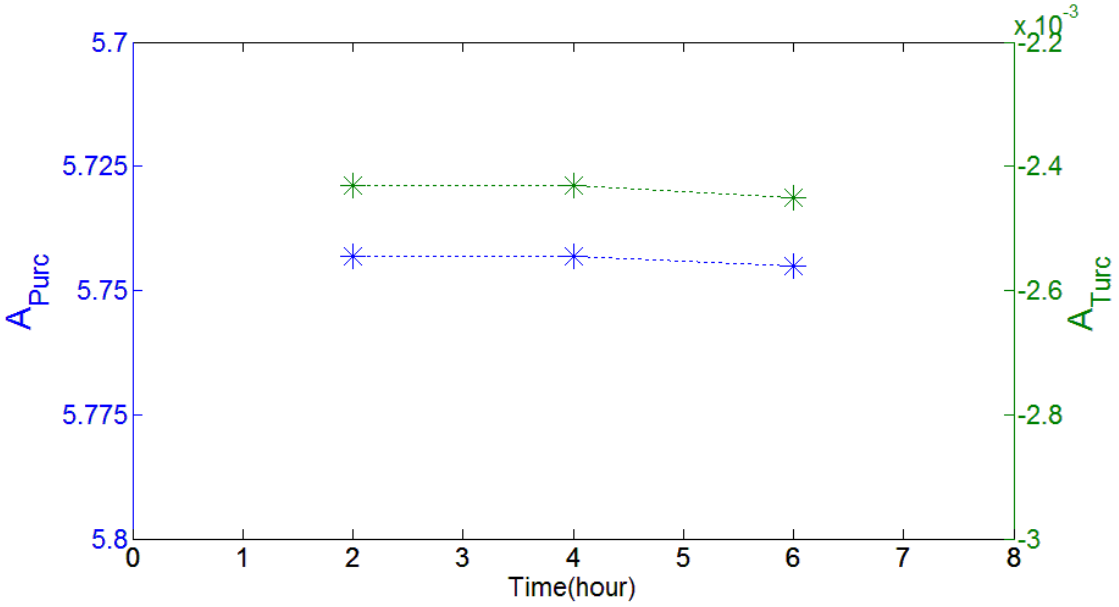

Figure 4-26：Linear system diagnostic from temperature and pressure data: constant value of the unit-rate-change coefficient A_{Purc} and A_{Turc} with time

4.5.3 Gas production base case – nonlinear system

Processed transient pressure data analysis

The flow-rate and down-hole transient pressure data acquired from a previously described gas well is shown in Figure 4-27. Figure 4-28 illustrates the processed pressure data. The WT detail coefficients A_P and unit-rate-change coefficient A_{Purc} are then calculated, as shown in Table 4-7.

Compared with the constant value of A_{Purc} in a single oil production linear system, the unit-rate-change coefficient changes with time in the nonlinear gas reservoir. As illustrated in Figure 4-29, A_{Purc} ranges from 2.229 to 2.308, which reveals the nonlinearity. Taking into account the impact of pressure-dependent fluid properties, the larger variations of unit-rate-change coefficient A_{Purc} maybe caused by the larger production rate, which leads to the down-hole pressure rapidly changing.

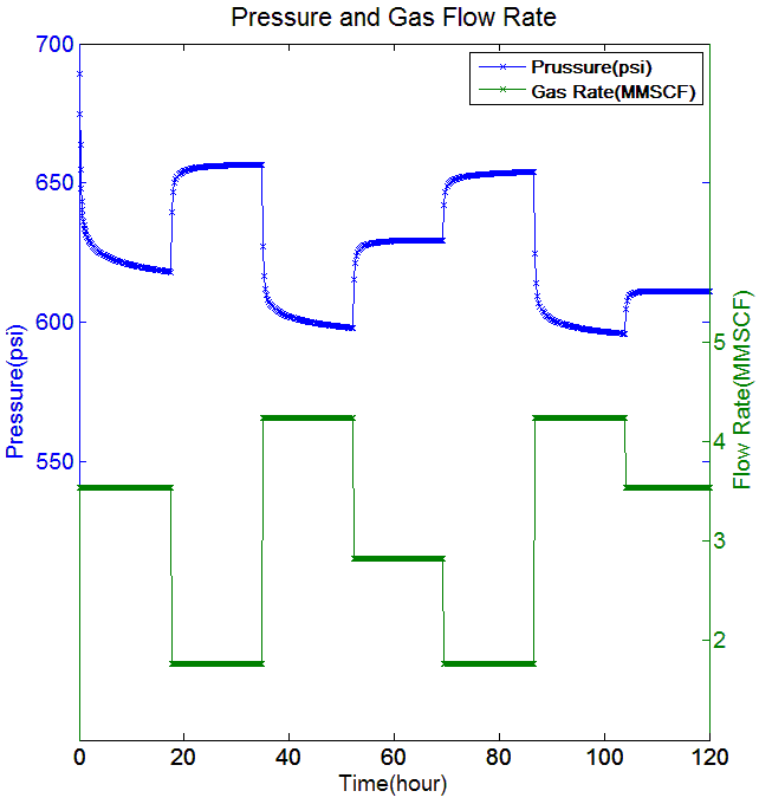

Figure 4-27：Production history and transient pressure data of the single gas phase scenario

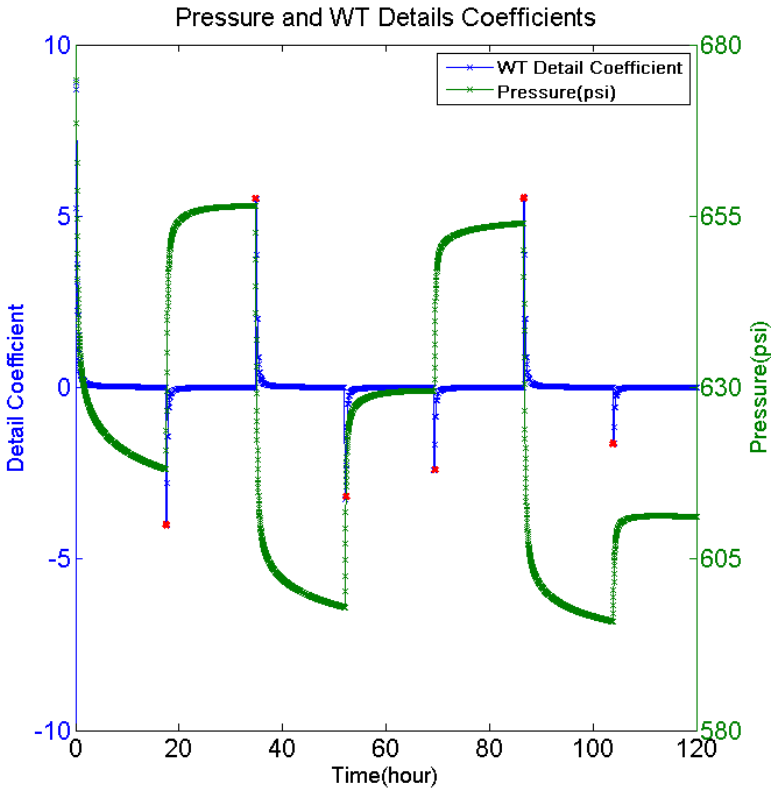

Figure 4-28：Transient pressure data processed by using Haar wavelet transform

The nonlinearities that are caused by reservoir and well properties changing are common in practice. As a result, the linearity assumption becomes invalid, which makes many conventional pressure transient analysis methods not applicable. In order to analyse those nonlinear down-hole pressure data, pseudo-pressure or pseudo-time should be used to linearize the pressure diffusivity equation. Furthermore, it is not easy to establish either isothermal or non-isothermal coupled wellbore-reservoir models and calibrate these models with the time-dependent parameters. Alternatively, transient temperature data can be regarded as another choice to diagnose the nonlinearity and interpret the reservoir.

Table 4-7：The unit-rate-change coefficient A_{Purc} in the gas production case changes with time

Time/t (hour)	Rate/q (MMSCF/day)	Rate Change/△q	WT Detail Coefficients/A_P	$A_{Purc} = = A_P/\triangle q$
0	3.532	N/A	N/A	
17.47	1.766	-1.766	-4.006	2.268
34.75	4.238	2.472	5.511	2.229
52.03	2.825	-1.413	-3.254	2.303
69.31	1.766	-1.059	-2.4	2.266
86.59	4.238	2.472	5.529	2.237
103.9	3.532	-0.706	-1.63	2.309

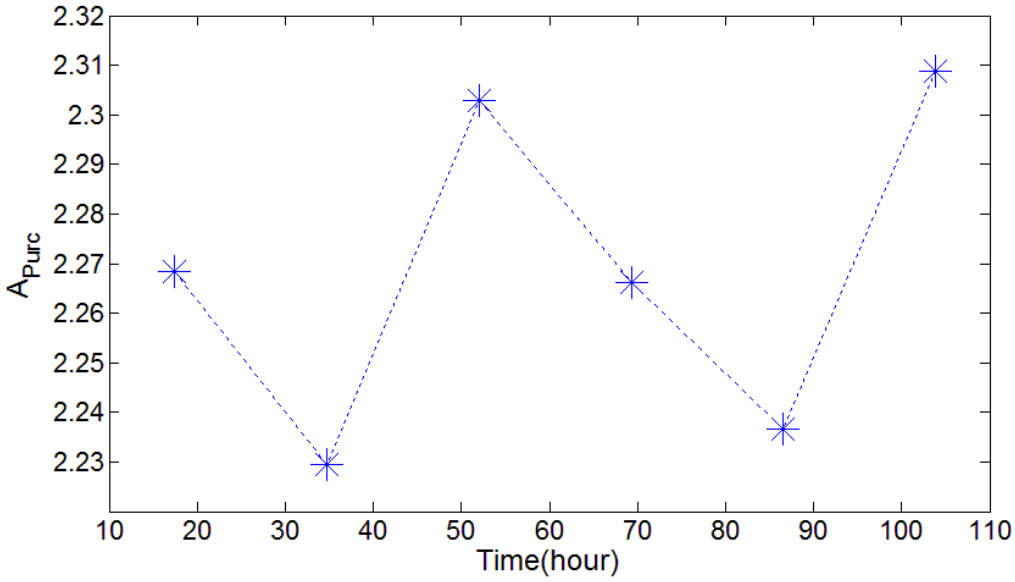

Figure 4-29：Nonlinear system diagnostic from pressure data: variations of the unit-rate-change coefficient A_{Purc} with time

Processed transient temperature data analysis

The down-hole transient temperature data which are correlated with the previously described pressure and flow-rate data are shown in Figure 4-30, and Figure 4-31 presents the processed temperature data. In contrast to the transient temperature performance in the single phase oil production case, in this nonlinear system, temperature first increases or decreases and then it gradually declines or rises. Therefore, the transformed temperature signals demonstrate two opposite amplitudes for every flow event. The earlier/later WT detail coefficients (A_{Tf}/A_{Tl}) and unit-rate-change coefficients (A_{Turc}) are calculated and shown in Table 4-8.

Generally speaking, the earlier WT detail amplitudes A_{Tf} correspond to the breakpoints which are caused by flow events, and the later WT detail coefficients A_{Tl} respond to flow-rate change. Next, the relationships between two kinds of WT amplitudes and flow-rate change are discussed separately.

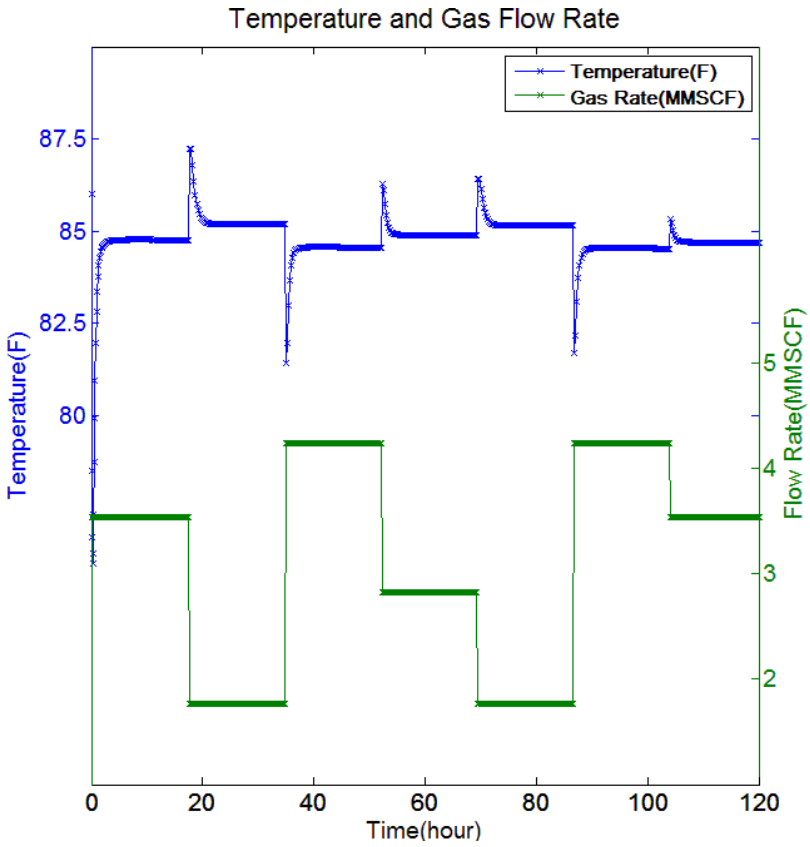

Figure 4-30：Production history and transient temperature data of the single gas phase scenario

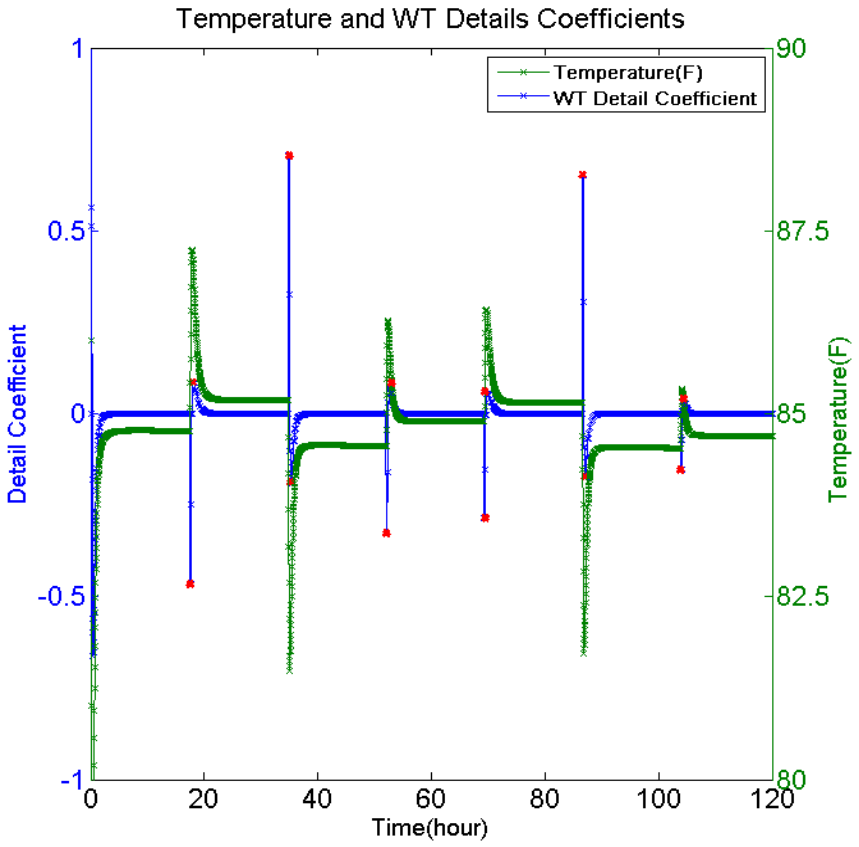

Figure 4-31：Transient temperature data processed by using Haar wavelet transform (gas production case)

For the early-time region (earlier amplitude - first WT detail coefficient)

The energy equation which describes the transient heat transfer in a formation can be notionally summarized as (Maubeuge et al., 1994; Sui and Zhu, 2009):

$$\overline{\rho C_p}\frac{\partial T}{\partial t} - \emptyset\beta T\frac{\partial p}{\partial t} = -\rho v C_p \nabla T + (\beta T - 1)v\nabla p + k_e\nabla^2 T \quad , \qquad 4.18$$

where: v = fluid velocity, β = fluid thermal expansion coefficient, $\emptyset$ = porosity, C_p = mass heat capacity at constant pressure, k_e = thermal conductivity of the formation, $\overline{\rho C_p}$ = average formation property of fluid and rock, $\overline{\rho C_p} = \emptyset\rho_f C_f + (1-\emptyset)\rho_r C_r = C_m$.

During the early region of each flow period (transient temperature data are divided by flow-rate changes), the non-negligible gas compression effect or expansion effect dominates the gauge measured temperature behaviour. It is safe to ignore all other effects

which also contribute to the heat transfer in reservoir in other flow regimes. After dropping the heat convection term, heat conduction term and Joule-Thomson effect term, the temperature change follows the pressure change and can be described as (Davies and Muradov, 2013):

$$\Delta T \approx \frac{\emptyset \beta T}{\overline{\rho C_p}} \Delta p \quad , \tag{4.19}$$

where β is the thermal expansion coefficient and C_p represents the heat capacity at constant pressure; T can be treated as a constant.

According to the previous introduction to the wavelet transform, it is a linear operation. Therefore, the earlier WT detail amplitudes A_{Tf} represent the temperature change:

$$A_{Tf} \propto \Delta T \tag{4.20}$$

Combining Eq. 4.19 and Eq. 4.20:

$$A_{Tf} \propto \frac{\emptyset \beta T}{\overline{\rho C_p}} \Delta p \tag{4.21}$$

Considering the fact that pressure-dependent fluid properties drive the pressure changes nonlinearly, Eq. 4.22 cannot lead to any linear relationship.

$$\mathrm{A}_{Tfurc} = \frac{A_{Tf}}{\Delta q} \propto \frac{\emptyset \beta T}{\overline{\rho C_p}} * \frac{\Delta p}{\Delta q} \tag{4.22}$$

A_{Tfurc} ranges from 0.217 to 0.285 with time, as shown in Table 4-8 and Figure 4-32, so A_{Tf} can only be used for diagnosing the breakpoint locations which are caused by flow events in nonlinear systems.

For the middle-time region (later amplitude - second WT detail coefficient)

Similarly to the superposition application in pressure interpretation, the temperature behaviour for the second increase or decrease consists of the temperature change initiated

by the previous alteration in flow-rate (compression or expansion effect) plus the temperature change caused by the increment or reduction in the flow-rate:

$$T_n(t) = T_{n-1}(q_{n-1}, t) + \Delta T_{ratechange}(q_n - q_{n-1}, t - t_{q\ change}) \quad 4.23$$

The simplified analytical solution that describes the sand-face temperature during this region for nonlinear systems has not yet been researched. This is treated as a part of my future work, and it will be discussed in Chapter 6.

However, as illustrated in Table 4-8 and Figure 4-33, the unit-rate-change coefficients calculated from the later amplitudes, $\mathrm{A}_{Tlurc} = \frac{\mathrm{A}_{Tl}}{\Delta q}$, are approximately equal to -0.048 during pressure build-up periods which are caused by flow-rate decrease. This verifies the constant reservoir parameters of the synthetic model.

A possible reason could be that the temperature changes during this period are dominated by the heat conduction effect which is usually ignored for fluid flow simulation. As can be seen in Eq. 4.18, the heat conduction term is affected by the thermal conductivity coefficient (the pressure gradient is removed), which in turn depends on different materials/saturated porous media. In other words, the third term of Eq. 4.23 is only contingent upon the reservoir and wellbore parameters such as porosity, skin factor and wellbore radius. The thermal conductivity coefficient is expressed as:

$\mathrm{k} = \frac{\Delta Q}{A\Delta t}\frac{x}{\Delta T}$,

where A is the cross-sectional area, $\frac{\Delta Q}{\Delta t}$ is the amount of conductive heat within unit time, x is the thickness of the thermal conductor, ΔT represents the temperature change.

In order to use the unit-rate-change coefficients for reconstructing the flow-rate history by temperature data, even in nonlinear systems (existence of pressure-dependent fluid parameters, but constant reservoir parameters), more research into the theory and evidence which can support the phenomena (constant A_{Tlurc}) needs to be carried out.

Table 4-8：The unit-rate-change coefficient A_{Tfurc} in the gas production case changes with time, but A_{Tlurc} is constant

Time/t (hour)	Rate/q (MMSCF/ day)	Rate Change/△q (MMSCF/day)	WT Details Coefficient/ A_{Tf}	WT Details Coefficient/ A_{Tl}	$A_{Tfurc} = A_{Tf}/\triangle q$	$A_{Tlurc} = A_{Tl}/\triangle q$
0	3.532	N/A	N/A	N/A		
17.47	1.766	-1.766	-0.4658	0.0859	0.2638	-0.0486
34.75	4.238	2.472	0.7049	-0.1885	0.2852	-0.0763
52.03	2.825	-1.413	-0.3271	0.0685	0.2315	-0.0484
69.31	1.766	-1.059	-0.2632	0.0511	0.2693	-0.0483
86.59	4.238	2.472	0.6532	-0.1724	0.2642	-0.0697
103.9	3.532	-0.706	-0.153	0.0343	0.2167	-0.0486

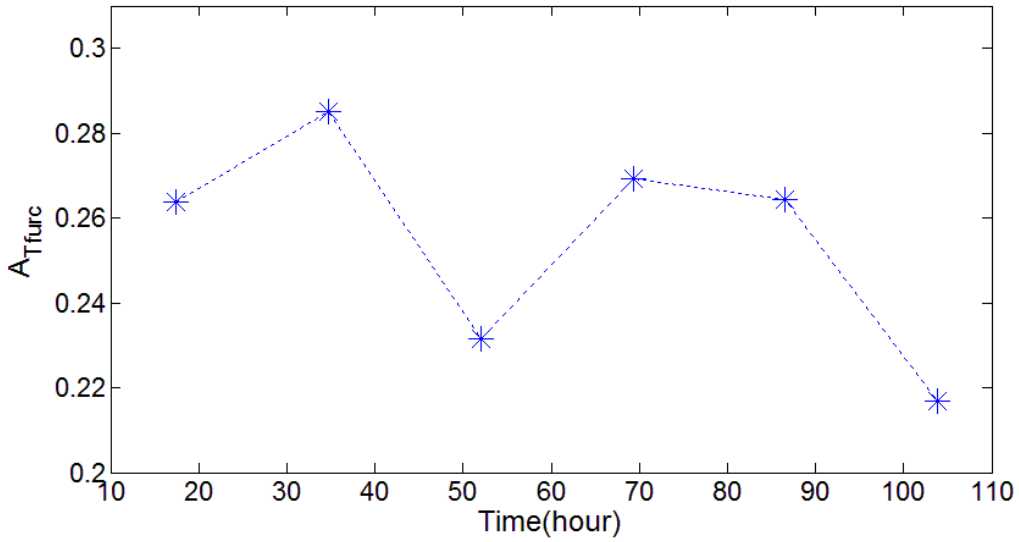

Figure 4-32：Nonlinear system diagnostic from temperature data: variations of the earlier unit-rate-change coefficient A_{Tfurc} with time

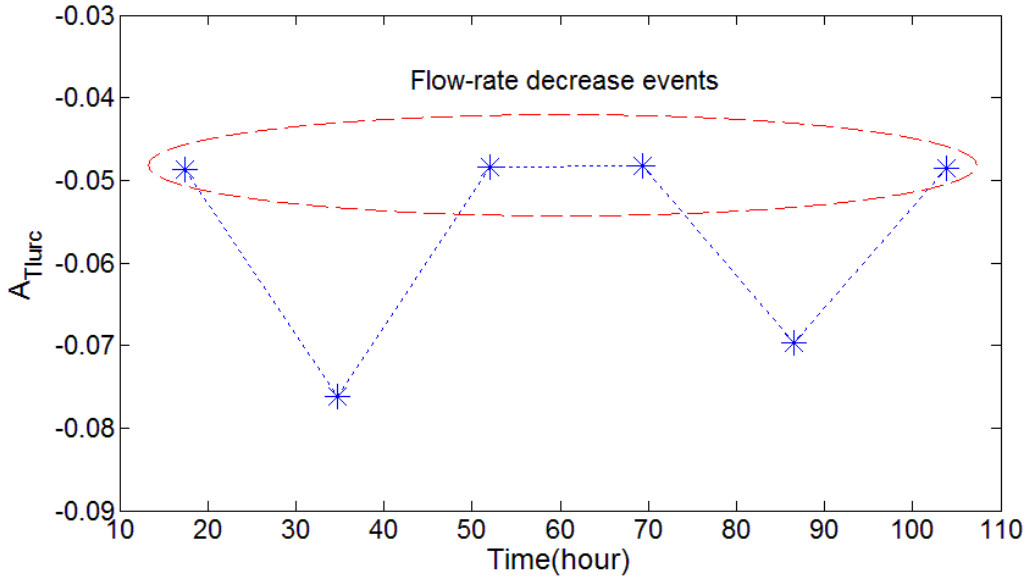

Figure 4-33：Nonlinear system diagnostic from temperature data: variations of the later unit-rate-change coefficient A_{Tlurc} with time

4.6. Sensitivity case studies regarding A_{Turc} function

How the unit-rate-change coefficients of pressure data perform with the changes of different reservoir-well parameters has been researched (Wang and Zheng, 2012; Wang, 2012). The case with single phase oil flow with constant reservoir-well parameters is a linear system. According to this, they conducted a sensitivity study on the constant coefficient A_{Purc} by analysing the transient pressure performance. As discussed in the previous section, temperature responds to changes in pressure, especially in linear systems. So temperature behaviour follows a similar rule in the wavelet transform based pressure nonlinearity diagnostic function in the single oil phase synthetic case.

However, in practice, the scenarios can be nonlinear or pseudo-linear. For a simple example, in the base case of single phase gas production, the transient pressure behaviour becomes much more complex than that in the slightly compressible fluid flow system (e.g. single oil phase), due to either high flow-rate non-Darcy flow or pressure-dependent gas properties, and the additional pressure loss will mask the typical pressure-transient characteristics. This nonlinearity could result in the previously mentioned URSR method being invalid. Thus, in order to interpret those nonlinear systems, pseudo-pressure, pseudo-time, or other appropriately transformed parameters should be used to linearize

the diffusivity equation (Al-Hussainy et al., 1966; Holditch, 1982; Agarwal, 1979; Meunier and Wittmann, 1987). Alternatively, the extended URSR method of transient temperature analysis, which has been proved effective on pressure build-up tests may provide another choice for nonlinear gas flow scenario interpretation.

In this section, how unit-rate-change coefficients (A_{Turc}) behave with the changes of different wellbore-reservoir parameters are researched. In oil/gas fields operations, the changes in some reservoir and fluid parameters such as geothermal gradient, reservoir thickness, and thermal conductivity coefficient are relatively small. After eliminating those minor parameters, the following parameters are tested: permeability of the formation, porosity, Joule-Thomson coefficient of the fluids, heat capacity, skin factor, and wellbore size.

The ranges of parameters shown in Table 4-9, including the wellbore size, permeability, porosity, skin factor, heat capacity, density and fluid Joule-Thomson coefficient, are based on information from the geology literature and field site measurements.

The ranges of fluid properties used for the synthetic models (Table 4-9) are based on common fluid properties (generated by an online system), including a Joule-Thomson coefficient ranging from 1.0E-3 K/psi to 1.2E-2 K/psi and fluid heat capacity ranging from 500 KJ/kg.K to 2000 KJ/kg.K. The ranges of reservoir properties (Table 4-9) are based on sandstone and carbonate properties for reservoir rocks, with permeability ranges of 10–300 mD and porosity ranges of 0.1–0.7.

Table 4-9: Initial ranges of fluid/reservoir properties used for transient temperature simulation

Property	Lower bound	Upper bound
Wellbore size (ft)	0.189	0.564
Permeability (md)	10	300
Porosity	0.1	0.7
Skin factor	0	30
Fluid J-T coefficient (K/psi)	1.0E-3	1.2E-2
Fluid heat capacity (kJ/kg.K)	500	2000
Fluid density (kg/m3)	0.6	1

4.6.1 Sensitivity case one - linear oil flow

As discussed before, the calculated unit-rate-change coefficients from processed temperature data and processed pressure data are both constants in a slightly compressible linear system.

$$A_{Turc} \propto -\frac{\mu * C_j\left(ln\frac{4A}{\gamma C_A {r_w}^2}+2S\right)}{4\pi kh} \tag{4.24}$$

Eq. 4.24 establishes a relationship between the unit-rate-change coefficients A_{Turc} and some typical reservoir-well parameters. In order to verify this equation and test the influence of different parameters on A_{Turc}, the base oil synthetic model was used for the first sensitivity study.

Permeability of the formation: According to Eq. 4.24, A_{Turc} (absolute value) declines with the increase of permeability, and a linear relationship exists between A_{Turc} and 1/k. The calculation results are illustrated in Figure 4-34.

Skin factor: Eq. 4.24 shows that A_{Turc} (absolute value) increases linearly with the addition of skin factor, and the intercept depends on $\frac{\mu * C_j\left(ln\frac{4A}{\gamma C_A {r_w}^2}\right)}{4\pi kh}$. A large skin factor not only causes extra pressure change but also leads to a large temperature change, which is represented by large unit-rate-change coefficients A_{Turc}, around the wellbore. The calculation results for different skin factors are shown in Figure 4-35.

Joule-Thomson coefficient of the fluids: Mathematically, A_{Turc} (absolute value) is proportional to C_j. Figure 4-36 verifies the linear relationship between them.

Wellbore size: As stated by Eq. 4.24, A_{Turc} has linear relationship with $ln\frac{4A}{\gamma C_A {r_w}^2}$. Therefore, the direct relationship between r_w and A_{Turc} can be defined as approximately logarithmic; Figure 4-37 demonstrates this connection. Compared with a large wellbore size, a smaller wellbore size can produce larger A_{Turc} (absolute value) which is good for noisy data interpretation.

The near wellbore area parameters, such as permeability and skin factor, are very likely to be variable during production. By using the unit-rate-change coefficient A_{Turc}, the variations of reservoir parameters can be diagnosed from transient temperature data.

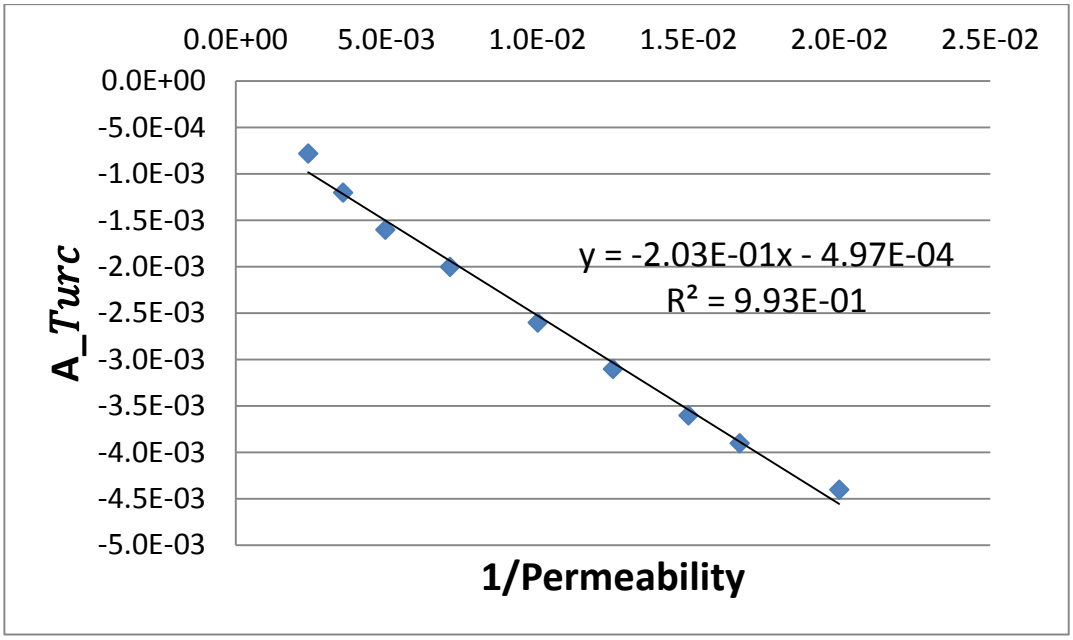

Figure 4-34：Linear relationship between unit-rate-change coefficient A_{Turc} and 1/k

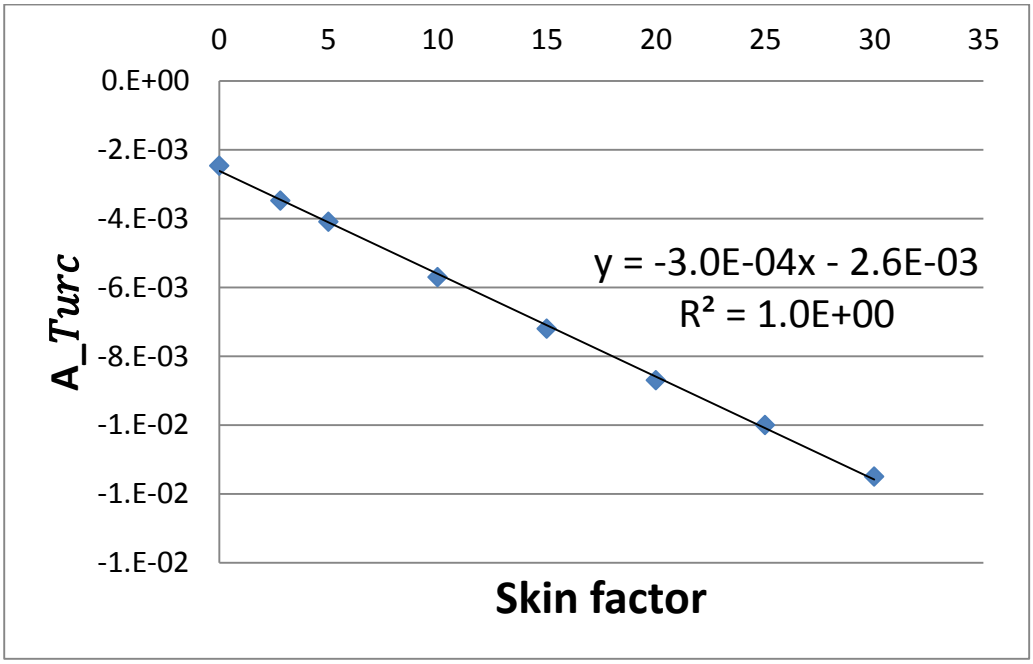

Figure 4-35：Linear relationship between unit-rate-change coefficient A_{Turc} and skin factor

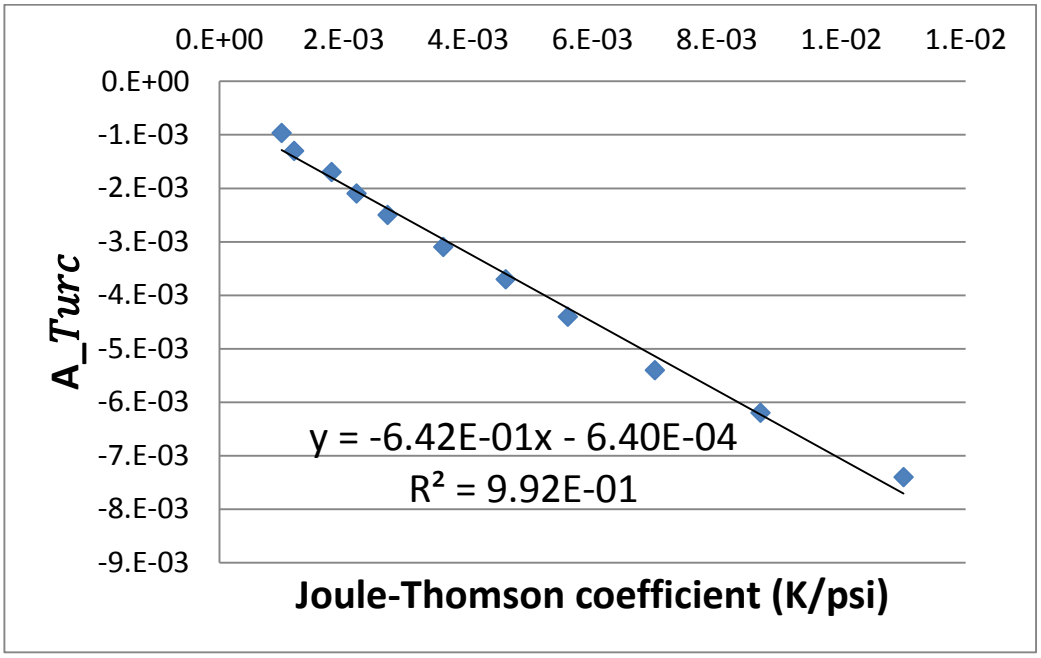

Figure 4-36：Linear relationship between unit-rate-change coefficient A_{Turc} and J-T coefficient

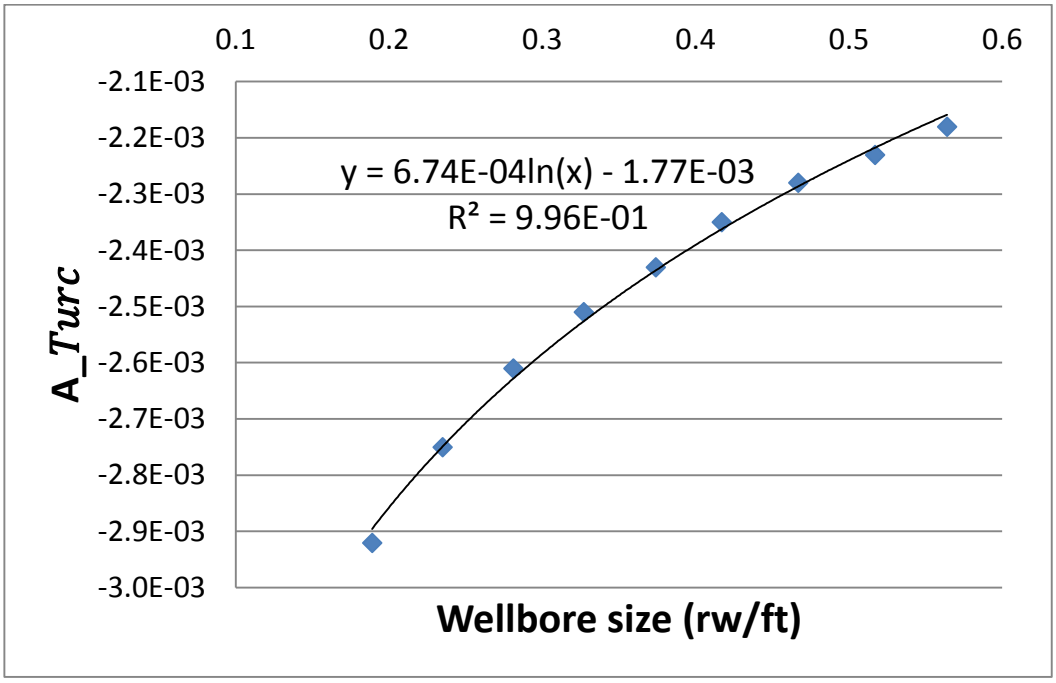

Figure 4-37：Logarithmic relationship between unit-rate-change coefficient A_{Turc} and wellbore radius

4.6.2 Sensitivity case two- nonlinear gas flow

This second sensitivity study focuses on the temperature behaviour in nonlinear systems, where the fluid flows with large compressibility. At the beginning of the temperature transient region, the adiabatic gas compression and expansion effect dominates the temperature behaviour. So the temperature change will follow the pressure change, as illustrated in Eq. 4.25:

$$\mathrm{A}_{Tfurc} = \frac{A_{Tf}}{\Delta q} \propto \frac{\emptyset \beta T}{\overline{\rho C_p}} * \frac{\Delta p}{\Delta q} \qquad 4.25$$

The transient-state pressure drop in a homogeneous infinite reservoir can be described as:

$$p_i - p_{wf} = -\frac{70.6qB\mu}{kh}\left[Ei\left(-\frac{948\emptyset\mu C_t {r_w}^2}{kt}\right) - 2S\right], \qquad 4.26$$

where B is the formation volume factor, $\mathrm{S} = (\frac{k}{k_{skin}} - 1)\ln(\frac{r_{skin}}{r_w})$.

If $\frac{948\emptyset\mu C_t {r_w}^2}{kt} < 0.01$, the exponential integral (Ei) behaves as a logarithmic function:

$$Ei\left(-\frac{948\emptyset\mu C_t {r_w}^2}{kt}\right) \approx ln\frac{1.78*948\emptyset\mu C_t {r_w}^2}{kt} = ln\frac{1688\emptyset\mu C_t {r_w}^2}{kt}$$

and the error is less than 0.25%.

Eq. 4.26 can be simplified as:

$$p_i - p_{wf} = -\frac{70.6qB\mu}{kh}\left[ln\frac{1688\emptyset\mu C_t {r_w}^2}{kt} - 2S\right] = \frac{70.6qB\mu}{kh}\left[ln\frac{kt}{1688\emptyset\mu C_t {r_w}^2} + 2S\right] \qquad 4.27$$

If flow-rate changes within a small time Δt, Eq. 4.27 can be rewritten:

$$\Delta p = \frac{70.6\Delta qB\mu}{kh}\left[ln\frac{k\Delta t}{1688\emptyset\mu C_t {r_w}^2} + 2S\right]$$

Combining Eq. 4.27 and Eq. 4.25, and eliminating the term for pressure drop with unit rate change,

$$A_{Tfurc} \propto \frac{\emptyset\beta T}{\rho C_p} * \frac{70.6B\mu}{kh}\left[ln\frac{k\Delta t}{1688\emptyset\mu C_t {r_w}^2} + 2S\right] \quad 4.28$$

Eq. 4.28 can be applied to analyse the relationship between reservoir-well parameters and the earlier unit-rate-change coefficient A_{Tfurc} . In order to verify the accuracy of Eq. 4.28, sets of synthetic cases with different parameters were simulated and the corresponding coefficients A_{Tfurc} were calculated. It should be noted that there are pressure-dependent gas properties (e.g. compressibility, FVF and viscosity) in the nonlinear system, so A_{Tfurc} is not absolutely constant. It is averaged within every synthetic case and the results of this sensitivity study are shown in Figure 4-38. The x axis stands for the change percent of every parameter with respect to the base value which given in Table 4-2; the y axis represents the calculated unit-rate-change coefficient. The changes of fluid and rock density are relatively small in practice, so they hardly affect A_{Tfurc}. The variation of wellbore size (approximately logarithmic relationship) has little influence on A_{Tfurc}, and the changes in porosity (approximately linear relationship), permeability (approximately logarithmic relationship), skin factor (linear relationship) and heat capacity (logarithmic relationship) have great impacts on A_{Tfurc}.

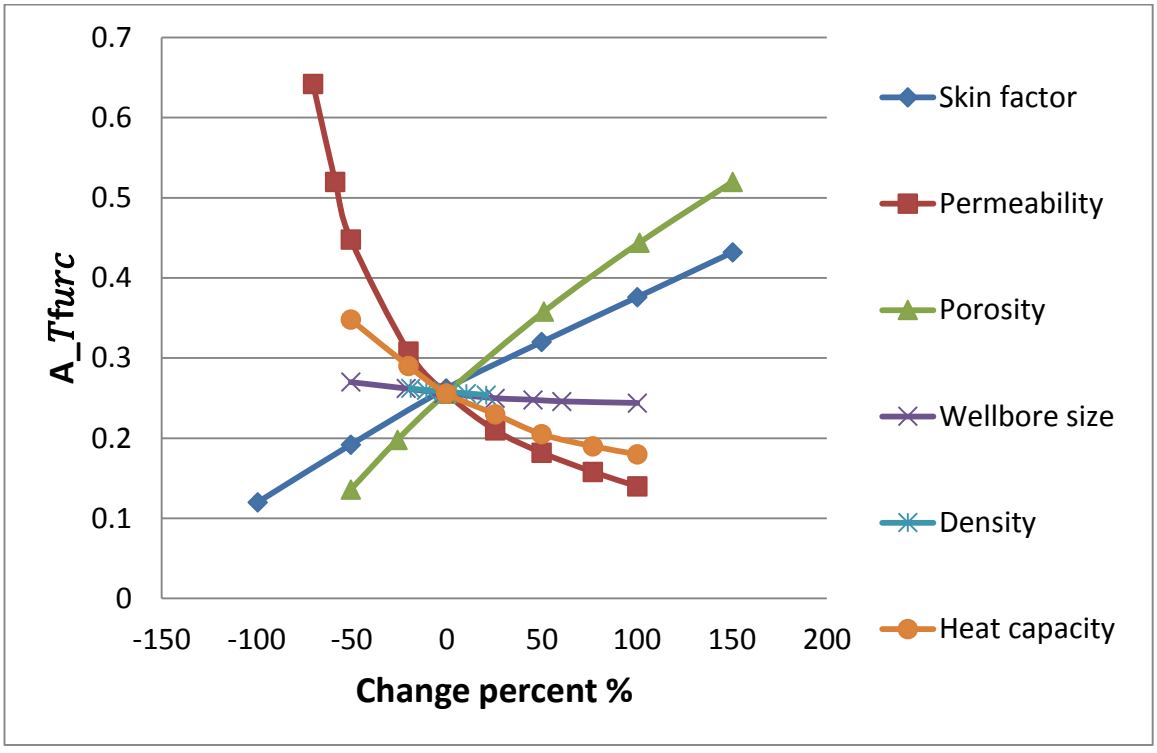

Figure 4-38：Sensitivity Study: relationships between unit-rate-change coefficient A_{Tfurc} and different parameters

The transient temperature gradually declines or rises as the effect of wellbore storage ends. For the middle time region, the analytical solution that describes the sand-face temperature for nonlinear systems has not yet been derived. For that reason, the sensitivity study regarding the later unit-rate-change coefficient A_{Tlurc} is treated as a part of my future work and it will be discussed in Chapter 6.

4.7. Other notes

4.7.1 Time interval

As described before in the data processing procedures, it is essential to keep the time interval coincident (synchronization issue) for processing transient temperature and pressure data and applying the interpretation method. Time intervals represent the sampling frequency of a dataset, and different intervals can result in different values of unit-rate-change coefficient (A_{Turc} and A_{Purc}). Generally speaking, a larger time step tends to obtain a larger value of unit-rate-change coefficient with lower accuracy, and vice versa. This regularity exists in both linear and nonlinear systems; the previously described sets of synthetic temperature and pressure data have been interpolated to have different time steps, as illustrated in Figure 4-39 and Figure 4-40. Figure 4-41 shows that there is a pseudo-logarithmic relationship between unit-rate-change coefficient and time interval. But considering the fact that a large time interval increases the uncertainty of the unit-rate-change coefficient, the regular time step should be less than 0.1 hour. In this circumstance, the relationship changes to a linear one, as shown in Figure 4-42.

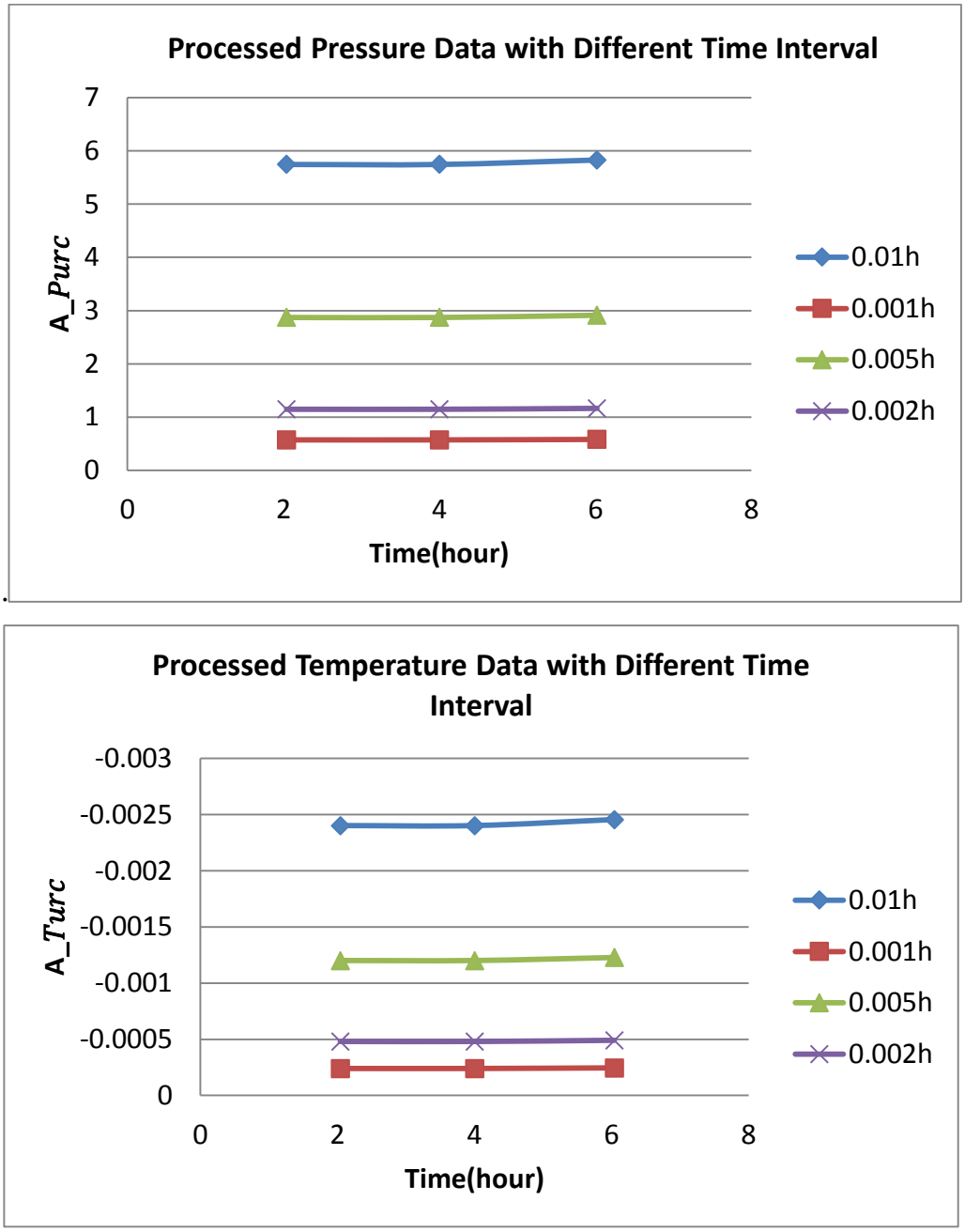

Figure 4-39：Linear system: unit-rate-change coefficients with different time intervals

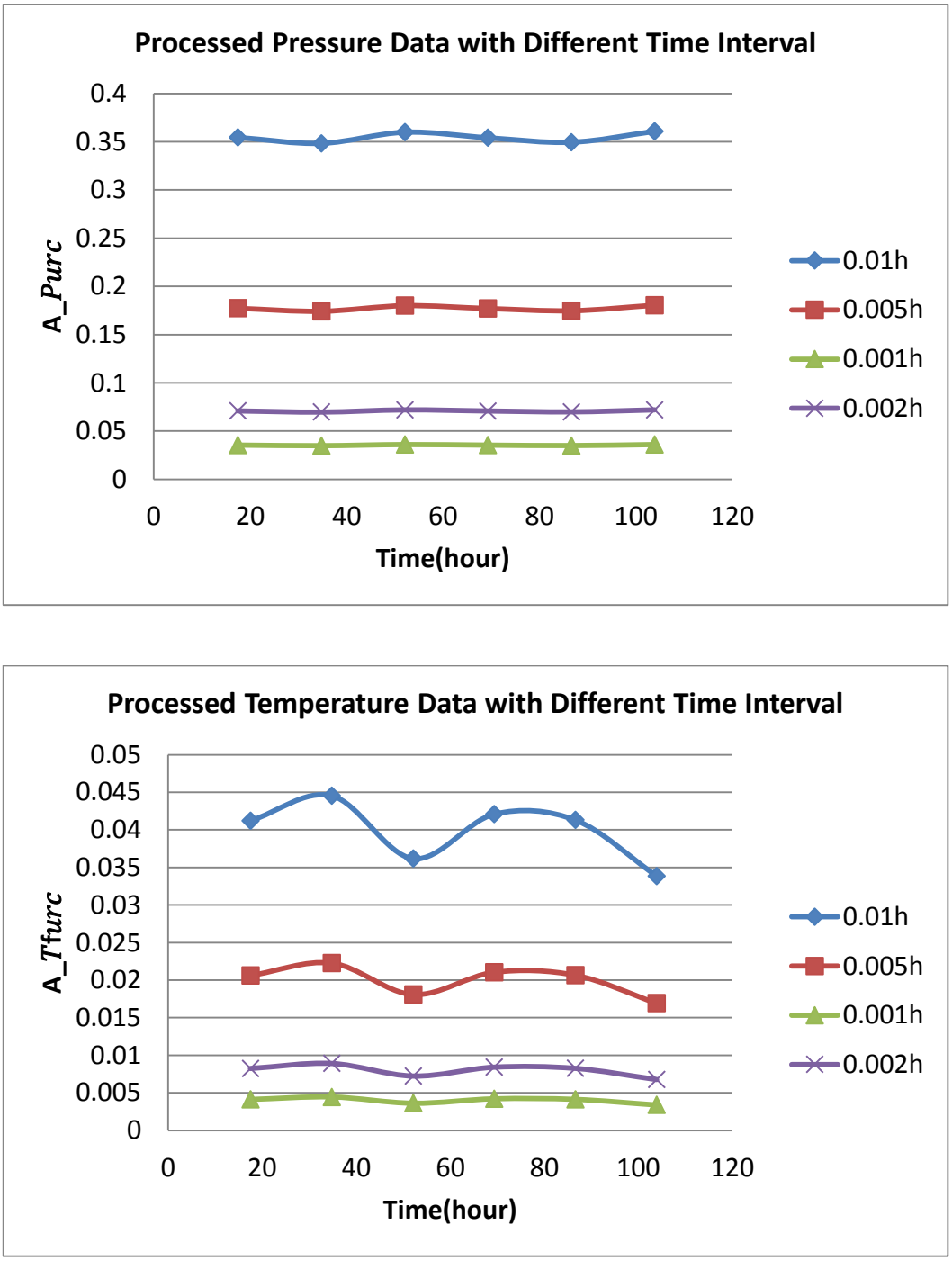

Figure 4-40：Nonlinear system: unit-rate-change coefficients with different time intervals

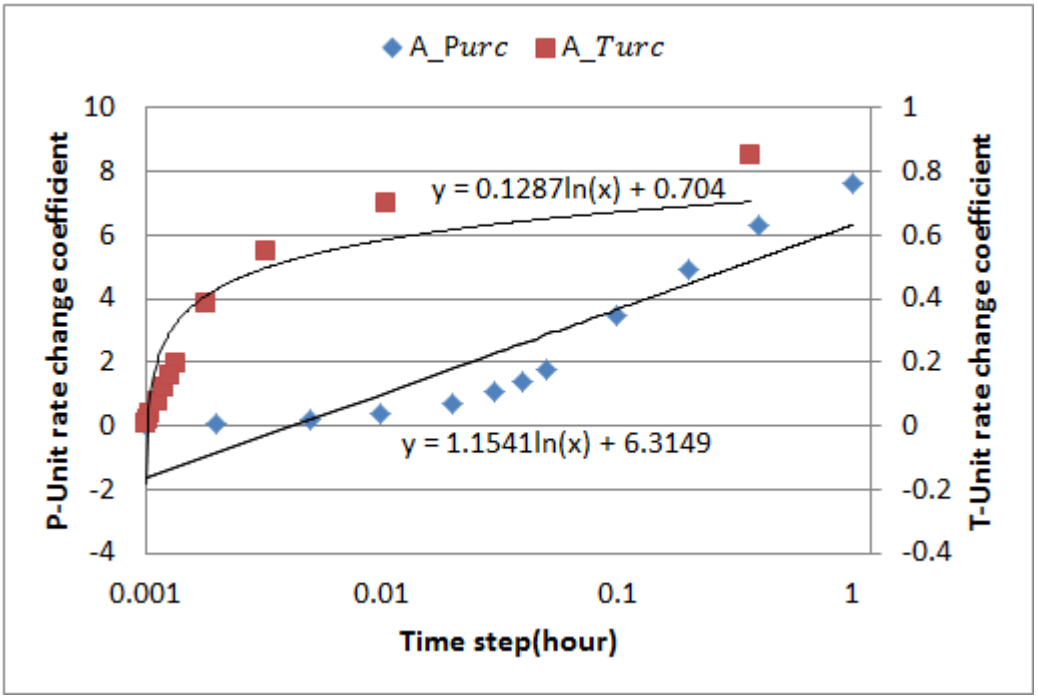

Figure 4-41：The logarithmic relationship between unit-rate-change coefficient and time interval

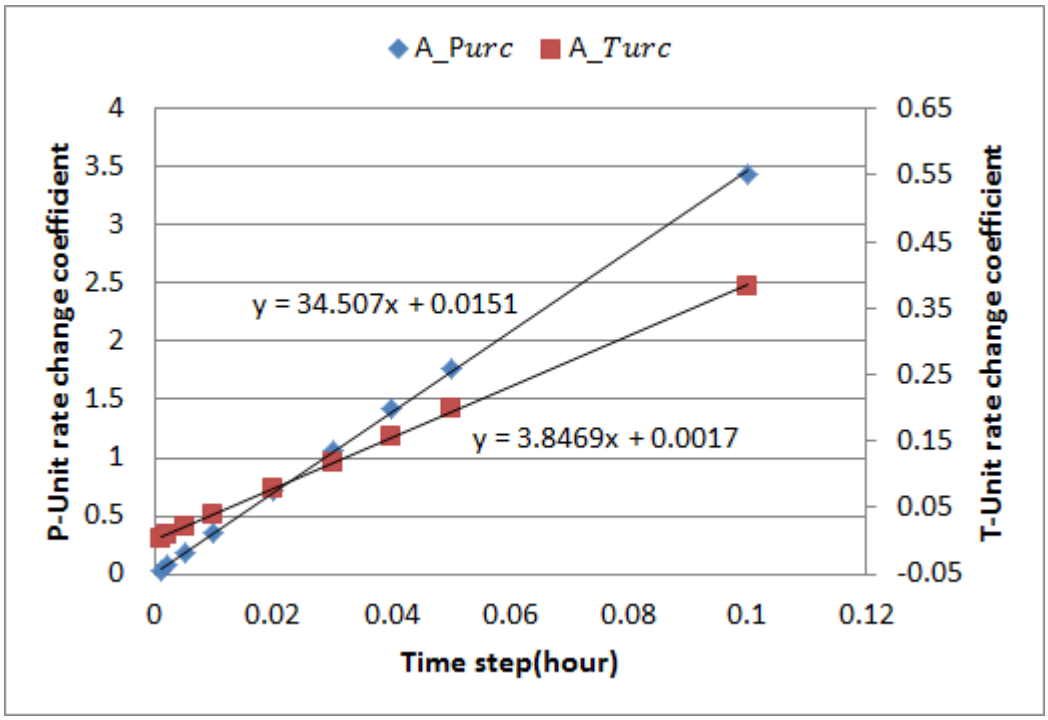

Figure 4-42：The linear relationship between unit-rate-change coefficient and time interval ($\Delta t < 0.1$ hour)

4.7.2 Scaling parameter selection

Selecting a suitable decomposition level (scale parameter s) is also a crucial problem and it usually depends on several factors. In this section, three main factors will be discussed: noise influence, identification resolution/data frequency and amplitude of WT detail coefficient. In general, as the scale parameter increases, the singularities caused by noise will be smoothed out and the resolution will be decreased. An oversized scale parameter can even remove the information contained in the signal's singularities.

Noise influence, identification resolution and data frequency

Field data always contain noise, due to the uncontrolled collection conditions. In order to apply the processing/interpretation method on noisy data and check the influence of scaling parameters on unit-rate-change coefficient, white Gaussian noise with 20% signal-noise ratio was generated randomly for synthetic temperature and pressure data.

Figure 4-43 shows Haar wavelet processed noisy pressure data with different scale parameters. It is not easy to identify the flow events from the noisy wavelet transform detail coefficients with a small scale, as illustrated in the second plot. With the increase in scale, the flow events stand out through the noisy coefficients with the decrease of resolution, as shown in the third and fourth plots. Particularly, for the large scale (7 and 9), either errors in the location of the breakpoint occur or the flow events are missed.

Figure 4-44 shows Haar wavelet processed noisy temperature data with different scale parameters. Compared with the noisy detail coefficients of pressure data, a larger scale is needed to identify the flow-events from noisy detail coefficients of temperature data. In addition, both the small flow event and the earlier/later amplitudes which make the transient temperature behaviour different from the transient pressure are merged by other opposite bigger amplitudes due to the decrease in resolution. This means the scale parameter of nine is too big in this case to process the noisy temperature data.

Unit-rate-change coefficients

Figure 4-45, Figure 4-46 and Figure 4-47 show the unit-rate-change coefficients with different scale parameters. Unit-rate-change coefficients (A_{Turc} and A_{Purc}) depend on

the values of wavelet transform detail coefficients. Although the WT detail coefficients increase with the addition of scale level, the variable scales (one to five) which are relatively small do not affect the time-invariant unit-rate-change coefficients. Moreover, linear relationships exist between the processed transient data (either pressure or temperature) and flow-rate changes. Oversized scales (seven and larger) increase the uncertainties and make the unit-rate-change function invalid. Therefore, finding a balance between noise removal and fine resolution is important for choosing an appropriate scale parameter.

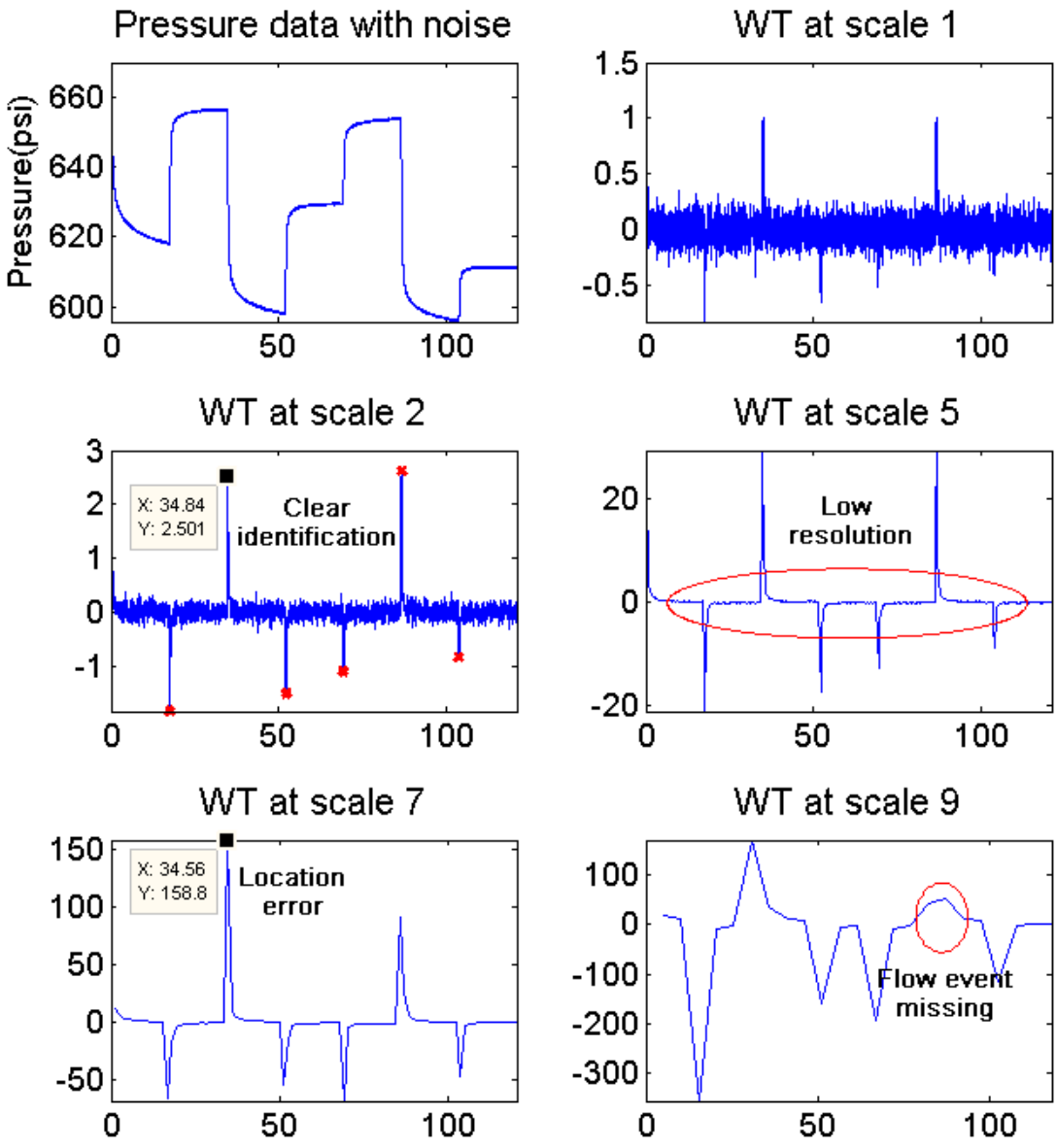

Figure 4-43：Haar wavelet processed noisy pressure data with different scale parameters

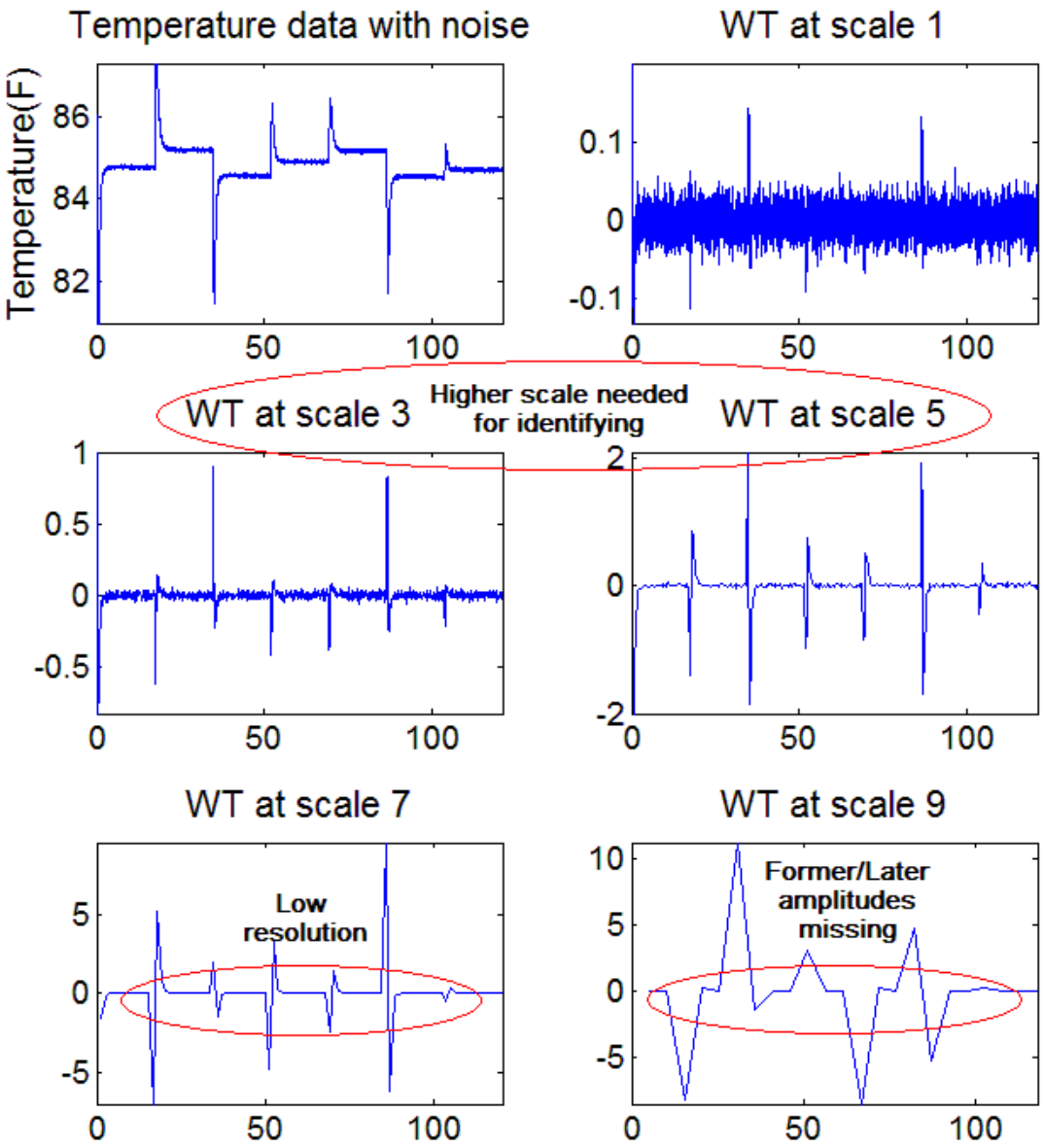

Figure 4-44：Haar wavelet processed noisy temperature data with different scale parameters

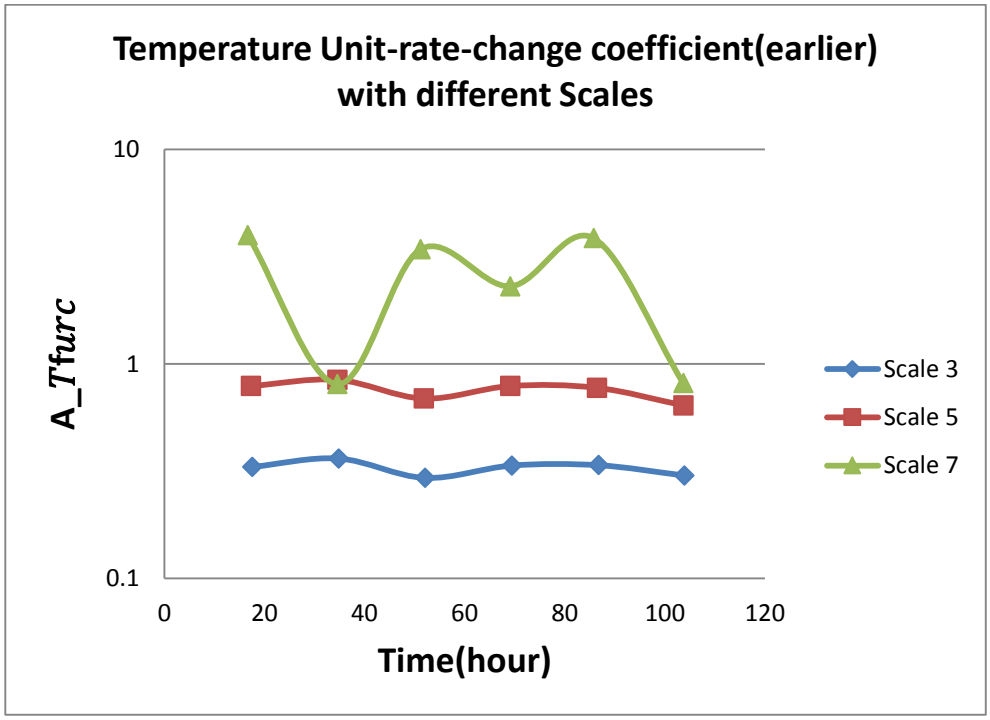

Figure 4-45：Temperature: earlier unit-rate-change coefficients with different scaling parameters

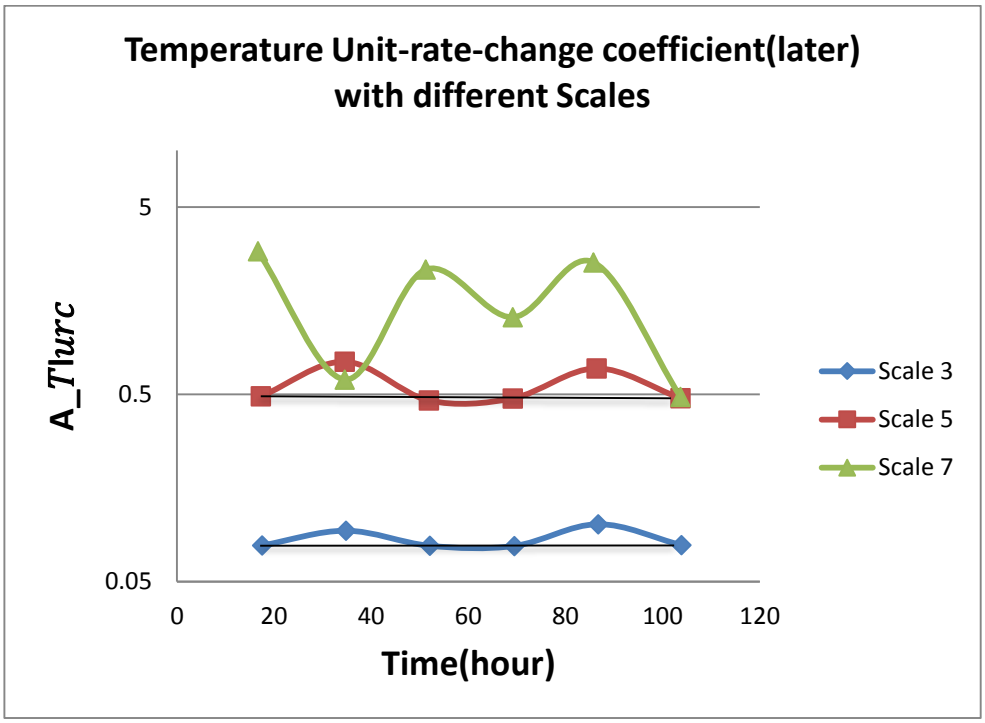

Figure 4-46：Temperature: later unit-rate-change coefficients with different scaling parameters

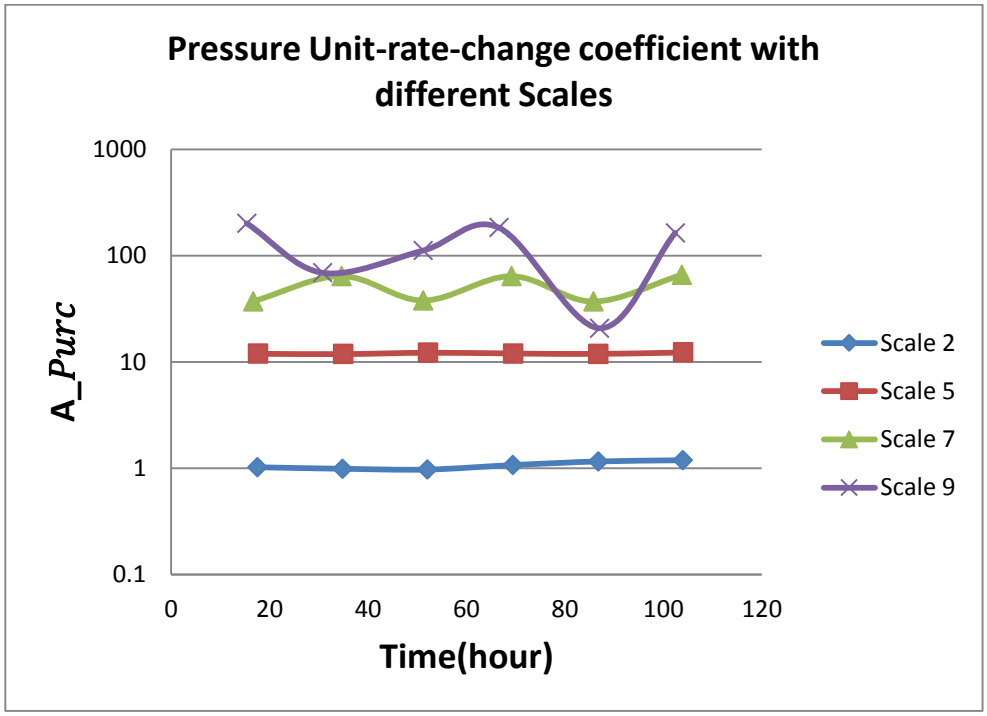

Figure 4-47：Pressure: unit-rate-change coefficients with different scaling parameters

4.7.3 Radius of investigation

Compared with the entire production history, the period between two consecutive flow events is relatively short, which is displayed as measured pressure and temperature changes within a limited time. For pressure transient analysis, the diagnostic radius can be calculated by using the equation of radius of investigation (Lee, 1982):

$$r_{investigation} = \sqrt{\frac{kt}{948\emptyset\mu C_t}}$$

The distance only relates to the elapsed time (since flow-rate change), reservoir and fluid properties, and is independent of the flow-rate. If the time is not long enough, the diagnostic radius will be as many as hundreds of feet around the well. The calculation algorithm of investigation radius may be not suitable for temperature transient analysis (More details about thermal investigation radius will be discussed in Chapter 5); however, through the utilization of unit-rate-change coefficient, any changes of reservoir and fluid properties in the near wellbore formation can be diagnosed. In addition, the early time region and flow-rate change can be easily diagnosed by transient temperature in nonlinear

systems such as gas flow and multi-phase flow, but pressure transient analysis is weak in these circumstances. This is because of the slow propagation of the thermal front, compared to the high speed of propagation of the pressure wave, which may cause the difficulties of interpreting near wellbore formation properties by pressure data. Temperature transient analysis can provide a useful complement.

4.8. Chapter Summary

This chapter has presented the analysis of the transient down-hole data by using a non-linear regression analysis method, known as ACE method, which shows that temperature responds to changes in flow rate and pressure. What is more, with the application of Wavelet Transform (WT), a novel model-independent approach has been developed not only to identify transient periods that are caused by flow-rate change operations, but also to diagnose nonlinearities from both transient pressure and transient temperature data. In addition, the specific relationships between WT coefficients and flow-rate change have also been summarized. These exist in both transient pressure and temperature for linear scenarios (oil production case), but can only be extracted from transient temperature for nonlinear systems (gas production case). The following detailed outcomes, findings and the conclusions that can be drawn from this park of the work can be summarised thus:

1. Temperature responds to changes of flow-rate and pressure, and those relationships can be determined from either an entire dataset or a selected representative transient region.
2. A wavelet based approach for transient pressure and temperature data processing has been used and a novel workflow has been described.
3. The Haar wavelet was utilized to identify the transient periods from both temperature and pressure data.
4. The necessity of combined interpretation of temperature and pressure data was highlighted. If flow-rate information is not available, these two kinds of data can provide constraints for each other (every confirmed transient period is an agreement between temperature and pressure).
5. Nonlinearities are caused by the near wellbore formation properties and flow conditions changes.

6. For the slightly compressible/incompressible fluid flow**,** unit-rate-change coefficient A_{Turc} can be used to diagnose nonlinearities of reservoir-well systems. A_{Turc} is constant for the linear system, but it varies with time if near wellbore parameters change.
7. According to the deduced equation of A_{Turc} and sensitivity case studies, larger changes of A_{Turc} mean higher nonlinearity. The degree of nonlinearity can be evaluated quantitatively through the changes of reservoir properties.
8. A_{Turc} is sensitive to the variations of permeability, skin factor, wellbore size and Joule-Thomson coefficient.
9. For the fluid flow with large compressibility, the earlier WT detail amplitudes A_{Tf} correspond to the breakpoints and the unit-rate-change coefficient A_{Tfurc} can be used to diagnose nonlinearities of reservoir-well systems. The later WT detail coefficients A_{Tl} respond to flow-rate change and A_{Tlurc} can be used to accurately reconstruct the flow-rate even in nonlinear systems.
10. According to the deduced equation of A_{Tfurc} and sensitivity case studies, the degree of nonlinearity can be evaluated quantitatively. The changes of permeability, skin factor, wellbore size and heat capacity are more sensitive to A_{Tfurc} .
11. The unit-rate-change coefficient A_{Turc} (or extended coefficient A_{Tfurc}) can be used to monitor the production wells. It is necessary to pay special attention to any abnormal increase or decrease of A_{Turc} which indicates the changes of production index (PI).
12. A larger time step tends to obtain a larger value of unit-rate-change coefficient with lower accuracy. If the time step is relatively small (less than 0.1 hour), there is a linear relationship between unit-rate-change coefficient and time interval; otherwise, the relationship changes to pseudo-logarithmic.
13. With the increase of scale parameter, the singularities caused by noise will be smoothed out and the resolution will be decreased. If the scale level is relatively small, its variations (one to five) don't affect the time-invariant unit-rate-change coefficients. Oversized scales increase the uncertainties and make the unit-rate-change function unavailable.

Chapter 5 Improved Analysis of Transient Temperature Data and Field Data Application

5.1. Introduction

During oil and gas field development, large volumes of high resolution and continuous down-hole information are obtainable. The interpretation of these real time temperature and pressure data can optimize well performance and improve reservoir characterisation.

Although the dynamic temperature data have been interpreted in practice to predict flow profiling and provide characteristic information for the reservoir, almost all of the approaches rely on established non-isothermal models which depend on thermodynamic parameters (Chapter 3). Another problem comes from the temperature transient analysis which is underutilized compared with pressure transient analysis.

In this chapter, the use of new procedures of transient temperature analysis is described, followed by diagnosing the wellbore storage regime, verifying the PTA interpretation results, reconstructing the flow-rate history and estimating the formation parameters by using transient temperature data. These interpretation methods are model-independent; several field case studies were then conducted to show their wide applications in different kinds of reservoirs.

5.2. New procedures for long-term transient temperature analysis

It is commonly accepted that conventional well test interpretation methods which are derived from traditional analytical models may be too simple to define the long-term pressure, temperature and flow-rate data (De Oliveira Silva and Kato, 2004). In order to interpret the extended duration of PDG records, an effective program which can divide the transient data and analyse them by different categories needs to be developed.

Although the transient temperature data have been interpreted in practice, a complete theory which can diagnose wellbore storage, indicate linear flow, calculate the flow-rate as well as evaluating the reservoir parameters integrally has not yet been published. In addition, compared with pressure transient analysis, temperature transient analysis is

extremely underutilized. It is therefore necessary to analyse temperature variation to overcome the problem of limited data when other down-hole information is less sufficient.

In this section, a novel analysis of long-term transient temperature data is presented in the order of the workflow followed. As shown in Figure 5-1, this interpretation procedure can be divided into five steps: temperature data processing and de-noising, transient identification, nonlinearity diagnosis and evaluation, temperature transient analysis, and information integration for reservoir management and model calibration.

Temperature data processing and de-noising:

In the first step, the acquired temperature, pressure and flow-rate data are processed by the usual procedures such as nonlinear regression analysis, synchronization, de-noising/outlier removal, data reduction.

Transient identification:

By utilizing the Haar wavelet transform, both the temperature and pressure data are able to yield satisfactory results and locate the exact points of flow-rate changes.

Nonlinearity diagnosis and evaluation:

The diagnosis and evaluation of nonlinearities are especially important before analysing transient temperature data, since they can distinguish different production scenarios, ensure the correct selection of data interpretation methods and reduce the need for analysis of uncertainties. The causes of nonlinearity include non-Darcy flow, multiphase flow and time/pressure-dependent fluid and reservoir parameters.

Through the application of extended unit-rate-change coefficients, A_{urc}, nonlinearity of the reservoir (invalid superposition principle) can be diagnosed by both transient temperature and pressure data, and the degree of nonlinearity can also be evaluated. Additionally, the two different nonlinearities either caused by pressure-dependent fluid parameters or reservoir parameters can be distinguished through integrating pressure and temperature interpretations.

Temperature transient analysis:

For the linear scenarios (e.g. single phase oil case), which can be proved by both pressure and temperature to perform with linearity, either conventional pressure-transient analysis (PTA) methods or a simplified temperature inversion algorithm are applicable. The transient temperature data is divided into two parts for interpretation: firstly, as temperature behaviour follows a similar rule to Pressure Unit Reservoir System Response (URSR), the flow-rate history can be reconstructed by A_{Turc} coefficients; and for later times, a modified radial flow solution can be used to calculate the down-hole temperature, which in turn can be used to estimate the reservoir parameters.

However, the systems which contain gas phase with large compressibility can be nonlinear, in practice, due to either high flow-rate non-Darcy flow or pressure-dependent properties. This nonlinearity could result in the previously mentioned Pressure Transient Analysis methods and URSR method becoming invalid. Alternatively, for the early time region, temperature data can be used to diagnose the end of wellbore storage and evaluate the near wellbore formation properties; then, for middle time region, the extended A_{Turc} coefficient on transient temperature analysis is able to reconstruct the flow-rate history for pressure build-up periods (temperature with linearity).

Furthermore, for the scenarios in which reservoir parameters change, both temperature and pressure data perform with high nonlinearity. It is recommended to apply the sliding window technique (Wang, 2012) and to divide the long-term transient data into several short linear periods for keeping A_{urc} constant within a tolerance. Otherwise, the numerical method which relies on an established non-isothermal wellbore-reservoir model can be used (as discussed in Chapter 3).

Reservoir management/model calibration:

The interpreted reservoir-well parameters and flow-rate information can be used for model calibration, production monitoring, real-time reservoir management.

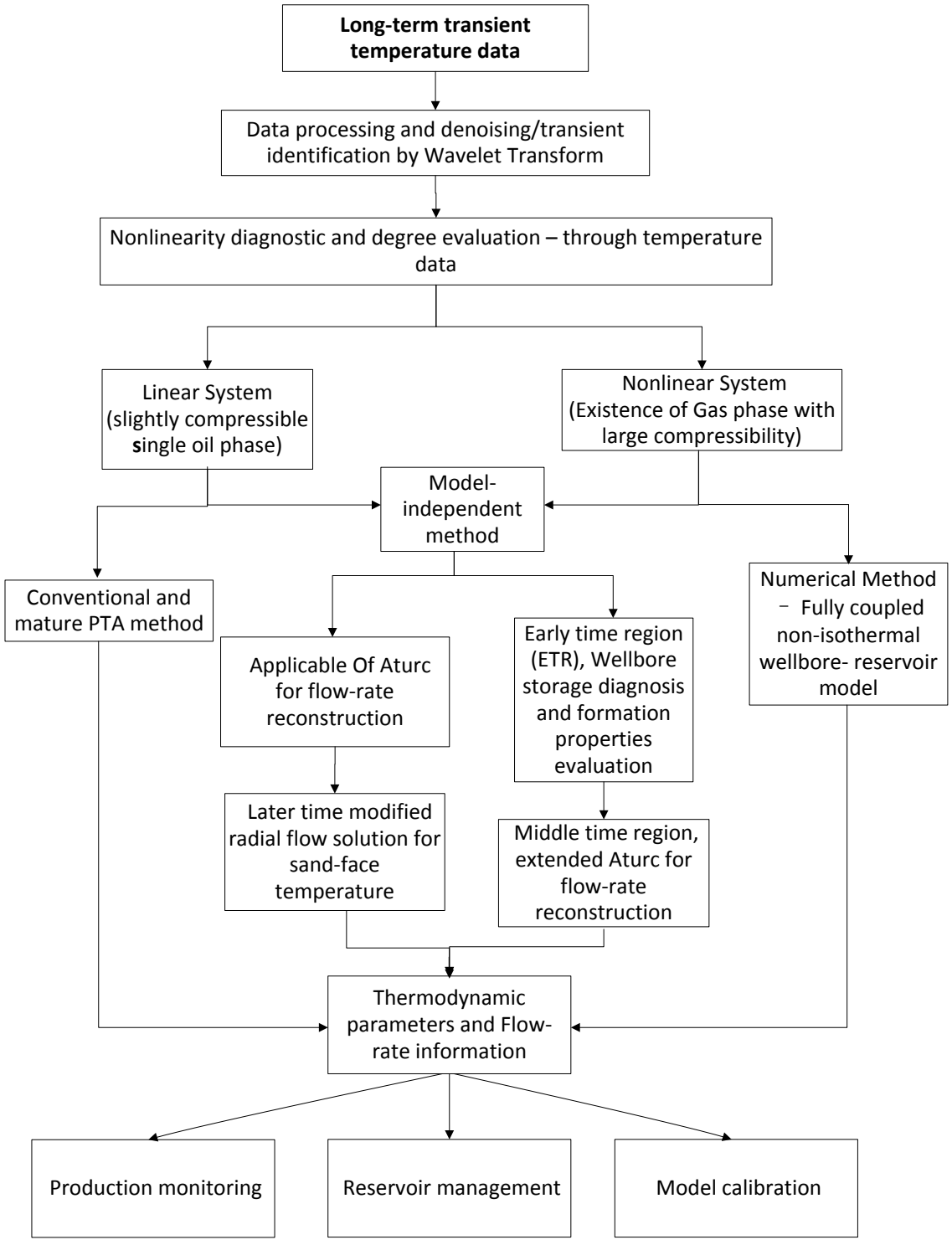

Figure 5-1：New procedures for long-term transient temperature analysis

5.3. Analysis of the early time region (ETR) transient temperature data for gas-presence nonlinear systems

Figure 5-2 shows a diagnostic log-log plot of the pressure and pressure derivative vs. elapsed time. Typically, the diagnostic plot can be divided into three regions. At early times, the unit slope line on both pressure derivative and pressure curves indicates wellbore storage. However, several effects such as formation damage, phase redistribution, stimulation and partial penetration can affect the early time pressure performance. Therefore, the conventional transient pressure diagnostic often fails to identify the exact timing of the end of wellbore storage, which significantly impacts on radial flow definition and well-test design.

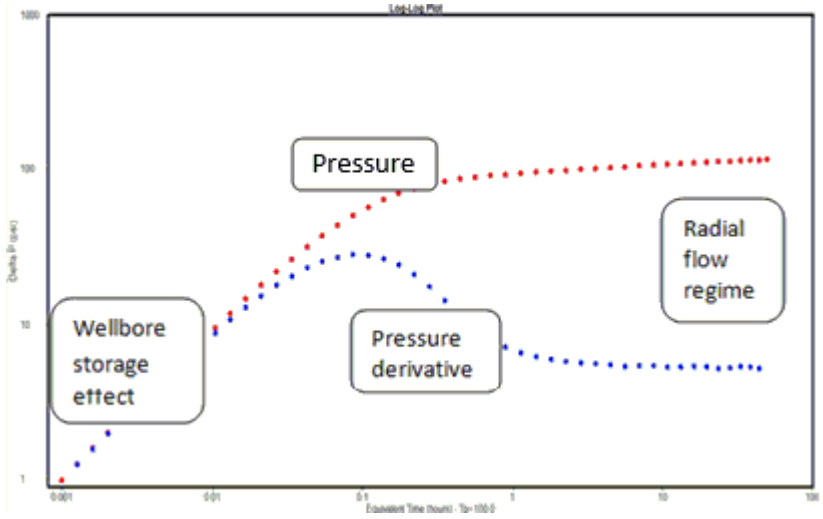

Figure 5-2：Diagnosis of wellbore storage and radial flow regimes on a typical log-log plot of pressure and pressure derivative curves

For the early time region (ETR), that is caused by well shut-in and opening resulting in rate-change operations, temperature increase or decrease is affected by wellbore storage in which the fluid compression and expansion dominates the temperature behaviour. Typically, temperature gradually declines or rises as the effect of wellbore storage ends. For a pressure build-up test of a gas well, the down-hole flow-rate decreases within a short time, which causes a sharp increase in temperature; the temperature then gradually declines as the effect of wellbore storage ends. This phenomenon has been presented in several synthetic case studies. Table 4-3 demonstrates the processed temperature data detected locations where wellbore storage ends for a typical gas production case. As

discussed in Chapter 3, the jump in temperature for the nonlinear scenario's build-up test can provide qualitative information on reservoir parameters, near wellbore pressure drops and well productivity index. Generally speaking, the jump in temperature can be very small in the case of high permeability, small skin and a small Joule-Thomson coefficient, but can be relatively large in the case of low porosity, large positive skin and high viscosity.

In this section, the application of early time temperature data for well testing interpretation is shown by using several field cases. Pressure build-up tests and pressure draw-down tests were conducted in an oil well and a gas well. In order to acquire the down-hole pressure and temperature data, both of the wells were tested by Drill Stem Testing (DST). Then, skin factor, permeability and other reservoir parameters were estimated using Pansystem^{TM}, as illustrated in the log-log plots of plateau pressure and pressure derivative curves. Also, the values were verified with early time temperature interpretation results.

5.3.1 Field case one - nonlinear oil, gas and water multi-phase flow production well

This vertical well is perforated for producing the oil zone from 718.5m to 846.5m; the details of pay zones, the production history, the fluid and reservoir parameters are shown in Table 5-1 and Table 5-2.

Table 5-1：Information for productive zones

Layer	No.	Perforation zone (m)	Perforation length (m)	Porosity（%）
T_2K_2	1	718.5-721.0	2.5	17.66
	2	725.0-726.5	1.5	17.66
	3	728.0-731.0	3.0	17.66
	4	733.5-735.5	2.0	17.66
	5	740.5-744.5	4.0	17.66
	6	814.5-817.5	3.0	17.66
	7	839.0-842.0	3.0	17.66
	8	844.0-846.5	2.5	17.66

Table 5-2： Production history and other inputs for pressure data interpretation

Daily liquid production (t/d)	11.27	Cumulative oil production	466.36
Daily oil production (t/d)	9.14	Cumulative gas production ($\times 10^4 m^3$)	1.8988
Water cut (%)	9.4	Cumulative production days	50.0
Production gas-oil ratio (m^3/t)	48.13	End date	2010.9.3
Porosity (%)	17.66	Fluid formation volume factor	1.068
Reservoir thickness (m)	21.5	Fluid viscosity (mPa.s)	8.72
Well radius (m)	0.062	Total compressibility (1/MPa)	0.000679
Stable production period (h)	1199.33	Average daily liquid production rate (m3/d）	12.62

Figure 5-3 below shows the plots of transient pressure and temperature data respectively for the oil production well during the first 150 hours of shut-in after it had been producing for sufficient time for the equilibrium state to be achieved between the well and reservoir. The early time region temperature and pressure performance can also be observed.

Figure 5-4 shows the pressure and pressure derivative curves plot of the pressure build-up test. The pressure derivative curve acts as the characteristic of a finite-conductivity vertical fracture reservoir; and the transient behaviour of the well was divided into three stages: early time wellbore storage regime, middle time transition period and later time bilinear flow regime (a quarter-slope line on the derivative curve, linear flow within the fracture to the well, and from the formation into the fracture).

The corresponding behaviour of temperature during the same period is shown in Figure 5-5; the x axis also stands for the logarithm of shut-in time and the y axis represents the temperature at the gauge location. The early time temperature increase is affected by wellbore storage, in which there is a down-hole flow-rate from the reservoir towards wellbore and a gradual decline in pressure. As the effect of wellbore storage ends, the main factor affecting the wellbore temperature changes to heat conduction between wellbore and formation, so that the wellbore temperature gradually declines towards the reservoir temperature at that depth.

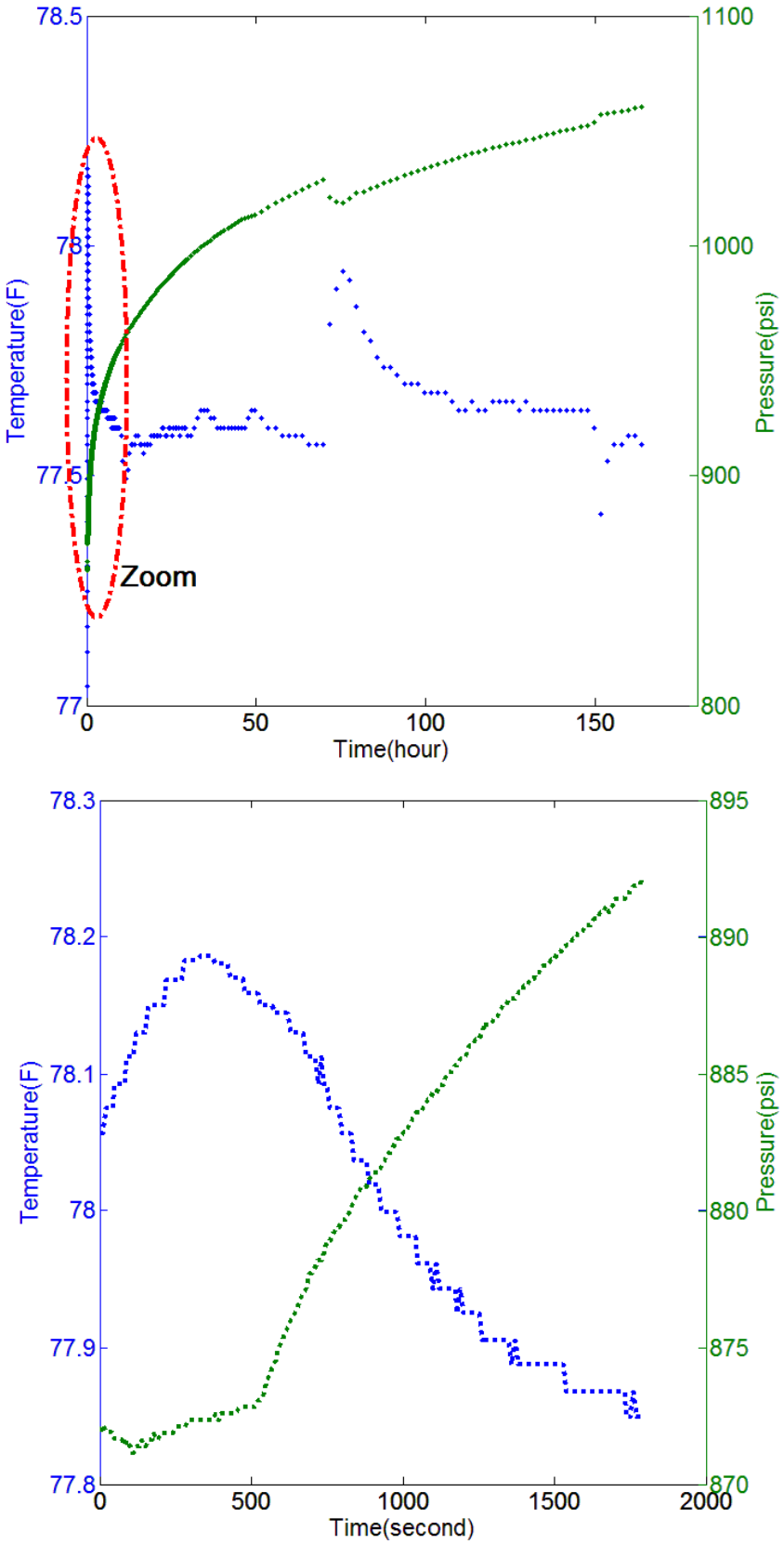

Figure 5-3：Transient pressure and temperature data during the first 150 hours of pressure build-up test and zoom in for early time region

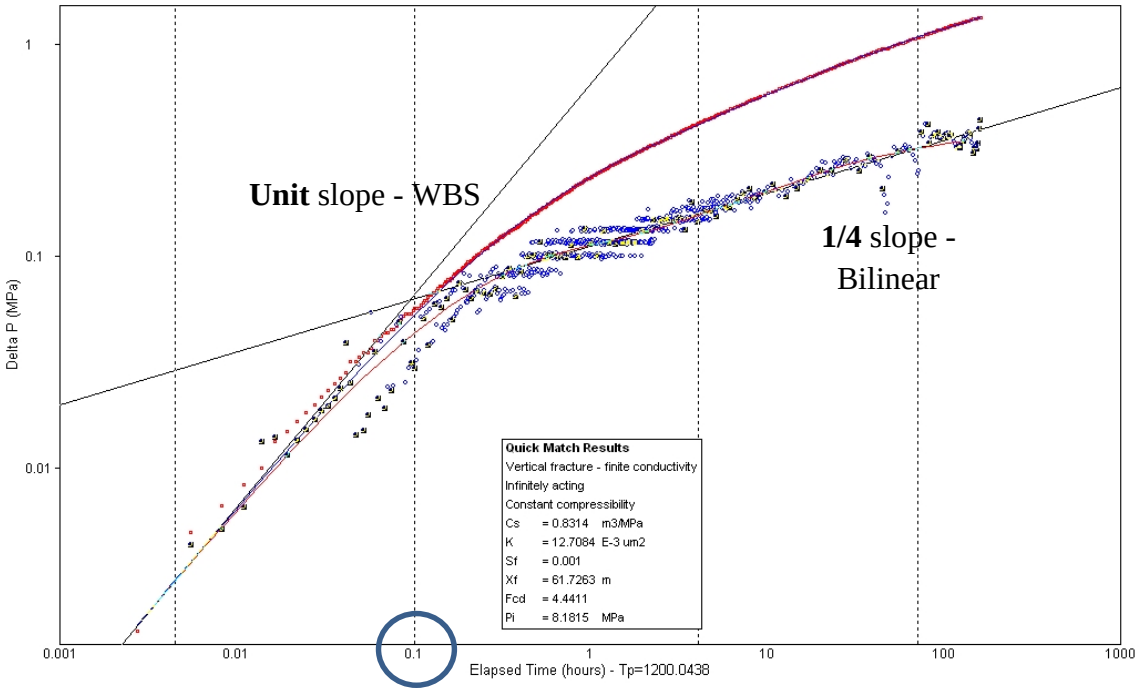

Figure 5-4：Log-log plot of down-hole pressure and pressure derivative during pressure build-up test

Table 5-3：Interpretation software, model selection and well test interpretation results using pressure log-log regression

Software: PanSystem™ V3.5			
Model selection	Wellbore model	Flow model	Boundary model
	Wellbore storage + skin factor	Vertical fracture-finite conductivity	Infinitely acting
Interpretation results			
Permeability ($10^{-3}\mu m^2$)	Skin	Formation factor = permeability*reservoir depth ($10^{-3}\mu m^2$.m)	Flow coefficient ($10^{-3}\mu m^2$.m /mPa.s)
12.708	0.001	273.222	31.333
Pressure transmitting coefficient	Mobility ($10^{-3}\mu m^2$/mPa.s)	Wellbore storage coefficient	Productivity index
0.0122	1.457	0.831	5.22

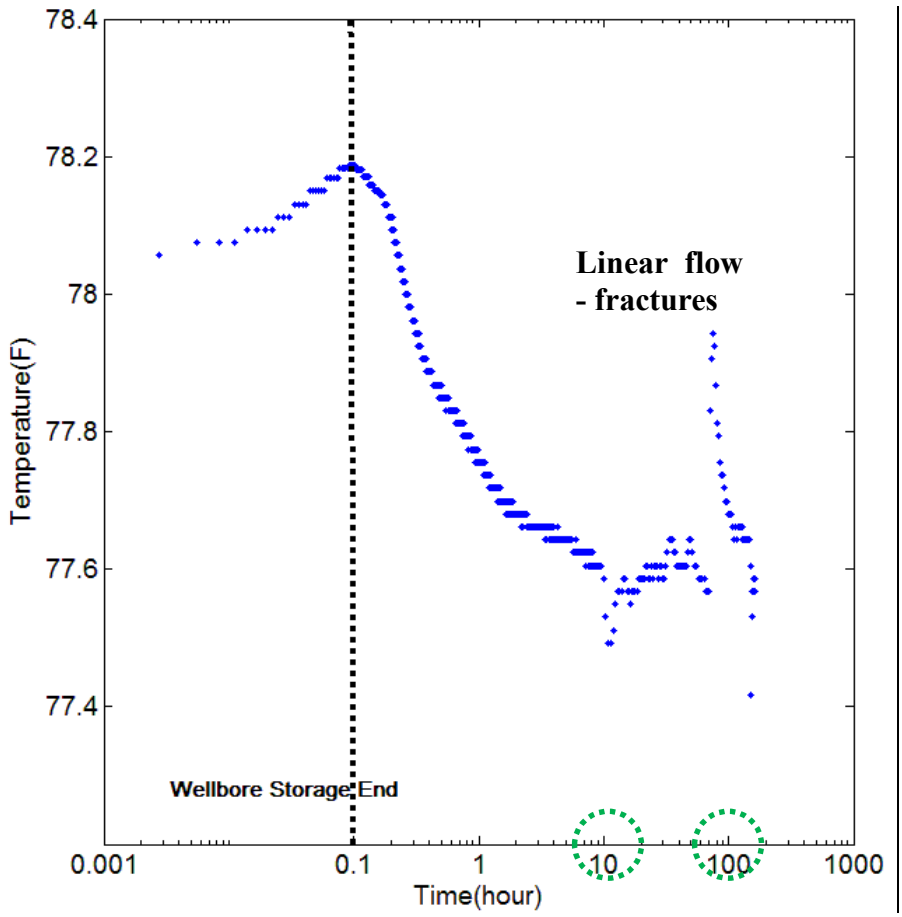

Figure 5-5：Semi-log plot of down-hole temperature during pressure build-up test

The end points of wellbore storage which have been marked in Figure 5-4 and Figure 5-5 almost coincide, at 0.1 hour. As shown in Figure 5-4, the plateau pressure derivative curves interpreted an average permeability, skin and productivity index of 12.708 md, 0.001 and 5.22 t/d/MPa respectively (Table 5-3). In addition, during this early time region, a small jump of approximately 0.2 °F in temperature indicates relatively high permeability (12.708 md) and small skin (0.001), which is coherent with the pressure interpretation results. In the near wellbore area, which is reflected by the early time region transient temperature data, the existence of perforation and skin cause an extra pressure drop, so the Joule-Thomson effect may be dominant. In this case, the small temperature jump means a small Joule-Thomson effect, which in turn implies a small pressure drop and small skin. The concaves on the semi-log temperature plot are located at 10 h and 100 h respectively, they represent the later linear flow regime which indicates the existence of fractures.

Moreover, the integrated interpretation of the sudden temperature increase and gradual pressure growth reflects the adiabatic coefficient (compression effect or expansion effect) which dominates the gauge measured temperature behaviour during the early time region. In this case, the transient temperature and pressure data were recorded every 10 seconds. The temperature increased from 78.05 to 78.2 °F and pressure rose by 2 psi within 360 seconds, as illustrated in Figure 5-3. The average adiabatic compression coefficient can be approximately evaluated from the maximal temperature and pressure increase:

$$\eta = \frac{\Delta T}{\Delta P} = 0.075\ F/psi$$

This estimated adiabatic coefficient is larger than the oil and water properties and smaller than typical values for gas. It verifies the nonlinear production scenario of multi-phase flow around the production layer (gas out of solution in the reservoir).

5.3.2 Field case two – nonlinear gas production well

This open-hole completion well is a vertical gas production well with designed well depth of 4300m. The daily gas production flow-rate was 14027-2431 m^3/day, during the second pressure draw-down period, and the average daily gas flow-rate was 3789m3/day. Other details of the test scheme, fluid sampling data, production history and reservoir parameters are shown in Table 5-4, Table 5-5 and Table 5-6.

Table 5-4：Test scheme and production parameters

Test layers	Layers	Well length(m)		Log interpretation
	6	3761.0-3984.5m		Gas layer, dry layer (poor reservoir properties)
Production management	First open	First shut	Second open	Second shut
	5-10min	24Hr.	4-8Hr.	24-72Hr.

Table 5-5：Pressure and temperature measurements recorded by four gauges at the end of second build–up test

Gauge No.	Depth(m)	Measurement range of the gauge (MPa/℃)	Pressure (MPa)	Temperature (℃)
1	3650.74	80/150	40.681	121.452
2	3650.24	80/150	40.709	121.195
3	3652.54	100/175	40.705	121.221
4	3652.79	100/178	40.622	121.937

Table 5-6：Fluid sampling data

Surface Gas properties						
Component	CO_2 (%)	Methane (%)	Ethane (%)	Propane (%)	Isobutene (%)	N-butane (%)
Natural gas	25.24	73.41	1.19	0.16	0.01	0.03
	Relative density：0.8141					
Formation Gas properties						
Fluid	Density g/cm^3	Viscosity mPa.s	Compressibility 1/MPa	Volume factor m^3/m^3	Gas deviation coefficient, Z	
Natural gas	0.278	0.0321	0.01337	0.00368	1.08156	

Table 5-7：Pressure and temperature measurements at different test stages

	Before setting	First open		First shut	Second open		Second shut
		Start	end	End	Start	End	End
Time	27^{th}, Sep						29^{th}, Sep
	10:04	10:10	10:20	15:10	15:10	22:00	22:14
Pressure (MPa)	38.309	9.383	9.863	39.127	10.227	9.6	40.705
Temperature (C)	115.64	117.48	118.34	118.45	118.85	118.45	121.452

Figure 5-6 shows the plots of transient pressure and temperature respectively for flowing and shut-in periods. During the production of gas wells, the pressure drawdown increases with time. Therefore, either a decreasing or an increasing trend in wellbore temperature can be observed, and the temperature behaviour depends on the dominant factor (the Joule-Thomson cooling effect or the frictional heating effect). In this case, during the seven hours of flowing before the second shut-in, the stabilized increase of wellbore temperature is a combination of the dominant frictional heating effect and the secondary Joule-Thomson cooling effect. However, at the beginning of flow-rate increase (second opening), a sharp reduction of about 10 °F in the wellbore temperature over a short time can be observed from Figure 5-6. This is because of the large fluid expansion and Joule-Thomson cooling effect caused by a sudden pressure drop at bottom-hole.

Subsequently, for the pressure build-up test (second shut-in), early time transient temperature data can still detect the end point of wellbore storage. The down-hole temperature will increase sharply as soon as the gas well is shut-in, due to the interaction of fluid compression and the end of Joule-Thomson cooling. The frictional heating effect will also vanish once down-hole flow-rate declines to zero and wellbore storage ends. At this point the only factor that is reducing the wellbore temperature changes to heat conduction. Therefore, not only in the build-up test of a multiphase well but also in the build-up test of a gas well, the wellbore storage starts when temperature increases and ends when temperature decreases.

Figure 5-8 shows pressure and pressure derivative plots for the second shut-in period. The corresponding behaviour of temperature during the same time period is shown in Figure 5-7; the x axis also stands for the logarithm of shut-in time and the y axis represents the temperature at gauge location.

This case study also shows the success of the wellbore storage diagnostic and linear flow regime indication with transient temperature data. The end points of wellbore storage are marked in Figure 5-7 and Figure 5-8; both are at 1 hour after the second shut-in. As shown in Table 5-8, the plateau pressure derivative curves interpreted an average permeability and skin factor of 0.00533md and -1.43 respectively. The relatively large jump of about 4 °F in temperature during this early time region indicates a low permeability (0.00533 md) and large skin (-1.43), which are coherent with the pressure interpretation results. The interpreted low permeability maybe caused by the long open hole section (more than

200m), and the thin gas layer (only 5m). The high rate gas flow (3789 m^3/day) may cause a rate-dependent skin, which manifests itself as a higher temperature jump and increased Joule-Thomson effect. In addition, a linear flow regime can occur in a channel reservoir, hydraulically fractured well or horizontal well. The concave shape on semi-log temperature plot and the 1/2 slope on pressure derivative curve represent the later linear flow regime.

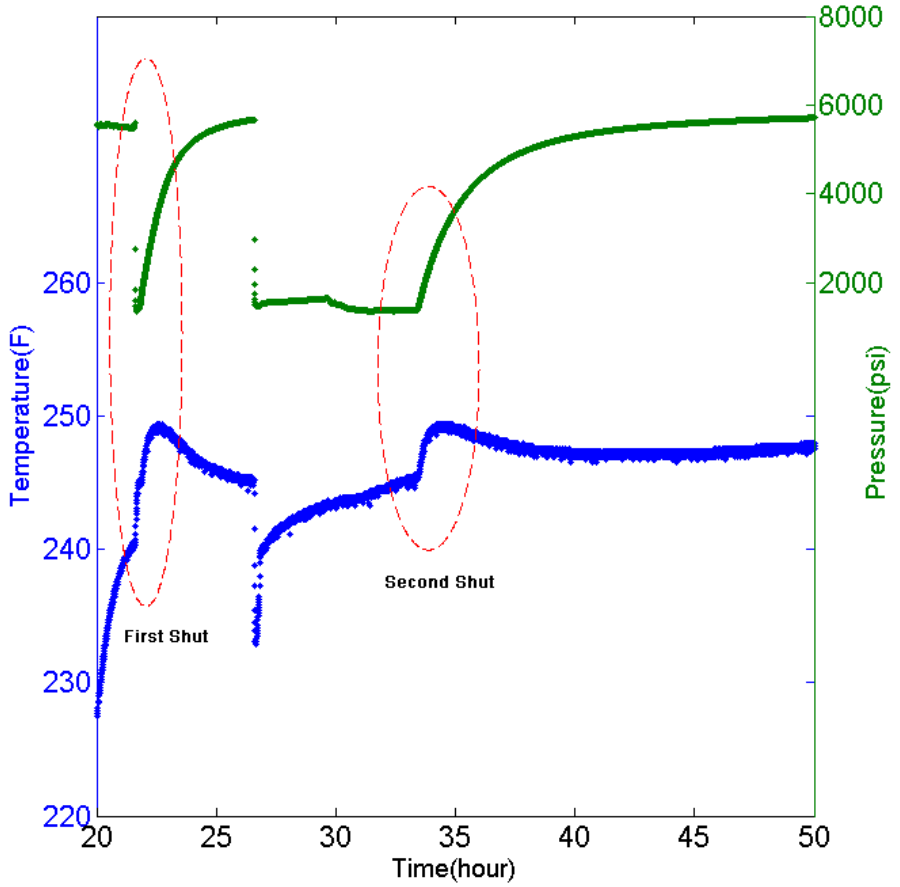

Figure 5-6：Transient pressure and temperature data during the 50 hours of pressure build-up and draw-down tests

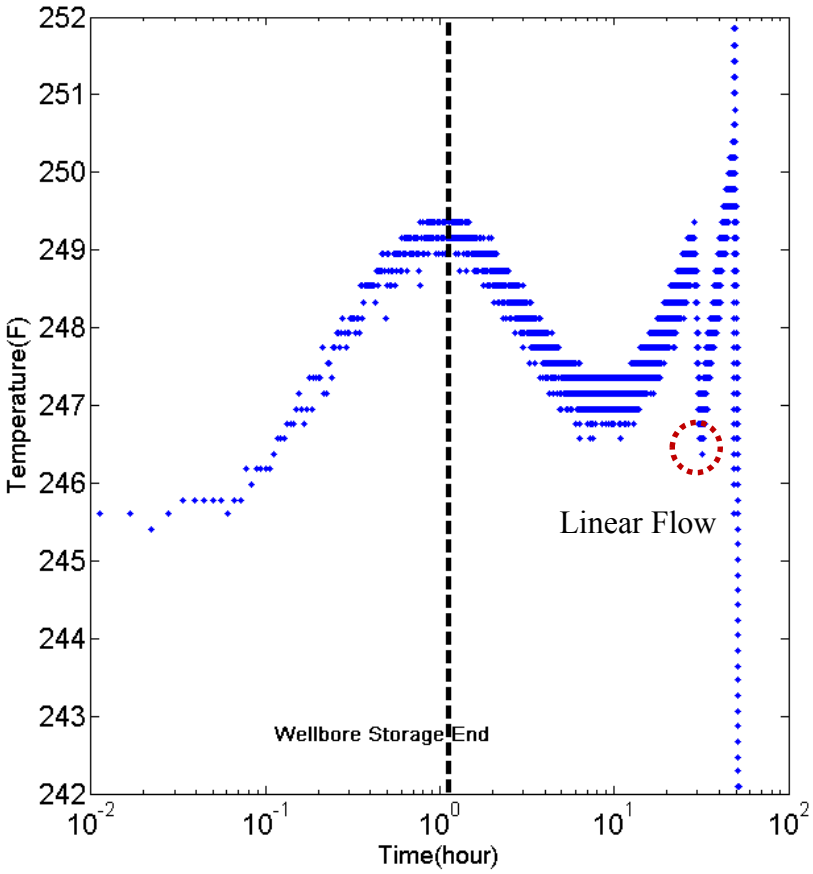

Figure 5-7：Semi-log plot of down-hole temperature during the second pressure build-up test

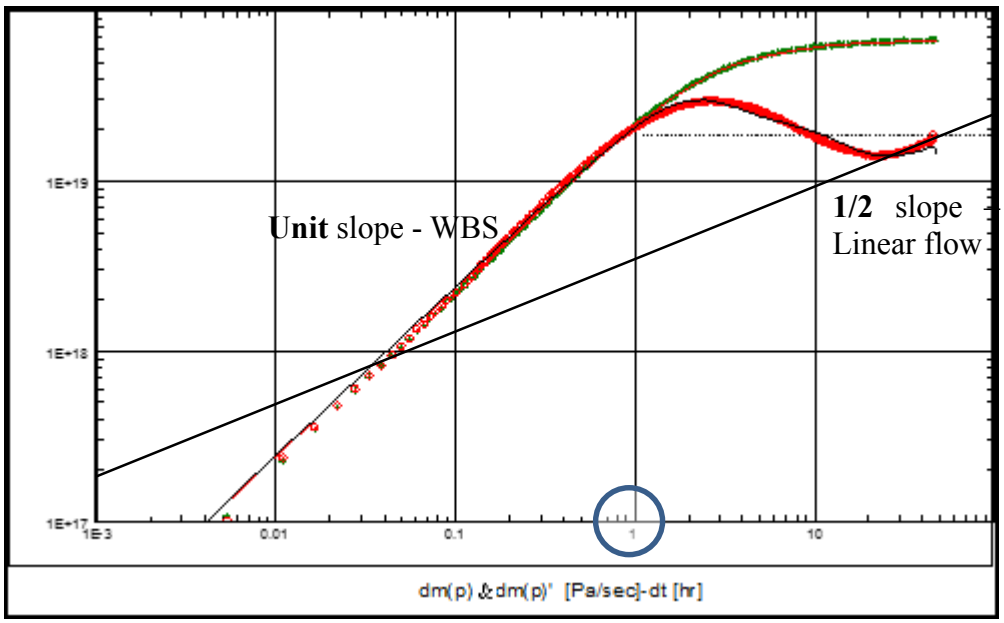

Figure 5-8：Log-log plot of down-hole pressure and pressure derivative during the second pressure build-up test

Table 5-8：Well-test interpretation results using pressure transient log-log regression

Software: PanSystem™ V3.5		Interpretation
Production rate	Oil（m^3/d）	
	Gas（m^3/d）	3789
	Water（m^3/d）	
Reservoir pressure (MPa)		44.05
Pressure coefficient (initial reservoir pressure/hydrostatic pressure)		1.16
Reservoir temperature (°C)		128.49
Geothermal gradient (°C/100m)		3.15
Formation parameter	Flowability coefficient（$10^{-3}\mu m^2$.m/mPa.s）	3.067
	Formation volume factor	0.0985
	Permeability ($10^{-3}\mu m^2$）	0.00533
	Skin factor	-1.43
	Wellbore storage coefficient (m^3/MPa)	0.149
	Coefficient of elasticity	0.0384
	Leakage coefficient	0.00109

5.4. Unknown flow-rate history calculation from down-hole transient data for both linear and nonlinear systems

In order to analyse transient down-hole data, monitor the production, and conduct model simulation for history-matching, detailed flow rate histories need to be acquired in advance. However, flow-rate data is not always available in practice; moreover, the conventional flow-rate measurement techniques such as flow metering measurements and production-logging tools are not only cost-prohibitive but also unreliable, especially in multiphase reservoirs. With limited utilization of down-hole flow meters in the oil fields, the common practice is the use of ‘combination of producers’ which means that the summation of the flow-rates is measured with surface separation equipment. This method has two major disadvantages. First of all, high-frequency tests are required to allocate accurate flow-rates back to individual wells. Secondly, the detailed flow-rate events are virtually unobtainable. Alternatively, it is also possible to reconstruct flow-rate history using established reservoir-wellbore models, as illustrated in Chapter 3. Because of the

complexity of building either isothermal or non-isothermal models, it is sometimes difficult to keep the errors and uncertainties away.

According to the previous relationship analyses and the convolution integral theory (WT), transient temperature is also related to flow-rate. Consequently, the detailed flow-rate history may be generated by calculating in advance the coefficient of relationship between flow-rate change and temperature WT amplitude, similarly to the flow-rate reconstruction algorithm from transient pressure data (Wang and Zheng, 2012). In this section, a new method of recovering flow-rate history from transient temperature and cumulative production data is applied. This method is model-independent and therefore has wide applications in different kinds of reservoirs. Generally speaking, if it is a linear system such as a single oil phase production well, the flow-rates reconstructed from pressure data are more accurate; however, if nonlinear gas flow (pressure-dependent parameters) exists in either reservoir or wellbore, the transient temperature data can reconstruct better results. In a word, the interpretation of transient temperature data is useful when there is a lack of other data.

5.4.1 Theoretical derivation

Although the entire flow-rate history contains many different flow events and each flow period consists of several flow regimes, flow-rate performs in accordance with down-hole pressure and down-hole temperature. If the sample interval time (impulse time) Δt is much smaller than the entire production time t, the extended unit-rate-change method on transient temperature analysis is able to reconstruct the flow-rate history. The unit-rate-change coefficient A_{urc} is a relative function which relates to the flow-rate change and provides the information regarding reservoir and well properties.

Based on the previous discussion on both linear and nonlinear cases, the flow-rate change Δq is proportional to the amplitude of temperature WT detail coefficients A_T and the pressure WT detail coefficients A_P in the oil case, but only responds to changes of the later temperature WT detail coefficients A_{Tl} in the gas production case.

Linear system: $A_{Purc} = \frac{A_P}{\Delta q} = constant$ $A_{Turc} = \frac{A_T}{\Delta q} = constant$

Nonlinear system: $\mathrm{A}_{Tlurc} = \frac{\mathrm{A}_{Tl}}{\Delta q} = \text{constant}$

The detailed flow-rate history can be generated by calculating the coefficient of the relationship in advance. For example, the second rate q_2 can be equated to the initial rate q_1 and first amplitude A_1 as:

$$q_2 = q_1 + \frac{A_1}{b} \quad , \tag{5.1}$$

where b represents the unit-rate-change proportional coefficient A_{urc}.

Then, for the second flow event (third flow period):

The third rate q_3 can be expressed with initial rate q_1, first Amplitude A_1 and second Amplitude A_2 as:

$$q_3 = q_2 + \frac{A_2}{b} = q_1 + \frac{A_1 + A_2}{b} \tag{5.2}$$

The remaining rates may be deduced by analogy and for the n-1 flow event (n flow period), the flow-rate q_n can be written as:

$$q_n = q_1 + \frac{\sum A_{n-1}}{b} \tag{5.3}$$

Assuming t_n is the specific flow time for rate q_n , the production for this flow period can be calculated as:

$$q_Q = q_n * t_n \tag{5.4}$$

Based on material balance, the total cumulative production Q is:

$$\mathrm{Q} = q_1 * t_1 + q_2 * t_2 + q_3 * t_3 \ldots + q_n * t_n \tag{5.5}$$

Substituting Eq. 5.3 into Eq. 5.5:

$$\mathrm{Q} = q_1 * \sum t_n + \frac{A_1 t_2 + (A_1 + A_2) t_3 + (A_1 + A_2 + A_3) t_4 \ldots + \sum A_{n-1} * t_n}{b} \tag{5.6}$$

Therefore, the constant b can be expressed as:

$$\mathrm{b} = \frac{A_1 t_2 + (A_1 + A_2) t_3 + (A_1 + A_2 + A_3) t_4 \ldots + \sum A_{n-1} * t_n}{Q - q_1 * \sum t_n} \qquad 5.7$$

Finally, by combining Eq. 5.7 and Eq. 5.3, the reconstructed flow-rate q_n for flow period n is:

$$q_n = q_1 + \frac{\sum A_{n-1}}{A_1 t_2 + (A_1 + A_2) t_3 + (A_1 + A_2 + A_3) t_4 \ldots + \sum A_{n-1} * t_n} * (Q - q_1 * \sum t_n) \qquad 5.8$$

With the detailed values of flow-rate and the exact time of flow-rate change, the flow-rate history can be reconstructed.

5.4.2 Application in Synthetic case one – Single oil phase production

A homogenous single phase oil production scenario is modelled, and the parameters used in this simulation are shown in Table 5-9. Figure 5-9 demonstrates the calculated pressure and temperature history in the first 16 hours. The cumulative production during this period is 320 bbl.

In this case, the initial flow-rate q_1 is assumed as a constant for reconstructing the next three rate changes from both pressure and temperature data.

Firstly, the two kinds of transient data are processed with Continuous Wavelet Transform by using the Haar wavelet. Figure 5-10 and Figure 5-11 show the processed data which identify the exact time of flow events. The specific values of flow-rate periods and the amplitude of WT detail coefficients are illustrated in Table 5-11. Secondly, the approximate proportional coefficients b_p and b_t are calculated and in this case, b_p=5.753, b_t=-0.00257. Finally, according to Eq. 5.8, the other three flow-rates can be calculated by using the constant *b* and initial rate q_1. The results reconstructed from the pressure and temperature data are compared and shown in Table 5-11. The errors in the flow-rate which was reconstructed from the transient pressure data are extremely small, less than 0.1%. Transient temperature data can also reconstruct flow-rate in this linear system, but the errors are much larger, up to 2.7%.

Table 5-9： Fluid, wellbore and reservoir parameters used in the synthetic model

Parameter	**Value**
Initial reservoir pressure, p_i	2900 psi
Permeability, k	100 md
Porosity, $\emptyset$	0.2
Total compressibility, C_t	6.89e-6 1/psi
Well radius, r_w	0.328 ft
Viscosity, μ_t	3 cp
Joule-Thomson coefficient, C_{JT}	2.76e-3 K/psi
Adiabatic coefficient of expansion/compression, η	9.65e-4 K/psi
Fluid thermal conductivity, λ_f	0.3 W/m.K
Fluid heat capacity, C_f	1500 J/kg.K
Fluid thermal expansion coefficient, β	N/A
Rock thermal conductivity, λ_r	7 W/m.K
Rock heat capacity, C_r	750 J/kg.K

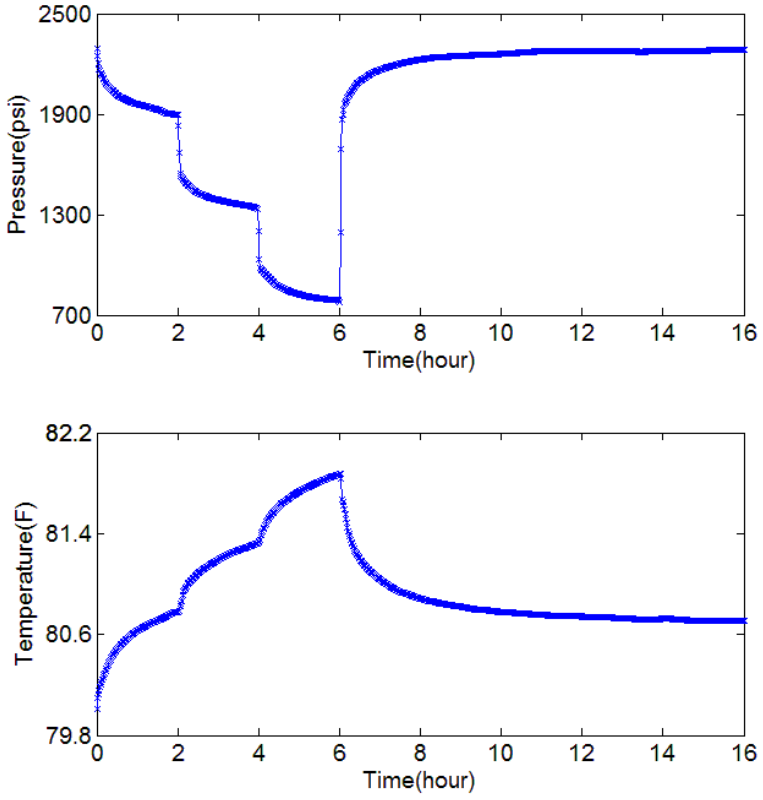

Figure 5-9： Transient pressure and temperature data used for flow-rate reconstruction

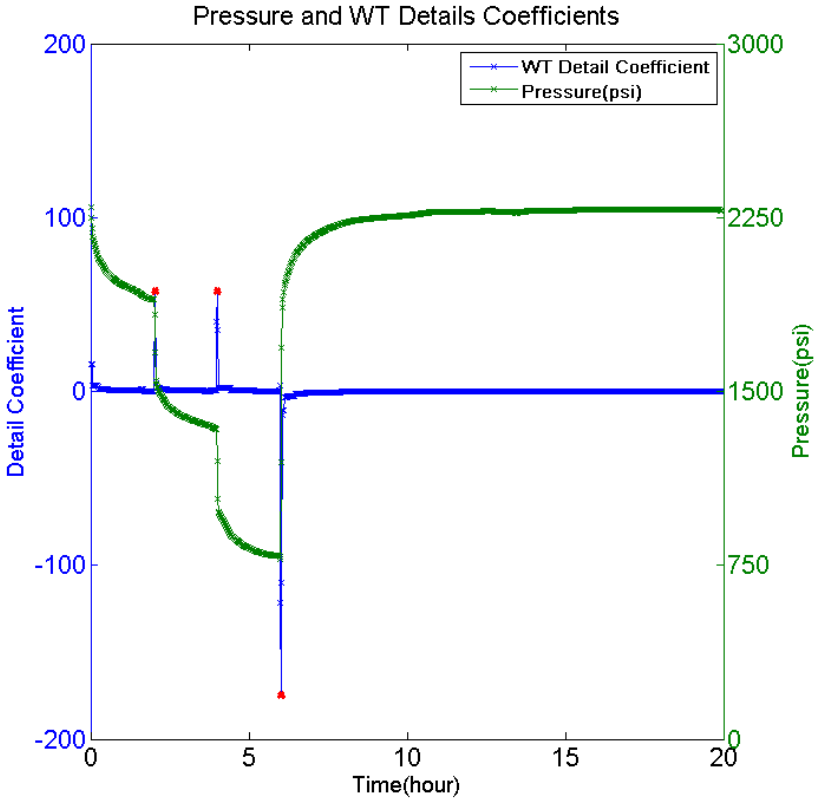

Figure 5-10：Processed transient pressure data using Haar wavelet transform

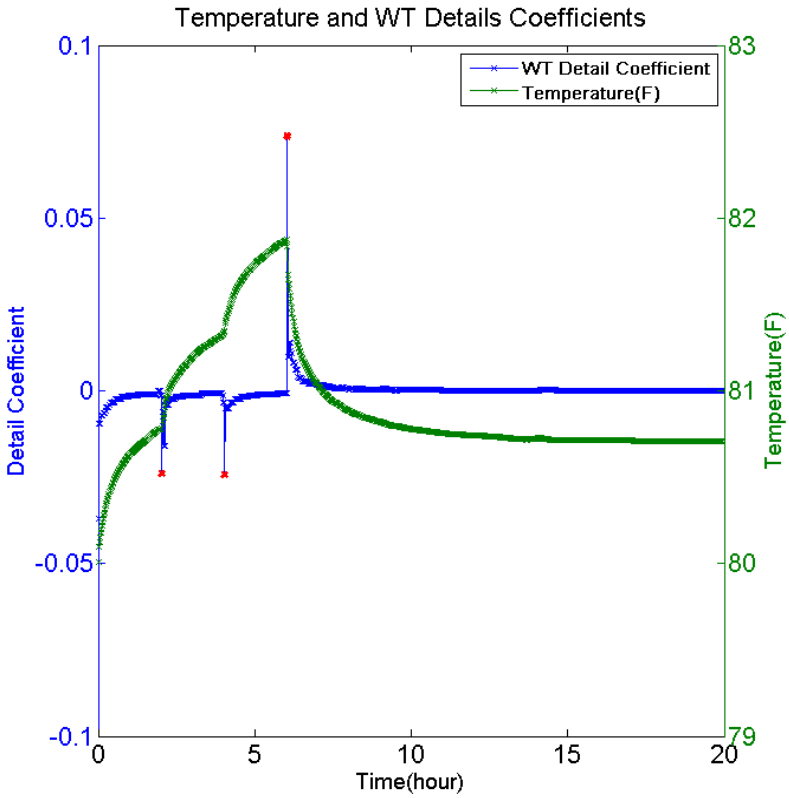

Figure 5-11：Processed transient temperature data using Haar wavelet transform

Table 5-10：Pressure data (b_p=5.753) reconstructed flow-rates are very accurate in linear system

Flow event beginning time (hour)	Flow event ending time (hour)	Flow event time period (hour) ti	Amplitude of WT coefficients A_j	Real rate (bbl/hour)	Calculated rate (bbl/ hour)	Error (%)
0	2	2	N/A	20	N/A	N/A
2	4	2	57.43	30	29.98	0.067
4	6	2	57.43	40	39.96	0.1
6	20	14	-172.35	10	10	0

Table 5-11：Temperature data (b_t=-0.00257) reconstructed flow-rates are not accurate enough in linear system

Flow event beginning time (hour)	Flow event ending time (hour)	Flow event time period (hour) ti	Amplitude of WT coefficients A_j	Real rate (bbl/ hour)	Calculated rate (bbl/ hour)	Error (%)
0	2	2	N/A	20	N/A	N/A
2	4	2	-0.0243	30	29.46	1.8
4	6	2	-0.0243	40	38.92	2.7
6	20	14	0.0737	10	10.24	2.4

5.4.3 Application in Synthetic case two – Single gas phase production

In order to test the performance of the rate reconstruction method and to demonstrate the differences between transient temperature and pressure data, another homogeneous single phase high flow-rate gas production case was simulated. The gas and reservoir parameters

used in this model are shown in Table 5-12 and Table 5-13. Figure 5-12 demonstrates the simulated production history during 120 hours. The cumulative production during this period is 441404 SM^3 = 0.000035*441404 = 15.449 MMSCF.

Table 5-12：Fluid, wellbore and reservoir parameters used in the synthetic model

Parameter	**Value**
Initial reservoir pressure, p_i	725 psi
Reservoir thickness, h	98.4ft
Permeability, k	Kx=ky=20md, kz=1md
Porosity, $\emptyset$	0.3
Rock compressibility, C_t	3.45e-5 1/psi
Well radius, r_w	0.328ft
Skin factor, s	3

Table 5-13：Thermal parameters used in the synthetic model

Parameter	**Value**
Fluid thermal conductivity, λ_f	0.003 W/m.K
Fluid heat capacity, C_f	2 kJ/kg.K
Rock thermal conductivity, λ_r	5.0 W/m.K
Rock heat capacity, C_r	750 J/kg.K
Joule-Thomson coefficient, C_{JT}	6.9e-3 K/psi
Adiabatic expansion coefficient, η	5.5 K/psi
Fluid thermal conductivity, λ_f	0.003 W/m.K
Fluid heat capacity, C_f	2 kJ/kg.K

According to the previous discussions in Chapter 4, the unit-rate-change coefficient A_{Purc} is not constant in this nonlinear system, because of the changeable gas properties. However, the extended URSR method for transient temperature analysis, which has been proven, and a constant $A_{Tlurc}$for pressure build-up tests can provide another choice for flow-rate reconstruction.

Firstly, these two kinds of transient data are processed with Continuous Wavelet Transform (on selected scale parameters) by using the Haar wavelet. Figure 5-13 and Figure 5-14 show the processed data which identify the exact time of flow events. The specific values of flow-rate periods and the amplitude of WT detail coefficients are shown in Table 5-14 and Table 5-15. Differently from case one, there is another table, Table 5-16, which shows the reconstructed flow-rate from the later amplitude of WT detail coefficients. Secondly, the initial flow-rate q_1 is also assumed as a constant and in this case, the approximate proportional coefficients are b_p=2.36, b_{tf}= 0.2555, b_{tl}= -0.0484. Finally, based on Eq. 5.8, the other flow-rates can be calculated by using b_p, b_{tf} and b_{tl} separately. The results reconstructed from the pressure and temperature data are compared and shown in Table 5-14, Table 5-15 and Table 5-16. Compared with the reconstruction results in the linear system, the errors in the flow-rate reconstructed from transient pressure data are much larger, in this nonlinear case, up to 3.8%. Again, using the transient temperature data (earlier WT detail amplitudeA_{Tf}) runs the errors up to 22.1%. However, the later WT detail amplitudes A_{Tl} reconstruct the flow-rate to a high accuracy, as illustrated in Table 5-16.

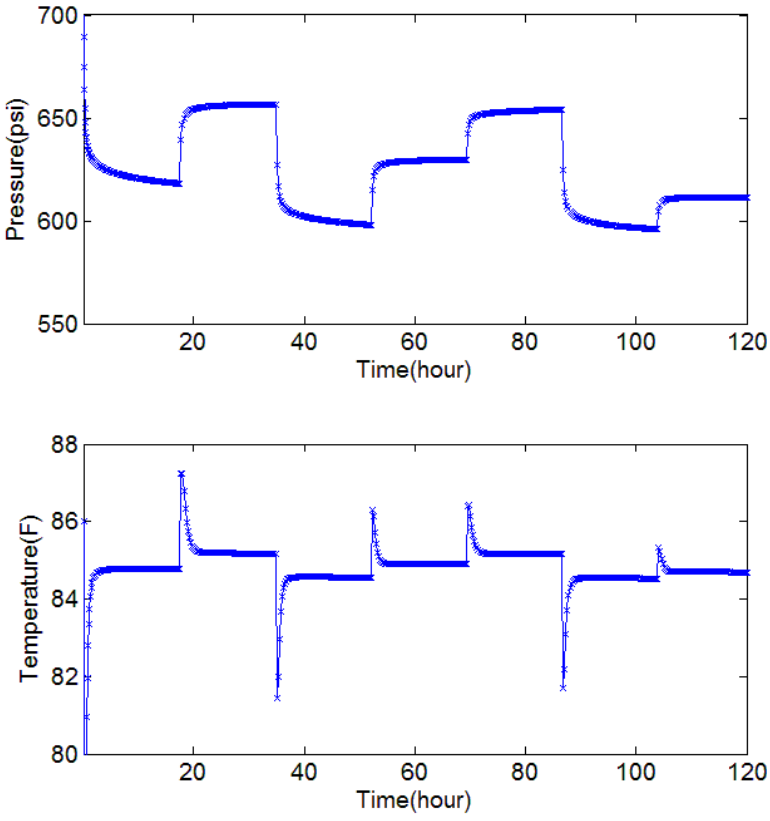

Figure 5-12：Transient pressure and temperature data for reconstructing flow-rate

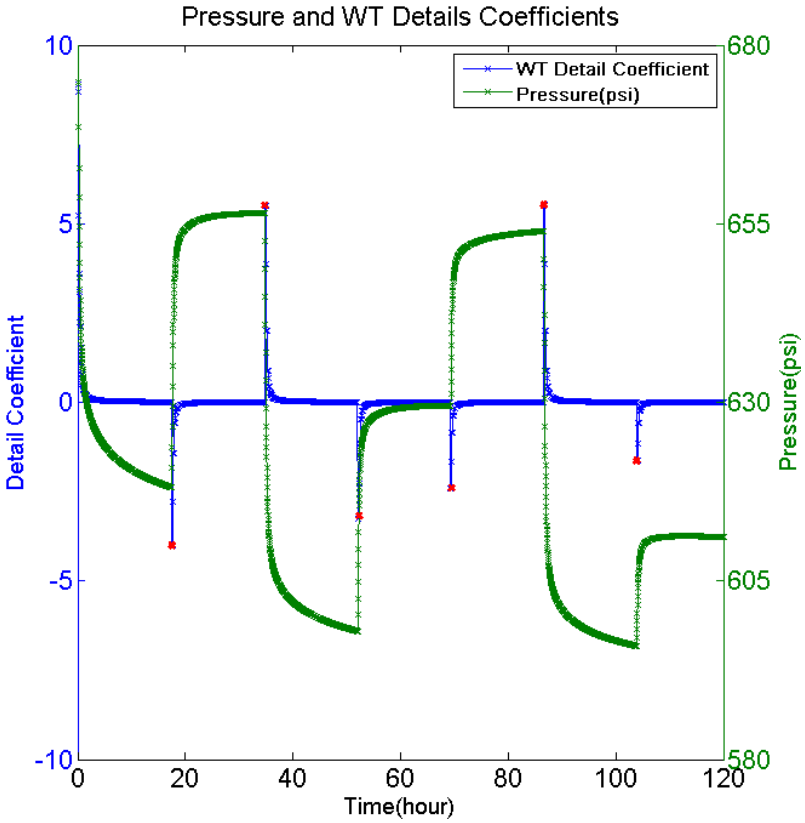

Figure 5-13：Processed transient pressure data using Haar wavelet transform

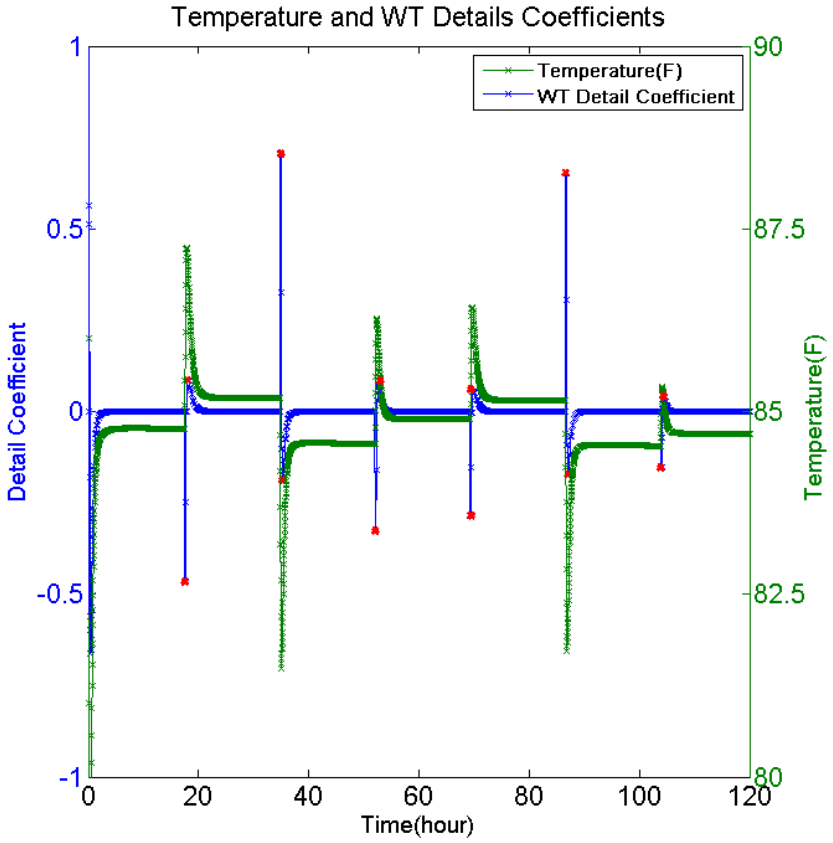

Figure 5-14：Processed transient temperature data using Haar wavelet transform

Table 5-14：Flow-rates reconstructed from pressure data (bp=2.36) are not accurate enough in a nonlinear system

Flow event beginning time (hour)	Flow event ending time (hour)	Flow event time period (hour) ti	Amplitude of WT coefficient A_j	Real rate (MMSC/ day)	Calculated rate (MMSCF/day)	Error (%)
0	17.47	17.47	N/A	3.532	N/A	N/A
17.47	34.75	17.28	-4.006	1.766	1.835	3.8
34.75	52.03	17.28	5.511	4.238	4.170	1.6
52.03	69.31	17.28	-3.254	2.825	2.791	1.2
69.31	86.59	17.28	-2.4	1.766	1.774	0.5
86.59	103.9	17.31	5.529	4.238	4.117	2.9
103.9	120	16.1	-1.63	3.532	3.426	3.0

Table 5-15：Flow-rates reconstructed from earlier temperature amplitudes (b_{tf}= 0.2555) have large errors in a nonlinear system

Flow event beginning time (hour)	Flow event ending time (hour)	Flow event time period (hour) ti	Amplitude of WT coefficient A_{tf}	Real rate (MMSCF /day)	Calculated rate (MMSCF/day)	Error (%)
0	17.47	17.47	N/A	3.532	N/A	N/A
17.47	34.75	17.28	-0.4658	1.766	1.709	3.2
34.75	52.03	17.28	0.7049	4.238	4.468	5.4
52.03	69.31	17.28	-0.3271	2.825	3.188	12.8
69.31	86.59	17.28	-0.2632	1.766	2.157	22.1
86.59	103.9	17.31	0.6532	4.238	4.714	11.2
103.9	120	16.1	-0.153	3.532	4.115	16.5

Table 5-16： Flow-rates reconstructed from later temperature amplitudes (b_{tl}= -0.0484) have very small errors even in a nonlinear system

Flow event beginning time (hour)	Flow event ending time (hour)	Flow event time period (hour) ti	Amplitude of WT coefficients A_{tl}	Real rate (MMSCF /day)	Calculated rate (MMSCF /day)	Error (%)
0	17.47	17.47	N/A	3.532	N/A	N/A
17.47	34.75	17.28	0.0859	1.766	1.757	0.50
34.75	52.03	17.28	-0.1885	4.238	N/A	N/A
52.03	69.31	17.28	0.0685	2.825	2.823	0.08
69.31	86.59	17.28	0.0511	1.766	1.769	0.18
86.59	103.9	17.31	-0.1724	4.238	N/A	N/A
103.9	120	16.1	0.0343	3.532	3.529	0.08

5.4.4 Application in field data

A set of field PDG temperature data which has been described in section 4.4 is used to reconstruct the flow-rate. Daily oil production was measured, but the detailed flow-rate history is not available. The original long-term temperature and pressure data may be affected by the skin and permeability change, so it is not easy to extract a constant A_{urc} coefficient which represents constant reservoir-well parameters for the whole production period. Figure 5-15 shows a subset of the entire time span which contains several flow events within 250 hours. The temperature data have been processed in advance and the early time temperature increase/decrease which is affected by wellbore storage can be ignored in this slightly compressible oil reservoir. Figure 5-16 shows the wavelet transformed temperature data; the points of flow-rate change can be identified with the amplitudes of detail coefficients. The amplitudes are positive for pressure build-up and are negative for pressure draw-down. The cumulative production can be calculated from the daily flow-rate, and the unit-rate-change coefficient can be calculated by Eq. 5.7. In this case, the initial flow-rate q_1=11630 bbl/day, the constant coefficient b=-0.0012, and the cumulative production Q=121807 bbl. Figure 5-17 compares the calculated flow-rates

and the measured daily flow-rates during this period. The reconstructed flow-rates can reflect all of the flow events within the acceptable errors, except for the marked daily flow-rate point. This uncertainty may be caused by the original data gap, because linear interpolation was conducted before wavelet transform.

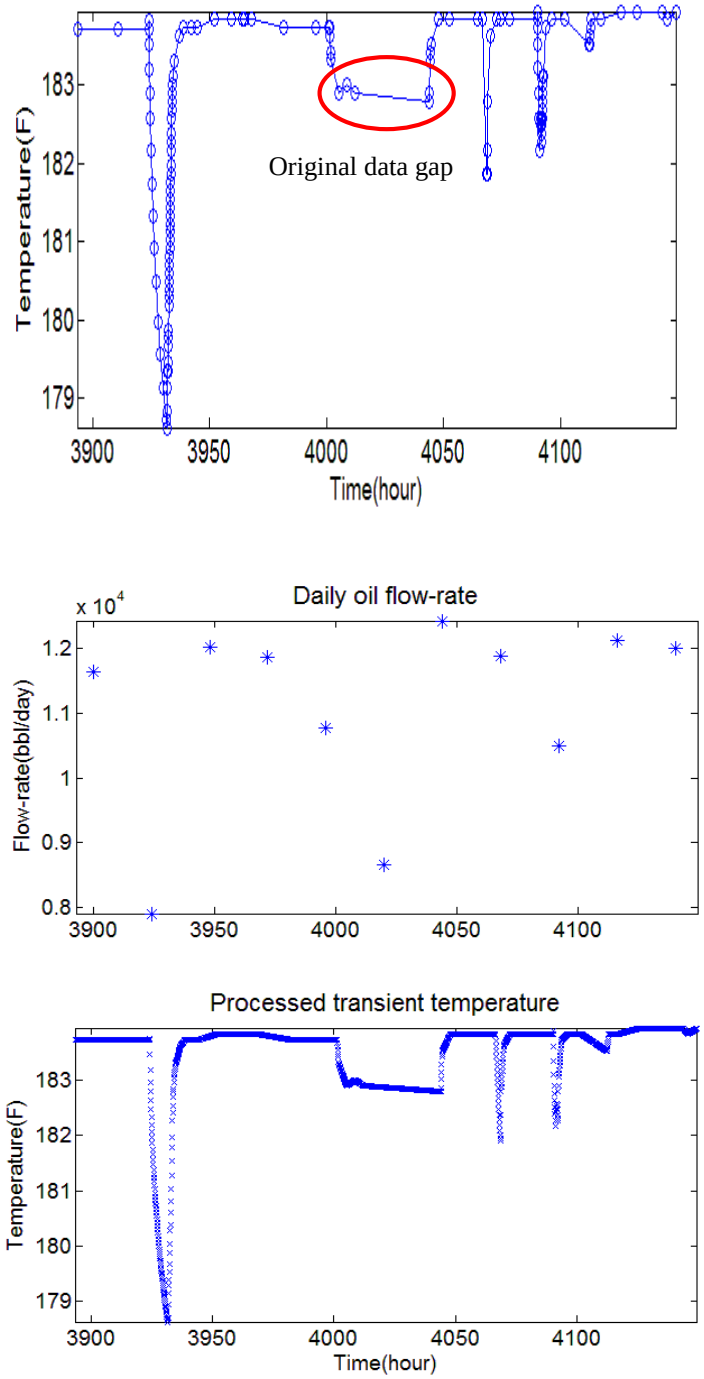

Figure 5-15： A subset of measured temperature data, daily flow-rate, and processed temperature data

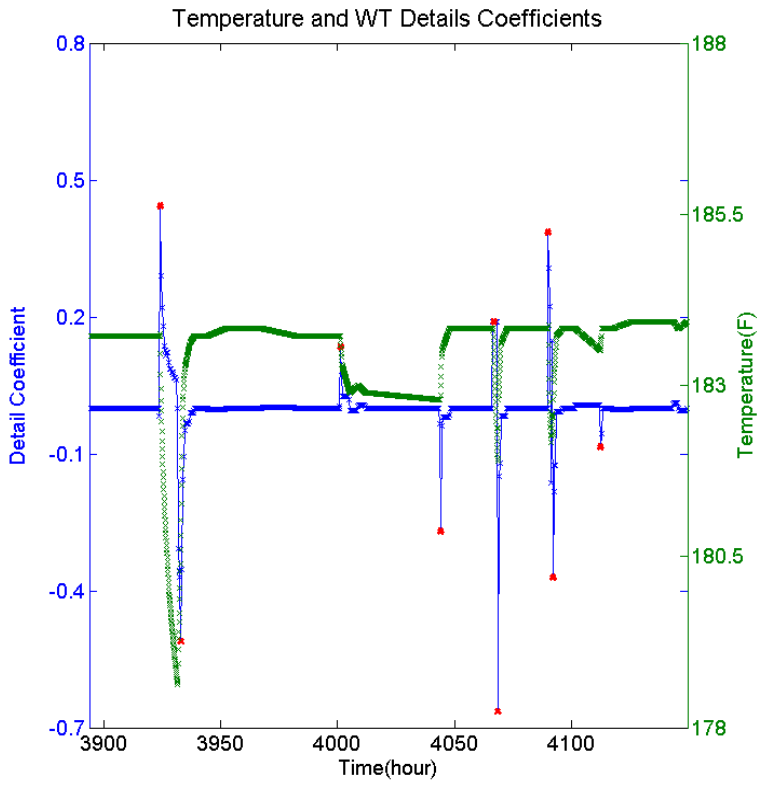

Figure 5-16：Processed transient temperature data and detected breakpoint locations

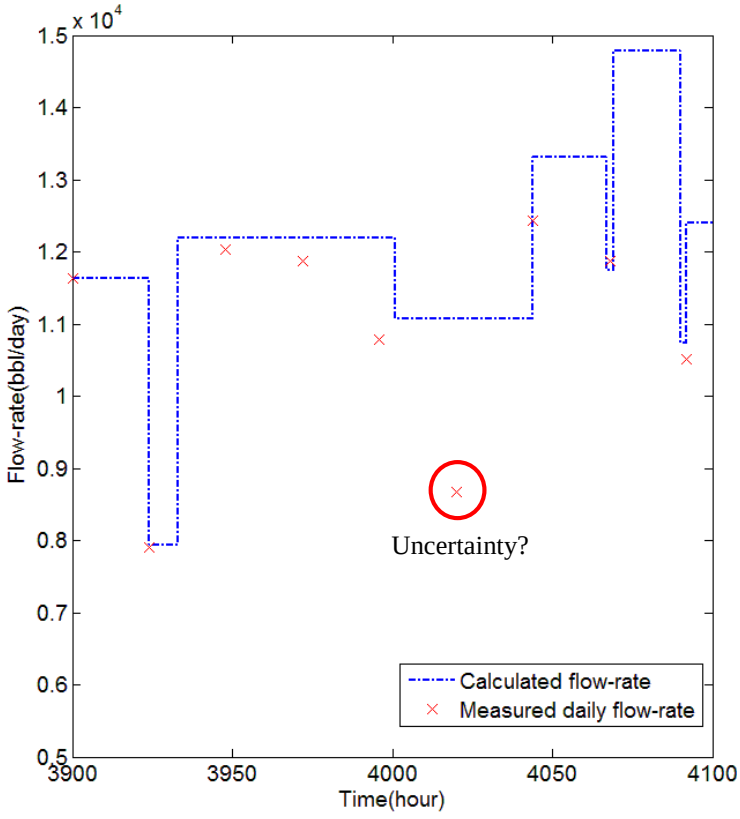

Figure 5-17：Measured daily flow-rate and calculated real-time flow-rate

5.5. Analysis of later-time region transient temperature data for reservoir parameters and radius of investigation estimation

The transient temperature and pressure are measured at second intervals, and the entire set of PDG data consists of many flow events. Generally, the flow regime changes, for example from early time flow to later time radial flow, for every transient period with constant flow-rate. In this section, a radial flow analytical solution which is able to calculate the sand-face temperature is introduced and the reservoir parameters, such as permeability and skin factor, are estimated with the previously calculated flow-rate.

The energy conservation equation for single phase fluid flow in a porous medium was described in Eq. 4.18, which demonstrates the effects of convective/conductive heat transfer and thermodynamic Joule-Thomason/adiabatic terms on temperature behaviour. Based on a series of assumptions such as neglecting the pressure/temperature-dependent fluid properties, the simplified sand face temperature solution for later times has been derived by (Valiullin and Ramazanov, 2010; Ramazanov and Valiullin, 2010):

$$\mathrm{T} = \frac{C_j q \mu}{4\pi k h}\left[ln\left(c\frac{q}{\pi {r_w}^2}\right) + lnt\right] \ , \qquad 5.9$$

where c is the ratio of the fluid heat capacity to the heat capacity of fluid statured rock.

It can be further simplified as:

$$\mathrm{T} = alnt + b$$

Therefore, Eq. 5.9 establishes a linear relationship between sand-face temperature at later times and the natural logarithm of time. The slope of the transient temperature curve depends on $\frac{C_j q \mu}{4\pi k h}$, and the intercept equals $\frac{C_j q \mu}{4\pi k} ln\left(c\frac{q}{\pi {r_w}^2}\right)$. Detailed flow-rate history was reconstructed from processed temperature data in advance, and C_j was treated as given information. Thus the permeability and mobility $(\frac{k}{\mu})$ of the formation within a time-dependent area (Eq. 5.11) can be estimated. Furthermore, the damaged/stimulated zones (near wellbore formation) which have different permeability can also be detected through the slope change (piecewise fitting approach); the skin factor and thermal radius of

investigation can be supposed according to Eqs. 5.10 and 5.11 respectively (Hawkin, 1956; Valiullin and Ramazanov, 2010):

$$s = (\frac{k}{k_s} - 1)\, ln \frac{r_s}{r_w} \qquad 5.10$$

$$r_{investigation} = \sqrt{{r_w}^2 + \frac{cqt}{\pi h}} \quad , \qquad 5.11$$

where k is the formation permeability and k_s is the reduced permeability of skin zone, r_s is the radius of skin zone and r_w is the radius of well (Further derivations of Eq. 5.9 and 5.11 are described in the Appendix).

The following three case studies are undertaken to illustrate how to evaluate the reservoir parameters from later time transient temperature data. It should be noted that this section only considers a simplified correlation for approximate analysis: more accurate interpretation results can be acquired by using a numerical model which simulates all the related effects.

5.5.1 Synthetic case one - oil production

The base case for single phase oil production is in a homogeneous reservoir with no skin factor. Other formation parameters and flow-rate details used in these estimations are shown in Table 5-17. Figure 5-18 shows the simulated transient temperature, and Figure 5-19 shows the second flow period's temperature change in semi-log coordinate.

Table 5-17：Synthetic oil case - given reservoir information and flow-rate data for four flow periods

Parameter	**Value**
Thickness	32.8 ft
Permeability, k	100 md
Porosity, $\emptyset$	0.2
Well radius, r_w	0.328 ft
Viscosity, μ_t	3 cp
Joule-Thomson coefficient, C_{JT}	2.76e-3 K/psi
Fluid heat capacity, C_f	1500 J/kg.K
Rock heat capacity, C_s	750 J/kg.K

Flow event beginning time (hour)	Flow event ending time (hour)	Flow event time period (hour)	Real rate (bbl/hour)	Calculated rate (bbl/ hour)
0	2	2	20	N/A
2	4	2	30	29.46
4	6	2	40	38.92
6	20	14	10	10.24

During the later time region, only one zone with constant slope is marked in the semi-log plot of transient temperature (Figure 5-19). According to the analytical solution and the theoretical definition of the curve's slope as described in Eq. 5.9, the permeability of the formation can be calculated:

$$\frac{C_j q \mu}{4\pi k h} = 0.1269 \text{ and } k = \frac{C_j q \mu}{0.1269 * 4\pi h} = \frac{4e{-}7 * 1.3e{-}3 * 3}{4 * 3.14 * 0.1269 * 10} = 99.2\ md$$

This estimation result is consistent with of the input (100 md permeability with no skin factor) of the numerical model which was used for generating the transient temperature data.

The duration of second flow period is 7200 seconds. Based on Eq. 5.11, the thermal investigation radius can be evaluated:

$$r_{investigation} = \sqrt{0.1^2 + \frac{1.5*7200*1.3e-3}{3.14*10}} = 0.676 \text{ m} = 2.217 \text{ ft}$$

During the limited steady production period (two hours in this case), the radius of thermal investigation is much smaller, compared with the pressure diagnostic radius of dozens of feet. This is as a consequence of the slow propagation of the thermal front. The high speed of propagation of the pressure wave may cause the difficulties in interpreting near wellbore formation properties by transient pressure data; however, temperature transient analysis can not only diagnose the early time region and flow-rate change, but also provide accurate estimations for the near wellbore formation (later time region).

Several notes and unit conversions used in these estimations are summarized: q=112.4m3/day=0.0013m3/s, C_j=4e-7K/pa, $c = 1.5$ dimensionless, μ =3 cp, 1 md = 0.9869e-15 m2. Additionally, the specific flow-rate ($\frac{q}{h}$) is calculated as uniformly distributed flow-rate (q) over the production layer thickness of 32.8 ft.

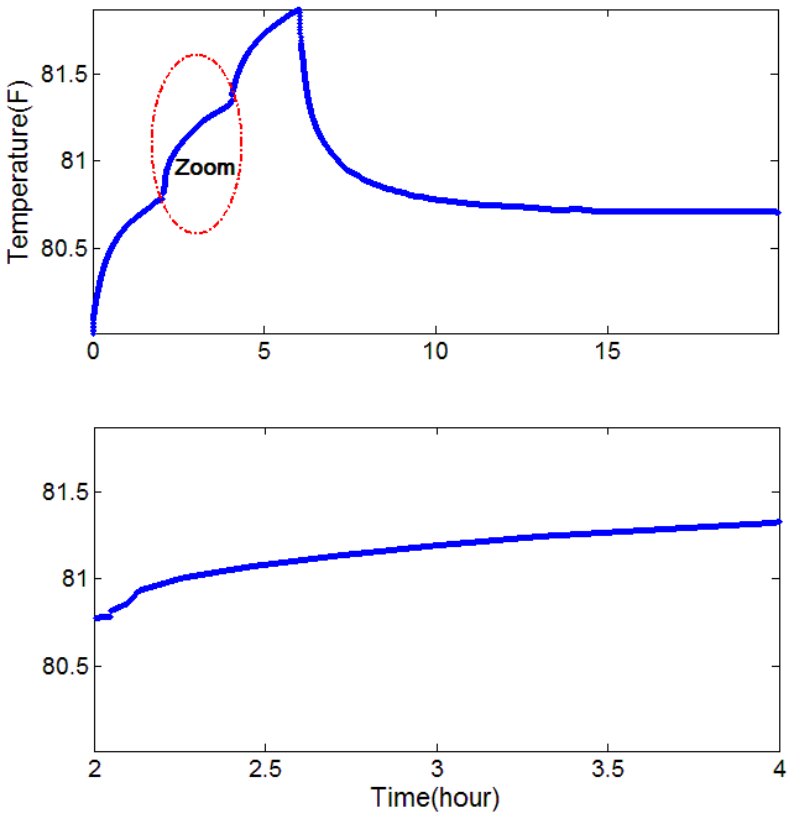

Figure 5-18：Synthetic oil case - transient temperature data and zoom-in for the second flow period

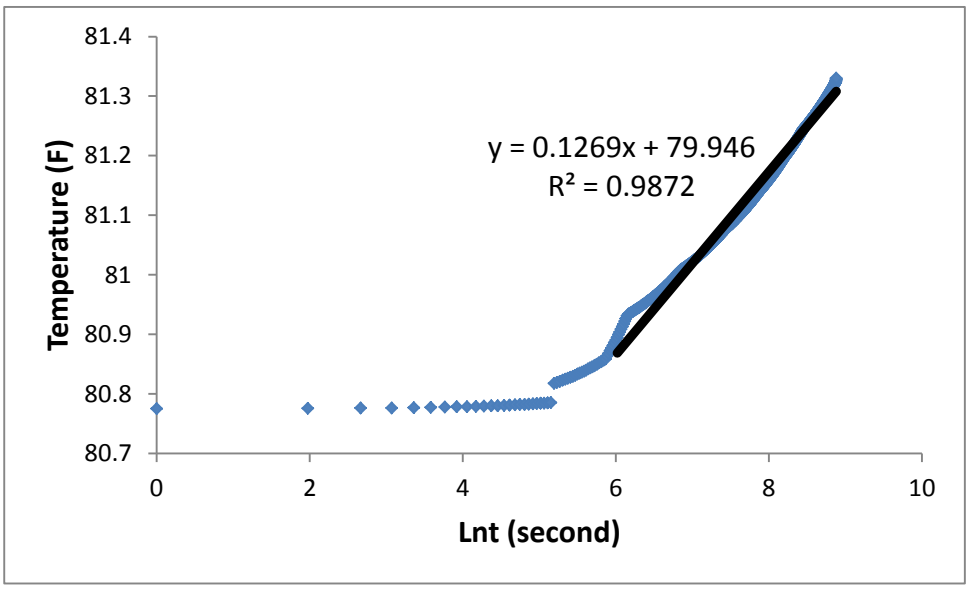

Figure 5-19：Synthetic oil case - temperature change and trend line in semi-log coordinate during second flow period

5.5.2 Field case application – gas production (negative skin)

The transient temperature data applied in this case study were acquired from a gas production well. Details of the formation properties, test scheme and fluid parameters were described in Section 5.3.2. Specifically, the gas viscosity does not change a lot for this high pressure scenario. Figure 5-20 shows the measured temperature data, and Figure 5-21 shows temperature change for the second pressure draw-down period in semi-log coordinates. During this flow period, the average gas flow-rate was 3789 m3 per day. The pressure transient analysis interpreted results of flowability coefficient ($\frac{\mathrm{kh}}{\mu}$) and skin factor are 3.067 md*m/cp and -1.43 respectively.

As demonstrated in Figure 5-21, two zones with different slopes are marked out. On the basis of the theoretical definitions of the slope change of the straight line, which has been described before, the ratio of near wellbore zone permeability (k_1) and the far formation permeability (k_2) can be estimated:

$$\frac{C_j q \mu}{4\pi h k_1} = 1.0492, \frac{C_j q \mu}{4\pi h k_2} = 1.9339$$

$$\frac{k_1}{k_2} = \frac{1.9339}{1.0492} = 1.84$$

The specific end time of the first slope is 3060 seconds, well radius r_w is 0.1 m, formation thickness h is 5 m, and the calculated c parameter equals 2. According to Eq. 5.11, the radius of the near wellbore zone can be evaluated:

$$r_s = \sqrt{0.1^2 + \frac{2*3060*0.04385}{3.14*5}} = 4.135\ m = 13.563\ \text{ft}$$

Then, skin factor can be calculated as:

$$s = (\frac{k2}{k_1} - 1)\ ln\frac{r_s}{r_w} = \left(\frac{1}{1.84} - 1\right) ln\frac{4.135}{0.1} = -1.69$$

After that, the fluid mobility (or flowability coefficient) in the reservoir can also be determined:

For the first slope, $\frac{C_j q \mu}{4\pi h k_1} = 1.0492$,

For the second slope, $\frac{C_j q \mu}{4\pi h k_2} = 1.9339$,

The specific gas flow-rate and Joule-Thomson coefficient are 0.04385 m3/s and 6.9e-3 K/psi respectively. The fluid viscosity is assumed as independent of temperature and pressure change. The calculated mobilities and flowability coefficients are:

$$\frac{k_1}{\mu} = \frac{C_j q}{1.0492*4\pi h} = \frac{1e{-}9*0.04385}{1.0492*4*3.14*5} = 0.666\ \text{md/cp}$$

$$\frac{k_2}{\mu} = \frac{C_j q}{1.9339*4\pi h} = \frac{1e{-}9*0.04385}{1.9339*4*3.14*5} = 0.361\ \text{md/cp}$$

$$\frac{k_1 \text{h}}{\mu} = 3.33\ \text{md} * \text{m/cp}$$

$$\frac{k_2 \text{h}}{\mu} = 1.81\ \text{md} * \text{m/cp}$$

Finally, given the flow duration of 24500 seconds, the thermal investigation radius in this gas production case is:

$$r_{investigation} = \sqrt{0.1^2 + \frac{2*24500*0.04385}{3.14*5}} = 11.69\ m = 38.343\ \text{ft}$$

Compared with the limited thermal investigation radius (near wellbore zone) in the oil production case, the analytical method can provide parameter estimations for wider formation in this gas production case, due to the high flow-rate gas flow and the extended production time.

In short, these estimation results are consistent with those of the transient pressure data interpreted parameters (Table 5-8). Therefore, later-time transient temperature analysis can provide a fast and reliable way of estimating the near wellbore and distant formation properties such as permeability, skin factor and fluid mobility.

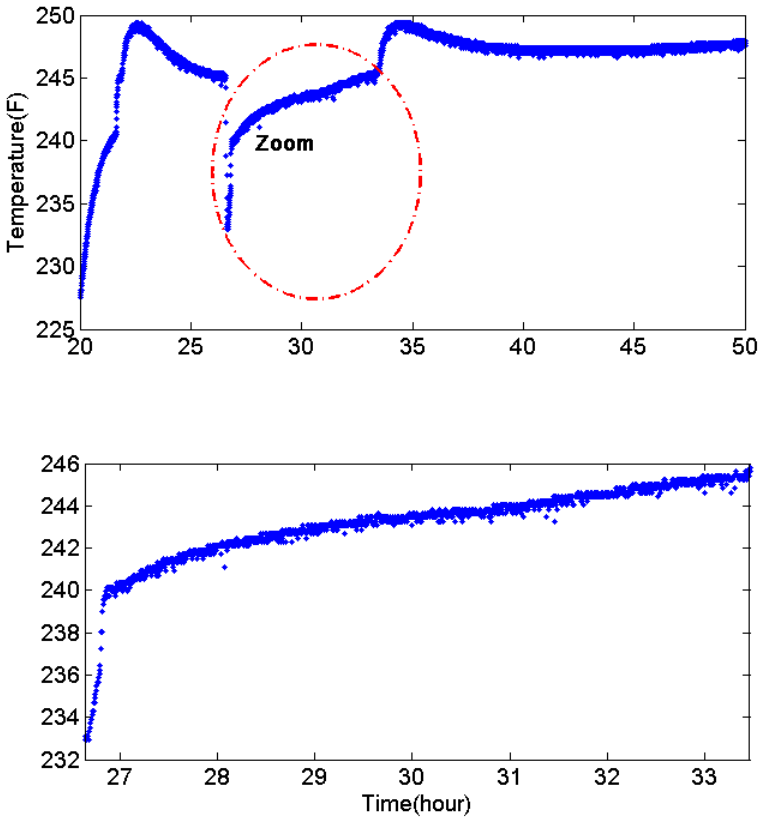

Figure 5-20：Field gas case - transient temperature data and zoom-in for the second flow period

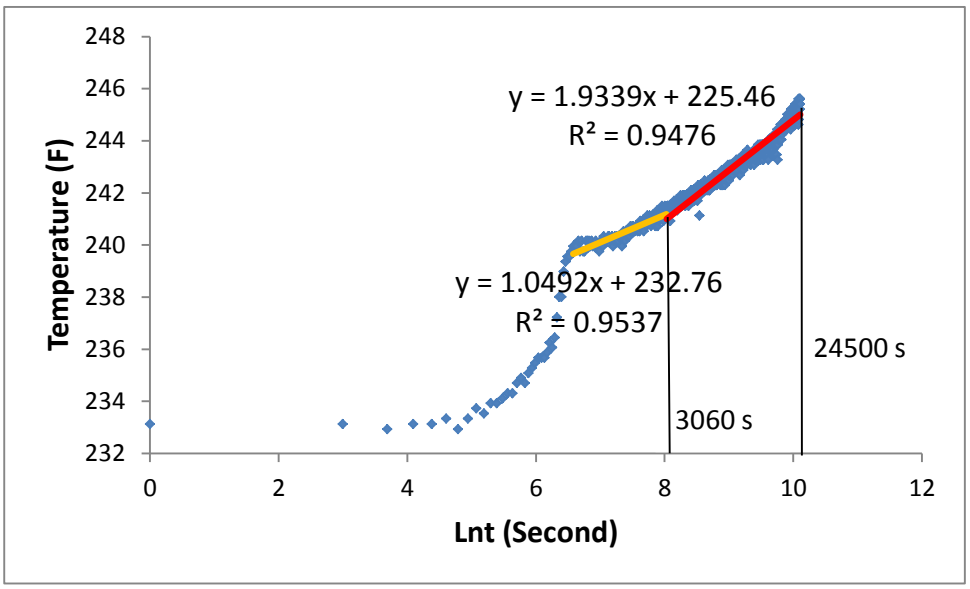

Figure 5-21： Field gas case - temperature change and trend lines in semi-log coordinate during second flow period

5.5.3 Field case application – oil production (positive skin)

A set of field PDG temperature data which has been described in section 5.4.4 is used to estimate the reservoir parameters. These transient temperature data were acquired from an oil production well. Daily oil production was measured and the detailed flow-rate history was reconstructed in section 5.4.4. According to the previous discussion about the flow-rate reconstruction algorithm, there is no skin and permeability change (proved by the constant A_{urc} coefficient) during the 250 hours of production period which contains several flow events.

The wellbore, formation parameters and reconstructed flow-rate details used in the estimations are shown in Table 5-18. Figure 5-22 demonstrates the measured transient temperature data, and Figure 5-23 shows the temperature change in the third flow period in semi-log coordinate. During this flow period, the calculated oil flow-rate is 12191 bbl/day.

Table 5-18: Field oil case - given wellbore/reservoir information and calculated flow-rate history

Parameter	**Value**
Formation Thickness	91.4 ft
Porosity, $\emptyset$	0.3394
Well radius, r_w	0.5104 ft
Viscosity, μ_t	0.506227 cp
Joule-Thomson coefficient, C_{JT}	4e-3 K/psi
Fluid heat capacity, C_f	1500 J/kg.K
Rock heat capacity, C_s	750 J/kg.K
Oil density	39.5757 lb/ft3

Flow event beginning time (hour)	Flow event ending time (hour)	Flow event time period (hour)	Calculated rate (bbl/day)
3900	3924	24	11630
3924	3933	9	7930
3933	4001	68	12191
4001	4044	43	11071
4044	4067	23	13319
4067	4069	2	11738
4069	4090	21	14778
4090	4092	2	10730
4092	4113	21	12408

As demonstrated in Figure 5-23 (semi-log plot of transient temperature), two zones with different slopes are marked out during the later time region. On the basis of the theoretical definitions of the slope change of the straight line, which has been described before, the ratio of near wellbore formation permeability (k_1) and the far formation permeability (k_2) can be estimated:

For the first slope, $\frac{C_j q \mu}{4\pi h k_1} = 2.162$; for the second slope, $\frac{C_j q \mu}{4\pi h k_2} = 0.2457$

$$\frac{k_1}{k_2} = \frac{0.2457}{2.162} = 0.1136$$

The specific end time of the first slope is 9660 seconds, well radius r_w is 0.5104 ft, formation thickness h is 91.4 ft and the calculated c parameter is equal to 1.6. According to Eq. 5.11, the radius of the near wellbore zone can be evaluated:

$$r_s = \sqrt{0.1556^2 + \frac{1.6*9660*0.02243}{3.14*27.866}} = 2\ m = 6.56\ \text{ft}$$

Then, the skin factor can be calculated as:

$$s = (\frac{k2}{k_1} - 1)\ ln\frac{r_s}{r_w} = \left(\frac{2.162}{0.2457} - 1\right) ln\frac{2}{0.1556} = 19.9$$

The specific oil flow-rate and Joule-Thomson coefficient are 0.02243 m3/s and 5.8e-7 K/pa respectively. With the two different slopes fitted piecewise, the permeability and fluid mobility of the reservoir can also be determined:

$$\frac{k_1}{\mu} = \frac{C_j q}{2.162*4\pi h} = \frac{5.8\text{e}{-7}*0.02243}{2.162*4*3.14*27.866} = 17.192\ \text{md/cp}\ ,\ k_1 = 8.703\ \text{md}$$

$$\frac{k_2}{\mu} = \frac{C_j q}{0.2457*4\pi h} = \frac{5.8\text{e}{-7}*0.02243}{0.2457*4*3.14*27.86} = 150\ \text{md/cp}\ ,\ k_2 = 75.934\ \text{md}$$

The large estimated positive skin factor and extra permeability change indicate the existence of pollution problems in near wellbore formation, such as mud infiltration, clay dispersion, the presence of cement, formation partially open, insufficient perforation and clogging. In order to increase the near wellbore formation permeability, stimulation techniques (e.g. acidizing and fracturing) should be adopted.

Finally, given the flow duration of 98160 seconds, the thermal investigation radius in this oil production case can be evaluated:

$$r_{investigation} = \sqrt{0.1556^2 + \frac{1.6*98160*0.02243}{3.14*27.866}} = 6.354\ m = 20.841\ \text{ft}$$

Compared with the limited thermal diagnostic radius of several feet in the synthetic oil production case, the selected steady production period is so long (about 30 hours) that the radius of thermal investigation is much larger in this real oil production case. Besides, higher flow-rate also leads to a larger radius of thermal investigation. In this circumstance, temperature transient analysis can provide accurate estimations for both the near wellbore formation and the wider formation.

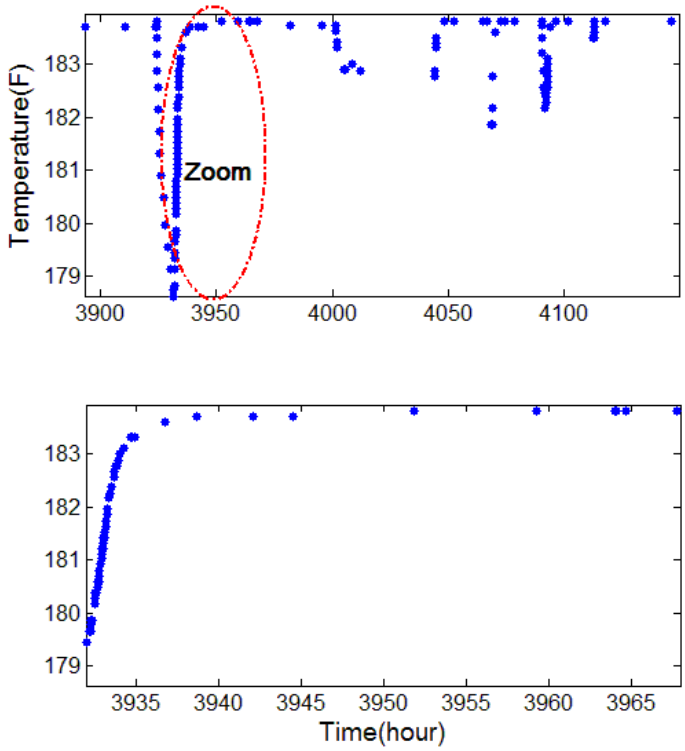

Figure 5-22: Field oil case - Transient temperature data and zoom-in for a flow period

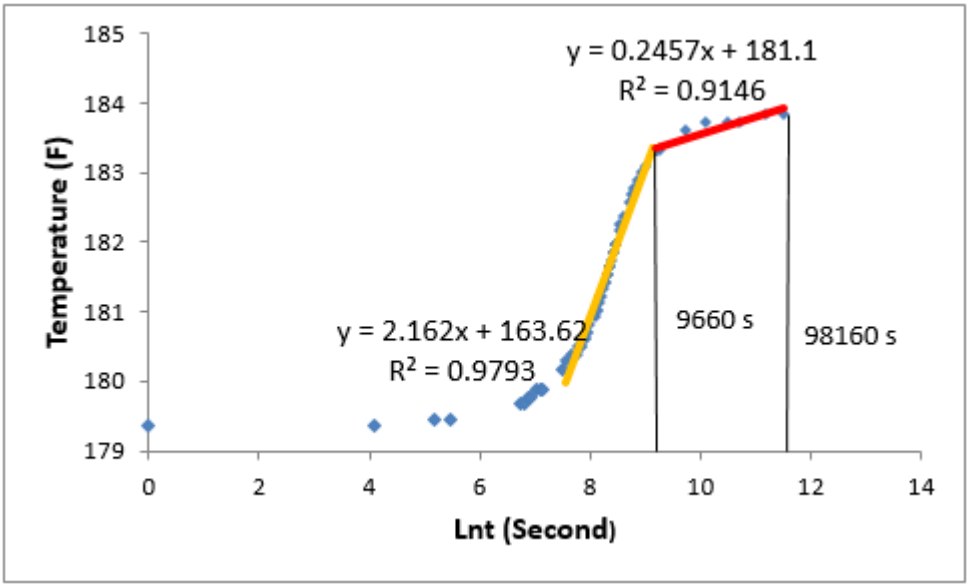

Figure 5-23: Field oil case - Temperature change and trend line in semi-log coordinate during a selected flow period

5.6. Chapter Summary

The main target of this chapter was analysing the transient temperature data and showing the field applications of these improved model-independent analysis methods.

Based on the previously described nonlinear diagnostic method, novel procedures of long-term transient temperature analysis have been presented.

The transient temperature was then divided into three stages for analysing. For the early time region caused by shut-in, opening or rate-change operations, temperature increase/decrease is affected by wellbore storage in which the compression/expansion dominates the temperature behaviour, and temperature gradually declines/rises as the effect of wellbore storage ends. Therefore, transient temperature analysis, along with the transient pressure analysis can greatly reduce the uncertainties in flow regime diagnostics. Several field case studies were conducted to show the success of wellbore storage diagnosis, linear flow regime (1/2 slope) indication and verification of conventional well-test interpretation parameters with transient temperature where large fluid compressibility exists (nonlinear gas production scenario).

For the middle time region, the detailed flow-rate history can be calculated from the cumulative production rate and transient temperature data (or transient pressure data). If it is a linear system such as single oil phase production well, the flow-rates reconstructed from pressure data are more accurate; however, if nonlinearity exists in either reservoir or wellbore, the transient temperature data can reconstruct better results. Additionally, in order to verify the reliability of the developed algorithms, sets of synthetic data which were simulated by a fully coupled wellbore-reservoir model and another real field dataset were utilized.

For later times, the flow regime changes to pseudo-radial flow. An analytical solution was developed to describe the sand-face temperature during this period. After integrating flow-rate data, the formation properties such as permeability, fluid mobility and skin factor could be evaluated quantitatively. The thermal investigation radius was also researched; generally, it can provide parameter estimations for wide formation in the gas production case, but it was much smaller and could only estimate the near wellbore formation in the oil production case.

It is necessary to analyse temperature variation to overcome the data limitation problem when other down-hole information is lacking (e.g. expensive and unstable flow meters). In summary, besides analysing pressure data, the transient temperature behaviour can also be used to provide flow-rate and reservoir information, and the methods described in this chapter provides a fast and reliable way to interpret transient temperature data.

Chapter 6 Conclusion, Discussion and Recommendation for Future Work

6.1. General conclusion

With the aim of utilizing transient temperature data acquired from down-hole gauges for reservoir analysis, several effective approaches have been developed in this work. Subsequently, the usefulness these approaches have been demonstrated by using both synthetic and real field data. The main contribution and general conclusions from the three main parts of this work are summarized as follows:

1. Model-dependent interpretation approach: a non-isothermal wellbore model for multiphase fluid flow was established and coupled with a reservoir model to account for transient temperature behaviour at location of gauges.
   - The reliability of the non-isothermal wellbore model has been verified by comparing it with other published models.
   - The established wellbore model can calculate temperature profile, integrate pressure data, and determine the flow-rate profile more accurately.
   - In accordance with the established non-isothermal well testing model (coupled wellbore-reservoir model), several synthetic cases were studied. It was found that the Joule-Thomson coefficient, viscosity, permeability and porosity are each very sensitive to transient temperature changes.
   - These representative thermodynamic parameters can be estimated by matching the simulated results with real temperature data.

2. Transient data processing and integrated interpretation of temperature and pressure for nonlinearity diagnosis.
   - The relationships within down-hole temperature, pressure and flow-rate data have been studied. It was established that temperature response to changes of flow-rate and pressure, and this optimal transformation function can be drawn out from either the entire dataset or a selected representative transient region.
   - Based on the theory of Haar wavelet transform, an approach which involves identifying the flow transients and removing the outliers by using processed temperature and pressure data together has been developed. This approach can

constrain pressure data by temperature measurements and therefore reduce the possibility of analysing spurious data points.

- The relationship between WT amplitude and flow-rate change has been studied in both linear and nonlinear systems. A unit-rate-change coefficient A_{Turc} was defined and its analytical solutions were derived.
- An approach for diagnosing the nonlinearity of the reservoir from transient temperature data has been developed. In linear systems (single oil), A_{Turc} is a constant; in nonlinear systems (single gas), the earlier A_{Tfurc} changes with time, while the later A_{Tlurc} is still constant with time during flow-rate decrease events.
- A_{Turc} can be used for reservoir management and production monitoring, and the near-wellbore variable characterizations such as skin and permeability can be evaluated both qualitatively and quantitatively.

3. Model-independent transient temperature data interpretation approaches.
    - Based on the preceding nonlinear diagnostic method described above, a novel and entire workflow of long-term transient temperature analysis has been presented.
    - The early time region (ETR) transient temperature data have been studied for detecting the wellbore storage regime and verifying the conventional well test (pressure analysis) interpretation parameters in nonlinear systems. Several field cases demonstrated that transient temperature analysis, along with the transient pressure analysis can greatly reduce the uncertainties in flow regime diagnosis.
    - Through the utilization of wavelet transform, unknown flow-rate history can be reconstructed from processed transient temperature and incomplete production data (either cumulative or daily flow-rate) in both linear and nonlinear systems.
    - For the single oil production case, although the results of temperature reconstructed flow-rate are acceptable, they have larger errors than the pressure reconstructed flow-rate; thus it is recommended to use pressure data to calculate the flow-rate in linear systems.
    - For the real gas production case, pressure calculated flow-rate tends to have larger errors than that in the oil case due to the high compressibility and other pressure-dependent gas properties. However, the later temperature WT detail amplitudes A_{Tl} are able to reconstruct high-accuracy flow-rate history.

Consequently, transient temperature data may provide another choice for interpreting nonlinear systems.

- A radial flow analytical solution which is able to calculate the later time sand-face temperature was introduced, and then the reservoir parameters such as permeability and skin factor as well as the thermal investigation radius were estimated through combining transient temperature data and the previously calculated flow-rate.

6.2. Recommendation for future work

In view of the fact that more accurate temperature data can be provided with the development of down-hole measurement tools, it is necessary to improve the temperature interpretation approach which is far from complete and perfect. Several future research directions are recommended as follows:

1. The unit-rate-change coefficients A_{Tlurc} that are calculated from the later amplitudes (temperature variation after wellbore storage regime) are constant during pressure build-up periods which are caused by flow-rate decrease. In order to use this function for reconstructing the flow-rate history even in nonlinear systems by temperature data, more studies about the theoretical evidence which can support the phenomena need to be completed. However, the analytical solution that describes the sand-face temperature during the middle time region for nonlinear systems has not yet been published. This should be treated as the priority of future work. The middle time temperature solution of linear flow presented by Davies and Muradov (2013) may be further modified for this request.
2. The non-isothermal wellbore model could be further extended for modelling the fluid flow in a horizontal section or a multi-lateral well. Additionally, the method of optimal matching could be developed for automatically matching the model results (transient temperature at gauge location) with real temperature data. After that, the model-dependent temperature interpretation approach would have a wider application range. Several steps can be done for numerical optimization in future:
   - Firstly, guessing the initial values of some unknown model parameters (such as porosity and J-T coefficient), and setting the upper and lower boundaries of them.
   - Secondly, optimization routine (nonlinear least square method) selection. Either the Genetic algorithm (GA) or Levenberg-Marquardt algorithm can be used.

- Thirdly, parameters estimation. Setting an objective function (e.g. Objective Function (P, q, t, T, unknown-parameter) = T_{data}-T_{model}) and searching for the exact values of the unknown parameters which minimize the objective function through the selected optimization algorithm.

3. The model-independent temperature interpretation approaches should also be improved. Current analysis of the 'temperature well test' is mainly for qualitatively interpreting the reservoir and correcting the pressure interpretation results. Developing temperature diagnostic plots (similar to the PTA analysis) or establishing the pressure well test theoretical plate including the thermal effect would be helpful.
4. The transient down-hole temperature data may contain interference caused by nearby production and injection wells. Even though it is not easy to analyze the influence of interference on temperature data, further study in this area should be encouraged.
5. Apart from PDGs, the DTS (Distributed Temperature Sensor) can also provide down-hole temperature information for production optimization and model calibration. The application of this kind of distributed wellbore temperature data could not only segregate the flow-rate from different layers, but also distinguish the wellbore nonlinearity from the reservoir nonlinearity, since the performance and effects of nonlinearity in the reservoir and the nonlinearity in the wellbore maybe different.

References

Achinivu, O., Zhu, D. and Furui, K., 2008. Field Application of An Interpretation Method of Downhole Temperature and Pressure Data for Detecting Water Entry in Horizontal/highly Inclined Gas Wells. SPE Annual Technical Conference and Exhibition, 21-24 September, Denver, Colorado, USA.

Agarwal, R., 1979. "Real Gas Pseudo-Time" - A New Function for Pressure Build-up Analysis of MHF Gas Wells. SPE Annual Technical Conference and Exhibition, 23-26 September, Las Vegas, Nevada.

Al-Hussainy, R., Ramey, H. J. and Crawford, P., 1966. The Flow of Real Gases through Porous Media. Journal of Petroleum Technology, pp.624-636.

Alves, I., Alhanati, F. and Shoham, O., 1992. A Unified Model for Predicting Flowing Temperature Distribution in Wellbores and Pipelines. SPE production engineering, November, pp.363-367.

App, J., 2009. Field Cases: Nonisothermal Behavior Due to Joule-Thomson and Transient Fluid Expansion/Compression Effects. SPE Annual Technical Conference and Exhibition, New Orleans, Louisiana, USA.

App, J. and Yoshioka, K., 2011. Impact of Reservoir Permeability on Flowing Sandface Temperatures; Dimensionless Analysis. SPE Annual Technical Conference and Exhibition, Denver, Colorado, USA.

Athichanagorn, S., Horne, R. and Kikani, J., 1999. Processing and Interpretation of Long-term Data from Permanent Downhole Pressure Gauges. SPE Annual Technical Conference.

Atkinson, P. G. and Ramey, H. J., 1977. Problems of Heat Transfer in Porous Media. SPE Annual Technical Conference, Denver, Colorado, USA.

Bahrami, H. and Siavoshi, J., 2007. A New Method in Well Test Interpretation Using Temperature Transient Analysis for Gas Wells. International Petroleum Technology Conference, 4-6 December, Dubai, U.A.E.

Baker, A., Jeffery, J., Thomas, A. and Unneland, T., 1995. Permanent Monitoring-Looking at Lifetime Reservoir Dynamics, Oilfield Review, No. 4, Vol. 7.

Bezerra, C., Da Silva, F. and Theuveny, C., 1992. Permanent Downhole Gauges: A Key to Optimize Deepsea Production. 24th Annual OTC, Houston, Texas, USA.

Bourdet, D., Whittle, T. M., Douglas, A. and Pirard, Y. M., 1983. A New Set of Type Curves Simplifies Well Test Analysis. World Oil.

Breiman, L. and Friedman, J., 1985. Estimating Optimal Transformations for Multiple Regression and Correlation. Journal of the American Statistical Association, September, pp.580–598.

Brown, G., 2006. Monitoring Multilayered Reservoir Pressures and Gas/Oil Ratio Changes Over Time Using Permanently Installed Distributed Temperature Measurements. Proceedings of SPE Annual Technical Conference and Exhibition.

Brown, G., Field, D., Davies, J. and Garayeva, N., 2005. Production Monitoring Through Openhole Gravel-Pack Completions Using Permanently Installed Fiber-Optic Distributed Temperature Systems in the BP-Operated Azeri Field in Azerbaijan. Proceedings of SPE Annual Technical Conference and Exhibition.

Chen, N., 1979. An Explicit Equation for Friction Factor in Pipe. Industrial & Engineering Chemistry Fundamentals, pp.296–297.

Cui, X., 2012. Wellbore Heat Transfer Model for Wax Deposition in Permafrost Region. Master thesis, University of Kansas.

Dake, L. P., 1983. Fundamentals of Reservoir Engineering. Elsevier.

Dakhnov, V. N. and Dyakonov, D. I., 1952. Temperature investigations of wells: Gostoptekhizdat.

Darve, E. and Le, H., 2008. CME 102 Matlab Workbook.

Davies, D. and Muradov, K., 2013. Some Case Studies of Temperature and Pressure Transient Analysis in Horizontal Multi-zone Intelligent Wells. EAGE Annual Conference & Exhibition incorporating SPE Europec, 10-13 June, London, UK.

De Oliveira Silva, M. I. and Kato, E. T., 2004. Reservoir Management Optimization Using Permanent Downhole Gauge Data. SPE Annual Technical Conference and Exhibition, Houston, Texas, USA.

Dietz, D., 1965. Determination of Average Reservoir Pressure from Build-up Surveys. Journal of Petroleum Technology, (10), pp.955–959.

Duru, O., 2008. Modelling of Reservoir Temperature Transients and Parameter Estimation Constrained to the Model. SPE Annual Technical Conference and Exhibition, (Student 6), pp.21–24.

Duru, O., 2011. Reservoir Analysis and Parameter Estimation Constrained to Temperature, Pressure and Flowrate Histories. Ph. D Thesis, Stanford University.

Duru, O., 2008. Modelling of Reservoir Temperature Transients and Parameter Estimation Constrained to A Reservoir Temperature Model. Master thesis, Stanford University.

Duru, O. and Horne, R., 2008. Modelling Reservoir Temperature Transients and Matching to Permanent Downhole Gauge Data for Reservoir Parameter Estimation. Proceedings of SPE Annual Technical Conference and Exhibition, Denver, Colorado, USA.

Duru, O. and Horne, R., 2011. Simultaneous Interpretation of Pressure, Temperature, and Flow-Rate Data Using Bayesian Inversion Methods. SPE Reservoir Evaluation & Engineering, April, pp.225–238.

Elshahawi, H., Osman, M. and Sengul, M., 1999. Use of Temperature Data in Gas Well Tests. SPE Annual Technical Conference and Exhibition, Houston, Texas, USA.

Eppelbaum, L. V. and Kutasov, I. M., 2006. Pressure and Temperature Drawdown Well Testing: Similarities and Differences. Journal of Geophysics and Engineering, 3(1), pp.12–20.

Fairuzov, Y. and Gonzalez, J., 1997. The Influence of Heat Transfer on the Two-Phase Flow Behavior in a Wellbore During Transient Pressure Tests. Latin American and Caribbean Petroleum Engineering Conference, 30 August-3 September, Rio de Janeiro, Brazil.

Gisbergen, S. Van and Vandeweijer, A., 2001. Reliability Analysis of Permanent Downhole Monitoring Systems. SPE Drilling & Completion, March, pp.60–63.

Gonzalez-Tamez, F., 1999. Truncation De-noising in Transient Pressure Tests. SPE Annual Technical Conference and Exhibition, 3-6 October, Houston, Texas, USA.

Griffith, P. and Wallis, G., 1961. Two-phase Slug Flow. Journal of Heat Transfer, August, pp.318–320.

Gringarten, A. C., Schroeter, T. Von, Rolfsvaag, T. and Bruner. J., 2003. Use of Downhole Permanent Pressure Gauge Data to Diagnose Production Problems in a North Sea Horizontal Well. SPE Annual Technical Conference and Exhibition, Denver, Colorado, USA.

Guan, L., Du, Y. and Li, L., 2004. Wavelets in Petroleum Industry: Past Present and Future. SPE Annual Technical Conference and Exhibition, September, pp.26–29.

Hagedorn, A. and Brown, K., 1965. Experimental Study of Pressure Gradients Occurring During Continuous Two-Phase Flow in Small-Diameter Vertical Conduits. Journal of Petroleum Technology, 17(4).

Hagoort, J., 2004. Ramey's Wellbore Heat Transmission Revisited. SPE Journal, December, pp.465–474.

Hasan, A. and Kabir, C., 2005. A Simple Model for Annular Two-phase Flow in Wellbores. SPE Annual Technical Conference and Exhibition, Dallas, USA.

Hasan, A., Kabir, C. and Sayarpour, M., 2007. A Basic Approach to Wellbore Two-phase Flow Modelling. SPE Annual Technical Conference and Exhibition, 11-14 November, Anaheim, California, USA.

Hawkin, M. F., 1956. A Note on the Skin Effect. Trans., AIME 207, pp. 356-357

Holditch, S., 1982. Application of Pseudotime to Buildup Test Analysis of Low-permeability Gas Wells with Long-duration Wellbore Storage Distortion. Society of Petroleum Engineers of AIME, December, pp.2877–2887.

Horne, R. and Shinohara, K., 1979. Wellbore Heat Loss in Production and Injection Wells. Journal of Petroleum Technology, pp.116-118.

Izgec, B., Hasan, A. R., Lin, D. and Kabir, C. S., 2010. Flow-rate Estimation from Wellhead pressure and Temperature Data. SPE Production & Operations.

Izgec, B., 2008. Transient Fluid and Heat Flow Modelling in Coupled Wellbore/reservoir Systems. Ph. D Thesis, Texas A&M University.

Johnson, D., Sierra, J., Gualtieri, D. and Kaura, J., 2006. DTS Transient Analysis: A New Tool to Assess Well Flow Dynamics. SPE Annual Technical Conference and Exhibition, 24-27 September, San Antonio, Texas, USA.

Earlougher, R. and Kersch, K., 1972. Field Examples of Automatic Transient Test Analysis. Journal of Petroleum Technology, pp.1271–1277.

Kabir, C. and Hasan, A., 1998. Does Gauge Placement Matter in Downhole Transient-Data Acquisition? SPE Reservoir Evaluation & Engineering, February, pp.64-68.

Khanlarov, S., 2012. Analysing Reservoir Thermal Behavior by Using Thermal Simulation Model, Engineering and Applied Science.

Khong, C. K., 2001. Permanent Downhole Gauge Data Interpretation. Master thesis, Stanford University.

Kikani, J. and He, M., 1998. Multi-resolution Analysis of Long-term Pressure Transient Data Using Wavelet Methods. SPE Annual Technical Conference and Exhibition, 27-30 September, New Orleans, Louisiana, USA.

Kin, K., 2001. Permanent Downhole Gauge Data Interpretation. Master thesis, Stanford University.

Kragas, T., Turnbull, B. and Francis, M., 2002. Permanent Fiber-optic Monitoring at Northstar. Journal of Petroleum Technology, 54(09).

Kragas, T., Turnbull, B. and Francis, M., 2004. Permanent Fiber-optic Monitoring at Northstar: Pressure/temperature System and Data Overview. SPE Production & Facilities, December, pp.86-93.

Kuchuk, F. J., Hollaender, F., Gok, I. M. and Onur, M., 2005. Decline Curves from Deconvolution of Pressure and Flow-Rate Measurements for Production Optimization and Prediction. SPE Annual Technical Conference and Exhibition, Dallas, Texas, USA.

Kutasov, I.M. and Eppelbaum, L. V., 2007. Well Temperature Testing-An Extension of Slider's Method. Journal of Geophysics and Engineering, 4(1), pp.1–6.

Lapuk, B. B., 1940. Thermodynamic Processes of Gassed Oil Moving in Porous Media. Azer. neftyanoye khozyaistvo, 2.

Lasseter, J., 1976. The Numerical Simulation of Heat and Mass Transfer in Multi-Dimensional Two-Phase Geothermal Reservoirs. Society of Petroleum Engineers.

Lee, J., 1982. Well Testing. New York: Society of Petroleum Engineers of AIME.

Lee, J., Rollins, J. B. and Spivey, J. P., 2003. Pressure Transient Testing. Richardson, TX: Society of Petroleum Engineers.

Li, X., 2009. Processing and Analysis of Transient Data from Permanent Down-hole Gauges (PDG). Ph. D Thesis, Heriot-Watt University.

Livescu, S., Aziz. K. and Durlofsky, L., 2009. Development and Application of a Fully-Coupled Thermal Compositional Wellbore Flow Model. SPE Western Regional Meeting, 24-26 March, San Jose, California, USA.

Lorentzen, R., Saevareid, O. and Nævdal, G., 2010. Rate Allocation: Combining Transient Well Flow Modelling and Data Assimilation. SPE Annual Technical Conference and Exhibition, 19-22 September, Florence, Italy.

Maubeuge, F., Didek, M. and Beardsell, M., 1994. MoTher: A Model for Interpreting Thermometrics. SPE Annual Technical Conference and Exhibition, 25-28 September, New Orleans, Louisiana, USA.

Meunier, D. and Wittmann, M., 1987. Gas Well Test Analysis:-Use of Normalized Pseudovaria es. SPE Formation Evaluation, December, pp.629–636.

Meyer, B., 1989. Heat Transfer in Hydraulic Fracturing. SPE Production Engineering, November, pp.423-429.

Michel, G. and Civan, F., 2008. Modelling Nonisothermal Rapid Multiphase Flow in Wells under Nonequilibrium Conditions. SPE Production & Operations, October, pp.24–27.

Morlet, J., Arens, G., Fourgeau, E. and Giard, D., 1982. Wave Propagation and Sampling Theory-Part I: Complex Signal and Scattering in Multilayered Media. Geophysics, 47(2), pp.203–221.

Muradov, K., 2010. Temperature Modelling and Real-time Flow-rate Allocation in Wells with Advanced Completion. Ph. D Thesis, Heriot-Watt University.

Nath, D., Sugianto, R. and Finley, D., 2005. Fiber-Optic Distributed Temperature Sensing Technology Used for Reservoir Monitoring in an Indonesia SteamFlood. SPE International Thermal Operations and Heavy Oil Symposium, Calgary, Alberta, Canada.

Olsen, S. and Nordtvedt, J., 2005a. Automatic Filtering and Monitoring of Real-Time Reservoir and Production Data. SPE Annual Technical Conference and Exhibition, 9-12 October, Dallas, Texas, USA.

Olsen, S. and Nordtvedt, J., 2006. Experience from the Use of Automatic Well-Test Analysis. SPE Annual Technical Conference and Exhibition, 24-27 September, San Antonio, Texas, USA.

Olsen, S. and Nordtvedt, J., 2005b. Improved Wavelet Filtering and compression of production data. Offshore Europe, 6-9 September, Aberdeen, United Kingdom.

Ortiz, C., Aguiar, R. and Pires, A., 2009. Wavelet Filtering of Permanent Downhole Gauge Data. Latin American and Caribbean Petroleum Engineering Conference, 31 May-3 June, Cartagena de Indias, Colombia.

Ouyang, L. and Belanger, D., 2006. Flow Profiling by Distributed Temperature Sensor (DTS) System? Expectation and Reality. SPE Production & Operations, August, pp.269–281.

Pourafshary, P., Varavei, A., Sepehrnoori, K. and Podio, A., 2008. A Compositional Wellbore/reservoir Simulator to Model Multiphase Flow and Temperature Distribution. International Petroleum Technology Conference, 3-5 December, Kuala Lumpur, Malaysia.

Prats, M., 1985. Thermal Recovery. SPE

Rai, H., 2005. Analyzing Rate Data from Permanent Downhole Gauges. Master thesis, Stanford University.

Ramazanov, A. and Parshin, A., 2006. Temperature Distribution in Oil and Water Saturated Reservoir with Account of Oil Degassing. Oil and Gas Business Journal, pp.1–16.

Ramazanov, A. and Valiullin, R., 2010. Thermal Modeling for Characterization of Near Wellbore Zone and Zonal Allocation. SPE Russian Oil and Gas Technical Conference and Exhibition, Moscow, Russia.

Ramazanov, A. and Nagimov, V. M., 2007. Analytical Model for the Calculation of Temperature Distribution in the Oil Reservoir during Unsteady Fluid Inflow. Oil and Gas Business Journal, (1), pp.1–8.

Ramey, H. J., 1962. Wellbore Heat Transmission. SPE Journal of Petroleum Technology, 14(4), 427-435.

Ribeiro, P., 2008. Use of Wavelet Transform in Pressure-data Treatment. SPE Production & Operations, June, pp.24-31.

Sahni, I. and Horne, R., 2005. Multiresolution Wavelet Analysis for Improved Reservoir Description. SPE Reservoir Evaluation & Engineering, February, pp.53–69.

Sanchez, A., Brown, G. and Carvalho, V., 2005. Slickline with Fiber-Optic Distributed Temperature Monitoring for Water-Injection and Gas Lift Systems Optimization in Mexico. SPE Latin American and Caribbean Petroleum Engineering Conference, 20-23 June, Rio de Janeiro, Brazil.

Sensornet Limited., 2007. DTS Advantages and Technology. www.sensornet.co.uk.

Schroeter, T. von, Hollaender, F. and Gringarten, A., 2001. Deconvolution of Well-test Data as a Nonlinear Total Least-squares Problem. SPE Annual Technical Conference and Exhibition, New Orleans, Louisiana, USA.

Shirdel, M. and Sepehrnoori, K., 2009. Development of a Coupled Compositional Wellbore/Reservoir Simulator for Modeling Pressure and Temperature Distribution in Horizontal Wells. SPE Annual Technical Conference and Exhibition, 4-7 October, New Orleans, Louisiana, USA.

Soliman, M. and Ansah, J., 2003. Application of Wavelet Transform to the Analysis of Pressure-transient Data. SPE Reservoir Evaluation & Engineering, April, pp.89-99.

Spindler, R., 2011. Analytical Models for Wellbore-Temperature Distribution. SPE Journal, March, pp.125-133.

Stone, T. and Bennett, J., 2002. Thermal Simulation with Multisegment Wells. SPE Reservoir Evaluation & Engineering, March, pp.206-218.

Sui, W. and Zhu, D., 2008. Determining Multilayer Formation Properties from Transient Temperature and Pressure Measurements. SPE Annual Technical Conference and Exhibition, 21-24 September, Denver, Colorado, USA.

Sui, W. and Zhu, D., 2009. Determining Multilayer Formation Properties from Transient Temperature and Pressure Measurements. Ph. D Thesis, Texas A&M University.

Tabatabaei, M., Tan, X., Hill, A. D. and Zhu, D., 2011. Well Performance Diagnosis with Temperature Profile Measurements. SPE Annual Technical Conference and Exhibition, 30 October-2 November, Denver, Colorado, USA.

Tardy, P., Chang, F. and Qiu, X., 2011. Determining Matrix Treatment Performance from Downhole Pressure and Temperature Distribution: A Model. International Petroleum Technology Conference, 15-17 November, Bangkok, Thailand.

Trina, S., 2012. An Integrated Horizontal and Vertical Flow Simulation with Application to Wax Precipitation. SPE Asia Pacific Oil and Gas Conference and Exhibition, Perth, Australia.

Trina, S., 2012. An Integrated Horizontal and Vertical Flow Simulation with Application to Wax Precipitation. Master thesis, Memorial University of Newfoundland.

Unneland, S.T., 1998. Permanent Gauge Pressure and Rate Measurements for Reservoir Description and Well Monitoring: Field cases. SPE Reservoir Evaluation & Engineering, June, pp.224-230.

Valiullin, R. and Ramazanov, A., 2010. Qualitative and Quantitative Interpretation: the State of the Art in Temperature Logging. North Africa Technical Conference and Exhibition, 14-17 February, Cairo, Egypt.

Veneruso, A., 1992. Computer-Based Downhole Data Acquisition and Transmission in Well Testing. SPE Annual Technical Conference and Exhibition, 4-7 October, Washington, D.C., USA.

Voss, H., 2013. Alternating Conditional Expectation Algorithm (ACE) to Calculate Optimal Transformations. www.uk.mathworks.com/matlabcentral/fileexchange.

Wallis, G. B., 1969. One-dimensional Two-phase Flow. McGraw Hill, New York.

Wang, D. and Murphy, M., 2004. Estimating Optimal Transformations for Multiple Regression Using the ACE Algorithm. Journal of Data Science, 2(2004), pp.329-346.

Wang, F., 2012. Diagnostic and Analysis of Long-term Transient Pressure Data from Permanent Down-hole Gauges (PDG). Ph. D Thesis, Heriot-Watt University.

Wang, F. and Zheng, S., 2012. Unknown Rate History Calculation from Down-hole Transient Pressure Data Using Wavelet Transform. Transport in Porous Media, 96(3), pp.547–566.

Wang, X. and Bussear, T., 2011. Real Time Horizontal Well Monitoring Using Distributed Temperature Sensing (DTS) Technology. Offshore Technology Conference Brasil, 4-6 October, Rio de Janeiro, Brazil.

Wang, Z., 2012. The Uses of Distributed Temperature Survey (DTS) Data. Ph. D Thesis, Stanford University.

Wang, Z. and Horne, R., 2011. Analysing Wellbore Temperature Distributions Using Nonisothermal Multiphase Flow Simulation. SPE Western North American Region Meeting, Anchorage, Alaska, USA.

Wu, X., Jiang, Y. and Sui, W., 2013. Innovative Applications of Downhole Temperature Data. SPE Middle East Intelligent Energy Conference and Exhibition, 28-30 October, Manama, Bahrain.

Wu, Y. and Pruess, K., 1990. An Analytical Solution for Wellbore Heat Transmission in Layered Formations. SPE Reservoir Engineering, November, pp.531-538.

Yoshioka, K., Dawkrajai, P., Romero, A., Zhu, D., Hill, A. D. and Lake, L., 2007. A Comprehensive Statistically-Based Method to Interpret Real-Time Flowing Measurements. The University of Texas at Austin.

Yoshioka, K., Zhu, D. and Hill, A., 2005. A Comprehensive Model of Temperature Behavior in a Horizontal Well. SPE Annual Technical Conference and Exhibition, 9-12 October, Dallas, Texas, USA.

Yoshioka, K., Zhu, D. and Hill, A., 2006. Detection of Water or Gas Entries in Horizontal Wells from Temperature Profiles. SPE Europec/EAGE Annual Conference and Exhibition, 12-15 June, Vienna, Austria.

Zheng, S. and Wang, F., 2011. Recovering Flowing History from Transient Pressure of Permanent Down-hole Gauges (PDG) in Oil and Water Two-Phase Flowing Reservoir. SPE/DGS Saudi Arabia Section Technical Symposium and Exhibition, 15-18 May, Al-Khobar, Saudi Arabia.

Zheng, S. and Zhang, Y., 2014. A Non-Isothermal Wellbore Model with Complex Structure and Its Application in Well Testing. International Petroleum Technology Conference, Kuala Lumpur, Malaysia.

Zheng, S. and Zhang, Y., 2015. Improved Analysis of Transient Temperature Data from Permanent Downhole Gauges (PDG). SPE Reservoir Characterisation and Simulation Conference and Exhibition, Abu Dhabi.

Zuber, N. and Findlay, J. A., 1965. Average Volumetric Concentration in Two-phase Flow System. ASME J Heat Transfer, pp.87-453.

Appendix A

This appendix studies the thermal behaviour which is affected by different reservoir-well parameters using commercial software Eclipse^{TM} 300 simulator. The transient temperature at the perforations and distributed temperature along the wellbore were simulated. Sensitivity studies were conducted to estimate and revisit the effects of different parameters which had been described in literature review, such as flow-rate, Joule-Thomson coefficient and drawdown pressure, on temperature. Consequently, the literature-related potential applications of temperature data for reservoir description, model calibrating and production monitoring are demonstrated.

Both vertical and horizontal wells' production scenarios were simulated. Through the established Eclipse model studies, several conclusions can be drawn:

1. Temperature responds to changes of flow-rate and pressure;
2. Compared with the homogeneous model, clear differences in temperature distribution along the wellbore in commingled reservoirs can be observed; this is because of the different permeability and skin factors within different layers;
3. If two or three phases of flow occur along the wellbore, the temperature profile will change from location to location even along the horizontal section, mainly because of the Joule-Thomson effect that leads to oil, water and gas entering the wellbore at different temperature.

Case one - vertical well production

In this gas production model, dual porosity which allows different temperatures in the rock and fluid was used. However, the pore volume in the matrix and the heat capacity of the fracture rock have both been set to zero (A simpler alternative is to use a single porosity model and ignore the energy stored in the rock by setting the rock heat capacity to zero, as is done here in the fracture cells). The effect of the geothermal gradient was ignored by using the keyword of RTEM.

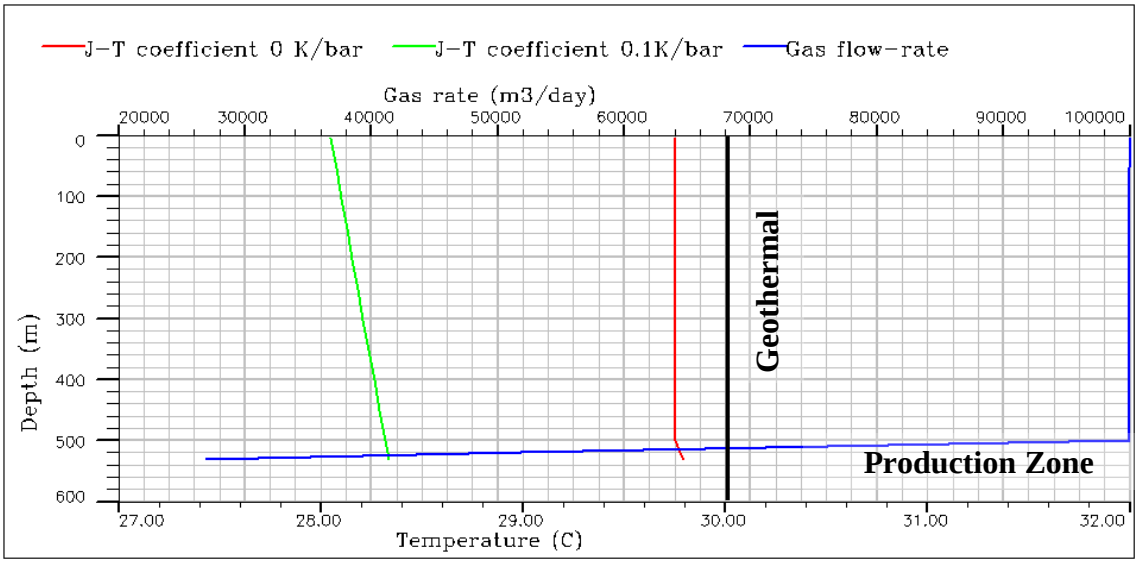

Figure A1：Joule-Thomson effect on temperature profile of a vertical gas production well

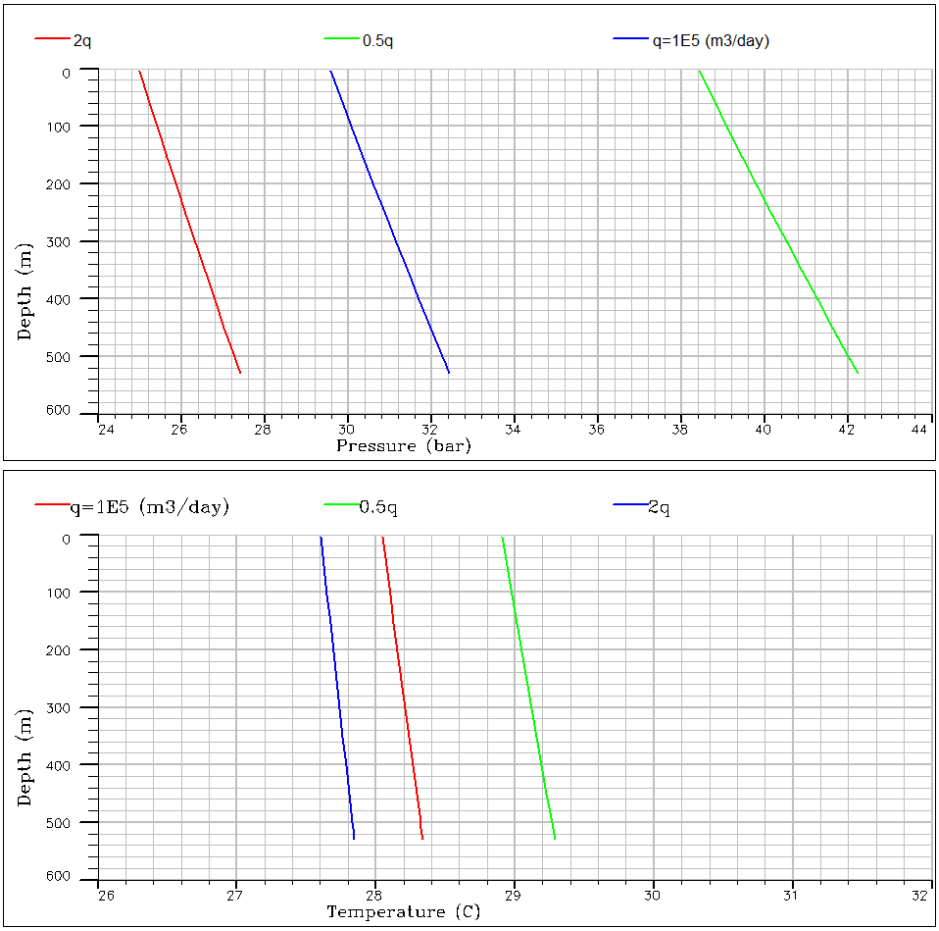

Figure A2：Flow-rate effect on temperature and pressure profiles of a vertical gas production well

Firstly, gas cooling caused by the Joule-Thomson effect can be observed clearly in Figure A1. The red line represents wellbore temperature distribution without the Joule-Thomson effect, and the green line is the temperature profile with the larger Joule-Thomson coefficient of 0.1. Gas flow-rate along the production zone is also displayed in Figure A1. The sensitivity of pressure and temperature profiles with respect to flow-rate change is demonstrated in Figure A2.

Secondly, a reservoir which consists of three layers with different permeability and skin factors was studied. This model contains water oil and gas three phases. Figure A3 illustrates the simulated temperature profile along the wellbore during about 100 days of production. The wellbore temperature increases slightly with the production. Figure A4 shows the oil flow-rate and gas flow-rate along the wellbore. The more the fluid entry, the higher the production rate and greater the deviation of wellbore temperature will be, and the deviation of the wellbore temperature from the geothermal is the core quantity used for flow profiling. Moreover, compared with the previously described homogeneous model, clear differences can be observed in temperature distribution along the wellbore in a commingled reservoir. This is because of the different permeability and skin factors within different layers. Thus the temperature distribution may be used for distinguishing if the formation is commingled.

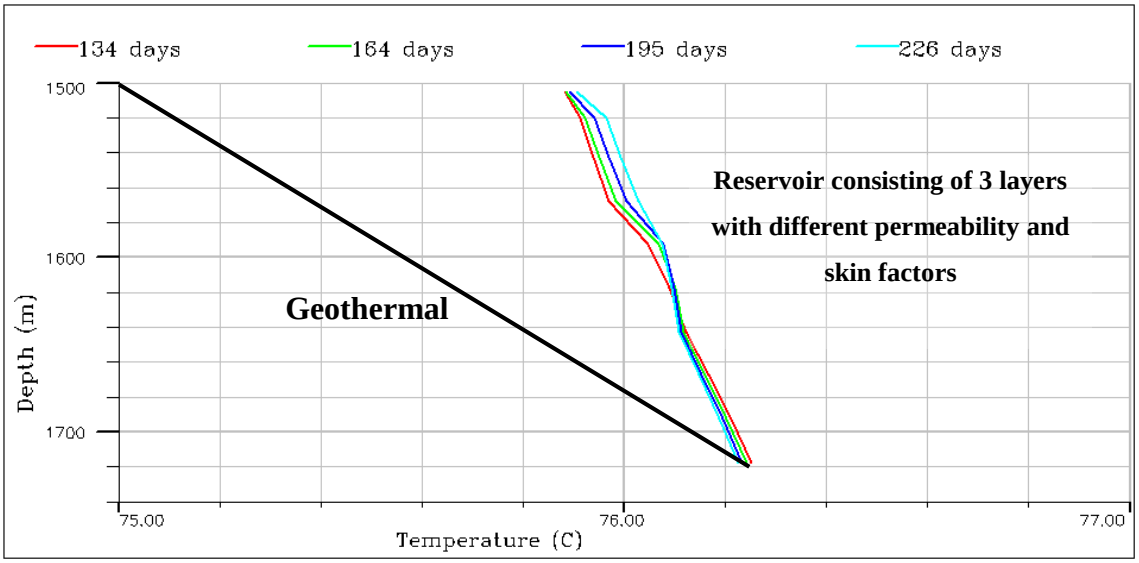

Figure A3： Temperature profile of a vertical well during 100 days of production

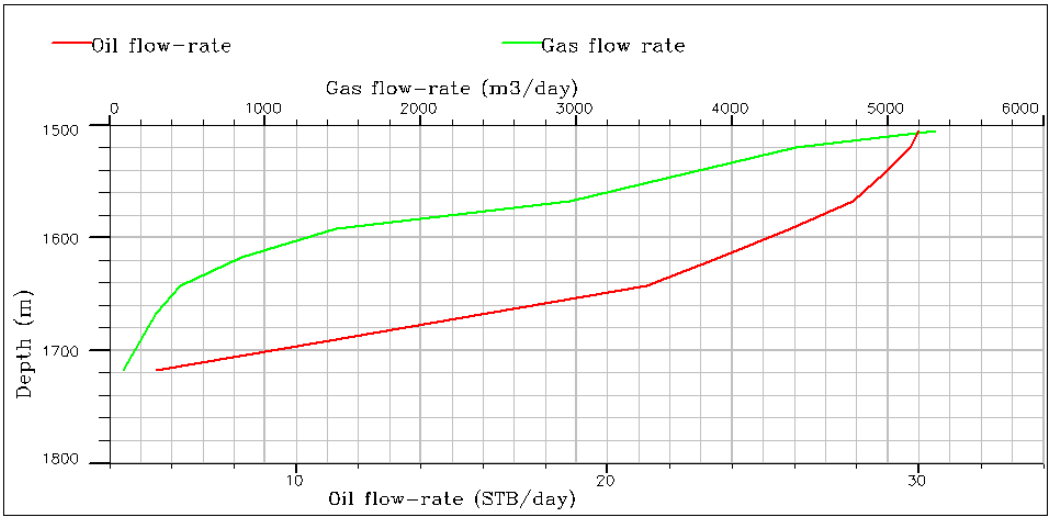

Figure A4：Oil and gas flow-rate along the wellbore

Case two – multi-phase horizontal well production

Single phase oil production has been studied by Ouyang and Belanger (2006). As they pointed out, fluid enters the wellbore at a higher temperature than the local geothermal temperature, due to the Joule-Thomson heating effect or the frictional heating effect. Figure A5 shows the impact of the Joule-Thomson effect on the wellbore temperature profile; the higher the pressure draw-down (from 50psi to 1000psi), the higher the Joule-Thomson heating, and the higher the temperature will be.

However, the wellbore temperature along the horizontal section does not vary from location to location. As illustrated in Figure A5 once fluid enters the wellbore, no matter how small the flow-rate is, the temperature will increase above the local geothermal temperature and will stay there. So it is difficult to identify the fluid entry using the wellbore temperature profiles. But if two or three phases flow occurs along the wellbore, the wellbore temperature profile will change from location to location, even along the horizontal section as shown in Figure A6. This is mainly because of the Joule-Thomson effect that leads to oil, water and gas entering the wellbore at different temperature. Moreover, in this model, wellbore temperature will increase with the decrease of pressure draw-down, due to the majority of gas flow (Joule-Thomson cooling effect) along the horizontal section Figure A7.

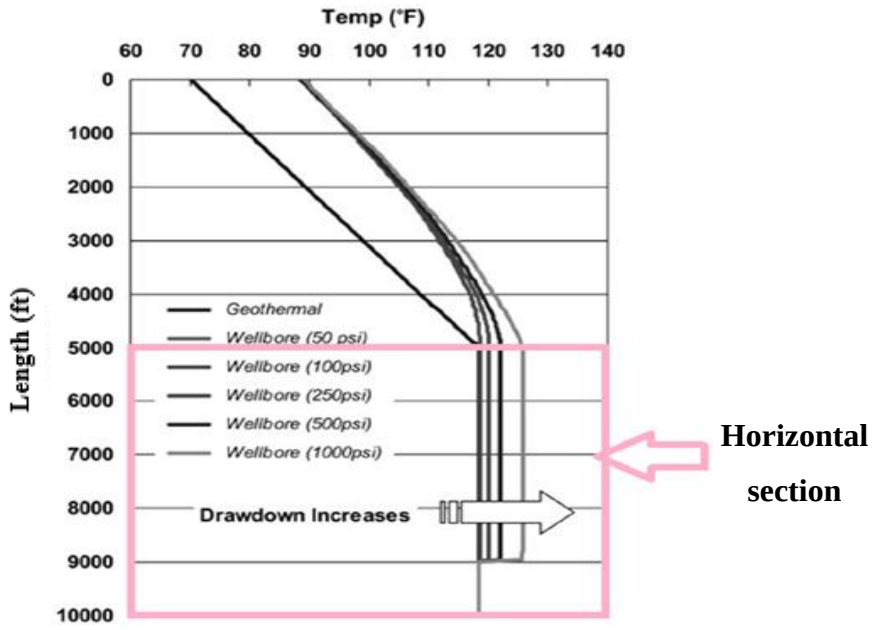

Figure A5：Impact of Joule-Thomson effect on predicted wellbore temperature profile (Ouyang and Belanger, 2006)

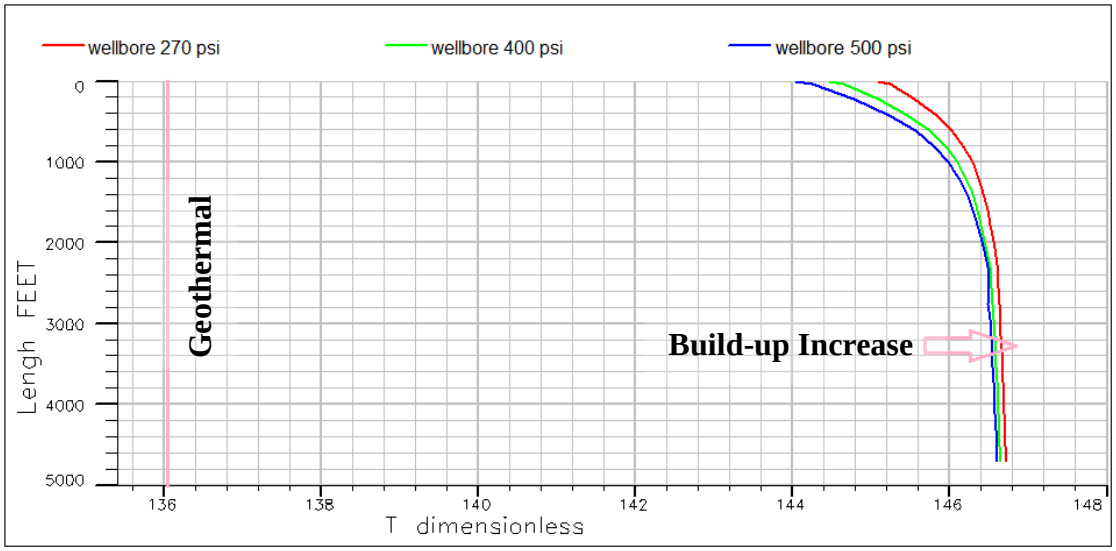

Figure A6：Three phase flow, horizontal section temperature distribution

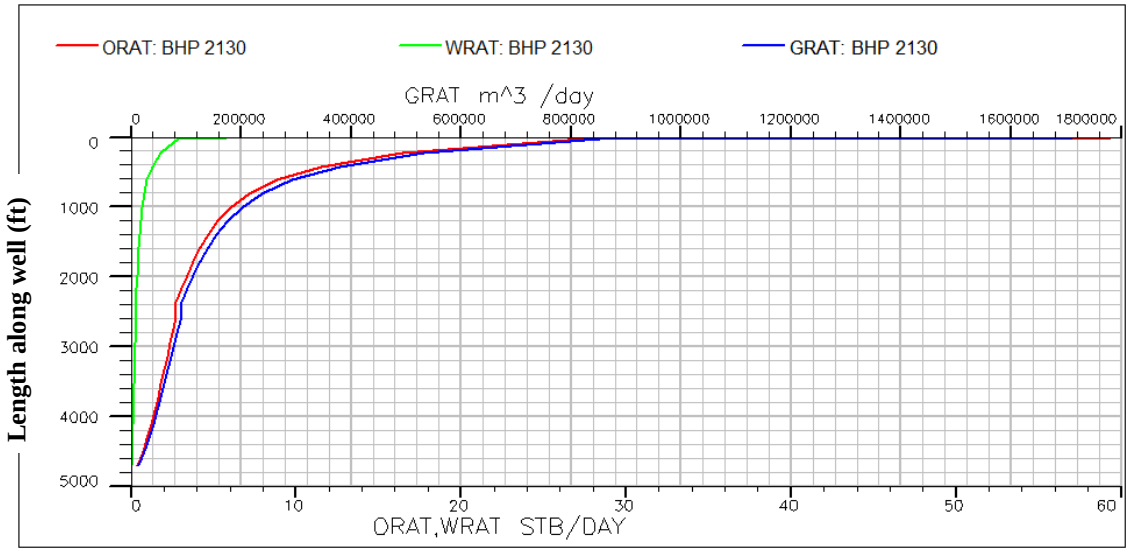

Figure A7：Gas, oil and water flow-rate along the horizontal section

Appendix B

This appendix explains the manipulation of equation 3.13. In addition, the derivations of equation 5.9 and 5.11 are also described in detail.

Section 3.3 - Modified Euler Method:

Through iteration, the Euler algorithm expresses the next step in terms of values at the current step. Compared with the basic forward and backward Euler methods which are referred to as the first order technique, the modified Euler Method is more accurate and can boost a larger stability interval. At the expense of increased algorithmic complexity, each time step produces a closer solution to the exact result (Darve and Le, 2008).

Two different points are introduced for the slope calculation so that the algorithm can be described as:

$$k_1 = f(z_n, T_{fn})$$

$$k_2 = f\left(z_{n+1}, T_{fn} + k\right) = f\left(z_{n+1}, T_{fn} + \Delta z * k_1\right)$$

$$T_{f(n+1)} = T_{fn} + \Delta z * \frac{1}{2}(k_1 + k_2)$$

For solving the ODE by using the modified Euler method, other input parameters include the segments domain (interval over which solution has to be computed, z) and the boundary condition (bottom-hole temperature, T_{fbh}).

Section 4.2.1 - ACE method description

An ACE regression model has the general form (Wang and Murphy, 2004):

$$\theta(\mathrm{Y}) = \alpha + \sum_{i=1}^{P} \emptyset_i(X_i) + e$$

where θ is a function of the response variable, Y (temperature data), and $\emptyset_i$ are functions of the predictors $X_{i,}\ i = 1, \ldots, p$ (pressure and flow-rate data). In other words, ACE method estimates p separate one-dimensional functions ($\emptyset_i$) and θ using an iterative method.

These transformations are achieved by minimising the unexplained variance (e^2) of a linear relationship between the transformed response variable and the sum of transformed predictor variables.

The error variance e^2 is:

$$e^2\left(\theta, \emptyset_1 \ldots \emptyset_p\right) = E\{[\theta(\mathrm{Y}) - \sum_{i=1}^{P} \emptyset_i(X_i)]\}^2$$

The minimisation of e^2 with respect to $\theta(\mathrm{Y})\ and\ \emptyset_i(X_i)$ is expressed as:

$$e^{*2}\left(\theta^*, {\emptyset_1}^* \ldots {\emptyset_p}^*\right)$$

where the transformations $(\theta^*(\mathrm{Y}), {\emptyset_1}^*(X_1), \ldots {\emptyset_p}^*(X_p))$ are regarded as the optimization of the regression.

In the transformed space, the response and predictor variables are related as follows

$$\theta^*(\mathrm{Y}) = \sum_{i=1}^{P} {\emptyset_i}^*(X_i) + e^*$$

where e^* is the error not captured by the use of the ACE transformations and is assumed to have a normal distribution with zero mean. The minimum regression error, e^*, and maximum mutiple correlation coefficient, ρ^*, are related by

$$e^{*2} = 1 - \rho^{*2}$$

Section 5.5 - Derivation of later time sand-face temperature solution and thermal radius of investigation

Eq. 4.18 describes the reservoir fluid temperature variation mechanisms.

$$\overline{\rho C_p}\frac{\partial T}{\partial t} - \emptyset\beta T\frac{\partial p}{\partial t} = -\rho v C_p \cdot \nabla T + \beta T v \cdot \nabla p - v \cdot \nabla p + k_e \nabla^2 T$$

Fluid thermal expansion coefficient, J-T coefficient and fluid velocity can be expressed as:

$$\beta = \frac{\eta C_f}{T},\ C_j = \frac{\beta T - 1}{C_f \rho_f} = \frac{1}{C_f \rho_f} - \eta,\ v = -\frac{k}{\mu}\nabla p$$

Rearranging Eq. 4.18:

$$C_m \frac{\partial T}{\partial t} + C_f \rho_f v\left(\nabla T + C_j \nabla p\right) - \emptyset\eta C_f \rho_f \frac{\partial p}{\partial t} = div(k_e \nabla T)$$

Neglecting the heat conduction and convection terms and defining the velocity of convective heat transfer as $u(r,t) = cv(r,t) = -c\frac{k}{\mu}\frac{\partial p}{\partial r}$. The energy equation can be simplified as:

$$\frac{\partial T}{\partial t} + u(r,t)\frac{\partial T}{\partial r} = -C_j u(r,t)\frac{\partial p(r,t)}{\partial r} + \eta^* \frac{\partial p(r,t)}{\partial t},$$

where $c = \frac{C_f \rho_f}{C_m}$, $\eta^* = \eta\emptyset c$.

Therefore, the fluid temperature change can be related to the fluid pressure change in the saturated porous media:

$$\frac{\partial T}{\partial r} = -C_j \frac{\partial p(r,t)}{\partial r}$$

$$\frac{\partial T}{\partial t} = \eta^* \frac{\partial p(r,t)}{\partial t}$$

Then, the temperature variation in both time and distance can be described as:

$$T = T_{initial}(r1) + C_j\left(p(r1) - p\left(r(t, r_1)\right)\right) - \eta^*(p_i - p(r_1))$$

For the homogeneous infinite reservoir with perfect well condition (no skin), the pressure profile can be expressed by a function of down-hole pressure and flow-rate:

$p(r) = p_w + \frac{q\mu}{2\pi kh} ln(\frac{r}{r_w}),\ \Delta p = \frac{q\mu}{2\pi kh} ln(\frac{r}{r_w})$

The velocity of convective heat transfer $u(r,t) = -c\frac{k}{\mu}\frac{\partial p}{\partial r} = -\frac{U_0}{r}$

$U_0 = c\frac{k}{\mu}\frac{\Delta p}{ln(\frac{r}{r_w})} = c\frac{q}{2\pi h}$,

where $r_{investigation} = \sqrt{{r_w}^2 - 2U_0 t} = \sqrt{{r_w}^2 + \frac{cqt}{\pi h}}$.

The temperature change at wellbore boundary is:

$$T(r_w,t) = \begin{cases} \frac{C_j q\mu}{2\pi kh}\left(ln\frac{r_{investigation}}{r_w} - \frac{\eta^*}{C_j} ln\frac{r_e}{r_{investigation}}\right) & ;\ \text{small time} \\ C_j(p_e - p_w) = C_j\frac{q\mu}{2\pi kh} ln\frac{r_e}{r_w} & ;\ \text{large time, stabilization} \end{cases}$$

If $\frac{\eta^*}{C_j} \ll 1$, an approximate equation can be used for the temperature calculation:

$T(r_w,t) = C_j\frac{\Delta p}{2lnR_{ci}} ln(1 + c\frac{qt}{\pi {r_w}^2})$, $R_{ci}$is the inner radius of the casing.

For great times, the term 1 can be neglected, rewrite above equation as:

$T(r_w,t) = \frac{C_j q\mu}{4\pi kh}(ln\left(c\frac{q}{\pi {r_w}^2}\right) + lnt)$